Fractals in Chemistry, Geochemistry, and Biophysics

AN INTRODUCTION

K. S. Birdi

Fractals in Chemistry, Geochemistry, and Biophysics

An Introduction

Fractals in Chemistry, Geochemistry, and Biophysics

An Introduction

K. S. Birdi

Department of General Chemistry
Royal Danish School of Pharmacy
Copenhagen, Denmark

Springer Science+Business Media, LLC

Library of Congress Cataloging-in-Publication Data

Birdi, K. S., 1934-
Fractals in chemistry, geochemistry, and biophysics : an introduction / K.S. Birdi.
p. cm.
Includes bibliographical references and index.
ISBN 978-1-4899-1126-1
1. Chemistry, Physical and theoretical--Mathematics. 2. Geochemistry--Mathematics. 3. Biophysics--Mathematics. 4. Fractals. I. Title.
QD455.3.M3B57 1993
541.2--dc20 92-30661
CIP

ISBN 978-1-4899-1126-1 ISBN 978-1-4899-1124-7 (eBook)
DOI 10.1007/978-1-4899-1124-7

Originally published by Plenum Press, New York in 1993
Softcover reprint of the hardcover 1st edition 1993

IN THE BEGINNING, God created the heaven and the earth. And the earth was without form, and void; and darkness was upon the face of the deep. And the Spirit of God moved upon the face of the waters. And God said, Let there be light: and there was light. And God saw the light, that it was good: and God divided the light from the darkness. And God called the light Day, and the darkness he called Night. And the evening and the morning were the first day.

—GENESIS *i, 1–5*

STRANGE is our situation here upon earth. Each of us comes for a short visit, not knowing why, yet sometimes seeming to divine a purpose.

—ALBERT EINSTEIN

Preface

We are all impressed by the patterns and shapes that nature has used all around us. In some cases these shapes and patterns are highly orderly. Man has always tried to understand the patterns and shapes found in nature: galaxies, clouds, snowflakes, ocean waves, coastlines, leaves, forests, patterns on skin and on butterflies, shapes and forms of crystals and molecules and macromolecules (e.g., synthetic polymers and proteins), shapes of biological cells and viruses.

Some decades ago, with the development of computers, the possibility arose of finding the geometrical laws that nature could have used (or uses) in these patterns and shapes. In order to characterize the so-called irregular geometrical structures, Mandelbrot (1982) developed and introduced a new kind of geometry, *fractal geometry* (different from Euclidean geometry). It was shown that many naturally occurring structures that are usually described as irregular, random, or chaotic actually have shapes that can be measured and categorized. Many shapes and patterns found in everyday life can be described on the basis of somewhat simpler geometrical considerations. In fact, fractal geometry can be considered a new way of looking at nature.

Later, some combinations with basic physical laws, such as those that describe the erratic motion of a dust particle in air (so-called Brownian motion), led to the discovery that in nature these shapes and patterns can be described by giving a dimension

to the geometrical analysis. This was called the concept of *fractal dimension* and is the subject described herein. Mandelbrot coined the word *fractal* from the Latin adjective *fractus* (Latin verb *frangere,* meaning to break, i.e., to create irregular fragments).

These developments have given rise to a very extensive literature. There are many excellent current textbooks that describe at various levels the elaborate theory that has developed about the fractal dimension and fractal geometry found in various natural systems and in technology. The aim of this text is to introduce the experimental methods and analyses of fractal dimensions in natural processes. The description is kept at a level such that anyone with a little mathematics and physical science training (high school and above) can succeed here. For those who feel that they need more advanced information, references are provided that give the appropriate guidance for high-level analyses.

Simple experimental procedures are described that will be useful for the reader in conducting experiments and verifying through analyses some of the fractal phenomena. Experimental data on all kinds of fractal systems are given, making it easier to follow the text as well as to compare and construct a model. The geometrical analyses, in some cases, are delineated with the help of computer (PC-computer-level) programs, which allow the reader to draw the shapes and patterns (although doing so is not a necessity for reading the text). Furthermore, the latest mathematical developments are included, which lead the reader to develop and analyze his or her own fractal shapes and patterns. Most recent developments are very useful for understanding the meaning and application of the fractal dimension to a variety of experimental data. These examples will further lead readers to find fractal dimensions in their own everyday observations. This point is emphasized wherever pertinent, since the usefulness of fractal geometry has now grown to such a level that it can be applied to a wide variety of phenomena.

The concept of fractals, as it is applied to problems in chemistry, geochemistry, and biophysics, is presented in separate sections. A short discussion is given to identify these structures, followed by a short review of the work pertaining to fractal measurements. The subject matter is arranged in such a way that

the volume can be used as a text. The book should be of value both to beginners and to professionals who have a continuing interest in fractal geometrical theory and applications.

I am very much indebted to many colleagues and students who have helped in various ways during the writing of this book. Finally, I am very thankful for the continuing support and encouragement given by my wife throughout this process.

K. S. Birdi

Contents

1

Introduction to Fractals

1.1. Fractals in Physics and Chemistry

Throughout the ages man has marveled at nature. The dimension of observation has increased from the eye to the electron microscope. All natural phenomena as observed by man seem very complex, at least at first sight. It may be the shape of riverbanks or hills or waves at the beach. Or it can be the shapes and colors of butterflies, leaves, and flowers, or the skin patterns (on the leopard or zebra). We may include here the shape of coastlines or of snowflakes. And we may also include the stars in the sky, the galaxy, and our solar system. The size range that has been studied varies from the shapes of craters on the moon, to the microscopic-level analyses of porous solid surfaces (catalysts, geological formations, oil reservoirs). Man is inquisitive, and therefore questions why he is here on earth, and whether the various phenomena mentioned above can be described by some mathematical geometry. Furthermore, man studies evolution and the ecological processes, which are in some ways related to these shapes and forms.

In nature one finds many patterns that are (seemingly) so irregular (e.g., shape of a leaf or flower) and fragmented that they cannot be described by Euclidean geometry. This is in contrast to Euclidean geometrical measurement, where one deals with length, depth, and thickness. As we know, the length of a line is

one-dimensional, the area is two-dimensional, and the volume is three-dimensional. All of these objects have the so-called characteristic length.

These dimensional descriptions cannot be useful if one examines in any detail the shapes of objects with irregular outlines, such as a leaf or flower, coastline, snowflake, skin patterns, ecological phenomena, trends of economic ups and downs, lightning, adsorption of molecules on solid surfaces, and so forth. The magnitudes covered are from 1 km (1000 m = 10^5 cm) to 10^{-8} cm (Å = molecular dimension). This was one of the reasons why many scientists became more and more interested in trying to find order behind such complex, and seemingly chaotic, systems in nature. Later, a new mathematical approach was invented that could be useful for analyzing those systems that deviated in shape and form from the Euclidean geometry. In recent developments, the role of the computer has become much more important, at various levels.

But one may question whether all of this could not be the outcome of some kind of organized natural phenomena, at some level of complexity not obvious to the naked eye, or the time scale available to the human being. One of the main limitations that man faces when studying the natural phenomena is the eye as used to observe these phenomena. Furthermore, on the time scale of evolution, one talks of (hundreds of) millions of years, whereas the duration of a very long laboratory experiment is overnight. In addition, the scale used for observation can also be an important parameter. Basically, the fractal theory revolves around analyses of irregular shapes and forms of objects (see general references). Herein the procedures are described through both a constructive approach and practical examples.

It is useful to introduce to the reader a simple approach for constructing a shape with some fractal geometrical dimension. After this example, we will proceed to discuss the basics of fractal dimension, and its application to everyday observations.

1.2. A Simple Fractal Shape [Personal Computer (PC)-Drawn Fractal Program]

The purpose of this example is twofold. First, a typical shape will be drawn in order to explain the need for fractal (geometry)

analyses. Second, a simple computer program will be used in drawing this shape. The impact of computers on many educational aspects of everyday life is becoming more and more important. A few (rather simple) computer programs mentioned here have much educational significance, but are not absolutely necessary for the general understanding of the subject matter. Those interested in more advanced computer fractal programs are given the necessary references. It will enable some of the descriptions given here to be interactive with the computer graphics, at a level such that any ordinary PC-compatible can be used. The programs (see Appendix programs) used to draw the figures are given in simple BASIC language. These can be easily rewritten to any language similar to BASIC. The following example is merely a typical program, which draws a shape with typical fractal dimension, as described later in much more detail. The reader is encouraged to look at these shapes as drawn by the program, and any difficulty that is encountered in understanding the procedure will be resolved in the next few pages.

Dragon: A Fractal Shape

As we learn in high school geometry, a straight line is the shortest distance between two points. Let us consider a simple example that can be used to introduce the fractal dimension for an object, starting from a straight line by using some geometrical rules. A few terms will be introduced to the reader through the patterns as drawn by using the fractal program DRAGON. The prime purpose of this example is to show how one can join by drawing a set of lines (*fractional lines*) from point A to point B, following various different procedures. As mentioned above, a straight line has a dimension *one*. A straight line, according to Euclidean theory, is the shortest and most easily seen connection between points A and B. Let us denote the distance between points A and B as L^1_{AB} (where index 1 denotes a straight line (the exponent here will be referred to as a dimension = 1)]. If one runs the program with $n = 2$, the distance between two points is traversed by four segments, where each segment has length = 1/2 $(=1/n)$ of the distance between the two points A and B $(=L_{AB})$. The total distance traversed then is $2L_{AB}$. Now, let us call this pattern the *generator*. If we put $n = 4$ in the next run, then each of

the four segments is again divided by four new but smaller segments [$=(1/2)^2 L_{AB}$], which gives 16 segments in going from point A to B. The distance traversed now is $16(1/2)^2 L_{AB}$. The distance traversed is thus found to increase from 2 ($=2^1$) to 4 ($=2^2$) to 16 ($=2^4$). This logarithmic increase (so-called *fractal dimension* = 2) is what one calls relations such as the *power law* dependence, as mentioned below. Mathematical analyses of the power law dependence show that there is a constant (=2 for the dragon) that gives rise to the increase in length as n increases.

The most fascinating result becomes obvious if we now look at the pattern generated when $n = 12$. It has the shape of a dragon. The generator which makes the first variation in going from point A to B is repeatedly used, and by decreasing the size of the steps, the figure obtained (Figure 1.1) looks like a figure with some known shape. In other words, if a dragon can be generated by using a simple generator, then we may expect that other more complicated patterns or shapes could be the result of other generators (perhaps not as simple as this generator). The generator could be imagined to be a perturbation to a system in any natural process (like a stone that is dropped into a pond, and the ensuing ripples). This will be shown in the many examples given throughout the text. A similar procedure is what has now become known as self-similarity and fractal dimension description of non-Euclidean shapes and patterns. *Self-similarity* implies that a structure is invariant to changes of scale, i.e., it possesses dilational symmetry and thus there exists no characteristic length scale associated with the structure. If we magnify the picture of this dragon, we will thus find that the generator appears at all magnifications. Of course, this depends on the magnitude of n. If say $n \approx \infty$ (which could be achieved if we were drawing this shape under a microscope), then an infinite number of magnifications can be carried out. Conversely, it is also self-evident that if one had started by looking at the shape of a dragon, and magnified the picture, one would end up with the generator at some level. However, this would disappear when further magnified. Furthermore, if the yardstick used was of molecular size (10^{-8} cm = Å = 0.10 nm), then the possibilities of drawing natural shapes and figures become numerous. Thus, the size of dragonlike shapes may vary from 1 km

(=1000 m = 10^5 cm) to 10^{-8} cm (Å = 0.10 nm). Additionally, two- or three-dimensional dragons are also possible with a bit more effort (it will be left to the more interested reader to pursue this matter!). It is also easily seen that in case we had a figure that looked like a dragon, then it could be simplified by using this fractal procedure. In fact, this is precisely why fractal theory has become so useful, since it can provide a procedure for analyses of such irregular shapes and forms. Thus, the straight line between points A and B has turned into a well-recognized shape through some simple geometrical generator step procedure.

This rather simple example thus suggests that one may find many shapes and forms, which when observed as we did with the dragon would repeatedly show self-similar characteristics. This observation has been reported in the literature and described in much detail (Mandelbrot, 1982).

The total distance traversed between points A and B thus is seen to increase as we diminish the yardstick of steps. From the difference between the lengths we can determine the fractal dimension (=2, as follows). Of course, similar rules would apply in the case of three-dimensional forms (Mandelbrot, 1982; Avnir, 1989; Takaytasu, 1990).

1.3. Basic Concepts and Terminology in Fractals

Fractal theory was found to be of necessity for those systems that could not be described by Euclidean geometry. Some general examples are as follows:

- Shape of a leaf or flower
- Shape of a cloud
- Shape of a riverbed
- Patterns of skin
- Patterns of a butterfly
- Surface of a porous solid
- Shape of a snow crystal
- Heartbeat rhythm
- Ecological phenomena
- Surface and shape of molecules

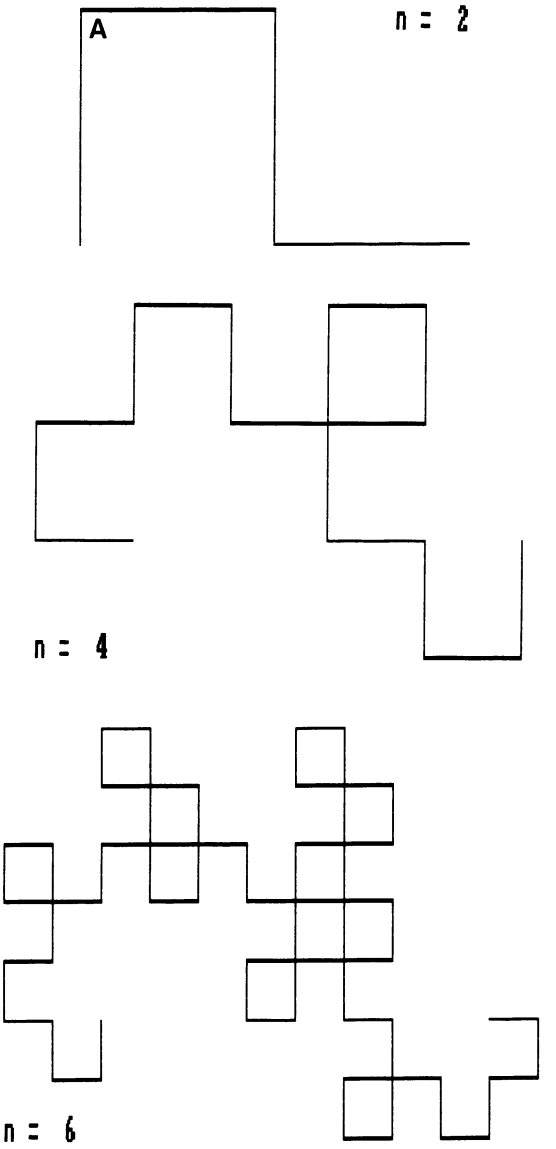

Figure 1.1. DRAGON (also called Harter–Heightway). The generator is shown in A. The increasing number of steps (n = 2, 4, 6, 8, 10, 12) can be drawn by the computer program, until a dragon shape is obtained. See Appendix A for computer program.

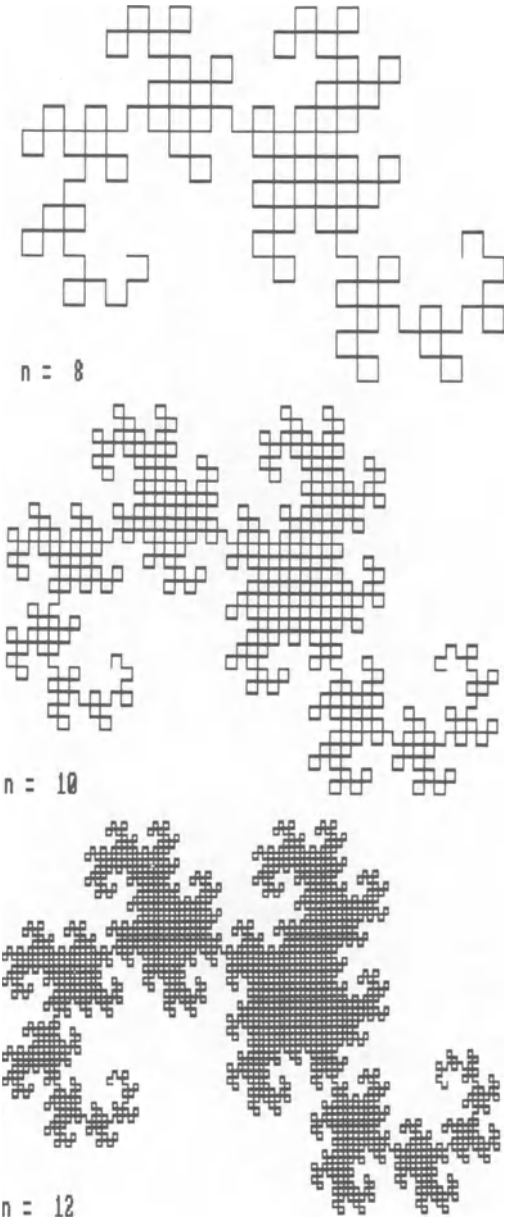

Figure 1.1. (*Continued*)

Fractal analyses thus attempt to give a more orderly picture of any (seemingly) disorderly systems (as might be evident from the above example of the dragon). It will be shown that the fractal analysis also adds increasing interest in the description of different systems through new ideas. These new analyses, as delineated here, would be expected to provide the reader with greater interest in natural phenomena with added vigor for application of this knowledge to some practical use, as compared to Euclidean geometry. This added interest to such mathematical analyses of natural phenomena is thus one of the aims of this monograph.

Moreover, fractal analyses as described herein will give a basic understanding both to beginners and to others who desire to investigate at a much higher level in this field. This is achieved through numerous examples from nature or everyday phenomena, where actual data are used to describe the procedures. A large number of typical examples are included, where experimental data are given from which fractal dimension has been estimated. In the latter systems, it is hoped that through this approach the reader can acquire a better practical understanding of fractal analyses. Another difference between natural fractal (e.g., of a leaf) and an ideal object is that the former is not self-similar over a range of length scales.

Further, we will point out at different places where the procedures described in these recent fractal theories are somewhat similar to the much older geometrical analyses. For instance, the magnitude of π was estimated by drawing a series of polygons of different side lengths, which is also used in fractal analyses of shapes and form (see Section 1.5).

According to Euclidean geometry, we know that length L (cm^1), area A (cm^2), and volume V (cm^3) are related to each other as (Figure 1.2):

$$L \propto A^{1/2} \propto V^{1/3} \tag{1.1}$$

If we consider a line of length L (say 1 cm), then a square of side L has $A = L^2$ (cm^2), and a cube of length L has $V = L^3$ (cm^3). In other words, the area of a square increases by exponent 2 and the volume by exponent 3, as L increases.

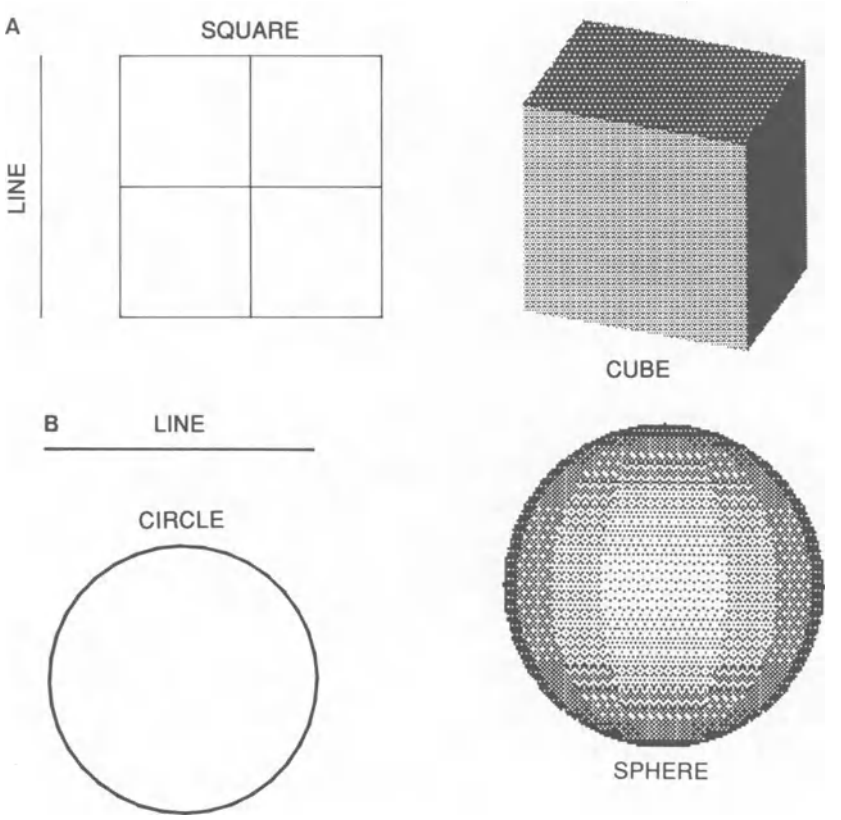

Figure 1.2. Simple geometrical shapes: (A) line, square, and cube; (B) line, circle, and sphere.

A similar relation holds in the case of area of a circle (cm^2) and the volume of a sphere (cm^3). It is also worth noting that if we increase L_{line} to $2L_{line}$ (by a factor of 2), then the magnitude of A_{area} increases by 2^2, and V_{volume} increases by 2^3. The exponents thus indicate that:

- L_{line} is one-dimensional
- A_{area} is two-dimensional
- V_{volume} is three-dimensional

Now if we consider the (irregular) outline of a leaf, and if we

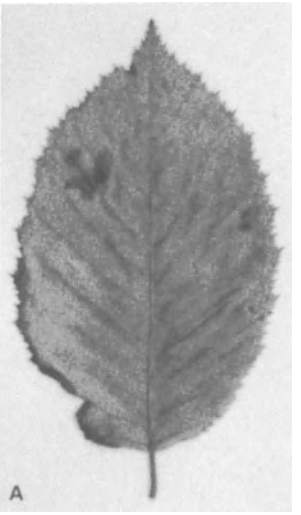

Figure 1.3. Outline of an elm leaf. (B) Magnification of A shows self-similar shape. The magnitude of $D_{leaf} = 1.5$ (see Section 1.3.2).

desire to determine the magnitude of its perimeter, we cannot perform this as easily as in the case of the square (Figure 1.3). We cannot use any of the ordinary geometrical (Euclidean) equations, like the circumference of the circle with radius R ($=2\pi R$). The leaf has no effective radius and therefore we need to develop some other appropriate procedure (described herein). Hence, in the case of non-Euclidean shapes and forms, we will have a quantity M, related to the above as follows:

$$L \propto M^{1/D} \tag{1.2}$$

where D is the fractal dimension. It will be shown herein that the value of D can be fractional, in contrast to the Euclidean (dimensions 1, 2, or 3) (Mandelbrot, 1982; Boccara and Daoud, 1985; Feder, 1988; Peitgen, 1988; Avnir, 1989).

Let us consider a somewhat different system. In general terms, a large molecule such as a protein or polyethylene is assumed to consist of a chain of segments connected in one dimension (same as

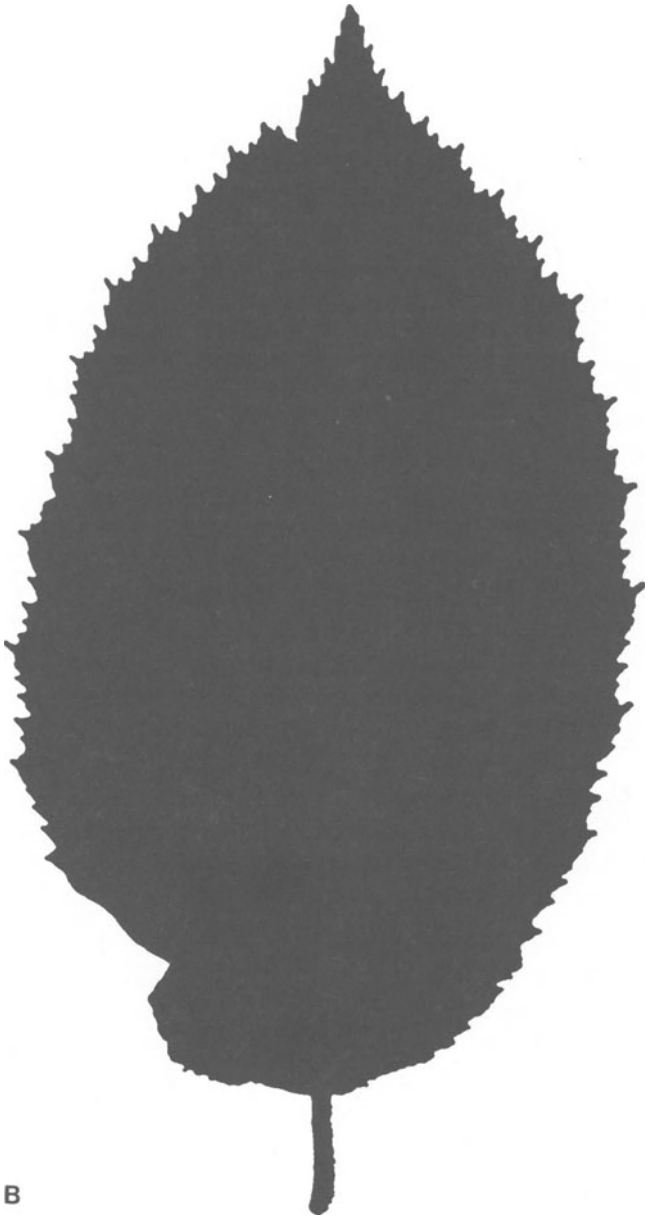

Figure 1.3. (*Continued*)

a string of beads). Similarly, the surface of a solid of any porous material is considered as two-dimensional. We thus find these two systems in varying dimensions as examples of perturbed states of an ideally ordered chain or surface. The ordered state can therefore be a periodic array of atoms (or molecular segments), a plane, a sphere, etc. The idea is that the disordered system inherits substantial physical and chemical properties found in the ordered system, provided that the deviation from the ordered system is of a degree that overall properties are the same. On the other hand, if the disordered state differs widely from the ordered state, then there is no way to estimate any useful physical properties from the ordered state. We thus introduce the usefulness of fractal analyses of irregular objects (Farin and Avnir, 1988). Unlike regular one-, two-, or three-dimensional geometrical objects, fractal objects will be shown to exhibit nonintegral dimensions. A randomly coiled polymer chain in solution will be shown to have a fractal dimension somewhere between 1 and 2, whereas the surface of a porous solid may be around 2 to 3.

The fractal description of any such disordered state is what has been most useful, based on comparisons with the ordered state. The fractal analysis is based on description of the disordered state as being intrinsic rather than perturbed.

In Figure 1.4, different types of disorder are given:

a: No disorder
b: Weak disorder
c: Anisotropic disorder (self-affine)
d: Isotropic strong disorder (self-similar)

It remains to be shown how these different kinds of disorder can be analyzed and evaluated by the following procedures. Further, one may also imagine certain phenomena that could be related to some combination of these states.

In the case of a solid, different subsets might be important. This could be the surface or the pore space of the solid. Further, it can only be the set of all edges and corners. Additionally, the shape of pores as a function of depth could be considered (described below).

As regards the local fractal structure, the analyses have shown

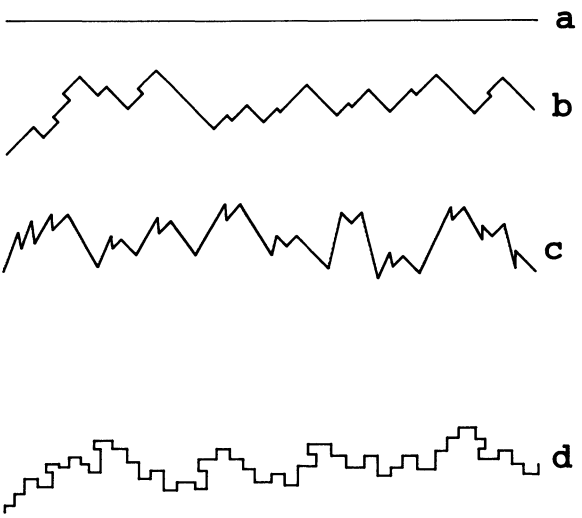

Figure 1.4. Different types of disorder (continuum model; see text) and their invariance properties. (a) No disorder; (b) weak disorder; (c) anisotropic strong disorder (self-affine); (d) isotropic strong disorder (self-similar).

that it can also provide many useful results. One can proceed by taking a reference point of any object, and then study the concentration of fractals about this reference point. In other words, one can estimate the local densities and distribution of fractals around the reference point. It is obvious that knowledge of the local form of a fractal is expected to be useful in the development of theory and in its application. The reference point may be arbitrary and would add information, i.e., variation of D with respect to the choice of reference point.

However, it is important to stress here that, depending on the yardstick used, the fractal dimension may or may not change drastically. The term *yardstick* means the degree of magnification used when observing the dragon shape. This point is clearly understood when considering Brownian motion and the mean free path of gas molecules (see Chapter 11 and Appendix B). Nevertheless, over a definite scale the analysis appears very much like fractals, and as such scales may usefully be regarded as fractals. The distinction between "natural fractals" and the mathematical "fractal sets" that

might be used to describe the objects was emphasized by various investigators (Mandelbrot, 1982; Stanley and Ostrowsky, 1986). This distinction must be kept in mind, for it seems to have become blurred in the current literature. Furthermore, one may also keep in mind that there are no true fractals in nature, just as there are no true straight lines or circles either! In the case of a circle, the circumference is equal to $2\pi R$. Since π is not an exact integer (see later), the exact value of the term $2\pi R$ will depend on the accuracy of π [π nowadays used in hand-held calculators or computers is given to an accuracy of 13 digits, whereas in ordinary calculations one generally uses $22/7 = 3.1428\ldots$, which differs from π by 0.00126448927 $(=22/7 - \pi)$]. There is no clear need for higher accuracy, since all of the large bridges are based on calculations where the magnitude of $\pi = 22/7$.

With regard to the notion of dimension (i.e., the size of the yardstick), let us consider a ball (made of threads) of 10 cm diameter, and proceed to describe how we (i.e., the eye) observe its outline at varying distances. Let us suppose that it is made up of thick threads of 1 mm diameter. Now, if someone saw the ball from a long distance away (say 1 km), it would merely seem to be a point. At a distance of 10 cm, it would look like a three-dimensional ball. From a very short distance away (10 mm), it would be a tangle of threads. As we approach even closer, the fibers make the ball look completely different from our original perception of it being a ball. This clearly shows that the perception of an object is dependent on the distance of observation, as far as the dimensionality is concerned. Furthermore, most natural fractal patterns have the property of scale invariance, which means that these patterns appear the same at all levels of magnification or resolution between upper and lower cutoffs.

An analogous example is the surface of the moon (although with a much larger dimension), as it looks quite smooth from the earth using the naked eye, whereas using a telescope it is seen to be completely pockmarked by craters. In fact, the first rocket equipped with a camera, which crashed on the surface of the moon (prior to the first manned landing) showed these features very clearly, so much so that the size distribution of craters (on the moon, earth, etc.) is found to be fractal.

1.3.1. Definition of the Fractal Dimension

Perhaps it is better to ask why it is necessary to use fractal analyses in the first place. This we can answer by showing how the shape of the dragon requires a non-Euclidean analysis, i.e., fractal dimension, provided such a dimension is indeed present. The question one may ask then is: how can one identify and measure the fractal dimension? Further, since by necessity we need some useful procedure to analyze these irregular shapes, the fractal theory is the most convenient.

What one does is measure the fractal dimension of objects in nature or of some appropriate model chosen to describe an experiment. This has given rise to much research activity in various fields of science. There are many different procedures that one may use in order to define the fractal dimension. In the continuum model, it is assumed that the structure remains so at any level of length scale. On the other hand, the lattice structure is based on larger length scales. If the structure is self-similar, then these two models are the same.

1.3.2. Self-similarity and Fractal Behavior

1.3.2.1. Exact Fractals

As already noted, Euclidean geometry is not sufficient to enable us to describe or analyze all of the shapes and forms in nature. One most remarkable shape that is completely lacking in any Euclidean analysis is that of the crack, be it in metal, cement, or earth. We generally notice that there are some patterns that repeat in the shape of these cracks. This repeating pattern is what we will discuss here. This is called mathematical fractals (Mandelbrot, 1982; Stanley, 1984; Pietronero and Tosatti, 1986; Stanley and Ostrowsky, 1986).

As an example, let us analyze the two-dimensional triangular shape, the so-called Sierpinski gasket (Figure 1.5). This is constructed by using a triangle as the initiator. The generator removes a part in the middle as indicated. The Sierpinski gasket can be drawn both by simple geometrical steps or with the help of a simple

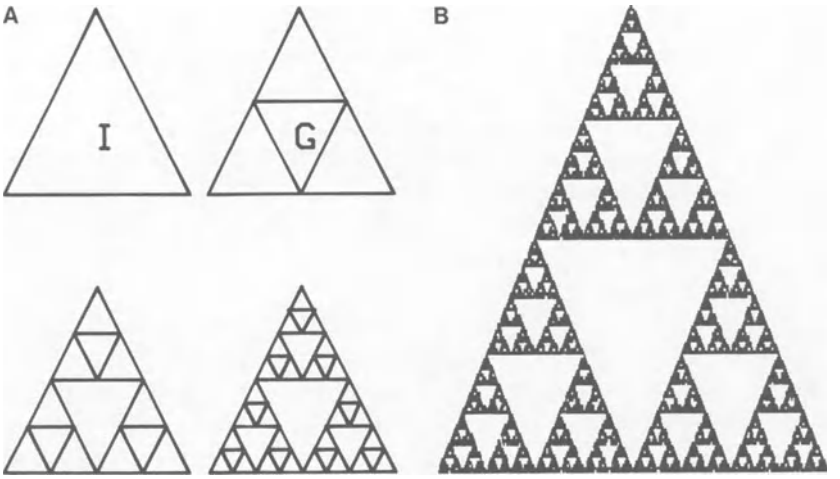

Figure 1.5. Sierpinski gasket. (A) The initiator (I) is the triangle that is initially filled; the generator (G) removes a central triangle as shown. (B) A more general Sierpinski triangle is generated by the computer program (see Appendix A). $D = \ln 3/\ln 2 = 1.58$.

computer program (see Appendix A). The algorithm is as follows:

- Draw an equilateral triangle
- Draw another triangle inside
- Draw triangles in each section
- Repeat the above procedure
- . . .

The magnitude of $D = \log 3/\log 2 = 1.58$. It is clear that if one examines this triangle under some magnification, one finds more and more empty space. The density thus changes when the length scale used for observation changes.

This observation does not seem to be in accord with everyday knowledge. According to Euclidean geometrical considerations, the area and volume of a square of cubic object increase as the length, L, of the side increases. However, let us consider an example to describe it in more detail. Say a container is full of sugar with mass M. If we increase the edge of the container from L

to $2L$, then the mass would increase by a factor of 8:

$$M_{2L} = 8M_L \tag{1.3}$$

$$= 2^3 M_L \tag{1.4}$$

A general relation can be written as:

$$M_{\epsilon L} = \epsilon^D M_L \tag{1.5}$$

where ϵ is any positive number and D is the fractal dimension. The relation in Eq. (1.5) is functional, and thus if $\epsilon = 1/L$, then we get:

$$M \propto L^{\delta} \tag{1.6}$$

The density δ is

$$\delta = M/L^D \tag{1.7}$$

Hence, the lower the density, the smaller are the amplitudes that appear implicitly in Eq. (1.7). Furthermore, no matter how low the density, the exponent in Eqs. (1.6) and (1.7) is always the dimension D.

It can be shown that the mass in the Sierpinski gasket is given as (Figure 1.6):

$$M_{2L} = 3M_L \tag{1.8}$$

$$= 2^{D_f} M_L \tag{1.9}$$

where

$$D_f = \ln 3/\ln 2 = \log_2 3$$
$$= 1.0986/0.693147 = 1.58496 \tag{1.10}$$

These fractals are called deterministic fractals since their patterns are completely determined by the generating process. This

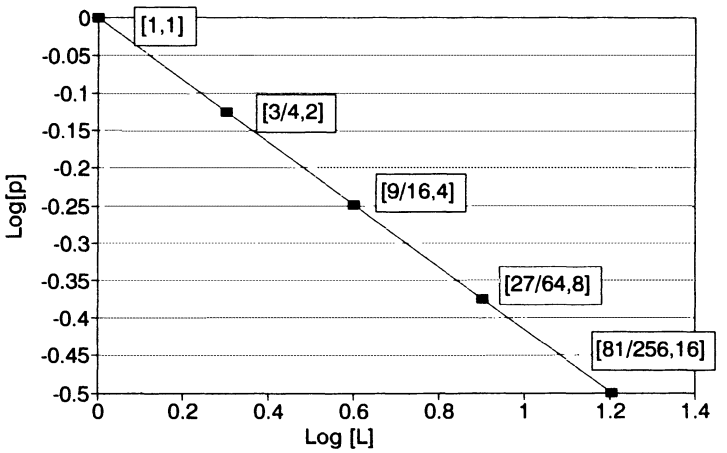

Figure 1.6. The prototype regular or exact fractal (Sierpinski), $D = 2$. On each iteration the density, p, decreases, which is a generic feature of fractal objects (plot of $\log p$ versus $\log L$).

means that one can calculate the coordinates of any point on the fractal. In other cases, some fractal structures exhibit a distribution of points that may be situated more or less at random. The latter do, however, obey the average scaling relationship:

$$N_R \propto R^D \tag{1.11}$$

These fractals are called stochastic or statistical fractals (Stanley and Ostrowsky, 1986).

Under similar considerations, the density can be given as follows:

$$\begin{aligned} \delta_{2L} &= (3/4)\delta_L \\ &= 2^{D_t - D}\delta_L \end{aligned} \tag{1.12}$$

where $D - D_t$ is called the co-dimension.

In general, fractal objects can be described by functional equations of the kind:

$$M_{\lambda L} = \delta^{D_t} M_L \qquad D_t < D \tag{1.13}$$

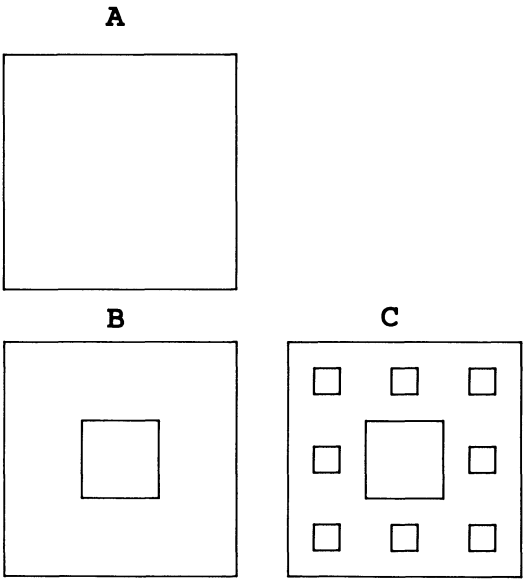

Figure 1.7. Square Sierpinski carpet. (A) Initiator: square; (B) generator; (C) second stage: eight squares.

The relation in Eq. (1.13) is the general fractal equation

$$M_L = L^{D_t} \tag{1.14}$$

for this exact fractal there are no "correction to scaling terms"—the leading "scaling" term suffices for all values of L. A similar analysis can be applied to the shape with initiator as square and the generator, Figure 1.7, where $D = \log 8/\log 3 = 1.89$. Actually, a variety of other shapes (polygons) can be obtained by using this procedure.

1.3.2.2. Statistical Fractals: Random Walk

The simplest example of a statistical fractal is an N-step random walk on, say, a square lattice (Figure 1.8A) (more later). The walker, for example a drunken sailor at the waterfront, takes one step per time unit (t), so that $N = t$. Since there are four

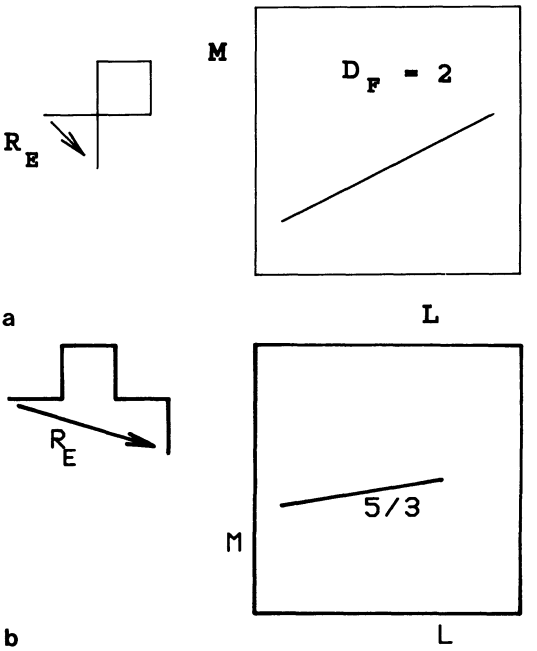

Figure 1.8. Schematic illustration of (a) a random walk and (b) a self-avoiding walk (SAW) (each of $M = t = 6$ steps). Only one of the 4^6 possible walks is shown, most of which have zero weight for the SAW case. The log–log plots show the relation between the characteristic length scale L (the mean end-to-distance R_e) and M, the number of steps.

choices for the drunk for each next step, after a time t there are a total of 4^t distinct configurations. Most configurations are not fractals, yet certain average quantities obey functional equations as obeyed by Sierpinski gasket.

As an example, let us use for the length scale L the "range" of the walk—the Pythagorean distance from the origin after the t steps, averaged over the ensemble of all t-step walks. Further, let $L_{t+1} = 1$ for the 4 one-step walks, $L_2 = 2^{1/2}$ for the 16 two-step walks, $L_3 = 3^{1/2}$ for the 64 three-step walks, etc. The general equation that one gets is:

$$L_t = t^{1/2} \tag{1.15}$$

This relation also holds for multidimensional systems.

A typical system where this type of model is used is when considering the shape and growth of a polymer by the polymerization of each monomer unit. As an example, let us consider that after each step a monomer is placed, and that the steps correspond to chemical bonds between monomers in a polymer. The random walk traces out a "free-flight" polymer that ignores the Archimedes's principle that two objects cannot occupy the same point of space. The mass of the polymer, M_{total}, after t steps is clearly proportional to t. The mean Pythagorean distance from the beginning to the end of a polymer chain [compare this to a necklace with the number of beads equal to t (i.e., each bead is a monomer)] with N monomers is given as:

$$t \approx M_L \approx L^2 \tag{1.16}$$

From these equations we get:

$$M_L \approx L^{D_w} \tag{1.17}$$

which in the random walk case gives:

$$D_w = 2 \tag{1.18}$$

The fractals are self-similar and the same is true for the self-avoiding random walk (SAW), which means that they look the same independent of the length scale at which they are observed. However, there are many systems in nature that exhibit different geometrical structures at different length scales (Ahrony *et al.*, 1987). Although they are homogeneous (on the average) for large length scales, they exhibit self-similarity on short length scales. In the latter case, such systems may be modeled by fractal structures. It is obvious that one may also ask how a fractal grows. It has also been mentioned that completely different growth mechanisms may lead to the same fractal object (Stanley and Ostrowsky, 1986).

1.3.3. Fractal Structures

One can describe the basic concepts underlying fractal spaces as follows. The mathematical fractals have been defined as those objects that exhibit *scale invariance,* which means that the pattern is self-similar. In other words, as already shown by the dragon example, the pattern remains unchanged under dilation operations (within some limits). The concept of self-similarity is basic to fractal analyses of forms and shapes, as shown for the dragon example. It can also be seen that through some variations, these self-similar phenomena can be expected to cover a rather large number of natural systems. Furthermore, one can draw both two- and three-dimensional objects (Mandelbrot, 1982).

Self-similarity and Fractals

We recall objects around us by associating them with their shapes and forms. Although the term *self-similarity* is well known, quantitative interpretations have only recently been exhaustively analyzed. Furthermore, this term is not found in Euclidean geometry. In other words, the shapes and forms that are easily analyzed by fractal geometry, cannot be described by simple Euclidean geometry. As already mentioned, for example, if one examines a crack in a cement wall or floor, one generally finds that some parts of the shapes repeat quite often. In fact, the same was described in the case of metal cracks some decades ago. In other words, even in such irregular shapes, one finds some similarity. Therefore, many scientists wondered whether such self-similarity could be analyzed by fractal theory. Another common observation is that ocean waves seem to be self-similar. This was known to ancient seafarers as mentioned in many old travel books.

Further, if one looks at a drop of rainwater, then one can easily be led to imagine that inside this drop must be other smaller drops, and that inside these there must be still smaller drops, and so on. In fact, the answer lies somewhere else. What colloid science has suggested is how water molecules must approach each other in the gas phase (so-called embryo), such that at some proximity and shape a first drop of liquid water will be formed (Adamson, 1982).

It has been found that there must be a minimum of ~30 molecules of water before an embryo can be formed for the phase transition from gas to liquid to take place. This also suggests that the distance and orientation of molecules remain the same as the embryo grows from ca. 30 molecules to ca. 30×10^7 molecules (a drop of rain). The self-similarity remains in this multitude of decades (approximately 7 decades). This is important to keep in mind whenever we mention the term *self-similarity*.

However, the notion of self-similarity is not new. It has been known that turbulence in rivers can be decomposed into small eddies, which remain self-similar (Figure 1.9). This may be one of the major reasons why rivers do not flow in a straight line.

The instability caused by an eddy in a river can be explained as follows. If one drops a stone into a pond, it gives rise to some waves, which disappear shortly. However, if one drops a stone down the side of a hill, it may hit a larger stone, and the latter might hit one still larger, and so on. This gives rise to an avalanche. It could be that rivers receive an input as a stone that gives rise to many eddies, which in turn makes the rivers flow differently on the banks. At a molecular level, this would be analogous to a toxic molecule entering a biological cell and destroying the lipid bilayer. This is the mechanism by which the same amount of snake venom injected into a human or an elephant is deadly.

1.3.4. Diverse Self-similar Fractals

At this stage it is useful to present typical examples illustrating the multitude of self-similar patterns that can be realized. A variety of self-similar patterns have been described in the literature (Mandelbrot, 1982). The simplest kind, as given in the dragon case, was mentioned earlier. Here we discuss a variety of self-similar patterns, furthering our general understanding of fractals and self-similarity. It is also hoped that through these examples one may be guided to proceed with construction of other types of fractal shapes. Although for the sake of simplicity only two-dimensional shapes are given here, it is also hoped that the reader through some help from computer programs can transform these shapes into three-dimensional space (especially with the help of

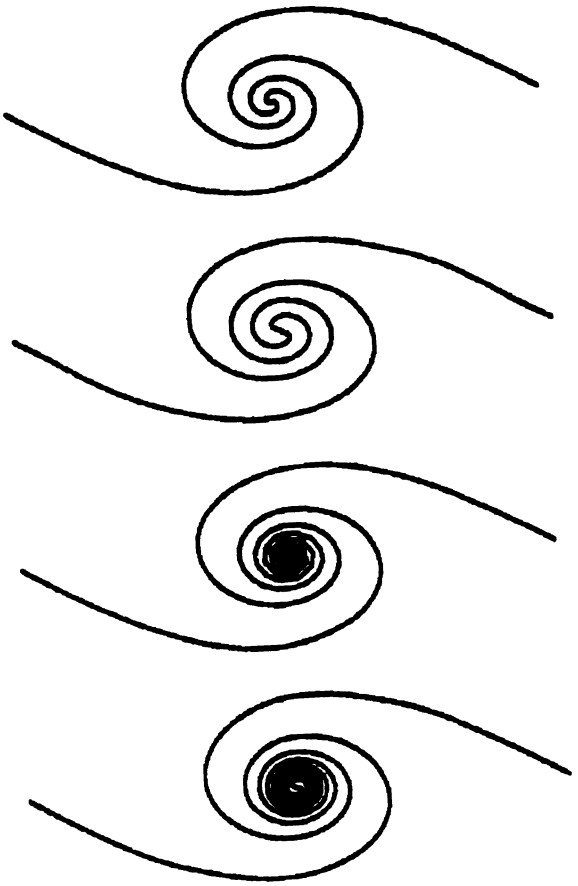

Figure 1.9. Small eddies (top) which are initiators and grow to larger vortex (bottom) (i.e., growth of self-similar shape).

simple computer-aided drawing programs). In a recent study, ray-tracing was applied to study such objects (Bouville, 1985).

Triadic Koch Island or Snowflake. These patterns are fractals that are generated by triangular shapes as the initiator. The analogous initiator square will be described in the next section.

The simplest shape occurs when the initiator is a triangle (Figure 1.10). Then each side is divided into thirds, and an equilateral triangle is constructed in the middle on each side, as the

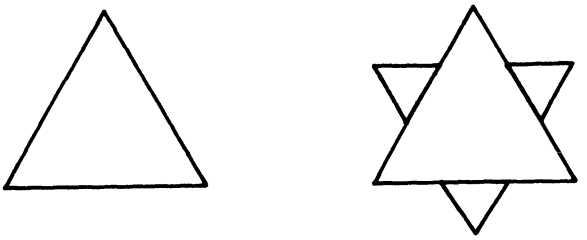

Figure 1.10. Self-similar construction of the triadic Koch curve (D = log 4/log 3 = 1.2628) (first two stages).

generator. The second stage is the star shape. The next stage merely subdivides the outer perimeter, which results in a pattern different from those that are open inside, such as the case of the Sierpinski. Further stages give a curve that is infinitely wiggly—there are no straight lines in it whatsoever. This pattern looks like a snowflake. A snowflake has been characterized as a result of nonequilibrium phenomena. The imbalance of forces gives rise to such shapes, which are well defined but the driving forces are chaotic (due to fluctuations as present around us arising from temperature, pressure, density, charges, etc.). In a recent study based on a more advanced model [diffusion-limited aggregation (DLA)], the structure and formation of snowflakes were reported (Meakin, 1986). The patterns produced by this computer simulation model are remarkably similar in appearance to real snowflakes observed in the microscope. As the structure grows, fluctuations of two general kinds appear. The first are radial extensions of the interface. These are rapidly destroyed as cluster mass accumulates on either side of the protrusion. The second type of fluctuations are depressions.

Quadric Koch Island. The initiator is square, and the generator is as given in Figure 1.11A. Each step ($\epsilon = 4$) is one-fourth of the total length of the straight line. There are in all 8 ($=N$) steps. This gives the magnitude of D:

$$D = \log 8/\log(4) \tag{1.19}$$

$$= 3/2 = 1.5 \tag{1.20}$$

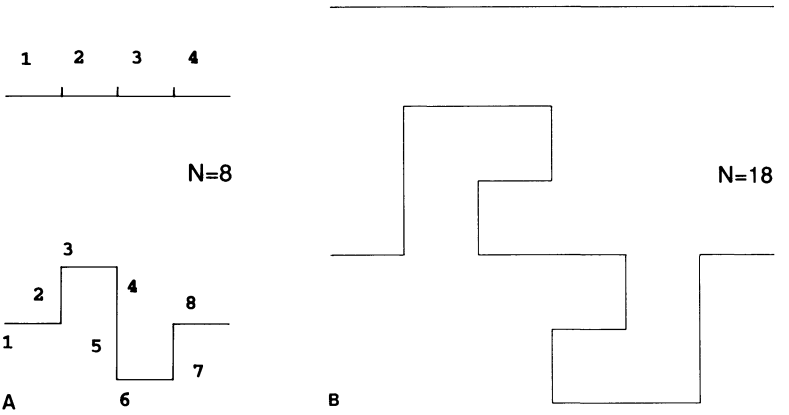

Figure 1.11. (A) Quadric Koch Island with $N = 8$, each step $= 1/\epsilon = 1/4$; $D = 3/2 = 1.5$; (B) curve with $N = 18$, $\epsilon = 6$, $D = \log 18/\log 6 = 1.6131$.

Another example is where $\epsilon = 6$ and $N = 18$ (Figure 1.11B). From this we can calculate the magnitude of D:

$$D = \log 18/\log 6 \tag{1.21}$$

$$= 1.6131 \tag{1.22}$$

If we consider the case where $\epsilon = 8$ and $N = 32$, D can be calculated as follows:

$$\begin{aligned} D &= \log 32/\log 8 \\ &= \log 2^4/\log 2^3 \\ &= 1.6667 \end{aligned} \tag{1.23}$$

The case where $N = 98$ and $\epsilon = 14$ gives:

$$\begin{aligned} D &= \log 98/\log 14 \\ &= 1.7373 \end{aligned} \tag{1.24}$$

The detailed analysis of these fractals has been given in the literature (Mandelbrot, 1982; Feder, 1988). It is obvious, however,

that by combining ϵ and N, different degrees of patterns with varying density can be obtained. In fact, when ink spreads after being carefully placed on water, it gives patterns with $D \approx 1.7$ [the result we get from the pattern from Eq. (1.24)]. This is a very important finding: magnitudes of D can be the same for two objects of different kinds.

The above are examples of a few typical fractals. The reader is encouraged to develop some variations of these and see what shapes develop. Furthermore, there are known random fractals analogous to the above-mentioned shapes (Falconer, 1990) (Figure 1.12). The dragon shape can also be easily transformed into a random fractal shape [by including a random command in the computer program (see Appendix A)]. For instance, one can draw curves instead of straight lines for each step, which gives a different shape. Or one may use dots for each step. We thus find that by combination of these various examples, one can draw almost any kind of shape or form that might be encountered in practice. This will be shown herein in more detail with the use of appropriate examples.

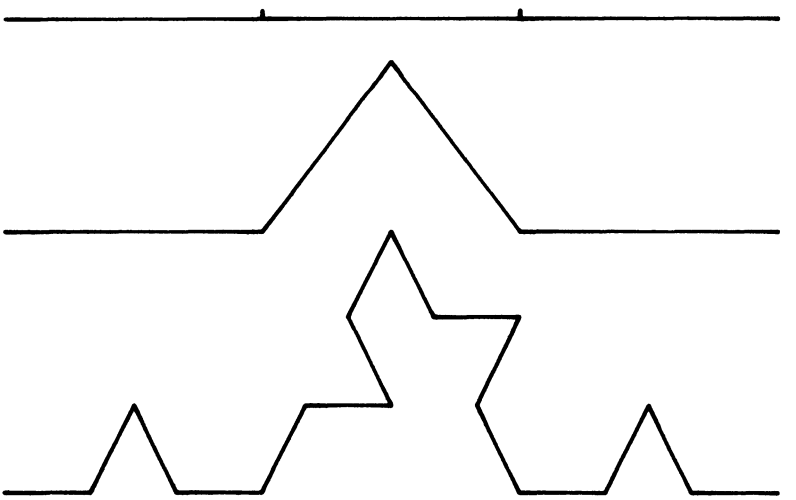

Figure 1.12. A random Koch curve. The shape at each step is determined by tossing a coin as regards to which side the segment is to be removed (three stages).

1.4. Fractal Dimension of Clouds, Rivers, and Coastlines: Length–Area–Volume Relations (Scaling Fractals)

Perimeter–Area Relation. As mentioned above, the shapes in the Euclidean regime exhibit some exact relationships between perimeter and area or perimeter and volume. In seemingly complicated natural phenomena, one often feels quite lost, since there is no possibility of analyses of natural systems by using Euclidean geometry. The latter defines the simplest shapes as lines, planes, or spaces. In addition, the language of physics uses density, temperature, pressure, or velocity, which are distributed in the homogeneous phase.

Furthermore, one can easily find the following relations between the perimeter and area inside any enclosed shape (Mandelbrot, 1982):

$$\text{Circle} \rightarrow \varphi = (\text{perimeter})/(\text{area})^{1/2} = 2\pi^{1/2} \tag{1.25}$$

$$= 2\pi r/(\pi r^2)^{1/2} = 2\pi^{1/2} \tag{1.26}$$

$$\text{Square} \rightarrow \varphi = (\text{perimeter})/(\text{area})^{1/2} = (2 + 2 + 2 + 2)/(2 \times 2)^{1/2} = 8/2 = 4 \tag{1.27}$$

$$\text{Equilateral triangle} \rightarrow \varphi = 6/3^{1/4} \tag{1.28}$$

It is also apparent that quantities of length, $(\text{area})^{1/2}$, and $(\text{volume})^{1/3}$ should provide ratios of any two, a parameter independent of the units of measurement.

In the case of area (A_δ) of any shape or form (e.g., island), by placing squares with side = δ (yardstick), Figure 1.13 is found to give (Mandelbrot, 1982):

$$\text{Perimeter} = L_\delta \tag{1.29}$$

$$\text{Area} = A_\delta \tag{1.30}$$

$$\varphi_D = (\text{perimeter})^{1/D}/A^{1/2} \tag{1.31}$$

$$= L_\delta^{1/D}/A_\delta^{1/2} \tag{1.32}$$

Unlike the circle (or square or other Euclidean shape or form), fractals are irregular geometrical objects that show greater and greater detail no matter how small the scale (Fogg, 1986), and additionally exhibit self-similarity. That is, the detail at small scales looks just like that at larger scales. Fractal geometry remains one of the most fascinating and useful areas of the physical sciences at all levels. Fractals are used to model natural phenomena such as turbulent flow, interactions of plant communities, Brownian motion, and the distribution of stars. Fractals can even describe the activity of the stock market (see Chapter 10).

1.4.1. Box-Counting Fractal Method

It thus becomes evident that in contrast to the Euclidean shapes (Figure 1.14A,B), we need other methods in order to estimate the magnitudes of length (L), area (A), or volume (V), in the case of fractal surfaces or shapes. The well-known Euclidean equations are not useful here, and we must find procedures by which the fractal length, area, or volume can be estimated for irregular shapes and forms.

For example, in order to measure the area of an irregular surface, one proceeds by using tiles, or boxes (Figure 1.14). The space is divided into cells of side length ϵ, and one counts how many are intersected by the curve or surface (Figure 1.14C,D).

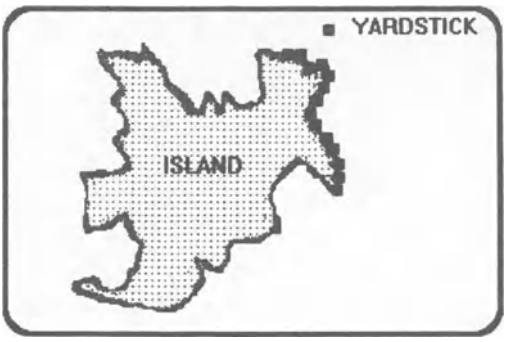

Figure 1.13. Fractal estimation of an irregular shape (e.g., an island) by box-counting method.

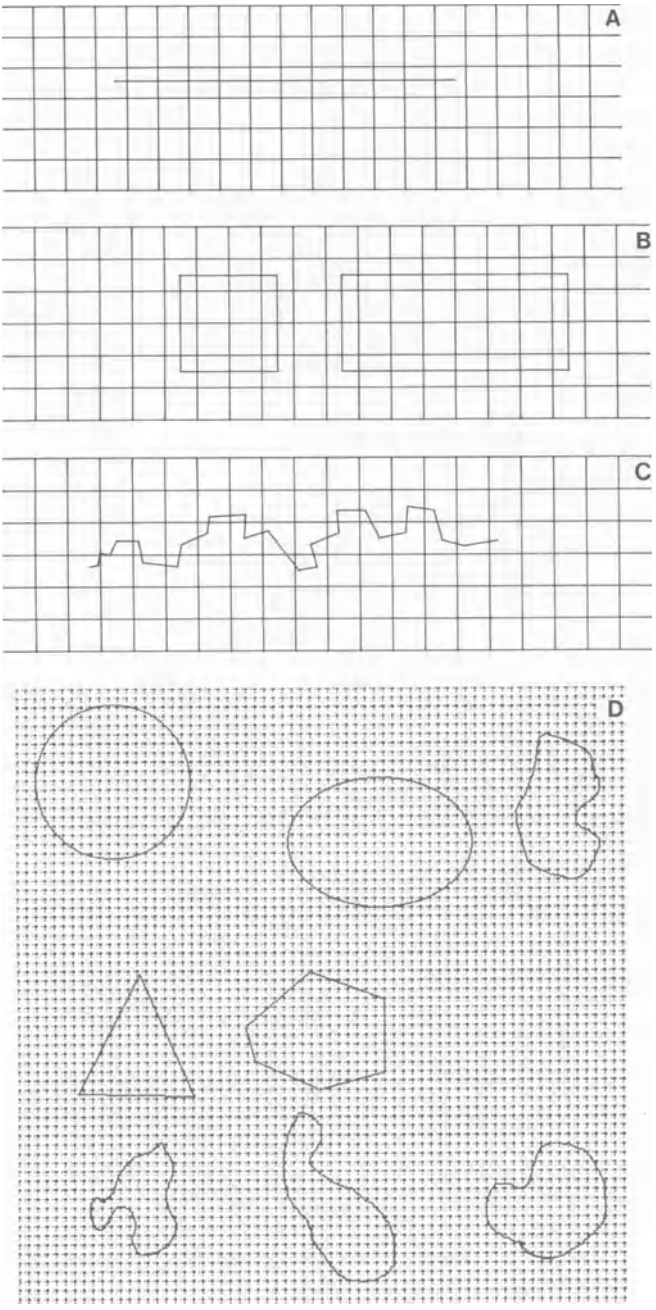
A
B
C
D

From this number of nonempty cells, $N_{box(\epsilon)}$, one gets:

$$\text{Length of curve as measured by box of size } \epsilon = L_\epsilon$$
$$= N_{box(\epsilon)}\epsilon \tag{1.33}$$

and

$$\text{Area as measured by box of size } \epsilon = A_\epsilon$$
$$= N_{box(\epsilon)}\,\epsilon^2 \tag{1.34}$$

where $A_\epsilon = \epsilon^2$. In other words, the magnitude of ϵ can be conveniently chosen to suit the measuring method [e.g., ruler, divider, magnifying glass, computer screen, microscope (e.g., electron microscope, scanning tunneling microscope)].

If we wanted to measure the fractal dimension of the coastline of an island or the geometry of clouds (Lovejoy *et al.* 1987), we would proceed as above. Let us suppose that the area of the island is A_{island} and the length of the coastline is L_{island}. As shown in Figure 1.13, draw a Cartesian lattice on the plane and make the squares as fine as possible. If using a computer, one can apply any of the graphic programs to perform such analyses. The squares that cover the coastline can be filled with colors. The number of squares or boxes can be counted, L_N. The area can be estimated from the unfilled boxes, S_N. As described above, both S_{island} and L_{island} are proportional to L_N and S_N. If there exists a fractal relationship between S_N and L_N for different islands, then the following relation will hold:

$$S_N^{1/2} \propto X_N^{1/D} \tag{1.35}$$

It is worth mentioning that whether a fractal dimension exists or not, or in most cases the variation of the fractal dimension, is expected to be dependent on the range of yardstick used for the

Figure 1.14. Fractal estimation of (A) a line; (B) a square and a rectangle; (C) an irregular line; (D) different (any) shapes.

analyses. Therefore, systems with such dependence will need to be analyzed with this bound. Further, there are systems where the fractal dimension is varying with the yardstick. The latter systems have not been extensively analyzed (Takayasu, 1990).

In the case of a straight line (Figure 1.14A), we thus find that since the magnitude of length L_ϵ is independent of size of ϵ used, then $N_{\text{box}(\epsilon)} \propto 1/\epsilon$. This shows that the system has a dimensional equal to 1.

The shape of a square (Figure 1.14B) has $A_{\text{box}(\epsilon)}$, where $n_{\text{box}(\epsilon)} \propto \epsilon^{-2}$; the exponent indicates that the surface has a dimension 2. Similarly, volume has a dimension 3.

For the irregular shape (Figure 1.14C), decreasing the magnitude of ϵ gives rise to an increase in length (as was seen for the dragon form), and thus $N_{\text{box}(\epsilon)}$ never approaches a dependence on ϵ^{-1}. From this we conclude that:

$$N_{\text{box}(\epsilon)} \propto \epsilon^{-D} \tag{1.36}$$

where D can be either integral or nonintegral.

We thus find the following:

$$\begin{aligned} D &= 1: \quad \text{curve} \\ D &= 2: \quad \text{surface} \\ D &= 3: \quad \text{solid} \end{aligned} \tag{1.37}$$

If we look at the winding curves in Figure 1.14D, we find that $D > 1$ due to these irregular shapes. The larger the value of D, the greater is the meandering (or disordered shape of the surface or solid). This kind of analysis can thus be useful for the characterization of surface roughness. In other words, the quantitative nature of fractal analyses can be very useful, under various conditions. A special application that has recently been adapted is the control of tumor growth in cancer.

Covering by Balls and Self-similarity. Box counting is a very simple and efficient method for determining the fractal dimension. $N_{\text{box}(\epsilon)}$ can be estimated as an average over all possible positions and orientations of the grid. However, if one estimates by box

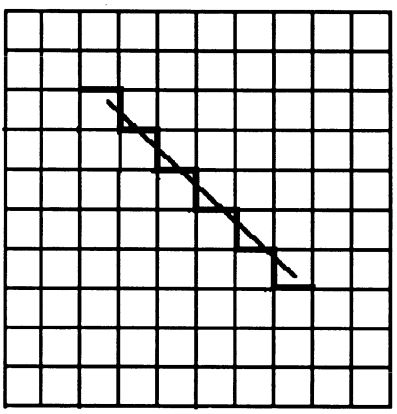

Figure 1.15. Overestimation of the length of a straight line by box counting. The estimated length N equals the length of the heavy stepped curve.

counting the classical length measurement [Eq. (1.33) or $D = 1$], it turns out that it is accurate to only within a factor of 2, and the same is the case for area. This arises from the fact that the length of a straight line, at an arbitrary angle with respect to the grid, is approximated by the length of a stepped curve (Figure 1.15). This leads to an overestimation of the length. Furthermore, the difference does not vanish as the box size is reduced (to zero limit). These discords can be avoided by using balls instead of squares or cubes, and estimating the length in terms of length as found from the diameter of the balls. Let $N_{\text{ball},r}$ be the minimum number of balls of radius r so that each point of surface lies on at least one ball. This procedure is termed covering by balls or spheres (Figure 1.16). From this we find:

$$\text{Length} = \lim_{r \to 0} N_{\text{ball},r} 2r \tag{1.38}$$

$$\text{Area} = \lim_{r \to 0} N_{\text{ball},r} 3r^2 \tag{1.39}$$

and instead of Eq. (1.36) one can write:

$$N_{\text{ball},r} \propto r^{-D} \tag{1.40}$$

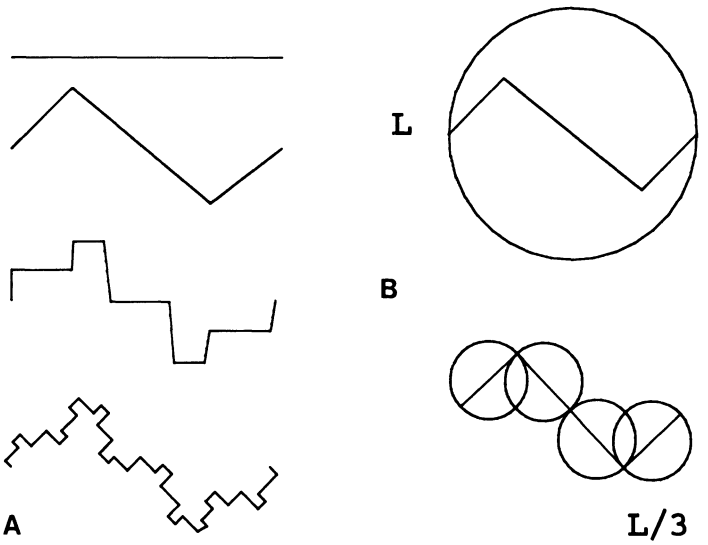

Figure 1.16. Definition of N and the construction of the curve. (A) The first stage is called the generator (top curve). It has end-to-end distance 1 and consists of four straight-line segments of length 1/3. If we replace each segment of stage k by the generator scaled down by the factor 1/3, we get stage $k + 1$ ($k = 1, 2, \ldots$). At stage k, the curve consists of 4^k segments of length 1/3. (B) Balls of size L and $L/3$ are shown (L = system diameter).

We find that the covering system by balls instead of cubes gives the correct estimate of length/area and a definition of D almost identical with Eq. (1.36). However, it is obvious that any other suitable shape (e.g., polygon) can be used.

Whether one uses cubes or balls or any other convenient reference probe (even molecules as mentioned later), this only affects the prefactor in Eqs. (1.39) and (1.40), and has no effect on the exponent. The only difference is that $N_{\text{ball},r}$ involves a nontrivial minimization problem, whereas $N_{\text{box}}(\epsilon)$ requires only averages. From the covering by balls in Figure 1.16, the value of $D = \ln 4/\ln 3 = 1.26186$. This relation is obtained as follows. The curve in Figure 1.16 consists of four copies of itself down-scaled by a factor 1/3, and hence of 4^k copies down-scaled by a factor of 3^{-k} (where $k = 1, 2, 3, \ldots$). The curve can therefore be covered by 1 ball of diameter L, by 4 balls of diameter $L/3$, by 16 balls of

diameter $L/9$, etc. Thus (Pfeifer *et al.*, 1985):

$$N_{\text{ball}}(3^{-k}L/2) = 4^k \tag{1.41}$$

$$= (3^{-k})^{-\ln 4/\ln 3} \tag{1.42}$$

for $k = 0, 1, \ldots$. Comparison with Eq. (1.42) gives $D = \ln 4/\ln 3 = 1.26$.

This example shows that a system can be decomposed into parts geometrically similar to the whole system, i.e., has *self-similarity*. The synonym *scale invariance* emphasizes the fact that the system looks the same regardless of the magnification used for its observation. The argument that leads to $D = \ln 4/\ln 3 = 1.26186$, for the curve in Figure 1.16, can easily be generated.

It is important to add that fractal dimension can be estimated by a suitable computer digitization procedure. Since there are many different procedures available, we merely point out that this technique will play a very crucial role in future fractal studies (for one-, two-, or three-dimensional systems). There are already reports of the use of the scanning tunneling microscope used for fractal analyses after digitization [at a yardstick on the order of 1 nm (10^{-9} m)].

1.4.2. Rivers: Shapes and Fractal Dimension

As exemplified in Figure 1.17, rivers meander and assume irregular shapes. Why don't rivers run straight? Further, it is of

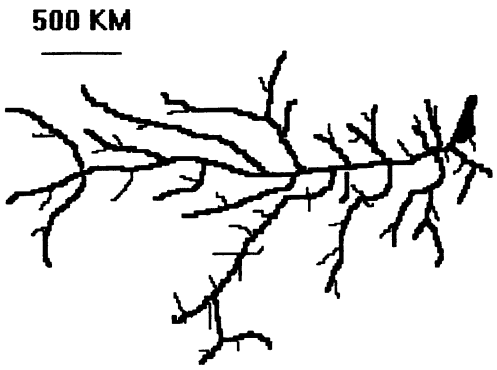

Figure 1.17. The shape (schematic) of the mainstream of the Amazon River.

interest to determine whether there is any self-similarity in such natural phenomena, with a geometrical fractal dimension.

For many decades the shapes of rivers has been the subject of much interest. The great rivers, such as the Danube, Ganges, Yangtze, and Mississippi, meander with curves and loops toward the sea. This vast movement of water along with the contents of suspended particles and dissolved material is an overwhelming natural process. In this fluid flow, as the water hits the banks it creates currents and eddies. As chaotic as the movement of a river may seem, its analysis may provide a coherent result. In turbulent flow, eddies of a range of sizes occur, leading to the suggestion of self-similar phenomena. Furthermore, turbulence results in heat evolution, i.e., the energy of the fluid motion is dissipated because of fluid viscosity. It is also obvious that this dissipation is not homogeneously distributed throughout the volume of the fluid, i.e., some parts are warmer than other regions. Gusts of wind would also contribute to this temperature difference. Thus, one would find secondary currents inside the primary currents. The spiral movement from one bank to the other produces more and more power due to any little perturbation. Since this multitude of perturbations results in the shapes of our rivers, we can imagine that nature creates other patterns with similar combinations of perturbations. In other words, small eddies are the cause of turbulence of a large scale. Despite many years of intensive investigations, turbulence in fluids is still not completely understood. Furthermore, there is no uniformly accepted definition of turbulent flow. This has the advantage that it can reasonably be identified with some convenient feature of a flow description.

From the analyses of the shapes of river tributaries and area (A_{river}), according to Hack's law (Hack, 1957; Takayasu, 1990), the length (L_{river}) and A_{river} are related:

$$L_{\text{river}} \propto 1.89 A_{\text{river}}^{0.6} \tag{1.43}$$

or

$$A_{\text{river}}^{1/2} \propto L_{\text{river}}^{1/2} \tag{1.44}$$

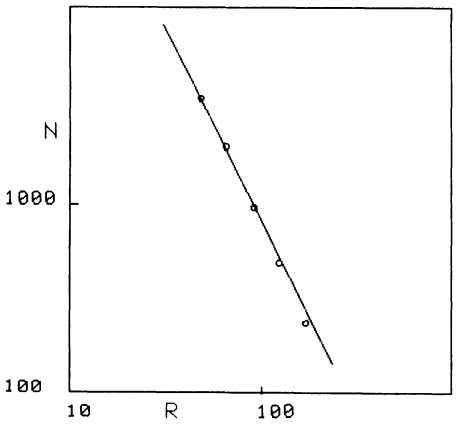

Figure 1.18. Plot of log (number of squares: N) versus length of the yardstick (R = km) for the Amazon (D = 1.85).

where $D = 1.2$. The values of D for various rivers are in the range from 1.1 to 1.9.

The shape of a whole river has been found to be fractal. The Amazon river was analyzed by the box-counting method. A plot of log N versus log $r_{\text{box size}}$ gave $D = 1.85$ (Figure 1.18). By a similar procedure, the value of D for the Nile was found to be 1.4. From these differences it was concluded that the magnitude of D is larger in the areas with higher rainfall (Takayasu, 1990). In other words, if the river branched out and flooded completely, i.e., $D = 2$, high rainfall in that area would be expected.

It has been further suggested that the variation of the water level in the rivers would be accordingly fractal. This gives a practical application of fractal analysis to water level control and other irrigation control projects. Further, these data can provide insight into the rather long-term changes in the environment (i.e., greenhouse effect, pollution effect, solar activity variations). Later, we will show, for example, how solar activity might affect economic variations. It must be stressed that in most systems, where diffusion processes are present, one expects a fractal basis (Unger *et al.*, 1987). This will become clearer as different theoretical developments are explained.

It is clear that concerning various ecological analyses of rivers and climatic changes, fractal analyses will find many useful applica-

tions in the future, e.g., fractal analyses of satellite photos after digitization. Theoretical models have been described that are useful for river shape analyses (Takayasu *et al.*, 1988; Hack, 1990).

1.4.3. Fractal Shapes of Clouds

In some of these examples the fractal dimension is correlated to the turbulence effects (Takayasu, 1990). This is especially seen in clouds and experiments where ink flows into another phase (so-called sumi-nagashi). In clouds the flow is regulated into streamlines of a fluid; the fractal dimension would thus be related to the turbulence and diffusion. The same considerations apply in the case of ink flow. These systems have been described by the so-called Richardson's 4/3 power law (Mandelbrot, 1982; Feder, 1988; Takayasu, 1990). This law postulates that the distance R between two particles floating along some turbulence flux increases with time, as follows:

$$d\langle R^2\rangle/dt \propto R^{4/3} \tag{1.45}$$

The flow of ink in a turbulent system is shown in Figure 1.19. Since ink spreads out isotropically, $\langle R^2\rangle$ is almost equal to the area covered by ink. This shows that the area increases as given by Eq. (1.44). The magnitude of D is thus $4/3 = 1.333$. The magnitude of D for clouds has been found to be ca. 1.35. From this we may conclude that the same kind of physical forces govern cloud formation and ink flow. This is the most important observation in

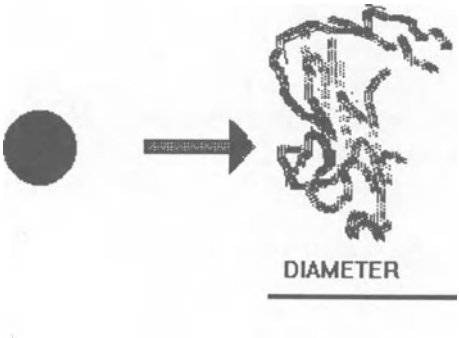

Figure 1.19. Turbulent diffusion pattern (Richardson's power law with $D = 4/3$).

the analysis of fractal geometry, as it shows how very different phenomena are interrelated. The fractals as described here in the case of clouds or smoke patterns are only short-lived. These are typical examples of fractal shapes that appear (are born) and disappear (die). The dynamics of fractals are discussed elsewhere.

1.4.4. Branching of Trees and Fractal Dimension

In various systems found in nature, growth is a very complex process, involving the optimization of many variables. It must be emphasized here that in the natural selection process the time scale is on the order of millions of years. As an example, it is known that the leaves of a growing plant tend to maximize their surface area and minimize the distance from the branches in order to maximize food production and minimize food transportation. The rings in a tree are exactly equivalent to 1 year, and sequoia trees in California have been so dated to be some 2000 years old.

It has been mentioned that the various shapes of different phenomena show a very strong resemblance. The shapes of tree branching are found to resemble very much those of rivers or dendrites, and show a well-defined pattern. The box-counting method applied to the branching of trees has found that $D = 1.3$ to 1.8. This is in contrast to the notion that being a three-dimensional structure the magnitude of D should have been greater than 2. This can be explained as follows. If the magnitude of D_{tree} was greater than 2, there would be more branches, and the lower branches would be in shadow and deprived of sunshine. Thus, the value of D_{tree} is less than 2, and more sunlight reaches the lower branches.

Analysis of fern leaves of different sizes shows some simple mathematical symmetry. The number of leaves of small size is 3, while in the next size it is $2^1 \times 3 = 6$. In a very large fully grown leaf there are now $2^2 \times 3 = 12$ sections. The leaves are growing by some factor 2^D, where $D = 2$.

In earlier observations (Leonardo da Vinci; see Mandelbrot, 1982), it was postulated that all of the branches of a tree when added together are equal in thickness to the trunk. A similar observation is found in biology, such as the branches in the lung or heart (Takayasu, 1990). A relationship between the diameters, d_D,

before and after bifurcation can be given as:

$$d_d^D = d_1^D + d_2^D \tag{1.46}$$

where $D = 2$. Similar considerations apply to other systems where growth and branching are present:

Lung bronchi	$D \approx 3$
Arteries	$D \approx 2.7$
Widths of rivers	$D \approx 2$

Different biological systems are discussed in Chapter 9.

1.4.5. Plants and Insects: Fractal of Size and Shapes

A wide variety of insects live on the leaves of different plants. Although it may not be obvious at first sight, it is reasonable to expect a correlation between the surface size and roughness of the leaves, and the size of insects that live on the leaves (besides other ecological factors). Further, it is known that population density and body weight vary for terrestrial habitats. This is also found to exhibit fractal relations (Marquet *et al.*, 1990).

Large insects must of necessity live on large leaves, and smaller insects on smaller leaves. Further, the surface roughness of leaves would be expected to determine the ecosystems of insects. In fact, analogous considerations have been used in the analyses of the theories given for the disappearance of dinosaurs.

In the case of insects and leaves, consider the following example (Takayasu, 1990). For $D_{\text{leaf}} = 2.5$ and insect size = 0.1 cm, the area used by this insect as compared to one of 1 cm is

$$10^{2.5-2} = 3.16 \text{ times} \tag{1.47}$$

The metabolic rate of insects (empirical) is given by

$$(\text{weight})^{0.75} \tag{1.48}$$

Consumption by a 1-cm insect is

$$1000^{0.75} = 178 \text{ times greater than for a } 0.1\text{-cm insect}$$

From these calculations, one can predict that the number of insects of size 0.1 cm is $3.16 \times 178 = 560$ times greater than the number of 1-cm insects. This has been analyzed in much detail (Takayasu, 1990). The size distribution of plant-supported insects thus is found to be related to power law under these assumptions (Morse, 1985).

Various algorithms have been used to analyze the fractals of plants (Prusinkiewicz and Lindenmayer, 1990). It is hoped that future studies will combine these correlations between insects and plant shapes and forms.

The relation between the population density and body size of different terrestrial habitats has been investigated (Marquet *et al.*, 1990). The data used were from natural rocky intertidal communities in central Chile, of the population density and body size for invertebrates. From log (individuals/m^2) versus log weight, slopes were found to vary from -0.77 to -0.96. Explanations proposed for the scaling power of animal population density with body size have considered the action of ecological and evolutionary processes. It has been proposed that population density scales to body size with a slope of -0.75, which would be the result of interspecific competition acting to keep energy use of all species within similar bounds (in other words, energy use is independent of body size). However, if the slope is -1.0, this would suggest that the total biomass per unit area is independent of body size (i.e., all kinds of species attain the same biomass), and that this pattern is the result of numerical and facultative responses of predators. It was concluded that the population density scaling is difficult to explain at this stage.

1.4.6. Coastlines: Fractal Dimension

Observing the jagged coastlines with self-similar shapes, one is led to wonder whether the shapes were carved out by some natural forces, and by some self-similarity that could be analyzed by fractal means (or random fractal shapes).

The shapes look very irregular and chaotic. However, besides other factors, one that is responsible for these coastlines is the pounding of the waves and the erosion by winds. The waves, although at first appearing irregular, do seem to suggest some pattern. In fact, surfers are known to regard each seventh wave as being the largest. This suggests that the coastlines have some fractal geometry, as indeed analyzed by various investigators.

The length of a coastline or boundaries between countries have been analyzed by many investigators (Richardson, 1961; Mandelbrot, 1982). For instance, as shown in Table 1.1, boundary lengths are variable.

In geography books, one finds that the coast of a particular country can be some 2000 miles long. But the question raised here is whether the yardstick used to measure the coastline has an effect on the measured distance. That is, the distance between two points must include harbors, bays, and ports as added length. This would become more evident as the resolution, ϵ, is varied from 100 km to 20 km or <1 m.

These data suggest that in the various measuring methods used, the dimension of the yardstick differed by a factor of ca. 2 (since $\log 2 = 0.3$, which corresponds to the 20% difference). The length measured would thus depend on the magnitude of the yardstick used. The length, if just set equal to a straight line, would be smaller than the actual length, if measured by walking along the coast (Figure 1.20).

If the length of each step is decreased (i.e., comparing the steps taken by a man and by a child), then the length traversed

Table 1.1. Lengths of Boundaries between Different Countries[a]

	Length (km)		
Countries	A[b]	B[b]	Ratio
Spain–Portugal	987	1214	1.23
Netherlands–Belgium	380	449	1.2

[a]Source: Richardson (1961).
[b]Data for A and B are from different atlases.

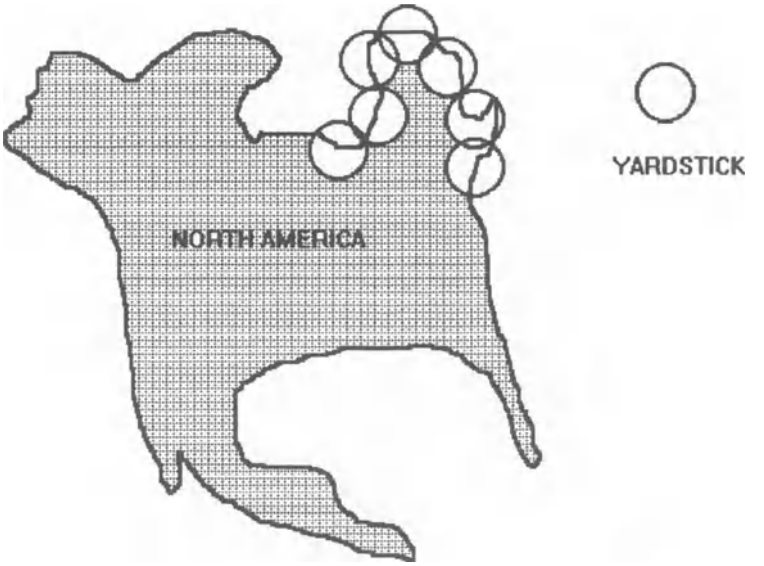

Figure 1.20. Estimation of the length of a coastline by the line segment method (yardstick = diameter of the circles).

would be even larger. In other words, the length, L_ϵ, would depend on the magnitude of each step, ϵ i.e.,

$$\text{length} = (\text{number of steps } N_\epsilon)\ (\text{magnitude of each step } \epsilon)$$

$$L_\epsilon = N_\epsilon \epsilon \tag{1.49}$$

This leads to the relation (Feder, 1988):

$$L_\epsilon = A\epsilon^{1-D} \tag{1.50}$$

where $A = L_N$ when ϵ is very small, and the exponent $D = 1$ in the case of a straight line or circle (see Figure 1.14). However, in the case of a coastline or boundary, we find that L_ϵ keeps increasing as the magnitude of ϵ is made smaller. This is due to the fact that as ϵ is decreased, one measures more detailed coastline, i.e., smaller bays or eroded coasts. There is in fact no limit on the increase in L_ϵ as ϵ decreases further. The magnitude of the

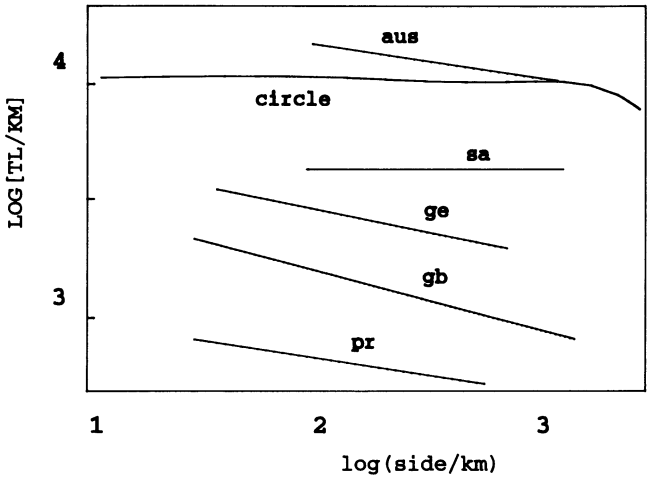

Figure 1.21. Estimation of D for coastlines of different countries. gb, Great Britain; pr, Portugal; aus, Australia; sa, Spain; ge, Germany; circle, $D = 1$, for small yardstick (for comparison). Redrawn with modifications from Mandelbrot (1982).

coastline length as measured would become infinity as $\epsilon \to \infty$, because the value of $D > 1$.

From the relation in Eq. (1.49) we find that a plot of $\log L_\epsilon$ versus $\log \epsilon$ gives the slope $(=1 - D)$, where D is the fractal dimension (Figure 1.21).

In a recent study, extensive tests were carried out on the fractal analyses of Random Island (situated near Newfoundland) from the digitized data of the contours of lake shores (Goodchild, 1982). The data were taken from a 1:50,000 scale topographic map and digitized to an accuracy of 0.01 inch. In the case of the shoreline, the data fit very well with the log–log fractal model. On the other hand, the log–log plots of lakes were sigmoid in shape, with D varying from 1.3 to 1.8. Thus, D is dependent on the yardstick used. Furthermore, the area/perimeter relationships showed that the contour envelopes and lake outlines were different for length/step size data. Similar investigations have been reported by other investigators (Mark and Aronson, 1984; Culling and Datko, 1987). The roughness of the San Andreas fault zone in

California has been analyzed (Aviles *et al.*, 1987; Power *et al.*, 1987).

Another argument can be given to support the finding that the magnitude of D for coastlines is very similar in different parts of the world. This may indicate that some movement in the oceans could be responsible for the erosion of the coast. This is supported by the observation that eight times within the past million years, something in the earth's climatic equation has changed. This has caused snow to remain in mountains where previously it had melted away. Furthermore, over the past 30 years, evidence has mounted that the glacial cycles are ultimately driven by astronomical factors: slow, cyclic changes in the eccentricity of the earth's orbit and in the tilt and orientation of its spin axis. Many scientists have proposed that the seasonal changes act directly on the ice sheets of the Northern Hemisphere (Broecker and Denton, 1990). A reduction in summer sunshine allows ice to build up, and an increase melts it away. The ice in turn alters the earth's climate. These cycles would affect evaporation and rainfall, and as well the ocean circulation. Thus, the overall effect could be that the fractal of coastlines would be more or less the same, as is observed.

1.5. Basic Mathematics of Chaos

In recent years, the word chaos has been mentioned in many contexts (Fisher and Smith, 1982; Kolb *et al.*, 1985; Holden, 1987; Pynn and Riste, 1987; Gleick, 1988; Avnir, 1989; Hecht, 1990). Before going into detail, some simple systems will be described as an introduction to basic ideas. For instance, the movement of a dust particle in a room was found to be erratic, due to collisions between gas molecules and the particle. However, the pressure exerted by a gas in a container can be described by a simple relation. The pressure (P) exerted by gas molecules arises from their collisions with the walls of the container with volume V at temperature T [273° + C = K (Kelvin)] (Figure 1.22). The gas law was derived from this theory (Berry *et al.*, 1980) (1 mole of gas):

$$PV = RT \tag{1.51}$$

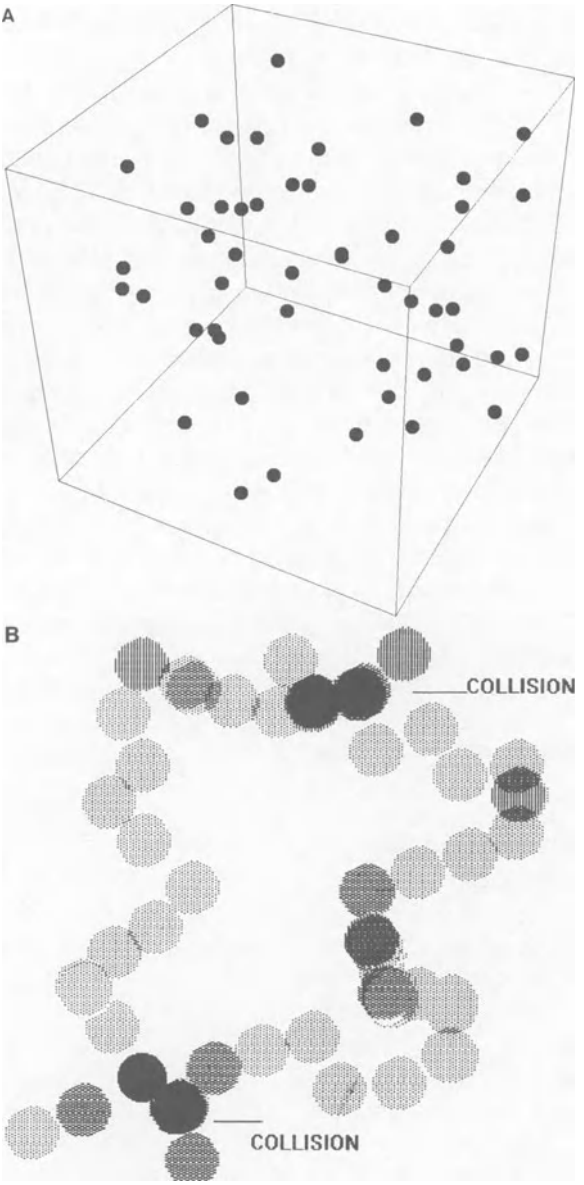

Figure 1.22. Movement of gas molecules. (A) Gas molecules and the walls of the container; (B) collisions between gas molecules and chaotic (random walk) movement.

where R is the gas constant [$=8.31441\,\text{J/(mole K)} = k(1.38 \times 10^{-23}\,\text{J/K})N_A(6.03 \times 10^{23}\,\text{mole}^{-1})$]. This equation can also be derived from the consideration that the total internal energy, U, of the gas is proportional to the pressure as: $P = (2/3)(U/\text{volume})$. Further, the energy per mole of gas is the average kinetic energy per molecule times the number of molecules: $(3/2)N_A kT = RT$. Combining these relations gives the expression in Eq. (1.51). It is supposed that a gas consists of a large number of very small molecules, moving about in all directions. Taking air as an example, there are 6×10^{23} molecules in 28 grams of air. Air weighs roughly 0.001 gram per liter. In 1 liter of air we thus have $10^{-3} \times 6 \times 10^{23}/28 = 2 \times 10^{19}$ molecules. In the case of an ideal gas, the kinetic theory postulates that the molecules are so small that their actual volume is negligible in comparison with the total volume of the gas, and that they exert no attraction upon each other. As a result of their continual movement in all directions, the molecules will frequently collide with each other and with the walls of the containing vessel, and it is the latter elastic impacts that, according to the kinetic theory, are responsible for the pressure exerted by the gas. Thus, the chaotic collisions of these tiny molecules give rise to the pressure (which is both easily measured and analyzed). The movements of the gas molecules are chaotic, but nonetheless one can derive the most fundamental equation in physics from this phenomenon (i.e., volume multiplied by the pressure exerted by the chaotic collisions of the molecules with the walls of the container = constant]. This is further related to the Brownian motion (see later).

Molecules in dense systems are known to move with a random, zigzag motion. This is easily observed in the motion of a macroscopic particle, such as a smoke particle in air or a colloidal particle in a liquid. Photographs of its motion reveal a chaotic trajectory. This motion has been analyzed by the theory of Brownian motion. It is known from kinetic theory that the molecule moves as it collides with other molecules. However, if the movement of the molecule repeats itself over a given length of time, this may create a starting pattern for larger time-scale patterns, just as a very small ripple in water looks the same as a very large vortex.

In another case, the heartbeat sometimes changes dramatically

from minute to minute and from hour to hour (Goldberger *et al.*, 1990). The interval between heartbeats is known to vary chaotically. Physiologists and physicians have attempted to quantify such chaotic phenomena through fractal procedures. These mathematical analyses can provide much useful insight into the disease treatment.

The word *chaos* has at least two levels of meaning. In the case of gas molecules, their movement is chaotic. However, the pressure exerted by these molecules when hitting the container walls is exactly described by the rather simple Eq. (1.51). Furthermore, a gas molecule moves a certain well-defined average distance (on the order of 1 nm) in space before it encounters another molecule or the wall. This average distance is called the mean free path, λ (Berry *et al.*, 1980). If one observes this movement under varying magnification in relation to the magnitude of λ, then the picture will be different for different magnifications. Interestingly enough, one finds systems in everyday life where these patterns exhibit self-similarity, i.e., the movements of molecules repeat their pattern at varying scales of magnification used for observation. The magnitudes of the mean free path, λ, also suggests that molecules move with very similar repetition.

Furthermore, chaos is actually all around us. From the swirling patterns of a hurricane on a radarscope to the eddies and swirls of a mountain stream, from the ups and downs of the stock market to the uncontrollable patterns formed by smoke as it rises, all of these phenomena seem totally unpredictable and out of control.

According to Ramsey's theory, complete disorder in nature is an impossibility. In the short time scale of man, the spatial arrangement of stars and galaxies seems to change very little. This supports the conjecture of Ramsey. This postulate, of course, has many direct relations to this monograph. The degree of order (including self-similarity) or disorder (chaos) in nature is the subject matter of this monograph. It was Henri Poincaré (1890) who proved that the motion of three bodies is very complicated when movement takes place under the influence of gravitational forces (Thompson and Stewart, 1988).

In the same way, the ecology of life around us is very complex and varying. The ecological chaos was therefore a subject of

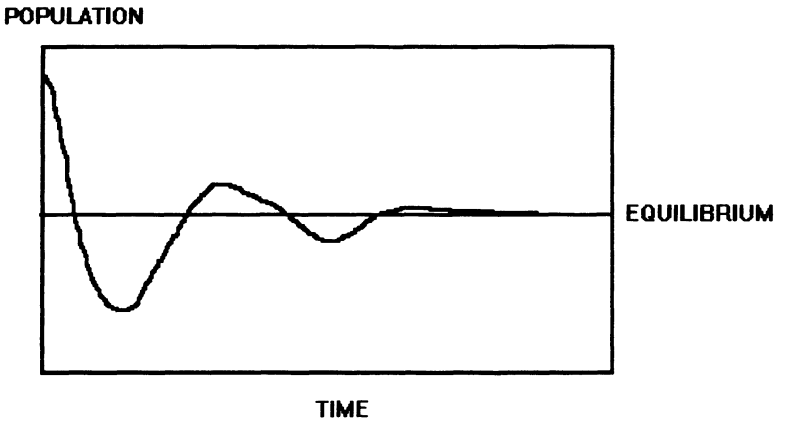

Figure 1.23. The rising and decreasing population approaching an equilibrium state (schematic).

interest to be analyzed by mathematical procedures. Of ecological phenomena, population growth is of the most interest. The growth is sometimes not easily visualized, since it may be rising steeply in the case of a small population and slowly in the case of a large population (for example, due to lack of food). Further, in most cases, this rise and fall brings the population close to some equilibrium (Figure 1.23).

Chaos is fascinating because of its interplay of mathematics, science, and technology. It is not clear what role chaos plays in real chemical processes, in living systems. On the other hand, a system may look chaotic or simple, depending on the scale of observation. Therefore, the term *chaos* is not sufficient for a large number of systems. It also requires some definition about the dimensional criteria of time and space. Since one finds self-similar characteristics in such phenomena, it is obvious that fractal dimension will be expected in some chaotic processes.

Chaos can be defined as some situation in which a dynamical variable x_t (at time t) is extremely sensitive to the initial precise value x_0 (at time $t = 0$). In some cases after a very short time only a statistical analysis is possible for the value of x_t, even when the nonlinear dynamical process is completely deterministic.

This kind of occurrence is called deterministic chaos, since it is not influenced by any external effects.

In order to describe this, the procedure of iteration has served as an example (Thompson and Stewart, 1988; Devaney, 1990). In mathematics, iteration can be used to estimate the value of x that would satisfy two equations at some value(s) of x, e.g., $y = x$ and $y = \text{function}(x)$. Iteration involves repeating a calculation process over and over again, using the result of the previous computation as the input for the next. In other words, one iterates by selecting an initial value as seed or input and then computing the value of a function. For example, to iterate the square root function, all we need to do is select an initial x value and calculate $\sqrt{x}$ several times. Let us proceed by selecting the value of $x = 256$:

$$
\begin{aligned}
y = \sqrt{x}, \qquad x_0 &= 256 \\
\sqrt{x} = \sqrt{256} &= 16 \\
\sqrt{16} &= 4 \\
\sqrt{4} &= 2 \\
\sqrt{2} &= 1.414214\ldots \\
\sqrt{1.414214\ldots} &= 1.189207\ldots \\
\sqrt{1.189207\ldots} &= 1.090508\ldots \\
&\vdots \\
&= 1
\end{aligned}
\tag{1.52}
$$

Continuing in this fashion, we see that repeated application of the function square root eventually yields the number 1, which then remains unchanged or fixed under subsequent iterations (Devaney, 1990). Moreover, if one selects the initial x value to be 0.6, it also leads to a value 1 after several iterations. This shows that regardless of the starting value, the function tends to the same

point in space (i.e., 1). This iteration procedure is depicted in Figure 1.24A. The crossing point, i.e., where $y = \sqrt{x}$ and $y = x$ have the same value, is the attractor (in the present context). This is an example where the iteration converges to a point. As a rule a strange attractor has a fractal dimension. For those who wish to pursue this further, a good survey can be found in the literature (Farmer *et al.*, 1983).

Let us consider another function, such as x^2, that leads to a different result. Here we find that on iteration the values tend to infinity (Figure 1.24B). This is an example where the iteration

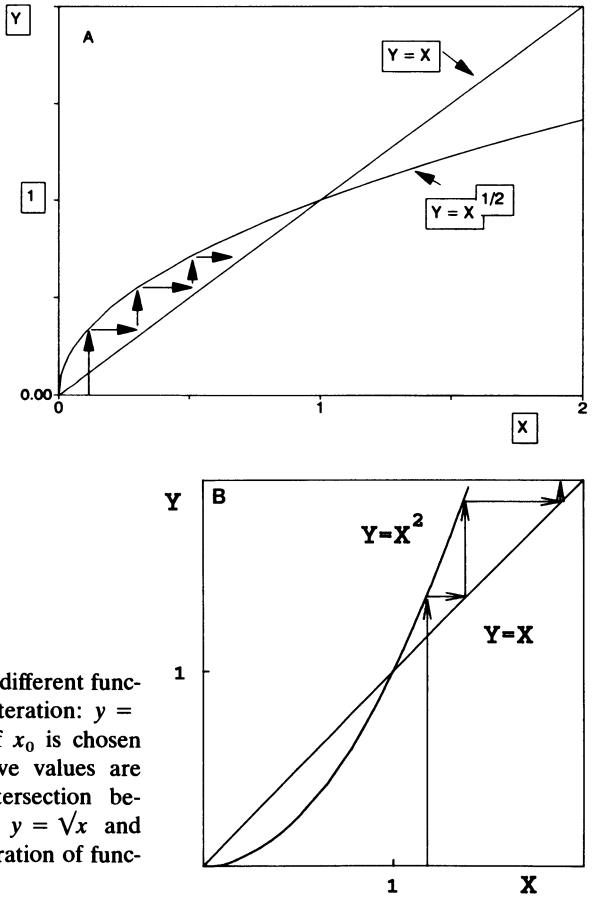

Figure 1.24. Iteration of different functions. (A) Convergent iteration: $y = \sqrt{x}$. The initial value of x_0 is chosen arbitrarily, and successive values are estimated from the intersection between the lines where $y = \sqrt{x}$ and $y = x$. (B) Divergent iteration of function $y = x^2$.

diverges and there is no attractor point. An iteration of $\sin x$ is found to tend to 0 but very slowly (the reader can confirm this by using any simple calculator or a computer). The reader can study other functions by this approach.

If we now look at the numbers, we find that it is these numbers that tend to 1 or infinity. As shown below, analogous numbers generated by simple mathematical equations can in fact produce a remarkable variety of data plots. Under certain conditions, these data can even exhibit chaotic phenomena as found in ecological cycles. In everyday life one has to find roots of an equation, i.e., where a certain value of x satisfies the relation that a function of x, $f_x = 0$. In the year 1225, Leonardo of Pisa investigated a function, $f_x = x^3 + 2x^2 + 10x - 20$ $(=0)$, and found that when $x = 1.368808107$, it satisfies the relation $f_x = 0$. If we rewrite the function (analogous to the above examples), such that some $x_n = 20/(x_{n-1}^2 + 2x_{n-1} + 10)$, then we discover whether as n increases (starting with $n = 1$, and guessing $x_1 = 1$) the value of f_x converges (or diverges). The value converges as given in Table 1.2. The rate of convergence is slow, but on a computer it would not be noticed.

Especially for a biologist or ecologist studying the growth or decline of the populations of different species of birds or fish or

Table 1.2. Iteration of a Function $f_x = x^3 + 2x^2 + 10x - 20$, for Various Values of n

n	x_n	n	x_n
1	1.538461538	13	1.368817874
2	1.295019157	14	1.368803773
3	1.401825309	15	1.368810031
4	1.354209390	16	1.368807254
5	1.375298092	17	1.368808486
6	1.365929788	18	1.368807940
7	1.370086003	19	1.368808181
8	1.368241023	20	1.368808075
9	1.369059812	21	1.368808122
10	1.368696397	22	1.368808101
11	1.368857688	23	1.368808110
12	1.368786102	24	1.368808107

animals or chemicals in rivers, an important goal is the selection of useful mathematical models that will give predictions on the population in the future. Or one might look backwards and try to understand (through appropriate models) the evolutionary processes. In these situations, it is obvious that some numbers tend to oscillate (as in a pendulum) or they tend to the same level of population size (or some other criterion). Here it will suffice to give an introduction using some simple examples. For those interested in more advanced mathematical models, suitable references are given.

Until the present decade, the study of nonlinear chemical reactions (i.e., reactions in which concentrations do not change regularly with time), multistability, traveling waves, and pattern formation, was generally the study of a single reaction.

In biology, where fluctuations in population of a single species are present, one finds that certain types of mathematical relations are very useful. Some of these might exhibit attracting or repelling periodic plots. They can be described by the plots obtained when iteration is carried out between two rather simple equations:

Constant reproduction rate (e.g., of children):

$$F_x = \mu x \tag{1.53}$$

Declining reproduction rate with increasing population [or a pollution effect in a macroeconomic model (Stutzer, 1980)]:

$$F_x = \mu x(1 - x) \tag{1.54}$$

The most interesting property of the relation in Eq. (1.54) arises from the fact that the magnitude of μ can give rise to a multitude of unstable phenomena as observed in nature, e.g., motion is periodic, ergodic (or mixing or chaotic). This simple mathematical equation can give rise to plots that are useful for describing phenomena, e.g., from simple chemical reactions to complicated ecological phenomena.

Let us examine the effect of different values of μ (Thompson and Stewart, 1988) in Eq. (1.54):

$$\text{for } \mu \leq 3 \tag{1.55}$$

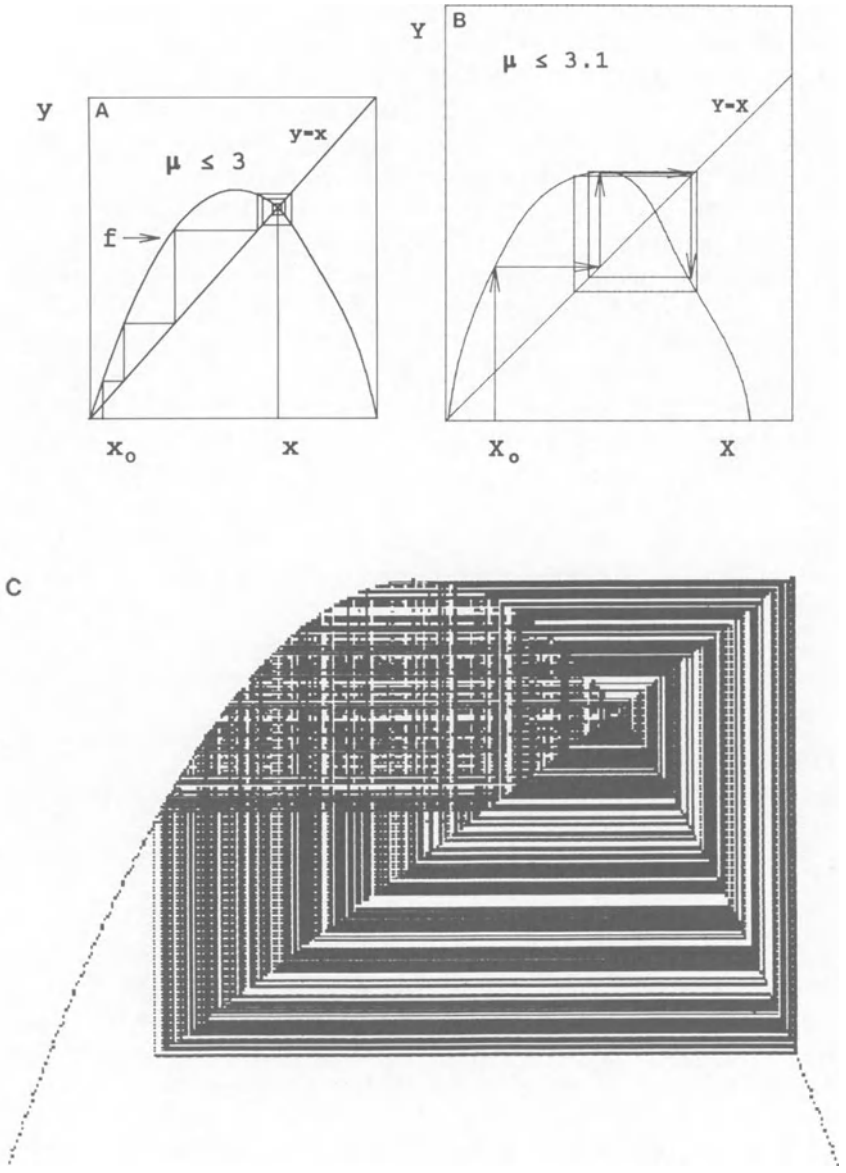

Figure 1.25. The effect of magnitude of μ in Eq. (1.54) on the iteration pattern. (A) $\mu \leq 3$; (B) $\mu < 3.1$ (period doubling); (C) $\mu > 3$ (chaos).

All initial population sizes evolve toward a unique stable equilibrium, which is the same as the point of bisectrix (Figure 1.25A):

$$\text{for } \mu \leq 3.1 \tag{1.56}$$

When the slope of $F_x = -1$, the equilibrium bifurcates by period doubling; this period 2 attracting limit cycle is shown in Figure 1.25B.

$$\text{for } \mu > 3 \tag{1.57}$$

The size and area of the limit cycle increase continuously when $\mu > 3$, with additional period doubling as μ increases (Figure 1.25C).

The period doubling is depicted in Figure 1.26. This is where the population does not settle down to a single number, but begins to oscillate (analogous to a pendulum) between two different levels yearly.

The example of period doubling is very important. It means

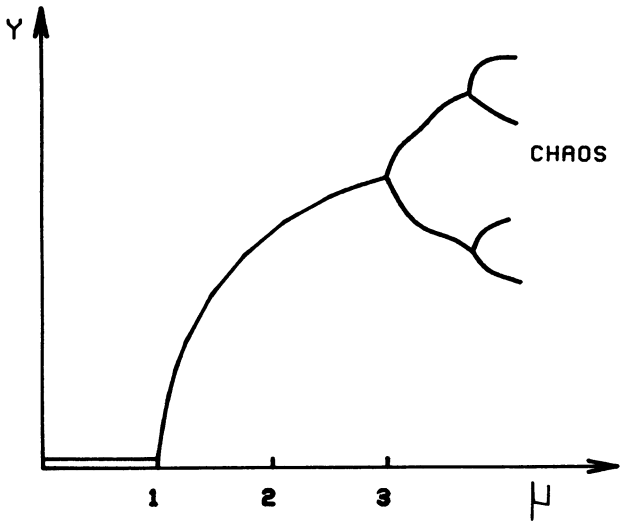

Figure 1.26. The state of period doubling leading to chaos.

that all systems starting with a large value settle down at a different cycle than those that start with a lower value. The 4-year cycle would be observed at larger μ values. The population is known to exhibit bifurcations as μ increases. Thus, even with such a simple mathematical plot, one can generate rather complicated systems. The period doubling may be put more qualitatively, as a plot where the period 1 > period 2 > period 4 > period 8 > period 16 > period 32 > period 64 > . . .

Thus, systems that look chaotic might just as well be partly periodic and partly steady, depending on the value of μ. In other words, mathematics need not be confronted with a hopeless case if one encounters chaotic data.

The logistic equation (1.54) exhibits chaos at infinitely many values of $\mu > 3$, while there is a dense set of values above 3 at which the system is periodic (i.e., nonchaotic).

Fractal objects are quite common in the theory of chaos in general and of turbulence in particular (Fisher and Smith, 1982). The interfacial instabilities described elsewhere are examples of colloidal turbulence and chaotic phenomena. Further, it has been suggested that chaotic attractor must have a fractal dimension (Thompson and Stewart, 1988). An important application of the theory of nonlinear dynamics is the analysis of erratic experimental data (or the variation of the line voltage) (Mayer-Kress, 1987). In this study a series of examples are discussed that should be fulfilled for serious dimension calculations, and applications of these methods to data from periodic signals are described. The effect of size of data set on the observed values of the dimension and the minimal number of data points required for a given sampling frequency are also delineated.

Various biological populations have been found to fit the following equations, which are mathematically equivalent to Eq. (1.54):

$$f_{\lambda,x} = \lambda \sin(\pi x) \tag{1.58}$$

or

$$f_{\lambda,x} = x \exp[\lambda(1 - x)] \tag{1.59}$$

$$= x[1 + \lambda(1 - x)] \tag{1.60}$$

or

$$= \lambda x/(1 + ax)^5 \tag{1.61}$$

By using these equations, we can describe phenomena with the following characteristics:

Steady state . . . Period doubling

.

.

.

Chaotic region

The relation between dynamic state and the magnitude of μ can be seen in Figure 1.27. These examples show that rather complicated fluctuations can be conveniently described by some simple mathematical analytical procedures. The reader may proceed on his or her own to further investigate the different features suggested from Eq. (1.54) and the value of μ.

The long-term unpredictability associated with chaos has been suggested to be undesirable in certain systems (Peng *et al.*, 1991). These analyses suggested that controlled chaos could be of importance in the self-regulation of living systems. This may be so

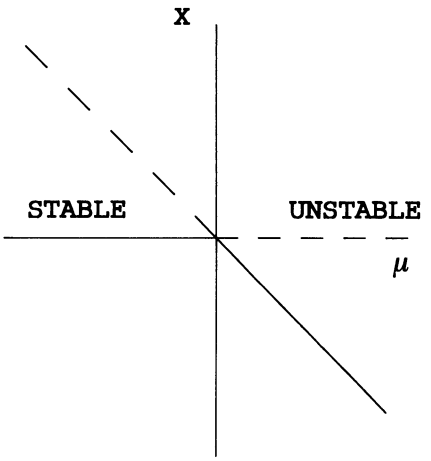

Figure 1.27. Schematic plot of relation between stability and the magnitude of μ (see Eq. (1.54)).

because of the fact that behavior is selected by some subtle feedback mechanisms. Three-dimensional phase portraits were developed by this model.

In a different context, there has been much interest in the mathematics of iteration of different kinds of planes, i.e., complex planes. The iterations used in these have been basically the theory described by Julia (1918) and Fatou (1919). These theories have recently been further advanced (Mandelbrot, 1980), which has given rise to a whole set of beautiful shapes and forms. A simple computer program describing the Julia set of a complex function has been given in a recent study (Devaney, 1990). The reader should consult these references in order to be able to pursue this fascinating area (Mandelbrot, 1980; Peitgen and Richter, 1986; Blanchard, 1984; Devaney, 1986; Saupe, 1987; Falconer, 1990).

1.5.1. Noise: Fractal Dimension

One way to introduce the term *noise* is as follows. If we measure the main voltage versus time, we find that the signal varies with a feature that looks like noise (Figure 1.28). This is one of the

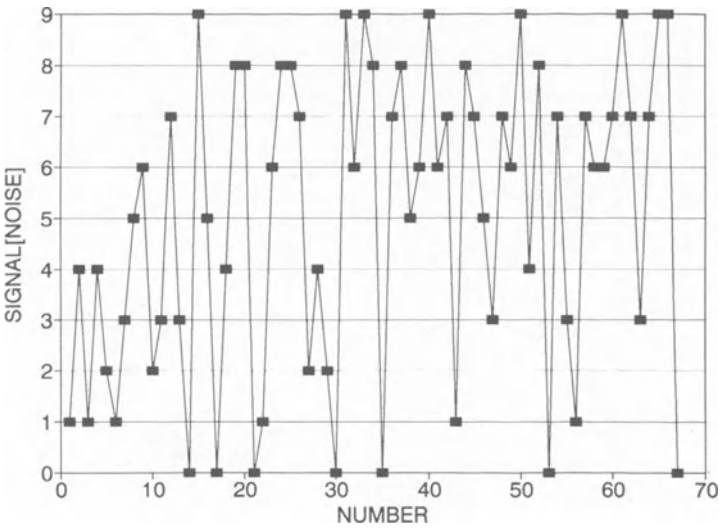

Figure 1.28. Typical plot of a signal considered as noise.

most common examples where noise is a daily experience, but at the same time without any effects, in general (D'Amico and Mazzetti, 1986; Holden, 1987). In a particular example, the noise signal as measured from the voltage of a turbulent jet was analyzed by the box-counting method (Barnsley, 1988). The magnitude of D was ca. 1.5. This observation is also a very good example that the Euclidean geometrical laws of the past 2000 years would not help in its analyses. We will show later that there are other signals, such as heartbeat, that can be analyzed by the same procedure as the noise. The same analyses can be applied for noise as for making measurements in the laboratory (e.g., pH, spectroscopy, conductivity).

Any such data, so-called noise, can be represented by sequences of numbers that can be used as signals. A typical example is to analyze the successive digits [100 digits are given, but more are available (up to 1 million through the use of supercomputers)] in the decimal representation of π:

$$\pi = 3.14159265358979323846264338327950288419716939937510$$
$$582097494459230781640628620899862803482534211706 8\ldots \tag{1.62}$$

The most famous of all numbers, π, and can be seen from the above, is a nonrepeating decimal and can thus be specified only approximately. It was in the 3rd century B.C. that Archimedes rounded off π to the fraction 22/7 (=3.142857...), and that was accurate enough for practical purposes, so much so that various mechanical machines have since been built to this day with this approximation. However, as early as 1596 the value of π was known to more than 20 decimal places.

Archimedes's method of estimating the value of π resembles somewhat the procedure discussed above for the estimation of the fractal length of coastlines. In the case of a circle, Archimedes inscribed a polygon with as many sides as possible. The magnitude of the perimeter is calculated from this polygon. As the number of sides of the polygon increases, the more closely it resembles the circle, and thus more accurately estimates π. From a hexagon one

gets π as 3. In order to get a value of 3.14, one needs a polygon of 96 sides! In order to get 20 decimal places, a polygon of 32,212,254,720 sides has to be used! The reason for this mathematical trial has many purposes. The most important of these concerns how closely π's digits resemble a random number sequence. One way mathematicians have defined a random string of digits is by a computer test: a truly random number is one that cannot be generated by a computer program shorter than the number itself. But another, less exclusive club to which π may also belong is as follows. According to mathematicians, a number is "normal" if any sequence of digits has an equal probability of appearing within it. In other words, each of the digits from 0 to 9 appears 10% of the time; each of the two-digit sequences 00 to 99 appears 1% of the time; each of the three-digit sequences appears 0.1% of the time, and so on. This concept of "normal" is close enough to "randomness" that in a loose talk mathematicians sometimes say "random" when actually they mean "normal." A plot of the first 100 digits of π are given in Figure 1.29. The plot looks like any noise signal one might measure. It is found that in almost all decimals the various digits repeat with uniform frequency.

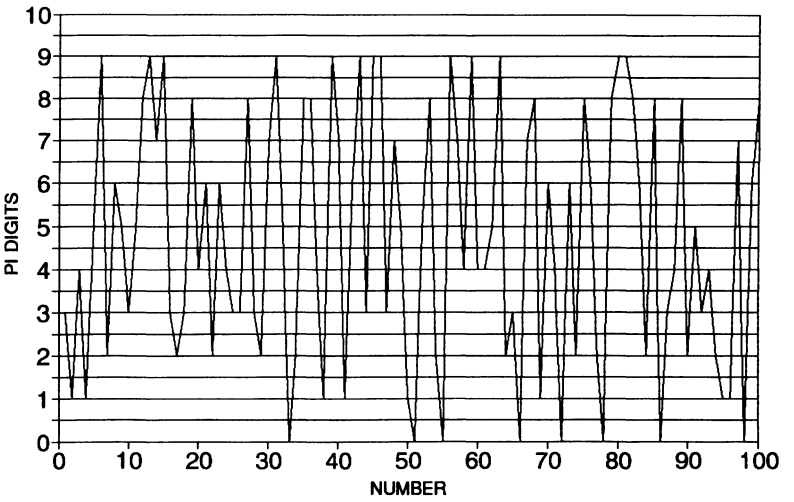

Figure 1.29. Plot of the first 100 digits in π (Shanks and Wrench, 1962).

In order to analyze the frequency of digits, let us denote the first digit as $y_1 = 3$, the second digit as $y_2 = 1$, the third digit as $y_3 = 4$, and so on. The sequence can be denoted as $\{y_t\}$ (100 digits):

$$\begin{aligned}\{y_t\} = \{&3\,1\,4\,1\,5\,9\,2\,6\,5\,3\,5\,8\,9\,7\,9\,3\,2\,3\,8\,4\,6\,2\,6\,4\,3\,3\,8\,2\,7\,9\,5\\ &0\,2\,8\,8\,4\,1\,9\,7\,1\,6\,9\,3\,9\,9\,3\,7\,5\,1\,0\,5\,8\,2\,0\,9\,7\,4\,9\,4\,4\,5\,9\\ &2\,3\,0\,7\,8\,1\,6\,4\,0\,6\,2\,8\,6\,2\,0\,8\,9\,9\,8\,6\,2\,8\,0\,3\,4\,8\,2\,5\,3\,4\,2\\ &1\,1\,7\,0\,6\,8\ldots\}\end{aligned} \tag{1.63}$$

The quantity of t may be associated with time, and the sequence of digits is represented per unit time interval. The mean of N digits can be given as:

$$\begin{aligned} m &= (y_1 + y_2 + y_3 + y_4 + \cdots + y_N)/N \\ &= 1/N \sum_{t=1}^{N} y_t \end{aligned} \tag{1.64}$$

The magnitude of m (for $N = 32$) $= 4.84$. If it is assumed that these digits are drawn from a uniform supply, then the mean m would approach a limit $\mu = 4.5$ as $N \rightarrow$ infinity.

Another procedure that could be used in calculating μ is to count the number of nines and multiply it by 9, multiply the number of eights by 8, and so on, and divide by N. Let a_y be the number of times the value y occurs (given in Table 1.3). From this we get:

$$m = (a_1 + 2a_2 + \cdots + 8a_8 + 9a_9)/N \tag{1.65}$$

$$= 1/N \sum_{y=0}^{9} y a_y \tag{1.66}$$

Table 1.3. Magnitudes of y, a_y, and a_y/N for Values of y from 0 to 9 ($N = 100$)

y	0	1	2	3	4	5	6	7	8	9
a_y	0	2	4	7	3	4	3	2	3	4
a_y/N	0.08	0.08	0.12	0.12	0.10	0.08	0.09	0.07	0.13	0.13

Thus, we obtain:

$$\mu = \lim_{N \to \text{infinity}} m \tag{1.67}$$

$$= \lim_{N \to \text{infinity}} 1/N \sum_{y=0} y a_y \tag{1.68}$$

$$= \lim_{N \to \text{infinity}} \sum_{y=0} y(a_y/N) \tag{1.69}$$

The magnitudes of y, a_y, and a_y/N are given in Table 1.3. The quantity a_y/N represents the fractional number of times the value of digit y occurs, and it is safe to assume that its limit for all values of y from 0 to 9 is 0.1. Thus, the probability, p_y, that a value y will occur can be given as:

$$p_y = \lim_{N \to \text{infinity}} a_y/N \tag{1.70}$$

Since $\sum a_y = N$, it is obvious that the term p_y exhibits the property that $\sum p_y = 1$, as required by any probability distribution.

The data termed noise can be analyzed by various procedures. One of these is the box-counting method (Feder, 1988). The term *noise* is thus found to cover a wide variety of systems and numbers. The chaotic pattern can be tamed and understood by these tools. The application of computer data treatment simplifies even further any such analyses that examine a large set of data. The phenomenon of noise was considered a nuisance a few decades ago. However, through these analyses it has been found that noise is actually an important source of information about the system. As described below, the Cantor set can also be applied in the analysis of noise.

1.5.2. Cantor Set (and Dust) and Devil's Staircase

It would be useful if one could draw shapes with some exact fractal dimension through simple procedures. In other words, if one has data of some observation, it would be useful to follow a

procedure such that one could draw a fractal shape. Another useful concept (Hausdorff dimension) was derived as a subset of a dimension D. This is the so-called Cantor set (with $0 < D < 1$), as shown in Figure 1.30 (Mandelbrot, 1982; Avnir, 1989; Takayasu, 1990). This is also one of the most important examples where the theory of fractal dimension is found to be very useful. In order to appreciate self-similarity as a symmetry property, we have to identify transformations that leave the system invariant. The calculation of any two such transformations will again leave the system invariant. It will be shown later how the Cantor set actually describes a wide variety of phenomena.

We find that in many ways the Cantor set is indeed the simplest of all fractals. The Cantor set as given in Figure 1.30 is constructed as follows. A line of unit length is divided into three equal segments, and the middle segment is removed. The same procedure (i.e., the generator) is carried out for the remaining two segments, and so on ad infinitum. This is called the Cantor set (1883), which proves that any two line segments regardless of their length contain an equal number of points and that a line segment has as many points as a two-dimensional surface or a three-dimensional volume.

The Cantor set (devil's stair; Figure 1.30B) can be easily constructed by using any computer program. The formula needed is defined as a macro, and can produce any kind of curve (see Appendix A).

It is seen that when s (step of the process) $= 0$, $\epsilon = 1$, which covers the unit line. When $\epsilon = 1/3$ ($s = 1$) and $N = 2$, cubes of side ϵ are needed to cover the set. At $\epsilon = 1/9$ and $N = 4$, cubes of side ϵ are needed. Thus, the general equation is:

$$\epsilon = (1/3)^s \tag{1.71}$$

$$N = 2^s \tag{1.72}$$

The limit as $s \rightarrow \infty$ in the process will give $\epsilon \rightarrow 0$, and one then reaches the end point of this Cantor set. This gives an infinite set of points very nonuniformly distributed with a Euclidean length of zero and a topological dimension of zero since no cuts can be made

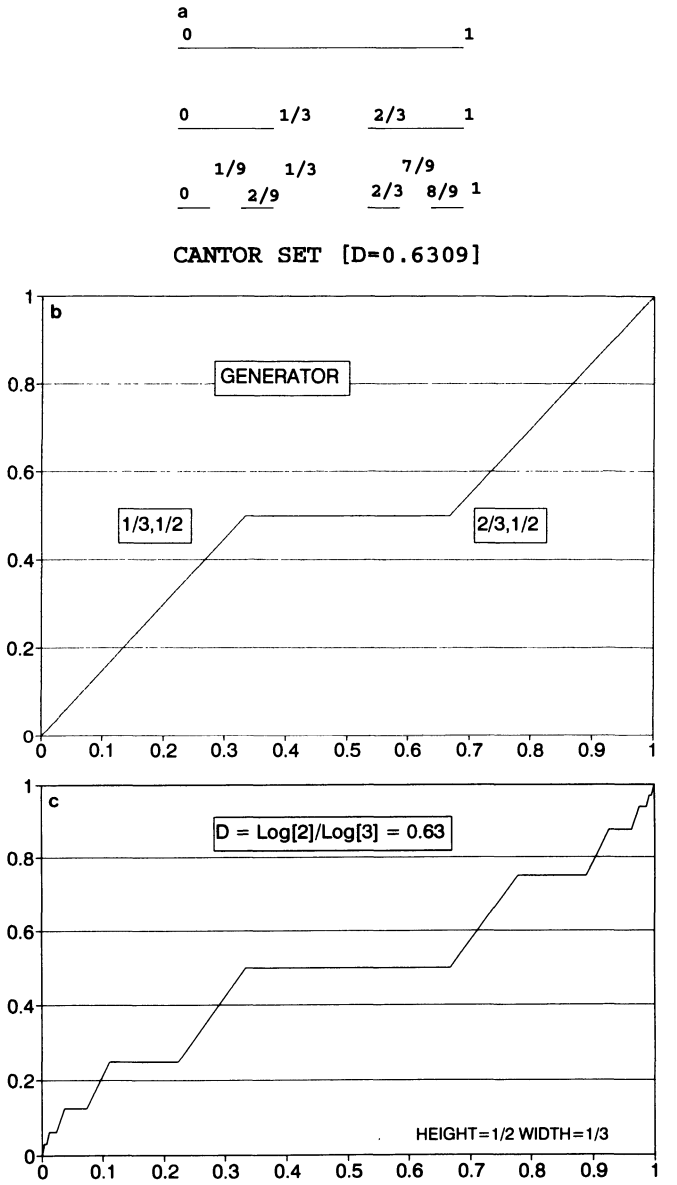

Figure 1.30. Cantor set. (A) The generator consists of two straight-line segments as subintervals of length 1/3 (top). The zeroth and first two steps in the construction of the Cantor set of fractal dimension $D = \log 2/\log 3 = 0.6309$. The process where every segment of the previous stage is trisected can be repeated ad infinitum. (B) Generator for the Cantor set curve. (C) Cantor dust, devil's stair.

in a set of points. The Hausdorff dimension, D, is given as:

$$D = \lim_{\lim \epsilon \to 0 (\text{as } s \to 0)} \ln (2^s)/\ln (3^s)$$
$$= \ln 2/\ln 3 = 0.6309 \tag{1.73}$$

This has been called a dust for $0 < D < 1$ regime. Notice the self-similarity or scaling nature of the final result. The full Cantor set between 0 and 1 looks the same as the part between 0 and 1/3 if this is magnified by a factor 3 or as the part between 0 and 1/9 if this is magnified by a factor 9, and so on.

It is found that after the 10th stage, there are 1024 intervals with length:

$$1/3^{10} = 1/59{,}049 = 0.0000169 \tag{1.74}$$

The Cantor set is found to be the basis for obtaining a wide variety of fractal shapes and forms. In fact, by using varying generator dimensions one can imagine all kinds of objects (see Chapter 5).

Further, the total length of all intervals removed from Figure 1.30 is:

$$\text{Length removed} = 1/3 + 2(1/3)^2 + 4(1/3)^3 + 8(1/3)^4 + \cdots \tag{1.75}$$

whose sum is $1/3/(1 - 2/3) = 1$. In other words, the length remaining must be zero.

The devil's staircase can be analyzed with the help of a function d_x:

$$d_x = \int_0^x C_s \, ds \tag{1.76}$$

It is important to notice that the derivative of this function is equal to zero almost everywhere. One can use this kind of Cantor set to analyze a variety of natural phenomena. As mentioned elsewhere,

the Sierpinski gasket is indeed a generalized version of the Cantor set in two-dimensional space. The Sierpinski gasket is obtained by continuously removing the centers of triangles on a plane. A similar procedure can of course be carried out in three dimensions. Later, we will construct a fractal surface (two- or three-dimensional) that corresponds to a Cantor set fractal dimension. By using these methods one can easily construct Cantor sets, such that the shape is similar to some known object [a metaphor of the Cantor set that represents lifeline has been described (Takayasu, 1990)]. The random analogue of the Cantor set has been investigated (Falconer, 1990). The procedure used to draw such a set is as follows. The middle third part may be randomized. In other words, the right or left third part may be randomized as the middle part under each step of construction. Actually, these random fractals do not have the self-similar shape as the nonrandom Cantor set. However, the random Cantor set resembles the shapes encountered in nature very closely, e.g., coastlines, topographical surfaces, clouds. The same procedures have been applied in drawing computer graphics of (for example) landscapes. A fractal can also be described in terms of numbers. The Cantor set provides numbers between 0 and 1, while the sets removed denote different sets of numbers. This can be used to represent noise (Falconer, 1990).

Products of Fractals—A Self-affine Set

A self-affine set can be constructed as shown in Figure 1.31 (Falconer, 1990). Each rectangle is replaced with an affine copy of the rectangles in E_1. After k subdivisions, E_k, we have 6^k number of rectangles of size $3^{-k} \times 4^{-k}$. Each of these rectangles may be covered by at most $(4/3)^k + 1$ number of squares of side 4^{-k}, by dividing the rectangles using a series of vertical cuts. Accordingly, we find that E_k may be covered by:

$$6^k \times 2 \times 4^k \times 3^{-k} = 2 \times 8^k$$

number of squares of diameter $4^{-k}\sqrt{2}$. This gives the width-to-height ratio as $k \to \infty$, $\dim_H F = \dim_B F = 1\frac{1}{2}$.

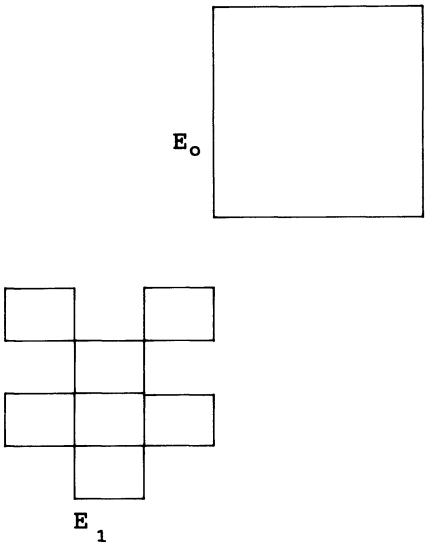

Figure 1.31. Product of fractals.

1.5.3. Nonlinear Dynamics and Chaos

We have mentioned that various phenomena can exhibit nonlinear behavior, before ascending to some of the more rarefied peaks of instabilities, bifurcation, and chaos (Barnsley and Demko, 1986; Thompson and Stewart, 1988). These systems can be found in many areas of everyday life, such as physical science (electrical) and nonphysical science (economics and politics). Fractal dimensional analysis of the reconstruction of phase portraits obtained from time series data in radar signals has been reported in the literature (King *et al.*, 1987). A complete discussion is beyond the scope of this text, and relevant references given herein should be consulted.

Most natural phenomena are intrinsically nonlinear, e.g., weather patterns and the turbulent motion of rapidly moving fluids or heartbeat. Although nonlinear effects are important in these and other physical phenomena, it is easier to introduce some of the important concepts in the context of theoretical ecology.

Example of a Nonlinear Chaos. We will study the example of how a population of insects varies from one summer to the next. The phenomenon is well known: the insects are born, lay eggs, and die in one summer and the process repeats itself the next summer. The population of insects during one summer, p_{n+1}, is related to the previous summer population, p_n, by a constant, μ, as follows:

$$p_{n+1} = \mu p_n \tag{1.77}$$

As the population grows and the role of survival of the fittest is applied (e.g., competition for food), the above equation will become less valid and another factor needs to be included, e.g., dynamic birth rate $\mu_{\text{eff},p}$:

$$p_{n+1} = \mu_{\text{eff},p_n} p_n \tag{1.78}$$

with

$$\mu_{\text{eff}} < \mu \tag{1.79}$$

$$\lim_{p \to 0} \mu_{\text{eff},p} = \mu \tag{1.80}$$

From this one obtains a simple form that satisfies these conditions:

$$\mu_{\text{eff},p} = \mu - \alpha p \tag{1.81}$$

where α is constant. Combining these equations gives:

$$p_{n+1} = (\mu - \alpha p_n) p_n \tag{1.82}$$

$$= \mu p_n [1 - p_n(\alpha/\mu)] \tag{1.83}$$

$$= \mu p_n (1 - x_n) \tag{1.84}$$

where we define $x_n = \alpha p_n / \mu$.

By eliminating the terms related to the populations in Eq. (1.84), we get the standard form of the nonlinear equation (see above):

$$x_{n+1} = \mu x_n (1 - x_n) \tag{1.85}$$

where

$$(1 - x_n) = p_{n+1}/(\mu p_n) \tag{1.86}$$

is the ratio of the insect population in the summer corresponding to $(n + 1)$ to what it would have been if the static model were valid. Further, x_n and $(1 - x_n)$ can only vary from 0 to 1, and μ must be in the range of 0 to 4, in order to keep x_n in this range in iteration. If μ is even slightly more than 4, the magnitude of x_n will tend to $-\infty$ on repeated iteration of Eq. (1.85). The phenomenon of bifurcation can be explained by the plot where pitchforklike curves are obtained when Eq. (1.85) is used (Holden, 1987).

The plots show that for $\lambda < 1$ only a population of zero is possible. When $1 < \lambda \leq 3$, then only a single stable nonzero population can exist. In the case when $3 < \lambda \leq 3.45$, the population will oscillate between the two values on the upper and lower branches of the plot. When $\lambda > 3.45$, the oscillation spreads over the four branches, and increases at higher values. The population becomes chaotic when $\lambda = 4$.

Pendulum Oscillation (An Example of Nonlinear Dynamic Motion)

Besides the great role geometry plays in the analysis and description of physical and natural phenomena, the systems that undergo regular and repeating motion are just as important. Examples are:

- Motion of the earth about the sun
- A pendulum as in a grandfather clock
- A plucked guitar string
- Oscillations of the atoms in crystalline solids
- Electromagnetic and atomic phenomena

It is important to note that the magnitude of distances under consideration in these examples differs by a few orders of magnitude. The same is true with regard to the magnitude of the frequency. In order to illustrate the important concepts involved with these oscillatory phenomena, it is useful to consider the motion in a simple pendulum (Figure 1.32). A simple pendulum

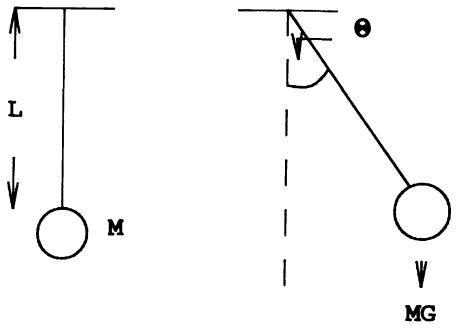

Figure 1.32. Motion of a simple pendulum. The sign of angle Θ is positive if the mass (M) is to the right of the vertical axis, and negative if it is to the left.

consists of a particle or "bob" of mass M attached to the lower end of a rigid rod of length L. In the following analysis the mass of the rod is assumed to be negligible in comparison to M. As the bob is set in moton by pulling it to one side from its equilibrium position, the swing is initiated in a vertical plane.

The position of the bob under its motion is given by the angle θ, since it traverses an arc of a circle of radius L. The linear velocity, v_{lin}, and acceleration, a_{acc}, are given as:

$$v_{\text{lin}} = L\, d\Theta/dt \tag{1.87}$$

$$a_{\text{acc}} = L\, d^2\Theta/dt^2 \tag{1.88}$$

If we neglect the bob–air friction, then the two forces that are acting on the motion of the bob are equal. The gravity component is $(Mg \sin \Theta)$, while the kinetic force is:

$$ML(d^2\Theta/dt^2) = Mg \sin \Theta \tag{1.89}$$

and we get:

$$d^2\Theta/dt^2 = -(g/L) \sin \Theta \tag{1.90}$$

The relation in Eq. (1.90) is very interesting. Since the plot of $\sin \Theta$ is nonlinear, we find that Eq. (1.90) is indeed an example of a nonlinear relationship. It is also known from differential equation

mathematics that most nonlinear equations do not have analytical solutions in terms of well-known functions. The relation as given in Eq. (1.90) is not an exception. In the limiting case, when the magnitude of Θ is very small, one finds that numerically $\sin \Theta \simeq \Theta$, from which we can rewrite Eq. (1.90) as:

$$d^2\Theta/dt^2 \simeq (g/L)\Theta \qquad \text{for } \Theta \ll 1 \tag{1.91}$$

here Θ is in radians.

As will be noticed throughout this text, one equation or relation is common to many varied systems. The relation in Eq. (1.90) is one such general relationship. In the case where $\Theta \ll 1$, the period of the simple pendulum, T, is found as:

$$T = 2\pi(L/g)^{0.5} \tag{1.92}$$

where T is time per oscillation.

The relation in Eq. (1.90) can be solved by numerical methods. The potential energy is considered. When the rod is situated at an angle, Θ, the bob is at the same time raised under the force of gravity by a height, h, as:

$$h = L - L\cos\Theta \tag{1.93}$$

The potential energy (PE) is thus:

$$\text{PE} = Mgh \tag{1.94}$$

$$= MgL(1 - \cos\Theta) \tag{1.95}$$

and the magnitude of PE is zero at $\Theta = 0$. The kinetic energy, KE, which is equal to PE, as required by the conservation of energy in the system, is given as:

$$\text{KE} = (1/2)(\text{mass} \cdot \text{velocity}^2) \tag{1.96}$$

$$= (1/2)Mv^2 \tag{1.97}$$

$$= (1/2)ML^2(d\Theta/dt)^2 \tag{1.98}$$

From this we can write the expression for the total energy, TE:

$$\text{TE} = \text{PE} + \text{KE} \tag{1.99}$$

$$= (1/2)ML^2(d\Theta/dt)^2 + MgL(1 - \cos\Theta) \tag{1.100}$$

As an example, consider a pendulum with $L = 150.3\,\text{cm}$ and $T = 246.7\,\text{sec}/100$ vibrations. The acceleration of gravity, g, can be estimated from:

$$g = (4\pi^2/T^2)L \tag{1.101}$$

$$= 9.75\,\text{m/sec}^2 \tag{1.102}$$

This value of g is in agreement with literature data. It shows that the simple pendulum movement can give much useful information about earth's gravity forces.

What is most important in this analysis of pendulum motion is that only one point in phase contains all of the information about the state of a dynamical system at any instant. In other words, if we know the position of the bob on one side, then we know exactly its position on the other side. Knowledge of the velocity and position is all that one needs. This merely points out that information of a large event can be embedded in just two simple data points.

Now let us consider a swinging pendulum, which we know will gradually come to a stop. This means that a phenomenon of swinging has taken place, but the pendulum moves toward a point where it always ends, regardless of its starting position. We can call this point a place that our system moves toward, or, as usually termed, the *attractor* of the phenomenon, e.g., a pendulum, oil price fluctuations, dollar exchange rate, population of bees, production of a product.

The pendulum motion constitutes both potential energy and kinetic energy terms. This indicates that attractors that are governed by energetic factors can be analyzed analogously to the pendulum motion. We know that the pendulum velocity is zero before it is set in motion. It even has a sign with reference to the center (negative on the left side). The magnitude of the velocity

increases and is a maximum every time it passes through the point 0,0 on the x–y plane.

If we analyze the magnitude of velocity, we find that the pendulum is attracted to the point where all motion stops. In such a pendulum the energy is lost and the trajectory is a spiral that is attracted toward the point.

The most important characteristic of pendulum motion is that it mimics different oscillating phenomena in everyday life. Even if one bumps into a pendulum clock, it switches back to its 60-second per minute frequency. This behavior is exactly analogous to other phenomena such as heartbeat, trajectory disturbance, and turbulence in a fluid.

A pendulum is a system that has a stationary equilibrium point at which all motion ceases. This archetypal example of oscillating motion, which was originally studied by Newton, returns to its vertical hanging point regardless of its starting position or velocity. This is characterized as a system with a point attractor. In order to conform pendulum movement to other systems (e.g., weather, economics), one may replace the parameters in the above equations with the appropriate variables (e.g., replace height with dollars, angle with interest rate). Or one may denote right and left movements as export and import. If perturbations are to be included, then the procedures described in the literature should be pursued (Thompson and Stewart, 1988).

Another important observation was reported by Foucault (Thompson and Stewart, 1988). Consider a pendulum set up at the North Pole. If started properly, it may vibrate as a simple pendulum in a vertical plane that is fixed in the Newtonian frame of reference. As the earth turns under the pendulum with angular velocity θ_m, the plane of vibration of the pendulum appears to an observer on the earth to turn with an angular velocity $-\Omega$. Foucault was the first to point out that a pendulum could be used to demonstrate the earth's rotation. It is not necessary that the pendulum be situated at one of the earth's poles; an apparent rotation (due to the rotation of the earth) may be observed at any latitude except on the equator.

2

Fractal Viscous Fingers

2.1. Introduction

Fluid motion or flow is generally uneventful. The fluid phase(s) is generally described by two main characteristics. One factor used to describe the flow is the viscosity. The second is the interfacial tension. As described elsewhere (Adamson, 1982; Chattoraj and Birdi, 1984; Birdi, 1989), when two fluid phases meet, the interfacial tension is proportional to the different forces that interact from one phase to the other. When the fluid flows, these two factors determine the characteristics of the system. However, the term *viscosity,* as used in the so-called Newtonian (as water) or non-Newtonian (such as toothpaste, cream, butter) case, requires some comments. The flow characteristics of fluid moving in any container or porous medium are quite common in everyday life (e.g., groundwater movement). However, the flow characteristics of two-phase fluid flow become much more interesting, and the latter type is also quite common and equally important. The flow phenomena concerning two phases (fluids) of different viscosity are somewhat special under certain conditions. The two fluids can be immiscible [e.g., oil–water (brine)] or miscible (groundwater; pollution). However, the investigation of such flow in three dimensions is obviously difficult because the motion will be quite complex, and the view of the interior parts will be obscured. In order to resolve this problem, a simplified cell was used by early

investigators (Hele–Shaw), which will be described herein. The data resulting from these investigations have achieved a very high level of information, besides simplicity (serving as a computer model). This model has been used to describe oil reservoirs, which may be located as deep as 5 km. Since we probably will never be able to visualize such reservoirs, these simple models thus become very useful. Further, in the case of oil recovery phenomena, viscous fingering in porous media has been considered an instability that occurs when a less viscous fluid (say brine) displaces a more viscous fluid (oil). In the oil industry, viscous fingering has resulted in serious problems when displacing viscous oil by miscible gas because it leads to a poor recovery of the hydrocarbon.

In these model cells, the flow between two transparent glass (or polycarbonate) plates has been investigated. The phenomenon of interfacial motion between two immiscible viscous fluids in the narrow gap (ca. 1 mm) between two parallel plates (Hele–Shaw cell) has been considered (Saffman, 1986). This type of flow is currently of interest because of its relation to pattern selection mechanisms and the formation of fractal structures in a number of physical applications (e.g., oil recovery processes, drug delivery from gels, pollution control). Attention is concentrated on the fingers that result from the instability when a less-viscous fluid (water) is implemented to drive a more-viscous (oil) fluid. (These phenomena when studied in the thin cells give rise to patterns resembling fingers, thus the term *viscous fingering.*) The cells were found to be useful for taking photographs of the flow patterns, and later for qualitative and quantitative analyses. In some cases, viscous fingering occurs in systems consisting of gas (air)–fluid (water) (Feder, 1988; Viesek, 1989). The energy dissipation in such turbulent flow systems has been analyzed (Benzi *et al.*, 1984; Pynn and Skjeltrop, 1985). The experimental data were found to exhibit dilation invariance, and multifractal behavior was present.

The flow phenomena were recognized to be very useful as models for understanding more complicated systems (e.g., the trapped oil in reservoirs, underground water pollution, gel chromatography, biological systems).

The two phases (fluids) under very special conditions exhibit fingerlike patterns only when the difference in viscosity (the term

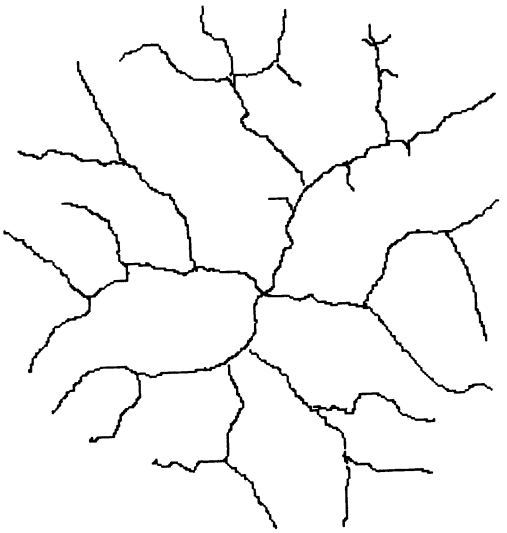

Figure 2.1. Typical viscous finger (digitized) phenomena [low viscosity: water (colored); high viscosity; gelatin (5 g/liter)]. $D = 1.7$.

viscosity needs special designation as given below) is >10,000 (in qualitative terms). The difference in viscosity primarily is found to give rise to a variety of finger forms (Figure 2.1). Typical systems which have been studied are described in Table 2.1. Viscous fingering has been extensively investigated in the current literature, not only because of its relation to some important industrial processes (oil recovery) and biological phenomena, but also because of purely academic interest. Moreover, the recently developed theoretical analyses of aggregation models and growth phenomena have been useful in describing the fingering shapes.

Table 2.1. Systems for Which Viscous Fingering Has Been Reported

High-viscosity medium	Low-viscosity medium
Polysaccharides (scleroglucan, guar gum, hydroxy ethyl cellulose)	Water (η = 1 cP), glycerol (η = 90 cP), corn syrup, polyvinyl alcohol (dyed with methylene blue)
Latex	Water
Gelatin	Water

In a recent report, extensive analysis of fractal systems has been reviewed (Ahrony, 1986). The paper reviews some recent results on random walks, nonlinear resistors, noise, spin dynamics, and viscous fingering.

It is known that ramified patterns can be obtained in viscous fingering if the capillary number is sufficiently high, i.e., nonlaminar flow (Saffman and Taylor, 1958; Saffman, 1986). However, the ramification is not very important if the fluids are miscible, since the low-viscosity fingers do not displace the viscous fluid as a plug and most of the time they are not steady with respect to time (Haberman, 1960). These major drawbacks can be overcome by the selection of appropriate experimental conditions. The displacement patterns so obtained can be investigated in much greater detail due to the simplifications these conditions bring to the flow equations.

Furthermore, various patterns are known to be formed in hydrodynamic systems during the approach to turbulent flow (Beloshapkin *et al.*, 1989). The various patterns, which are observed under a wide range of conditions, have a symmetry typical of crystals or quasi-crystals. These pattern elements are also found to be divided by thin layers that form a web, within which the streamlines are chaotic. It is interesting to note that within the web channels, transport occurs which is associated with dynamical chaos.

Basically, viscous fingering is an interfacial instability phenomenon and in conjunction with the viscosity criteria, therefore, one should analyze the fractal dimension of its boundary. In most cases, it is the mass of the finger that has been analyzed rather than the surface. For DLA (diffusion-limited aggregation)-type fractal patterns, which contain no loops and where the width of the individual branches (fingers) is statistically constant, both dimensions are equal. Thus, in the general case, each dimension contains specific information and is accordingly useful.

The so-called Hele–Shaw cells (Figure 2.2) have been used in such studies. Unlike packed beds or etched network models, these model cells are perfectly isotropic. The viscous fluids generally used are of non-Newtonian type (described later). This gives rise to a pluglike motion of the interface.

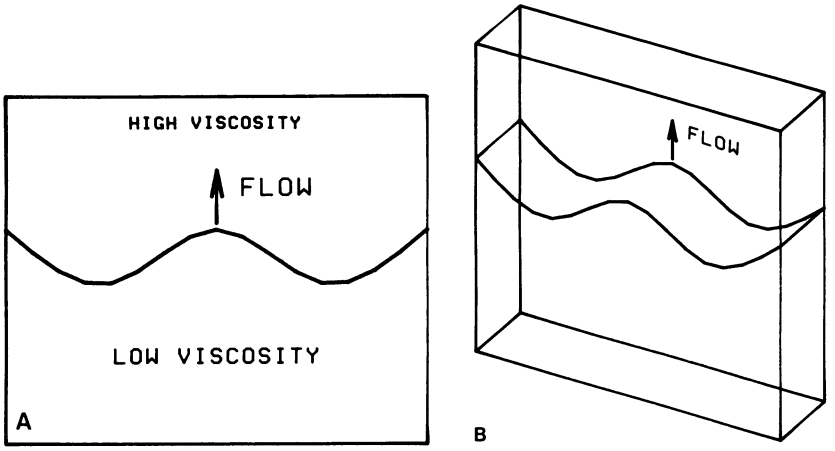

Figure 2.2. Geometry of the Hele–Shaw cell (schematic): (A) two dimensions; (B) three dimensions.

With regard to viscosity, it is necessary to describe this term somewhat elaborately here (in a qualitative sense) (Bird *et al.*, 1987; Goodwin, 1982). This is necessary because the term is not a simple physical property of a fluid (or solution). In general terms, the viscosity of a fluidlike phase is defined as:

- Newtonian (fluids such as water, alcohol, glycerol)
- Non-Newtonian (fluids such as thick oils, toothpaste, saliva)

A Newtonian fluid is one that exhibits the same viscosity no matter how fast (within certain flow rates) it flows through a tube. Some fluids or solutions decrease (or in a few cases increase) in viscosity as the flow rate increases (non-Newtonian). This arises from the fact that the increased flow rate (shear rate) progressively aligns or breaks up large-scale structures made by the polymer molecules or the colloidal particles. In some fluids we may also find memory and elastic effects (such as in toothpaste or gel-like fluids or saliva). When *viscosity* is used in this text, we mean any of this multitude of phenomena, and it is apparent that viscous fingering is quite complicated. The flow of gel-like fluids consists in the rearrangement of molecular interactions which is dependent on the relaxation time constant. For flow rates much slower than the

slowest microscopic motions, the structure of the fluid is able to adapt itself synchronously to the external conditions, and the system flows. On the other hand, for flow rates faster than the fastest microscopic motions, the structure of the fluid does not have the time to adapt itself to the external conditions and the structure of the system breaks down. Despite many years of extensive investigations, the turbulence in fluids is still far from fully understood (despite the fact that many natural and industrial systems are turbulent).

If the difference in viscosity is small, then the two phases may be analogous to the mixing of two fluids (Ottino *et al.*, 1988). This is studied by injecting a colored fluid into another fluid and analyzing the color patterns. The chaotic mixing has been found to mimic the movement of matter inside the earth. Self-similar patterns can be useful in understanding various technical and natural processes.

In these systems there are a limited number of degrees of freedom. This could be ascribed to the intimately chaotic nature of the flow (turbulence) or reactive flow. This is again related to the fact that in chaotic phenomena, as described herein, the system is basically sensitive to the initial conditions. This was shown to be based on the observation that at some time two systems might look quite similar, but they will diverge at a later time, due to the initial conditions being different. But the most interesting feature of viscous fingering experiments is that one can easily visualize such observations.

Turbulent flow is a phenomenon typical of low-viscosity and low-molecular-weight fluids (i.e., air and water). In fluid flow the turbulence is determined by the magnitude of a quantity called the Reynolds number, R_e (one could call this a kind of degree of turbulence) (Moloy *et al.*, 1985):

$$R_e = V_{\text{fluid}} L_1 / (\mu/\delta) \tag{2.1}$$

where V_{fluid} is the average velocity of the fluid, L_1 is the length, and μ/δ is the ratio of the viscosity, μ, and the density, δ (kinematic viscosity). Actually, the term R_e is proportional to the ratio of internal forces to viscous (internal friction) forces. It has been

observed that turbulence appears when the magnitude of $R_e > 10^3$, regardless of the values of length and viscosity. This means that turbulence would occur at enormous velocities in the case of heavy and high-viscosity fluids.

In order to understand the physical meaning attached to the magnitude of R_e, it is useful to consider the patterns of fluid flow past a cylinder as visualized for different Reynolds numbers (Figure 2.3). For small R_e (<20), fluid velocity is constant with time. In the case of larger R_e values, the velocity exhibits two values with some periodicity. At even larger R_e values (>10^4), turbulent or chaotic flow sets in. In fact, viscous fingering is a mixture of chaos and turbulent flow, characteristic of such fluids.

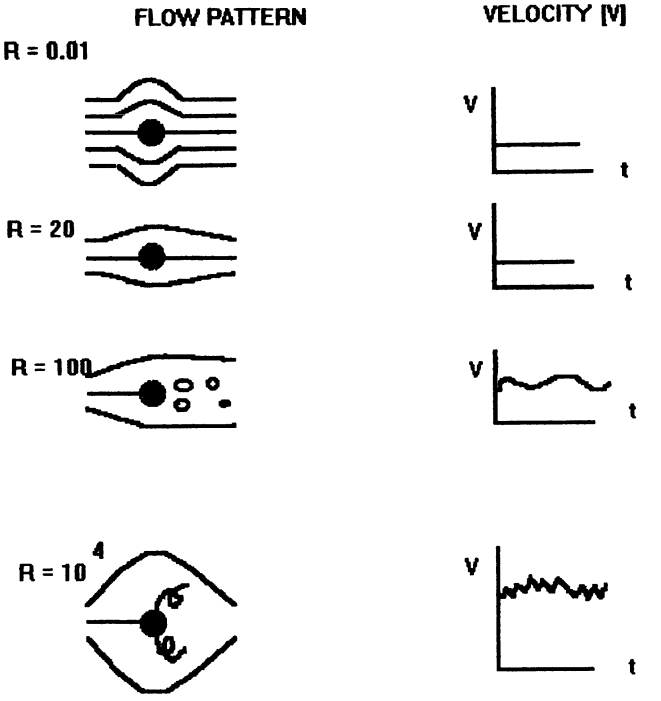

Figure 2.3. Visualization of patterns of fluid flow past a cylinder for fluid of different Reynolds number (R_e). The breakup (chaotic) flow at high R_e is depicted (schematic).

The motion of the interfaces under equilibrium distribution of forces can be described as follows (Feder, 1988; Vicsek and Kertesz, 1990). Assuming that the fluids under consideration are incompressible, the change in velocity is zero:

$$\nabla u = 0$$

and

$$\nabla^2 u = 0 \tag{2.2}$$

where u is the distribution of pressure (viscous fingering) (or temperature in crystallization or electric field in electrodeposition). The normal velocity of the interface, v_n, is given by:

$$v_n = -kV_u n \tag{2.3}$$

where k is a constant. The value of u on the interface Γ is given as:

$$u_\Gamma = -d_0 k - \beta v_n^\tau \tag{2.4}$$

where the capillary length d_0 is proportional to the surface tension, k is the local curvature of the interface, and τ is an exponent depending on the physical process considered. The first term on the right-hand side is related to the local thermodynamic equilibrium. The second term accounts for the departure from equilibrium arising from the velocity-dependent term with the kinetic coefficient β.

Various analytical procedures have been developed in order to use these equations. The role of interfacial tension on the pattern formation has been demonstrated. The magnitude of the interfacial tension can be varied by the addition of amphiphilic molecules (e.g., detergents or other molecules with hydrophobic–hydrophilic character). The hydrophobic interaction plays a very important role in such interfacial phenomena (Ben-Naim, 1980; Tanford, 1980; Birdi, 1982). The random walk method has been applied in the DLA models, used to describe these phenomena (Stanley and Ostrowsky, 1986; Avnir, 1989).

2.1.1. Apparatus and Experimental Procedure

The experimental setup that is generally used is relatively simple, consisting of two closely spaced rectangular glass (or polycarbonate; acrylic) plates (relatively stiff) closed along the sides (for linear cell) or open on all sides (for radial cell).

A schematic diagram of the experiment is shown in Figure 2.4. The fluids are injected into the cell, and the displacement patterns can be recorded by different methods.

A linear cell (length ca. 10–90 cm, breadth ca. 10–90 cm, and thickness adjustable from 0.1 to 3 mm) is shown in Figure 2.5.

A radial cell consists of two plates with spacing, but here the fluid is injected in the center. The difference between the axial and radial cell is that in the latter the sides are open to the surroundings.

The procedure used is, however, the same in both cells. The spacing between the plates is filled carefully with a high-viscosity fluid (gel phase and non-Newtonian). A low-velocity fluid (water or the like or gas) is then slowly pushed into the cell at a constant speed by using an appropriate pump. In order to visualize the flow pattern, suitable dyes as markers are generally used.

In order to avoid bubbles, one should fill the high-viscosity fluid carefully and remove the bubbles (if present) by careful tilting and vibration. Spacers can be made of layers of thin polyethylene or Teflon tapes. For accurate studies the patterns are photographed and digitized by a convenient method. In more advanced procedures, computer image analysis has been used. However, digital analysis of photographs is still the most accurate and inexpensive, even though tedious and time-consuming in some cases.

The fingering phenomenon has also been studied for such systems as clay particles in water (as paste) and water in Hele–Shaw cells. The dimensions of the cell were:

$$1\,\text{m} \times 0.3\,\text{m} \times b$$

where b is the thickness between the plates. The magnitude of b can be varied by using suitable spacers. The water phase was injected through a 1-mm hole in the closed part of the cell.

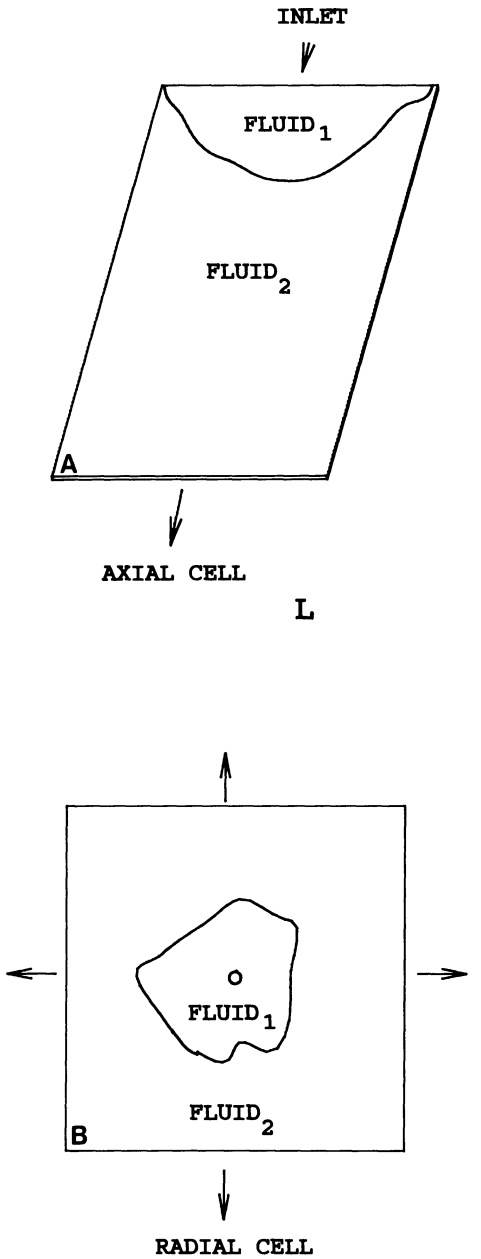

Figure 2.4. Diagram of Hele–Shaw cell. (A) Axial cell (note that the cell is closed along the long sides); (B) radial cell (open on all sides).

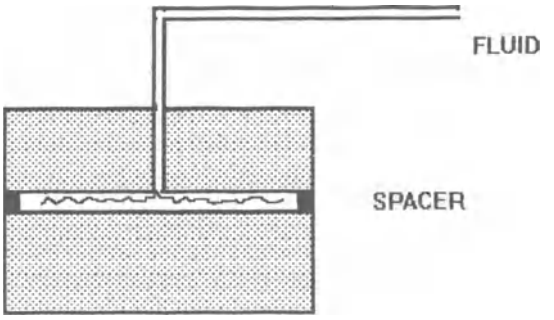

Figure 2.5. A typical experimental cell for viscous finger studies.

Even though the patterns observed are never exactly the same from one experiment to the next, the fractal analysis shows that the magnitude of D estimated is exactly the same.

The solid (clay)/water ratio in the paste was varied from 0.05 to 0.1 w/w. Bentonite pastes were used since they exhibit viscoelastic shear-thinning suspensions, with a threshold for flow.

In another study (van Damme *et al.*, 1986a,b), a radial Hele–Shaw cell of dimensions $0.5 \times 0.5 \times 0.0003$ m was used. The low-viscosity fluid (water) was injected through a syringe needle at the bottom of the plate center. The injection rate was between 1 and 2 ml/sec. Slurries of composition 4–15% clay/water were used.

2.1.2. Viscous Finger Width and the Cell Separation

The most fascinating observation is that one can obtain all sorts of patterns with such a simple setup. If we inject water into water (with dye or ink for visibility), we merely see drops of one phase spreading into another phase, with no fingering. Now if we inject water [$\eta \approx 1$ cP (centipoise)] into some thick fluid such as glycerol ($\eta \approx 1000$ cP), we see a circular-shaped fluid spreading into glycerol.

The dependence of the finger width on the separation of the cell has been investigated (van Damme, 1987). In these studies the cell thickness, b, was varied from 0.2 to 6 mm. The data showed

that the finger thickness, l_{finger}, was linearly related to b as follows:

$$l_{\text{finger}} = 6.5^{\alpha} \tag{2.5}$$

where $\alpha = 1$. A similar linear relationship has been reported by other investigators for the case of polymer solutions, where b was varied from 0.2 to 1.2 mm (Daccord *et al.*, 1986).

From Newtonian viscous fluid theory, the relation for the linearly unstable wavelength, λ_m, is given as:

$$\lambda_m = 4b \tag{2.6}$$

It is seen that this relationship predicts a value lower than the experimental data. However, it is clear that one cannot expect such clear correlations for complicated systems.

The pressure inside the low-viscosity fluid is quasi-constant, and therefore any defect in the interface gives rise to an increase in the pressure gradient toward the outlet in the high-viscosity fluid phase (Figure 2.6). Since the fluid velocity is directly proportional to the pressure gradient (i.e., an increase in pressure produces an increase in flow velocity), this gives rise to acceleration of the more

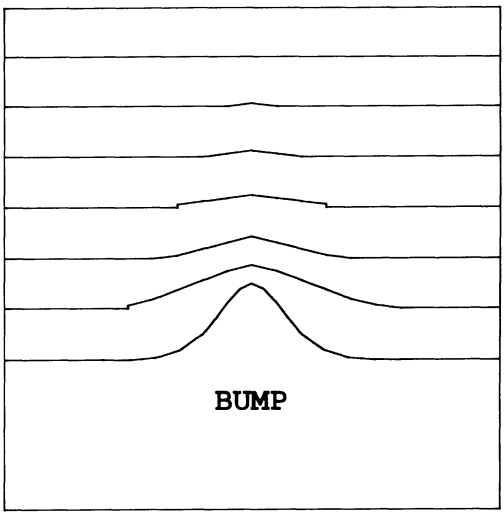

Figure 2.6. Pressure isobars that are found whenever a defect (bump) is present.

viscous fluid in front of the bump. Accordingly, as the less viscous fluid moves forward in the Hele–Shaw cell, the interface ripples (the degree would be dependent on the interfacial tension), and leads to a meandering pattern. It has been observed that very clear fractal behavior is obtained only by increasing the non-Newtonian character of the high-viscosity phase. The fingers are of constant width in such systems. If the non-Newtonian character is very large, lowering of the interfacial tension yields very little effect. However, some observations indicate that even if differences are small, the systems might exhibit some other significant variations (like the angles of branches).

As known from surface chemistry (Chattoraj and Birdi, 1984), the interfacial force (interfacial tension) tends to stabilize the pattern. It is only recently that the theoretical description has been given for why one well-defined finger width is selected among other possibilities.

2.2. Determination of Fractal Dimension of Viscous Fingers

The rather complicated patterns obtained have been extensively analyzed by fractal theory. This approach was used in order to determine the interfacial forces under which the fingers are formed. The structures appeared to be self-similar, the lower cutoff corresponding to the finger width and the upper being higher than the maximum size of the cell. In growth processes the structure is self-similar and the volume or mass of the region bounded by the interface, M, scales with the increasing linear size R of the object in a nontrivial way:

$$M \sim R^D \tag{2.7}$$

where D is the fractal dimension. D is reported to be 1.7 ± 0.05 for a wide variety of systems.

However, it has been argued that no universal value should be attached to the values of D. The case of the fractal dimension of the patterns generated in radial cells, where wall effects are absent

and no perturbation on growth is expected, gives more general values of D. For a wide variety of systems (e.g., polysaccharide solutions, latexes, clay suspensions), $D = 1.7 \pm 0.05$. It must be emphasized that no two systems give exactly the same pattern, even if D is the same. In other words, the finger width, angle, and length may vary appreciably. This has been found to be dependent on the various properties of the two fluid phases, as mentioned.

The fractal value of a water–polysaccharide solution has been estimated (Nittmann *et al.*, 1985; Daccord *et al.*, 1986). The fingers showed some fattening. The value of D was 1.4, which is low for such fractals (compared to $D = 1.7$).

Influence of the Thickness of the Gap. The thickness of the linear cell was investigated using values from 0.1 mm to 3 mm. This did not affect the nature of the pattern, which was always self-similar, but the average width of the fingers was found to be roughly proportional to the thickness, between 5 and 10 times the gap.

Decreasing the gap narrows the range of conditions for obtaining steady fingers. Seepage and closed loops have been observed simultaneously for 0.1-mm gaps.

2.3. Instability of the Diffusion Front

It is well known from everyday observation that when a liquid drop is subjected to some violent force, it breaks up. This is commonly observed when a fluid drop lands at high speed on a solid surface. In fact, the breakup results in the formation of very symmetrical shapes, which is analogous to the instabilities observed here. The interface between a low-viscosity fluid pushing a high-viscosity fluid will be unstable, as found from physical forces (Figure 2.7). The dynamic behavior of the diffusion front has been analyzed by simulation calculation. This is explained by assuming that during the diffusion process, some microscopic event in the motion of single particles (Stanley and Ostrowsky, 1986) may induce semimacroscopic changes of the front. There exist relatively long periods when nothing happens, which are separated by such remarkable events. A preliminary study of these dynamics of the

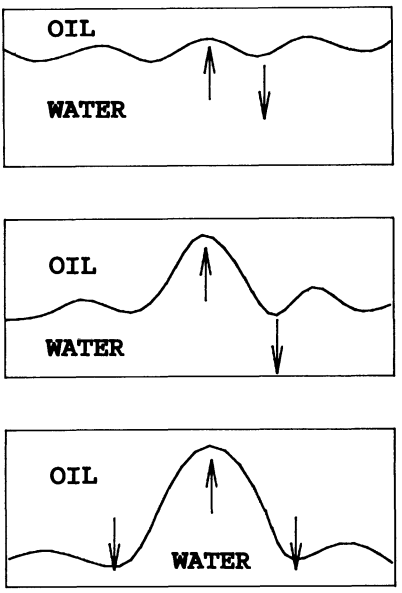

Figure 2.7. Unstable conditions at the interface between a low-viscosity fluid [water, or gas (air)] and a high-viscosity fluid (e.g., oil).

diffusion fronts has shown that the variation of the number of points during a time follows on the average a power law. However, the most remarkable feature about front fluctuations is their very high frequency, which is much higher than the hopping frequency. For a fluctuation to appear, it is sufficient that one particle near the front move to a position such that, for example, a cluster is made a part of the front itself. One can predict the existence of an interaction noise at high frequency. It has been suggested that this erratic dynamic behavior of the diffuse form could have practical implication. This is an entirely new kind of noise source occurring in an inhomogeneous system.

2.3.1. Newtonian Finger Formation and Noise

All of the data reported so far suggest that Newtonian viscous fingers strongly resist destabilization. The interface between immiscible fluids in Hele–Shaw channels has been shown to exist between critical wavelength and the capillary number.

When the flow velocity is very high, the appearance of

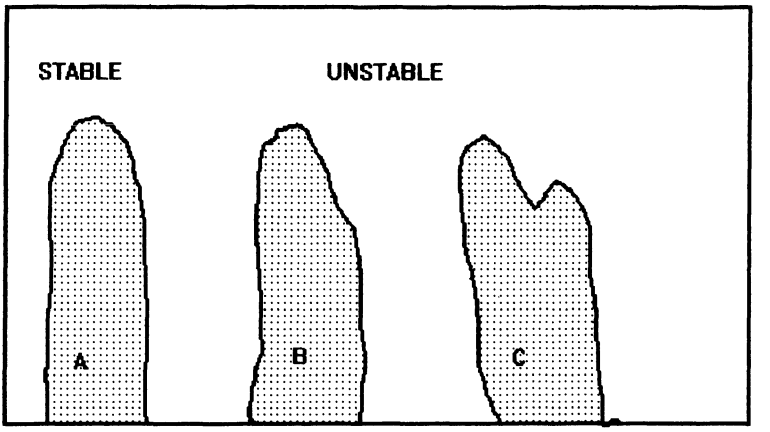

Figure 2.8. Tip splitting (of the low-viscosity phase or fluid) arising from instability at the curved fluid interface.

asymmetric fingers leads to tip splitting (Figure 2.8) (Tabeling *et al.*, 1987). In these various theoretical analyses, the effect of interfacial tension and velocity has been described. Numerically, the critical noise amplitude necessary to drive the system unstable in axial cells was found to be an exponential function of the control parameter. It was found that the critical noise amplitude decreases extremely quickly with velocity.

2.3.2. Branching Angle and Finger Stability

In the viscous finger experiments, one observes branching with varying angles, in all kinds of systems. As mentioned elsewhere herein, the branching angles are also of consequence in other natural processes, such as trees, rivers, and thunder. These were associated with the least work principle. This means that the system strives to minimize the work of pressure forces (Murray, 1926, 1927; Stevens, 1974). Thus, a narrow side branch will split off from the main branch at close to a 90° angle because this minimizes the work of pressure driving the fluid in the narrow branch. On the other hand, if the main and side branches are close to the same size, the fluid will, with little energy, switch over to the side branches and such side branches will grow away from the main branch at angles considerably narrower than 90°.

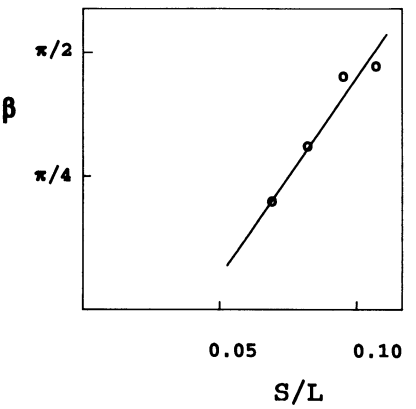

Figure 2.9. Variation of the branching angle, β, with ratio between solid (S) and liquid (L). (Redrawn with modifications from van Damme, 1987.)

As shown in Figure 2.9, the average branching angles are related to the solid/liquid ratio as follows:

$$25° \text{ at solid/liquid} = 0.06$$

$$85° \text{ at solid/liquid} = 0.10$$

It seems that the branching angle changes from almost parallel branching to perpendicular branching.

Recent studies (Birdi, 1992) have shown that branching angles and shapes may be self-similar at a given radius from the center (water–gelatin systems). This observation shows that similar kinds of forces are operating at a circular symmetry. In other words, a power law of the kind:

$$\text{Pressure} \propto \text{radius}^{D} \tag{2.8}$$

exists in the Hele–Shaw cells. These data also show that the fluid flow is circular and symmetrical, when using the experimental conditions described above. It is obvious that such observations are useful for the analyses of water injection in the oil recovery process, where the injection well is located at some geometrical pattern.

2.4. Chemical Dissolution of Porous Medium

One of the most important phenomena on the earth's surface is erosion. Rains are responsible for many dissolution processes when penetration takes place in porous rocks. Daily, rivers carry away millions of tons of dissolved minerals into the sea. The dissolution process in these natural phenomena is not always easy to follow. Therefore, some model systems need to be used in the laboratory. Analogous to the above, the process of dissolution has been studied (Daccord, 1989) by using a cast of 1-mm-thick plate of plaster ($CaSO_4 \cdot 0.5H_2O$) between two transparent plates (glass or Plexiglas), and water is injected at the center. Since plaster is slightly soluble in water, it creates a pattern that looks like a viscous finger. The etched pattern is made visible by filling it with Wood's metal, and subsequent removal of the plaster by an acid solution. These patterns look very much the same as described above. The magnitude of the fractal dimension was found to be 1.6. These data on interfacial instabilities in colloidal fluids are related to turbulence and chaotic phenomena. The transition from fractal fingering to turbulence or chaos in dynamic systems still remains to be investigated.

The chaotic phenomena can be explained by these procedures. The data reported in the literature are concerned with spatial aspects of the fingers and patterns (instability modes, i.e., finger shapes). There is a need for other parameters to be investigated, such as the temporal aspects (i.e., pressure fluctuation, velocity fluctuation).

Critical analysis has concerned whether the pore topology of porous glass (Vycor) is fractal or effectively one-dimensional. Porous glass has been examined in various fractal kinetic studies. In one recent study, the fractals and fractal-like concepts in chemical analyses of controlled pore glass oxide surface were reported (Mottola, 1990). These analyses have supported a one-dimensional topology. More studies are needed employing this methodology.

In nature, since many phenomena occur in gel-like structures, it may be that the viscous finger process is much more important than has been realized. In the interior of the earth, such processes

are taking place under conditions of very high temperature and pressure. The object of this postulate is the origin of the so-called geological dendrites (see Chapter 4) that are formed in many clayey or carbonate sediments. It can be argued that these dendrites are in fact viscous fingering patterns that have been fossilized (over many millions of years) by a crystallization process occurring in the finger after the pattern was formed. Another very important example is the fetus in the womb. It may be that the origin of life is regulated by such fractal finger phenomena. Strong evidence for the latter is the fact that some dendrite structures do not grow after reaching a certain dimension. This is exactly what one finds for the fetus.

3

Colloidal Fractal Aggregates

The size of a solid particle is known to play a very important role in both natural and technical phenomena. There are various reasons for this observation. The simplest arises from the fact that as the particle is reduced, the magnitude of surface area per gram increases. For example, if a cube of a solid of side 1 cm weighs 1 g, then the surface area = 6 cm^2. Now, if we subdivide this solid into cubes of 1 mm (e.g., by grinding), then the volume of each cube is 0.1^3 cm^3. The number of small cubes is 1/0.001 = 1000. The surface area of each of the smaller cubes is $6(0.1^2) = 6(0.01)$ cm^2. Thus, the surface area of the smaller cubes is $1000(6)(0.01) = 60$ cm^2. This gives an increase in surface area by a factor of 10 when each side of the cube is reduced by a factor of 10. It is easily seen that in the case of even smaller cubes, this increase would be tremendous. The magnitude of surface area per gram for such powders as active charcoal is ca. 1000 m^2/g. This enormous surface area gives very special properties to such powders (e.g., adsorption of pollutants from drinking water). Further, in many cases when the particles are not smooth, the edges and corners will give rise to special characteristics. Another important parameter that is related to particle size is light reflection. As the size decreases, the degree of light reflection changes, such that in some cases one sees a bluish tinge. In nature, diverse phenomena are based on the aggregation

of small particles, e.g.,

- Aerosol
- Colloidal aggregation
- Soot, smoke particles
- Polymer aggregation
- Immunology
- Phase transitions
- Critical phenomena

These aggregates are classified into two types:

- Particle–cluster aggregation: freely moving particles are able to approach close enough to stick together to form clusters (e.g., electrodeposition, crystal growth)
- Cluster–cluster aggregation: where larger clusters are formed.

The fractal geometry has been found useful in describing these aggregates quite satisfactorily. Modern techniques have been used to analyze these phenomena. In some cases, the computer simulations have provided further theoretical analyses for better understanding of such phenomena. The importance of diffusion (Brownian motion; Appendix B) in colloidal aggregation has been recognized for many decades. However, only in recent years has it been practical to undertake computer simulations [diffusion-limited aggregation (DLA)] (Meakin, 1984; Stanley and Ostrowsky, 1986).

3.1. Colloidal Aggregation

The term *colloid* means gluelike. A particle is called colloidal when its size is on the order of 0.001–1 μm. It is customary to express size in micrometers (1 μm = 10^{-6} m), angstroms (1 Å = 10^{-8} cm), or nanometers (1 nm = 10^{-9} m). Because of its importance in a wide variety of natural and industrial processes, colloidal aggregation has been the subject of considerable interest for many decades.

Colloidal particles may be spherical, or they may exhibit needlelike or platelike shapes. Colloidal particles aggregate to form

larger particles, in the case when the aggregated state is at a lower energy state than the single particle. A typical colloidal sol of gold is generally prepared by electrical charge, yielding a diameter of ca. 100 Å (Weitz and Oliveria, 1984). If we add pyridine to this negatively charged sol, the particles are attracted to each other by van der Waals forces as the charge is neutralized. As known from the kinetic theory of gases (Berry *et al.*, 1980), the energy of a particle is related to its temperature. The particles being very small give rise to an energy of attraction that is much larger than the thermal energy [$=kT \approx 600$ cal/mole ≈ 2400 joule/mole, where k ($=1.38 \times 10^{-23}$ J/K $= 1.38 \times 10^{-16}$ erg/K) is the Boltzmann constant and T (Kelvin) is the absolute temperature] (see Chapter 1). This means that the particles stick almost irreversibly on contact. Since these particles move under the force of Brownian motion, small clusters are formed. Brownian motion is said to be a statistically self-similar process. Systems that qualify under these forces are:

- Soot (carbon black)
- Paint
- Snow pack
- Blood clot

It is worth mentioning that an analogy exists among these phenomena, since the same analytical procedures can be applied in the analyses. An overview has been given in a recent study (Witten and Cates, 1986). A fractal cluster interpretation of laser scattering and extinction measurements in a sooting flame has been reported in a recent study (Hall and Bonczyk, 1990). These systems are examples where both temperature effects and kinetics become important parameters. Much of the behavior of these small particles may be explained by their very large surface-area-to-weight ratio.

It has long been known that the kinetics of aggregation can be classified into two kinds: slow and fast aggregation, each with different rate-limiting physics. These mechanisms can be related to the Derjaguin–Landau–Verwey–Overbeek (DLVO) theory of colloidal particle pair interaction potential (Verwey & Overbeek, 1948; Adamson, 1982; Chattoraj and Birdi, 1984). The interfacial

potential that is present between two colloidal particles in a stable state exhibits a "well" when the distance of separation is short, which arises from the van der Waals attractive force, while at larger distances there is another repulsive force arising from the electric double layer (at the surface of each particle). The sufficient reduction in the repulsive forces brings about fast aggregation, because particles can easily come close enough to stick (due to the attractive van der Waals forces). The slow aggregation process is induced by the remaining relatively small barrier. The resulting clusters have also been found to possess different fractal dimensions and different size dimensions. A correlation between cluster size and fractal dimension remains to be investigated. Further, ions that move toward the solid surface will have to give up some loosely bound water in this process. This has obvious consequences on the dielectric constant around the ions. Since the potential is related to the dielectric constant, we thus find that such ion movement becomes dependent on the colloid surface roughness.

Clusters formed by the aggregation of metal colloids, soot, or coagulated aerosols are characterized by their tenuous, chainlike structure. Iron particles can be formed in dense helium gas by a large pulse of electric current through a fine tungsten wire electroplated with ion. This evaporated the iron coating to form small iron particles with a diameter of ca. 70 Å. The particles were found to aggregate, forming tenuous, chainlike structures. Transmission electron microscope images showed that the iron aggregates were statistically self-similar with a fractal dimension of ca. 1.6 (determined from mass versus radius^D plot) (Matsushita *et al.*, 1984).

An aggregate of fine soot particles has a fractal dimension of 1.5–1.6 (Forrest and Witten, 1979). The size of these particles was ca. 35 Å. This size is important, since it shows that the fractal dimension remains of the same magnitude as long as DLA is the driving force.

In another example, gold sols were studied. These sols are produced by the reduction of aqueous Na $AuCl_4$ solution with trisodium citrate (Weitz and Oliveria, 1984). An aqueous suspension of gold particles (150 Å) is stable owing to the screened electrostatic repulsion between the gold particles, which have a net

charge as a result of ions adsorbed on their surfaces (electric double layer). A similar effect is obtained when excess electrolyte is added to the suspension (i.e., salting-out effect). This causes clusters to stick to one other upon each collision (fast aggregation), and thus the aggregation is solely determined by the diffusion forces. This process has been called diffusion-limited cluster–cluster aggregation. Under these conditions, the number of particles, N, has been found to be related to the radius of the aggregate, R, as follows:

$$N \sim R^D \tag{3.1}$$

where $D \approx 1.77$. However, if the charge–charge repulsion is very large, then more compact aggregates are formed. This gives $D \approx 2.05$, resulting from the slow aggregation. Thus, in such aggregation processes the value of D can tell the experimenter whether it is a fast or slow aggregating system.

Similar data were obtained for colloidal silica (Ludox). The values of fast and slow D were 1.75 and 2.08, respectively (Aubert and Cannell, 1986). A variety of other systems have provided much useful data (Table 3.1).

Two-dimensional experiments are obviously simpler than three-dimensional ones by an order of magnitude, and thus simple and useful model systems. A number of experiments have explored cluster–cluster aggregation in two-dimensional systems (Hurd and Schaefer, 1985).

The aggregation of silica microspheres confined to two dimen-

Table 3.1. Various Aggregation Systems and the Fractal Dimension[a]

System	D_{fast}	D_{slow}
Gold (aqueous)	1.77	2.05
Silica (aqueous)	1.75	2.08
Polystyrene latex (aqueous)	1.65	—
Silica (vapor phase)	1.84	2.34
Silica aerogel	1.75	—
Proteins (immunoglobulin)	2.56	—

[a]Source: Avnir (1989).

sions at an air–water interface has been investigated (Hurd and Schaefer, 1985). In the experiments, silica particles (0.3 μm) were suspended in methanol and spread on a salt solution (1.0 N $CaCl_2$). The cluster micrographs were analyzed by determining the radius of gyration, R_G, as a function of particle number, N, in order to obtain the fractal dimension:

$$N \approx R_G^D \tag{3.2}$$

The data gave a value of $D = 1.2$, which is well below the simulated value for diffusion-limited cluster–cluster aggregation models [$D = 1.47$ in two dimensions (Kolb *et al.*, 1983; Meakin, 1984)]. The lower value of D was ascribed to electrostatic forces around the growing clusters.

The aggregation of polystyrene and polyvinyltoluene microspheres (0.2–2.0 μm) has been investigated (Armstrong *et al.*, 1986). D was found to be 1.42 in these systems. A special case is where the aggregation of charged colloids (e.g., silica or Al_2O_3) can be induced by the adsorption of a polymer (generally of opposite charge). This kind of system has been reported to have very important industrial applications. The molecular weight, and hence the length of the polymer, is known to have a determining effect. In the case of long polymer chains, the chain can collect by adsorption many colloidal particles. This may serve as a fractal with both a self-similarity character as well as a dimension (Jullien, 1987; Jullien *et al.*, 1987). Computer simulations have given $D = 1.7$, which agrees with the experimental observations. These models are being developed further in order to include three-dimensional aggregates (e.g., smoke).

In nature, however, geometrical clusters (e.g. tumors, gels, soot) are usually grown. A review of these aggregates has appeared (Herrmann, 1986). The growth of a single cluster as well as the growth distribution of clusters are found to be of importance. Growth models can be developed that consider the dimensionality and the specific rules of the growth. The fractal dimension and its relation to the growth phenomena are discussed.

3.2. Gelation (A Flocculation Phenomenon)

The physical structure of a gel plays a very important role in everyday life. The human body is some 70% water. A great part of this water is actually found in gel form in various parts of the body. Fish (and other aquatic animals) are ca. 80% water, in the form of gel structure. From the very beginning of life, in the womb, the gel structure plays an important role, namely the egg has a very characteristic gel-like fluid. The function of gel structures in life processes is therefore of much fundamental importance. In some polymer systems, gelation is also observed prior to precipitation.

The kinetics of gelation (Family and Landau, 1984) can be best depicted by the structures in Figure 3.1. This is analogous to the process described for aggregation phenomena. To begin with, one has clusters, which (slowly or quickly) aggregate through time and form a gel structure. Gelation occurs when one big cluster is formed, instead of small aggregates (Herrmann *et al.*, 1982).

The lattice model of gelation has been described by the percolation theory (Desai *et al.*, 1989). A linkage or bonding is automatically assumed to take place between two polymers, giving rise to a cross-linked polymer. Because of this automatic linkage of nearest neighbor occupied sites, there is effectively no interaction between the monomers. The onset of a tortuous (fractal) connected path of nearest neighbors that reaches from one side of the lattice to the opposite side, thus represents the onset of gelation.

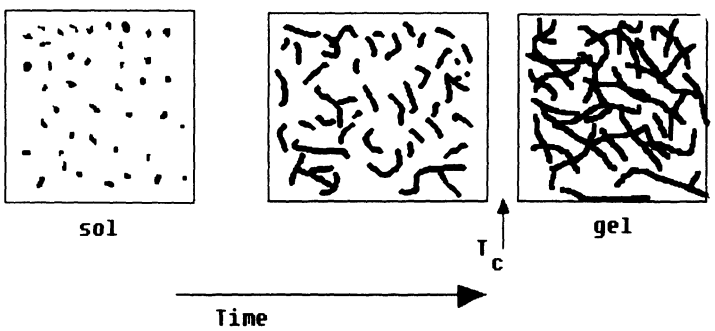

Figure 3.1. Sol–gel kinetic equilibria. T_c denotes some critical time where transition to infinitely large cluster appears.

As described in Chapter 8, the swelling of a gel is another example of a fractal process. The addition of solvent to a polymer (e.g., gelatin) induces swelling. The volume of swelling may be ten times the original volume in some cases. This has found use in the gel chromatography employing different polymers, especially Sephadex (polydextrans) (Birdi, 1988). The initial solvent–polymer interaction proceeds with less excluded volume effect, and the fractal dimension of the gel is that of percolation. According to the Flory polymer theory (Flory, 1971), the mass (M) in a volume element with radius χ_i is related as follows:

$$M \approx \chi_i^{5/2} \tag{3.3}$$

where χ_i is related to the gel fraction (G_{gel}):

$$\chi_i \approx G_{gel}^{\nu/\beta} \approx G_{gel}^{-2} \tag{3.4}$$

As more and more solvent is added, the phase corresponding to the sol is washed out of the gel phase. At this stage there is no screening effect and the gel exhibits the fractal dimension of random animals. Then the same mass, M, is contained in the volume of radius R_f, where $D = 3$:

$$M \approx R_f^2 \tag{3.5}$$

From these considerations the swelling ratio, Q, is derived:

$$Q \approx G_{gel}^{-3/2} \tag{3.6}$$

It is thus observed that the degree of swelling ratio may become very large when the gelation threshold is approached. With regard to the sol–gel transition and the dynamics of sol clusters, the experimental and theoretical aspects have been described in the literature (Martin, 1987). In this study the kinetics of growth of the sol beneath the gel point have been discussed based on the spatial correlation length in undiluted gels. Much of this research on the dynamics of gels is new, so the theoretical ideas are either

qualitative or, in some cases, essentially nonexistent. Further, the swelling properties of flexible gels are found to be important. Some of these properties are described below in the section on polymers. These analyses have been applied to the swelling of vulcanized linear polymer chain systems (Daoud *et al.*, 1986).

Fractal Nature of Gels

Casein Gels

The aggregation of colloidal particles has been much investigated in recent years. The discussion of fractal-type structures in nondilute systems is much more complicated, due to the interpenetration of the clusters and the formation of the gel state. These gels are homogeneous on the macroscopic scale, but heterogeneous and possibly of a fractal nature at small scales (Kolb *et al.*, 1983). Higher concentrations should lead to a higher fractal dimensionality, owing to an increase in interpenetration between the developing clusters, leading to a dimensionality of 3 in the case of gelation.

Consider casein (a macromolecule), the main component involved in the structure of gels made from milk. Casein includes a family of different casein molecules, whose common characteristic is that they are insoluble at pH 4.6. Under the natural conditions of milk, they are associated into large spherical particles, so-called casein micelles (aggregates). These aggregations consist of casein, water, and salts (mainly calcium and phosphate). At lower pH (i.e., acidic), the calcium phosphate, which is essential for the integrity of casein micelles at the natural pH of milk, goes into solution together with part of the casein. At pH 5, the calcium phosphate is completely dissolved but most of the casein is still aggregated. At even lower pH (4.6), the casein becomes fully aggregated again in particles which are stable at lower temperatures. The average diameter of these micelles is ca. 120 nm. At higher temperatures, the casein micelles are no longer stable, which can be ascribed to the weakening of the hydrogen bonding between water molecules. This leads to very large aggregates and eventual gelation.

Consider that the aggregates are present on lattice sites, and that the lattice sites are occupied either by a particle or by solvent. The fractal nature on the lattice can be expressed as (Bremer *et al.*, 1989):

$$N_p = (R/a_l)^D \tag{3.7}$$

where N_p is the number of lattice sites occupied by a particle, R is the radius of the fractal, and a_l is the radius of one lattice, which can be equal to the radius of one primary particle if the lattice site is the same size as the particle. D is the fractal dimension of the aggregate. In real systems the magnitudes of both R and a_l are not well defined. Moreover, the aggregates are generally not spherical and the primary particles are not monodisperse (i.e., all particles of the same size).

In the case of a three-dimensional lattice, the total number of lattice sites that have been occupied by an aggregate is:

$$N_a = (R/a_l)^3 \tag{3.8}$$

The expression for the volume fraction of particles in an aggregate is:

$$\begin{aligned} \varphi &= N_p/N_a \\ &= (R/a_l)^{D-3} \end{aligned} \tag{3.9}$$

This indicates that the fractal clusters grow until they jointly occupy the total liquid volume, i.e., the stage where gelation takes place. This suggests that the fractal dimensionality is retained in the gel. On the other hand, when $a_l \gg R$, the gel is homogeneous and obviously has a dimension of magnitude 3.

The sum of all sites occupied by the individual fractal aggregates $N_{a,i}$ will be equal to the total number of lattice sites in the gel (N_t):

$$\sum_{i-1}^{n} N_{a,i} = N_t \tag{3.10}$$

and

$$\sum \varphi_{s,i} N_{s,i} = \varphi_t N_t \tag{3.11}$$

where φ_t is the overall volume fraction of the particles and n is the total number of aggregates of casein. From these equations we get:

$$\varphi = \sum R_i^D / a^{D-3} \sum R_i^3$$

$$= (R_{3D}/a)^{D-3} \tag{3.12}$$

with

$$R_{3D} = \left(\sum R_i^3 / \sum R_i^D \right)^{1/3-D} \tag{3.13}$$

where R_{3D} is the three-dimensional average cluster radius.

The magnitude of D has been estimated to be 1.7 from model computer calculations for diffusion-limited cluster–cluster aggregation, and $D = 2$ for reaction-limited cluster–cluster aggregation. For more concentrated systems a higher D is anticipated. In these investigations the casein gels gave values of D around 2.23–2.39. The effect of ethanol on the aggregation of casein micelles was investigated (Horne, 1987). The aggregates formed were dependent on the ethanol concentration, especially when the concentration was >29%. The magnitude of D was measured as a function of ethanol concentration. The magnitude of D increased from 2 to 2.3, and was constant after ca. 29% ethanol. The value of $D = 2.2$ is somewhat higher than that found for gold sols (1.7). This could be explained by the fact that casein micelles are rearranging when aggregates are formed, while gold sols are hard particles and rearrange very quickly.

Gelatin Gels

Gelatin is known to form stable gels in water solvent. In a recent study, gelatin-containing water-in-oil microemulsions were found to form clear gels at certain temperatures and polymer concentrations (Quellet *et al.*, 1991). The difference between the

latter and the former was ascribed to the different properties of the solvents. The sol–gel transition here is known to be related to the aggregation of gelatin-filled aqueous droplets (of nanometer size). During this process, conductivity increases fourfold, which is related to the percolation threshold of the system (in other words, a state where an infinite sized cluster is formed, as mentioned above). Viscosity data indicated the onset of interdroplet cross-linking. The fractal nature of both sol aggregates and polymer network was found to give a power-law dependence. Based on the assumption that a percolation-like phenomenon is present, the magnitude of fractal dimension was found to be $D = 2.05$. From these analyses it was concluded that the gel consisted of a swollen, tenuous network that also extended into the apolar phase of the dispersed medium.

3.3. Geometrical Floc Structures

Interesting features relating to floc structures are found in many reports in the current literature. Flocculation of particles involves their aggregation without the destruction of their individuality (i.e., size and shape) and differs fundamentally from the processes of sintering and particle growth. Flocculation occurs spontaneously if it is accompanied by a decrease in the total free energy of the system (which means that particles when flocculated exhibit lower energy than when separated). The floc diameter is reported to obey the power law, i.e., the density is related to the radius. Further, one also finds a self-similarity in these analyses (Adachi and Ooi, 1990). The approach of a single particle to the floc has been described as a random walk (Figure 3.2). The Brownian motion of the approaching particles causes a self-similar structure of the formed floc.

In a recent review (Sood, 1987), light-scattering results were presented on static and dynamic properties of ordered colloidal suspensions of charged polystyrene particles and fractal colloidal aggregates. The studies discussed the static structure factor, $S(Q)$, of ordered monodisperse colloidal suspensions and binary mixtures of particles with different particle diameters, measured by angle-

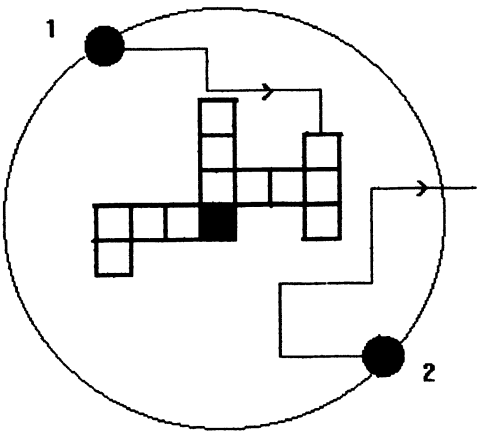

Figure 3.2. A random-walk model of floc aggregation (schematic). The particle at position 1 is able to move and stick to the aggregate, while from position 2 the particle moves away without sticking.

resolved Rayleigh scattering. This includes determination of bulk modulus using gravitational compression and observation of colloidal glass [inferred from splitting of the second peak in $S(Q)$]. Dynamic light scattering, with real-time analysis of scattered intensity fluctuations, is used to obtain information about Brownian dynamics of the particles. Recent advances in the field of light scattering from colloidal aggregates that show fractal geometry are also discussed.

Polystyrene–latex (PSL) particles of spherical shape and uniform size have been investigated (Adachi and Ooi, 1990). PSL particles of 8.04 μm diameter were used. These particles consisted of spheres with a uniform diameter and a specific gravity of 1.05, which is equal to that of a 1.19 M KCl solution at 25°C. Therefore, by using a thick KCl solution the gravity effect becomes negligible. The electrochemical properties were also investigated. As the charge–charge effect was negligible, the Brownian coagulation was due to the van der Waals potential. The flocs used were from solutions with concentrations from 6.4×10^7 to 1.6×10^{10} l/cm^3.

The flocs of size (i) as large as 10^8 particles were investigated. These flocs were found have a compact structure. The results of the table-tennis-ball simulations were also used for the precise analysis of the floc structure.

It is known that floc structure can be described by many

different methods. The relation between the radius of gyration, R_g, and the number of particles, i, is often used to evaluate the calculated result of computer simulation. This relation is reported to obey the following so-called power law:

$$R_g \propto i^{1/D} \tag{3.14}$$

Using the cluster model, the value of D has been reported to be 1.85. However, in large-size simulation the value of D approaches 2.0. From experimental studies of flocs, using electron micrographs of gold aggregates, the value of D was found to be 1.75 (Weitz *et al.*, 1985, 1988). In another study the silica aggregates were studied by using dynamic light-scattering (Schaeffer *et al.*, 1984). The value of D was 2.12. However, other investigators found a dependence of D on concentration of silica and time, where D was reported to vary from 1.75 to 2.05 (Aubert and Cannell, 1986). The effect of pH has also been reported. In a recent study, the agglomeration of hydrogenated amorphous carbon/potassium chloride was reported (Liu *et al.*, 1990). These systems were used as a crystallization fractal model for scaling property of aggregation phenomena. The fractal properties of polystyrene spheres suspended in aqueous salt solutions have been described in a recent study (Zhou and Chu, 1991).

The relation between the projected area of the floc, S, and R_g was found as follows:

$$S \propto i^{\alpha} \tag{3.15}$$

$$D_m \propto i^{\beta} \tag{3.16}$$

where α and β are constants, which can be regarded as indexes of structure. Plots of S versus i were found to be linear. These indexes are reported to be useful when considering other physical properties. The relation in Eq. (3.8) can also be expressed as:

$$S \approx a\pi i^{\alpha} \tag{3.17}$$

where the constants a and α can be dependent on the short-length scale.

In a recent study, agglomeration of titanium oxide aerosol was investigated (Dziedzini and Botet, 1991). The fractal clusters formed by titanium oxide were analyzed. Excitation energy transport in fractal aggregates has been investigated (Dewey, 1991).

Self-similarity can thus be recognized as a phenomenon that contains symmetry information across scale. From physics, we can easily show that there is a limit as to how far one can continue enlarging a shape or form ad infinitum. This is due to the fact that as one approaches some molecular scale, the symmetry must break down. One cannot magnify an atom of hydrogen and compare it with a similarly enlarged picture of another atom, say nitrogen. On the other hand, one should rather consider self-similarity at some macroscale, in order to get a better working understanding of the fractal geometry.

So far we have described cluster–cluster aggregation occurring in some liquids. In these systems the cluster trajectory is expected to be Brownian. On the other hand, in an atmosphere of very low pressure or very high temperature, the cluster trajectory is linear. This kind of situation is present in the case of various soot aggregates produced by rapid evaporation of metals, combustion of fossil fuels, aerosols, or similar phenomena. The aggregation behavior of iron particles in liquid argon has been investigated (Tence *et al.*, 1986). The cluster is composed of spherical shapes with sizes ranging from 100 to 2000 Å. The magnitude of D was found to be 1.9. The degree of polydispersity had no effect on the magnitude of D. Soot aggregates formed by the combustion of acetylene in a burner were investigated (Samson *et al.*, 1987) and the cluster found to be of ultrafine carbon particles 200–300 Å in diameter. These particles were analyzed by transmission electron microscopy. Particles in the range 5–12 μm were found to have a fractal dimension of $D = 1.82$. The smaller clusters with diameters < 1 μm had smaller values of $D = 1.55$. This finding is of much importance for pollution control in everyday life.

3.4. Electrodeposition and Aggregation

The technology related to electrodeposition is vast. The process of electrodeposition has been considered as an important

aggregation phenomenon. The complex structures observed in such processes have been analyzed by fractal geometry methods. In the case where the deposition is controlled only by diffusion, the aggregation represents statistically simple, self-similar, i.e., fractal structures, aggregates. This is argued from the fact that in such processes the driving force is Brownian motion.

The chaotic dynamics in several solid-state systems have been reviewed (Jeffrie, 1985). In each case the physical system is described, relevant equations of motion are given, experimental results are presented and interpreted, more or less from the relevant equations, including numerical solutions. The systems are: (1) an electron–hole helical plasma density wave in a Ge (germanium) crystal in parallel electric and magnetic fields; this shows period doubling and quasi-periodic routes to chaos. (2) Standing mode spin wave packets in ferrite spheres, excited by driving ferromagnetic resonance of the uniform mode; this system shows period doubling to chaos and periodic windows. (3) Resonantly driven p–n junctions in Si (silicon) show extremely nonlinear behavior due to charge stored during injection; one junction shows period doubling to chaos and period adding (i.e., frequency locking); coupled junctions show, in addition, quasi-periodicity, entrainment, and behavior generic to coupled nonlinear oscillators. The fractal dimension has been measured for these systems. In a recent study the simulated fractal formation in electrochemical switching of conducting polymer film into an insulating form on the basis of the conductive zone was reported (Aoki, 1991). In this report the electric conductivity, electric switching, and fractal properties of polymers were analyzed.

Fractal Electrodes (Battery Efficiency and Fractal Dimension)

The discharge of a battery may take place under varying conditions, e.g., constant load, constant current, or constant power. The surface reactions that take place at the interface of an electrode are generally irreversible processes, which can be analyzed by fractal theory in order to explain these practical examples in electrochemistry. The procedure used has been to analyze an electrode on which an electrochemical reaction takes

place, and to determine the surface behavior in terms of fractal theory. In these reports, fractal volume relaxation was given in terms of electrical analogues, e.g., the transport properties of recrystallized ionic conducting polymer such as the ionic complexes of polyoxyethylene. The relaxation spectrum of the impedance of the system Li/solid electrolyte/Li revealed two main modes of relaxation. It was concluded that if the fractal has no thickness (i.e., $D < 2$) and is perpendicular to the flow, then it can be described as a Sierpinski grid (see Figure 1.5).

The correlation between battery efficiency and the fractal dimension of the electrode has been the subject of various studies. The power available from a battery is generally determined by the fractal dimension of one or both of the electrodes and the test may easily be made by measuring the efficiency of the batteries associated with a change in the current (Fruchter *et al.*, 1986). In this case, the capacity of the battery, $Q_{t,E}$:

$$Q_{t,E} = I^* t_E \tag{3.18}$$

under galvanostatic conditions one gets;

$$I^{*(D-1)} Q_{t,E} = C_E \tag{3.19}$$

where the subscript E is the cutoff potential (the interfacial polarization, ohmic drop being neglected), C_E is a constant depending on E, and t_E is the time for accessing the local polarization E of the electrode. It has been found to be easy to test the diffusion limitation in fractal electrode media, for instance by lowering the temperature or by increasing the current.

Furthermore, as seen from the relation in Eq. (3.18), all of the discharge curves are self-affine in a ratio related to D.

The correlation between fractal dimension through X-ray scattering, impedance measurements, and battery efficiencies has been experimentally established in the case of Li/$SOCl_2$/carbon batteries.

The electrode can be drawn with the help of the Cantor set (Figure 3.3), where each groove has two branches. Each branch is self-similar to the whole groove with a magnification, f_m (Takayasu,

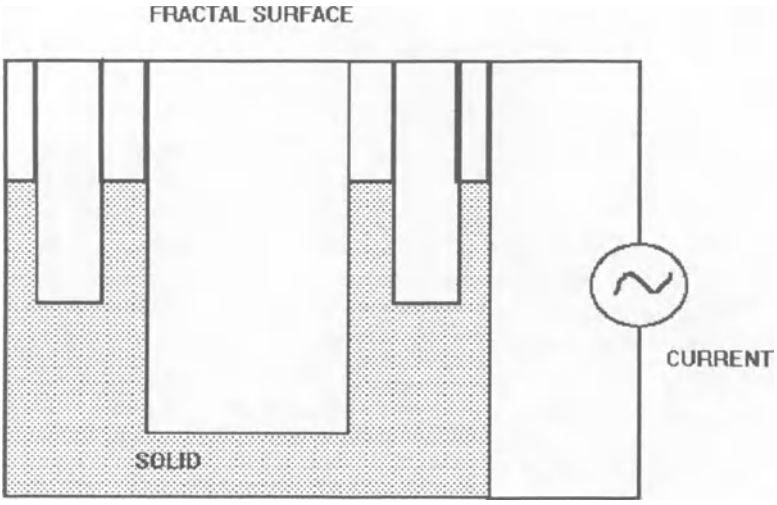

Figure 3.3. A fractal electrode with current characteristics determined by the Cantor set (see text).

1990). The dimension of this electrode surface is $D = 2 + \log 2/\log f_m$. When current is measured, it branches from the bottom to the top. The resistance measured increases by the ratio f_m in each branch. By combining the capacitance, one can write an expression for the impedance of this electrode surfaze, Z (Takayasu, 1990):

$$Z \propto w_f^{\alpha} \tag{3.20}$$

where $\alpha = 1 - \log 2/\log f_m = 3 - D$.

Other diverse electrochemical reactions that have been analyzed by nonlinear dynamics are: electrode dissolution of copper in an acidic environment (Albahadily *et al.*, 1989; Schell and Albahadily, 1989); the oxidation of formaldehyde or formic acid on a platinum surface (Xu and Schell, 1990). All of these electrode systems have exhibited typical far-from-equilibrium behavior like multistability, oscillations (e.g., periodic, multiperiodic), and chaos. A simple three-variable model satisfactorily described the mixed-mode and the chaotic oscillations observed

during the reduction of indium(III) at a mercury interface, in the presence of thiocyanate.

This kind of correlation is very important for those who are investigating battery efficiency and performance. The investigations need to be expanded to include chemical kinetics in heterogeneous media, and further the entropy and the equilibrium thermodynamics (see Chapter 10). The dynamics of bioelectrode interfaces have also been analyzed by fractal methods (Onaral *et al.*, 1987). The analyses have been more tutorial than in-depth discussions. The implications of the interfacial electrical properties in bioelectric stimulation and sensing and in the design of new-generation chemical sensors are summarized. Mathematical models showing the fractal nature of the interface dynamics are also discussed.

3.5. Phase Transition and Critical Point

Matter consists of molecules in motion. The distance traveled by a molecule before hitting another depends on the structure of the matter (see Chapter 1). The state of all such materials is defined on the basis of distance between molecules, since both the attractive and the repulsive forces are determined by the average distance between molecules. In order to follow a phase change, it is useful to consider the distance between two molecules in each phase. As an example, consider the differences between distances when molecules are either in the gas or liquid state. The volume occupied by 1 mole ($= 6 \times 10^{23}$ molecules) of water is:

Liquid state: 18 cm^2

Gas state: 22,000 cm^3

$Volume_{gas}/volume_{liquid}$: ca. 1000

From this we can estimate that the distance between molecules in the gas state is ca. 10 times larger than in the liquid state. The distance between molecules in the liquid phase is, in general, some 10% larger than in the solid phase. As a solid is heated, the molecular motion increases such that at the melting point, a very sharp change in structure is observed. This suggests that all of the

temperature input within a very short interval is converted into increased molecular motion (which was an increase in distance by ca. 10%). This is defined as the entropy effect (Berry *et al.*, 1980). As mentioned above, the state of matter that is approaching the transition region, the molecules that are going to change from $\text{phase}_{\text{solid}}$ to $\text{phase}_{\text{liquid}}$, must undergo rearrangement. The process of this rearrangement has been analyzed by different investigators.

Furthermore, in the vicinity of the critical point, many bulk properties (e.g., density, surface tension, specific heat, magnetization) of the material exhibit power laws. Phenomena observed near a critical point are referred to as *critical phenomena.* A mechanical variable that is undetermined, namely the density δ (Berry *et al.*, 1980) in the liquid–gas case, is referred to as the *order parameter.* At or near the critical point, these quantities or their derivatives are divergent. At the molecular scale, we may ascribe this to the divergence of the correlation length. Since the correlation length is a quantity that characterizes the system, the divergence implies that the system becomes invariant.

This is best described by the following. Water is added to a glass capillary tube such that the liquid phase fills ca. one-fourth of the container, and the container is then sealed. On heating, the liquid phase expands and the pressure inside increases. At the critical point (i.e., when $T = T_c$ and $P = P_c$), the liquid and gas phases merge into each other as an opalescent mass. The reason for this is that at the critical point, both of the phases exhibit identical physical properties (e.g., density, surface tension). In the case of water the critical temperature and pressure are 647 K (374°C) and 218 atm, respectively. The material exhibits opalescence owing to the random reflection of light of any wavelength.

A general relationship has been given, i.e., the physical property (e.g., density, surface tension)

$$(1 - X/X_c)^D \tag{3.21}$$

where X is the variable (temperature or pressure) and the subscript c denotes the critical point. The magnitude of D thus provides information about the fractal dimension of the measured physical property.

It is further observed that critical phenomena in many different materials near various kinds of critical points have quite a few features in common. This immediately suggests that near the critical point the molecular movements are in some way similar.

It is of interest to determine whether such a transition state of matter can exhibit fractal dimension. What we mean is whether the molecular movement during the change from one phase to another goes through some fractal structuring. As described elsewhere herein, the percolation problem is analogous to a phase transition fractal.

3.6. Percolation and Cluster Size Distribution: Basic Concepts

The term *percolation* is used to describe many different phenomena as regards fluid flow through porous media (and other systems such as insulators, ferromagnets). Actually a coffee percolator describes the process quite accurately, i.e., movement of fluid (water) through a porous medium (coffee). Another common system is water drainage in the earth. A qualitative description is that fluid moves through the porous medium (coffee or earth) and breaks up into small or large domains (also called ganglia in oil recovery processes). The movement of the fluid and its distribution within the porous medium, whether connected or disconnected, is the percolation termed *fluid flow* (Stauffer, 1985). If the pore size distribution is such that the fluid flows in connected form, this means the surface tension and the pore size are of some appropriate magnitudes. The pore surfaces are recognized to be irregular. The irregularities are also known to repeat themselves over several length scales or degrees of magnification. On the other hand, due to interfacial forces present in such curved fluid surfaces, the fluid may break up and become disconnected. The percolation experiments involve the investigation of these phenomena. The breaking up and rejoining of the fluid mass that takes place in the percolation process thus is a dynamic process. The percolation process is found in many types of disordered systems (Domb and Sykes, 1961; Broadbent and Hammersley, 1957), e.g., fragmentation and fractures, gels, forest fires, epidemic.

The forest fire and its relation to the distance between each tree is a good example for describing some of the principles involved here. If a tree catches fire in a forest, then it can ignite a neighboring tree only if the flames are large enough to reach the neighboring tree. However, if the distance between trees is large enough, then the fire cannot spread. House planning in Greenland is pursued similarly: If the maximum flame that can be produced around a house is say 10 m, then the flame cannot spread to a neighboring house situated 20 m away.

A more dramatic example is the observation that a balloon remains floating in air at the outlet of an air nozzle. This means that as air flows around the balloon, it gets fixed in position. A similar phenomenon is observed when water is injected into oil reservoirs in order to push the oil. In many cases, however, one finds that instead water flows around the trapped oil ganglia. These examples are comparable, but on a qualitative level.

More extensive results can be found in a recent review (Sokolov, 1986) of the studies of the dimensionality characteristics of percolation clusters. The purely geometric nature of a percolation phase transition and the great variety of the quantities exhibiting critical behavior make this geometric approach both informative and useful. In addition to the fractal dimensionality of a cluster and its subsets (such as the backbone, hull, and other dimensionalities), it is necessary to introduce additional characteristics. For example, the maximum velocity of propagation of excitations is determined by the chemical dimensionality of a cluster, and the critical behavior of the conductivity, diffusion coefficient, etc. is determined by spectral (or related) dimensionalities. Scaling relationships between different dimensionalities, as well as relationships between these and conventional critical exponents are discussed. The application of supercomputers to understanding fractal growth and form has become very important (Auerbach *et al.*, 1987). In the past few years, many physicists have developed theoretical models related to the clusters. The different questions addressed are: how can we give quantitative detail of the form of an object and what are the forces that are responsible for these phenomena? However, everyone concerned agrees that these model studies must be regarded with some reservation.

Let us divide the system into many lattice sites. We can then give names to each site. A site is randomly occupied with probability p, and randomly empty with probability $1 - p$. A cluster is denoted as a group of sites occupied with neighbors. A cluster thus indicates a continuous medium. A typical example is the process where water (flood) displaces the oil in a reservoir (Feder, 1988). The situation with $p_c = 0.59273$, which corresponds to a critical state, occurs when the oil phase breaks through (Bunde, 1986). This means that if oil is spread out in disconnected drops, then any medium surrounding it, like gas or brine, cannot push the oil as effectively as when oil is present connected (i.e., as ganglia).

It is known that in different processes the diffusion and percolation can look alike. As mentioned earlier, the phase transition is like many other processes. Let us consider percolation: an experiment that can be considered is fine metal powder distributed over an insulator. Under the condition that each conducting metal particle is separated from the others, no current can pass and therefore the surface is an insulator. The surface becomes conducting when all of the metal particles touch each other at a coverage of degree 1.

Between these two extremes there is found a critical ratio p_c, where the metal layer behaves as (Hughes and Ninham, 1983):

- An insulator when $p < p_c$
- A conductor when $p > p_c$

This is analogous to the phase transition where the system changes from phase I to phase II (see above).

The different stages of p values are shown schematically in Figure 3.4. Clusters of large size are depicted as dark areas. The values of p in panels (a) and (b) correspond to the insulator phase, or to the nonpercolating cluster. The stage in (e) obviously is the conducting cluster. The intermediate stages in (c) and (d) are near the critical point where we find rather large clusters that can conduct. Accordingly, the critical point, p_c, corresponds to the stage where with the smallest value of p we can start to observe conduction or percolation breakthrough. The magnitude of p_c in these experiments was found to be ca. 0.75.

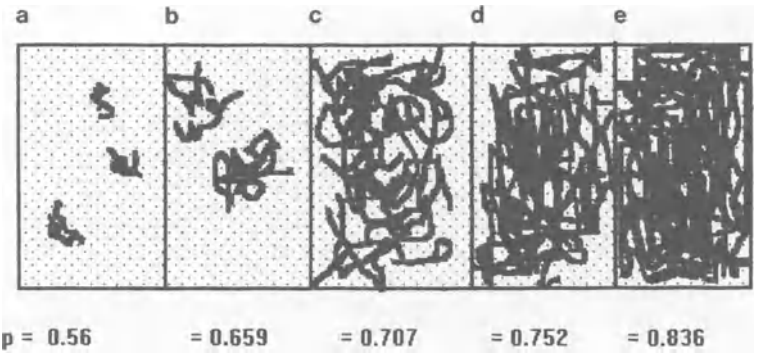

Figure 3.4. Schematic random metal configurations for different values of p. Dark shade indicates conducting phase. The metal is conducting in (e).

Now it becomes important to determine the fractal dimension of the cluster size. This is carried out by calculating the total mass, M_r, of a connecting metal cluster within a radius r:

$$M_r \propto r^D \tag{3.22}$$

[this is analogous to the procedure used when analyzing the size distribution of craters on the moon (Chapter 7)].

A detailed presentation of percolation theory is beyond the scope of this book, and the reader should refer to the more advanced literature (Kersten, 1982). It is known from the general theory that at a concentration p not too far from p_c, the mean-square distance between two connected point is finite. This particular distance is called the correlation length, η:

$$\eta \propto [p - p_c]^{-\nu} \tag{3.23}$$

where the exponent ν depends only on the dimension D of the lattice. A rather simple computer program has been described by Takayasu (1990).

Oil reservoirs: in the water-flooding process, the pores that are filled by the oil phase are going to be pushed by another fluid (i.e., water). This important process has been studied by percolation theories in the current literature (Feder, 1988).

4

Dendrite Growth and Fractal Dimension

The aggregation of molecules to form crystals is one of the most common examples both in nature and in industry. Analogous to the movement of gas molecules (Chapter 1), molecules in dense phases collide and invariably stick together to form crystals or dendrites. The crystals can be those of sugar, salt, copper sulfate, quartz or other minerals. The salt crystals (mainly NaCl) near the oceans are formed under the sun's heat and ordinary temperature and pressure. On the other hand, quartz crystals (dendrites) found in nature are formed over a long time scale and under very high pressure and temperature. Dendrite growth has been suggested to be an interface-controlled crystal growth process.

Theorists have long attempted to describe the complex spatial patterns found in nature, e.g., snowflakes or dendrites. The theory of dendrite growth has been described based on instabilities dependent on surface tension (Langer and Muller-Krumbhaar, 1978a,b). The dendrite growth mechanism, however, needs to be given more extensive attention. This is due to the fact that dendrite growth takes many millions of years, whereas most crystal growth processes in the laboratory last at the most overnight! This difference thus requires some other kinds of process kinetics that occur in the laboratory time scale. Furthermore, dendrites grow under very high pressure and temperature (conditions that are not

easily attainable in the ordinary laboratory). It is also recognized that surface tension acts as a stabilizing agent and prevents the formation of deformations. These lead to beautiful shapes (such as the sixfold symmetry in snowflakes) during the growth process. The reason why dendrites grow under well-defined paths is thus the main interesting feature. The diffusion-limited aggregation (DLA) and diffusion-limited deposition models have also provided a basis for the development of more extensive and realistic models for dendrite growth and solidification (Szep *et al.*, 1985; Vicsek, 1984, 1985, 1987; Nittmann and Stanley, 1986, 1987; Family *et al.*, 1987; Chen and Wilkinson, 1985; Liang, 1986).

Recent progress in the understanding of the structure of fractal aggregates has been reviewed (Jullien and Botet, 1987). After describing a typical aggregation experiment leading to fractal aggregates, the concepts of fractal and fractal dimension are introduced and experimental methods are described to measure the fractal dimension of aggregates. Then, the two main theoretical models, particle–cluster and cluster–cluster aggregation, are introduced, emphasizing their connections with experiments. Computer simulations have been used to describe the time evolution of a dendritic pattern growth mode.

Let us consider an experiment where a fluid is pushed into a solid in resin form, and then allowed to polymerize. In this way, one would be able to fossilize the viscous finger. In nature, such processes did indeed take place some millions of years ago. This refers to the so-called geological dendrites found in various clay or carbonate sediments (Figure 4.1). It can be argued that dendrites are formed by crystallization process in the finger (analogous to the viscous finger phenomena) after a pattern has formed.

4.1. Experimental Methods for Making Dendrites in the Laboratory

In a typical procedure, a solution of zinc sulfate ($ZnSO_4$) of concentration 2 M is placed in a petri dish (ca. 5 mm deep) (Matsushita, 1985). A layer (a few millimeters thick) of organic liquid (immiscible with water), such as *n*-butylacetate (BA), is

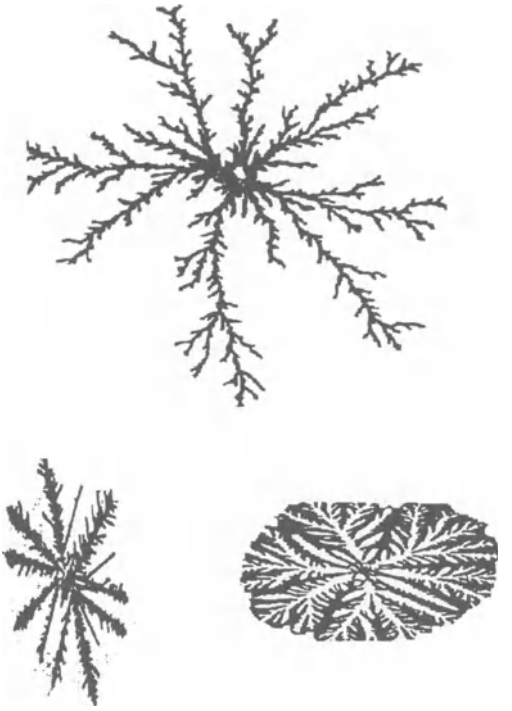

Figure 4.1. Typical dendrite shapes (schematic).

poured on top of the $ZnSO_4$ solution, thus giving an interface with very low interfacial tension [ca. 2 mN/m (=dyne/cm)]. The negative electrode is placed in the center of the dish, while the positive electrode (zinc) is placed at the edge (Figure 4.2). When a current of 5 volts is applied, a dendrite-shaped leaf forms after a few minutes. The magnitude of D is found to be ca. 1.7 [from the relation log(mass) versus log(radius)]. This compares with the magnitude of D_{finger} of viscous fingers, described above.

In another procedure (Matsushita *et al.*, 1984), experiments on the electrodeposition of zinc on a linear cathode were carried out. Rectangular cross-sectional pencil cores were used as cathode. In these metal forests the fractal dimension was also found to be 1.7, as expected from theory.

Copper has been deposited from aqueous $CuSO_4$ solution onto the exposed end of an otherwise insulated thin copper wire. A

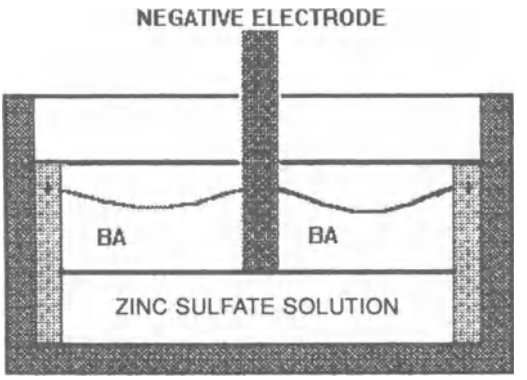

Figure 4.2. Experimental setup used for dendrite growth of Zn. BA, *n*-butylacetate.

polymer (polyethylene glycol) was added to avoid convection (by increasing the viscosity), while excess electrolyte (Na_2SO_4) was added to screen the electric field. The whole process thus is carried out under conditions where the growth is conducted by diffusion of copper ions to the cathode. The path followed by Cu^{2+} ions is governed by Brownian motion, due to the electric field between cathode and anode. The magnitude of D was found to be 2.4, which is somewhat larger than the previous values. The dendrites of $CuSO_4$ grown under similar conditions (Evesque *et al.*, 1986) have been investigated after digitization of the patterns.

The reaction that occurs is the dissociation of $CuSO_4$ into Cu^{2+} and SO_4^{2-} ions in aqueous media, which drift around randomly (Brownian motion). The copper ions that hit the cathode are deposited as copper after receiving two electrons ($Cu^{2+} + 2e^- = Cu$). The Cu^{2+} that contact any copper are also deposited. Assuming that these ions move in a random manner, following Brownian paths, the ions will more likely hit the exposed fingers rather than the protected interior of the dendrite. These dendrites have been described by DLA theory (Evesque *et al.*, 1986). Theoretical analyses showed some differences between this and the experimental data. This was ascribed to different factors. The DLA model is known to be an ideal model for describing electrodeposition. The model does not take into consideration any transport properties which could be very important. In the case of electrode-

position, the Cu aggregates have a loose, porous structure instead of a compact, crystalline structure. This would also lead to some degree of defects in the aggregates, and to an increase in resistance. This affects the current density, and thus the rate of deposition is faster at the end of radial branches than at the end of more tortuous branches having the same distance from the center. The inhomogeneous depletion of the Cu ion concentration during the deposition is another possible reason. Stirring is not feasible due to the fragile nature of the dendrites. In all natural processes, stirring is always absent.

The fractal analyses of such electrodeposition processes are of much practical importance. These experiments mimic processes that take place in batteries and similar systems (undercharging/discharging). In other words, both battery performance and lifetime could be investigated by means of such fractal experiments.

Precipitation fingers (Alsac *et al.*, 1990) can be obtained by pushing an aqueous solution of iron(II) sulfate ($FeSO_4$) at pH 3 into a clay suspension at pH 10. The ion Fe^{2+} (ferrous) is oxidized to Fe^{3+} (ferric) when the two fluids meet at the interface, where precipitation of iron(III) hydroxide [$Fe(OH)_3$] takes place as red-brown dendrites.

It is worth mentioning that various systems—e.g., aggregation of solids, viscous finger formation of fluid flow, lightning discharge, cracks in rocks, and the dendrite patterns—all have about the same magnitude of $D \approx 1.7$. These systems have also been analyzed by model simulations, stochastic models, and deterministic models. Dendrite growth has been analyzed by DLA theory (Evesque *et al.*, 1986). Typical copper aggregates are shown in Figure 4.3.

The patterns show a very strong radial symmetry. In these experiments, the dendritelike patterns formed branches of characteristic width, R_0. The magnitude of R_0 was 1–5 mm. R_0 was found to be related to the thickness of the electrolyte and the applied voltage. The patterns could not be reproduced exactly, thus the value of R_0 was varying. The data were analyzed by the mass versus radius relation:

$$M_R \propto R^D \tag{4.1}$$

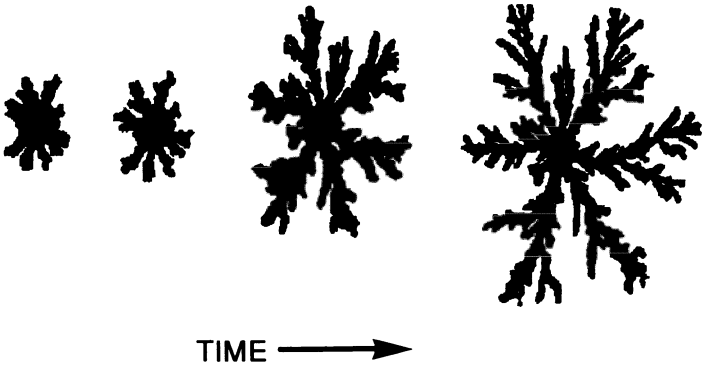

Figure 4.3. Copper aggregate patterns at different stages of growth. (Voltage = 2 volts; copper ion concentration = 0.5 M; complete time of growth = 50 h.) The patterns show a very strong radial symmetry. (Redrawn with modifications from Evesque *et al.*, 1986.)

The average value of D was found to be 1.6. It is to be noted that such shapes could not be analyzed by Euclidean geometry.

Studies on the fractal dimension of a fracture surface formed during slow stable crack propagation in steel have been reported (Long *et al.*, 1991).

4.2. Fractal Growth in Lipid Monolayers

When a very small amount of a virtually insoluble and nonvolatile organic substance is placed on the surface of water, which has a relatively high surface tension, either of the following results may be observed:

1. The substance may remain as a compact drop (or as a solid mass), leaving the rest of the liquid surface clean.
2. It may spread out as a monomolecular film over the entire available surface of water.

The formation of a stable monolayer by any substance is determined by the interactive forces between that substance and the subphase, i.e., water. In other words, a stable monolayer is formed when the work of adhesion between the substance and

water is greater than the work of cohesion of the substance itself. Under these conditions, the substance spreads over the entire available water surface and forms a stable film. Similar energetic considerations would apply for the formation of monomolecular films for other interfaces (Birdi, 1989), e.g.,

- Oil–water
- Mercury–water
- Solid–water (or other fluid)

The lipid molecules (amphiphiles) are known to form stable monomolecular films when spread on the surface of water (Chattoraj and Birdi, 1984; Birdi, 1989). This is a two-dimensional arrangement of amphiphiles as formed at the interface of air–water (or oil–water). The alkyl chains pack together avoiding water molecules, while the polar part of the lipid molecule interacts with water molecules (through hydrogen bonding). In some cases we find liquid-crystal structures (Birdi, 1989, 1992). These monolayers of lipids have been found to be useful cell membrane models. It is remarkable that a few micrograms of lipid (such as fatty acids, fatty alcohol, or lecithin) is enough to cover a few hundred square centimeters. The molecules rearrange to form a monomolecular film. The growth of such two-dimensional assemblies thus is an important system for investigation, as regards the fractal geometry.

In these two-dimensional monolayers, fractal growth of crystalline domains in phospholipid [L-α-dimyristoyl-phosphatidylethanolamine (DMPE); Miller and Mohwald, 1987] and fatty alcohols (Birdi, 1989) at an air–water interface has been observed. In the former studies, a fluorescent dye was used to visualize the crystalline domains. The magnitude of dendritelike domains was found to be 1.5. This suggests that the growth mechanism may be determined by the two-dimensional diffusion of dye from the solid–substrate boundary of the phospholipid. Analogous investigations of organized assemblies of lipid (palmitoylphosphatidylcholine) vesicles have been reported (Lianos, 1990). Also consistent with these results is the finding that emerged in a lattice-based study of sequestering and the influence of domain structure on excimer formation in spread monolayers (Politowicz and Kozak, 1988). In these monolayers, the changes in lifetime of

the diffusing, excited-state monomer probe molecule, studied experimentally by monitoring the excimer-monomer steady-state photoexcitation of the probe, were examined. An overall conclusion was that the lifetime of the probe molecule was always longer on domains of lower coordination valency. More studies are needed at this stage, in order to understand these two-dimensional fractal growths in monolayers.

4.3. Fractal Character of Interfaces

In many different natural systems, it is apparent that various processes take place at the line of contact between a liquid phase and a solid phase. Although much interest has been shown regarding the fractal structures in bulk phases, much less has been reported about these structures at interfaces (e.g., gas–solid–liquid or liquid_1–solid–liquid_2). The molecules in the liquid phase can move larger distances than those in the solid phase. Therefore, since the molecules in the solid phase are well fixed, it is in general not possible to study the surface forces of the solid phase in the same way as for the liquid phase. Furthermore, there exist surface defects and irregularities on a solid surface that account for such special properties as catalysis. The interfaces play a very important role in diverse industrial fields, especially in the heterogeneous kinetics of catalysis and their overall selectivity (Meakin, 1986). In a recent study (Pospisil, 1988), the AC technique was applied to the investigation of the growth of a compact film of bis(2,2′-bipyridine) cobalt(II) perchlorate at the mercury–aqueous solution interface. From the capacitance (C) versus time (t) measurements, it was concluded that the electrode exhibited surface roughness, which affected the electrode impedance. A model based on a rough surface with grooves and pore branches was developed, in terms of fractal geometry. The roughness effects are observed experimentally as the power-law dependence of the electrode impedance (Nyikos and Pajkossy, 1985):

$$Z_w \propto (iw)^{-\alpha} \tag{4.2}$$

Table 4.1. Hexagonal Surface Arrangement

	No. of particles (○)			
	○ → 7	○ → 49	○ → 343	○
Mass	7^1	7^2	7^3	
Size	3^1	3^2	3^3	

○ denotes particles.

where $0 < \alpha \leq 1$. The exponent α has a direct relation to the effective fractal dimension D as follows:

$$\alpha = 1/(D - 1) \tag{4.3}$$

as long as the deviation of the rough electrode surface from the smooth plane has an average self-similar property. Since the mercury drop electrode would behave as an ideally smooth interface with $\alpha = 1$, its use is suitable for detecting the fractal structure during the compact film growth.

The magnitude of D was found to be 2.14–2.16. In the case of a smooth two-dimensional surface, $D = 2$. Further, in the case of a rough surface with hexagonal packing, $D = \log 7/\log 3 = 1.771$ (Table 4.1).

The experimental value of D (=2.16) compares with the fractal structure obtained by dividing a square (or cube) by a factor of two, thus producing four subsquares (Matsushita, 1985). One of these squares survives, while the other three squares are again divided by two, and so on. This gives a fractal of dimension $D = 2.16$. This is in agreement with earlier observations that the fractal nature of objects can be experienced over a large range of dimension. More investigations are needed in order to evaluate D for different electrochemical systems with other crystallographic structures.

5

Porous Solid Media (Fractal Surfaces)

The porous media are of much importance in different aspects of technology, e.g., geoscience (evolution), oil recovery, catalysis, water seepage and drinking water treatment, chromatography [high-pressure liquid chromatography (HPLC)]. At the microscopic scale, chemical reactions in soil take place at the interface between water, air, mineral grains, and organic complexes; fluids through soils and rock pores. At the macroscopic scale, fluids are stored in reservoirs or move through rock fissures. Caves in limestones are the result of solution reactions involving dissolved carbon dioxide to enlarge initial weaknesses along joint, fracture, or rock inhomogeneities. A major theoretical and practical difficulty with heterogeneous porous media is the problem of relating laboratory-scale data to the field scale.

The problems of porous media are now being analyzed using fractal models. In some cases, as in oil recovery, it is necessary only to be able to model a reservoir that is situated perhaps 5 km deep. Furthermore, porous materials, aggregates, and ramified structures are known to exhibit frequently self-similarity, i.e., their structure is associated with power-law density–density correlation function.

In the past (Reich *et al.*, 1990), the measurement of surface areas and pore volumes of porous solids by gas adsorption and liquid intrusion (Hg porosimetry method) has led to variable and

often ambiguous results. The range of surface areas of solids is rather large, i.e., ca. 1000 m^2/g (e.g., active charcoal or talc powder) to a few square meters per gram (e.g., most powders used in paints) (Chattoraj and Birdi, 1984; Birdi and Vu, 1991). A powder, or solids in general, are characterized by surface roughness. The detailed nature of a solid surface is studied by adsorption. The variable surface roughness is naturally of much interest, as regards the surface interactions. For example, the surface areas appeared to vary enormously according to the method used to determine these areas (e.g., using either N_2 or CO_2 as adsorbed gas) (Unger *et al.*, 1987; Birdi, *et al.*, 1991; Birdi, 1992).

Furthermore, soil physicists have been applying in recent years the scaling methods in an attempt to rationalize the heterogeneity and nonlinearity they encounter when studying the movement of water through soil (Miller, 1980). These procedures have been applied in situations where the movement of soil water is constrained only by the physical dimensions of the porous media. For example, scaling soil-water movement from a fine silt to a coarse sand allows demonstrations and laboratory experiments to be speeded up greatly. Scaling methods were found to be less successful, however, when adsorption and movement of water are governed by chemical and physical properties that result from different kinds of soil particles and their size. For example, the finest soil particles ($<2\,\mu m$) are very often clay colloids whose physical behavior is strongly dependent on their crystalline structures. This behavior is often well understood, and it is not necessarily helpful to adopt a fractal approach for their analysis. Further, recent work suggests an analogy between viscous fingering at an infinite viscosity ratio and diffusion-limited aggregation (DLA), and hence that the fingers may be fractal with D = ca. 1.7 (in two dimensions). This observation leads to some unanswered questions regarding the nature of the fingered patterns at a finite viscosity ratio. In some analyses the rock has been modeled as a lattice of capillary tubes of random radius through which miscible displacement takes place. The fractal dimension has been found to be important as it gives a measure of the efficiciency of oil recovery processes.

The surface roughness can thus be easily compared (qualita-

tively) with the coastline problem previously described, and hence the fractal surface. The surface adsorption processes are well defined, as discussed in various surface chemistry textbooks (see References). We will mainly be concerned here with adsorption processes where no chemical reaction takes place (systems where reactions occur on solid surfaces are discussed elsewhere).

It has been extensively reported that there is good reason to expect fractal structures in natural geological or artificial porous media. The interfacial phenomena at the fluid–solid interface will be described below. The porous solid can be expected to exhibit fractal features at three different levels:

- The pore space
- The solid phase
- Solid–pore interface

This clearly shows the complex nature of porous solid surfaces. It is accepted at this stage in the literature that flow in porous media is not satisfactorily understood due to the absence of an adequate description of the material itself and due to the difficulty in its mathematical analysis. However, it is hoped that fractal analysis will provide one key to a more complete description of these media.

A systematic treatment of microstructure has been proposed (Avnir, 1989). This structural level of solid matter includes all features that do not belong to the bulk structure, or phase structure (crystals, gas). Zero to three-dimensional discontinuities in the phase structure are defined as microstructural elements. Prototypes of two-phase microstructures are dispersion, net, cell, and duplex. Further, it has been recognized that a high-energy particle colliding with lattice atoms would create a disordered region of damage and that the central region of this damage would be rich in vacancies while the outer part would be rich in interstitials (Williams *et al.*, 1987). Fractals thus have enabled the recognition of a characteristic structure in the spatial distribution of the vacancies and raise the issue of describing the order of electronic features due to this cascade structure. There may exist microstructural order, gradients, anisotropy, as well as mixtures and transformations of microstructural elements and types. Microstructural energy is given

by the product of the density of a microstructural element and its specific energy. The scale of microstructure must be based on relation to properties. Fractal analysis may become useful for the description of rugged, fissured, and branched microstructure.

The pore space of various sandstone specimens was found [from scanning electron microscopy (SEM)] to be fractal, with D in the range of 2.57–2.87, with pore size ranging from 10 nm to 100 μm.

The method used to estimate the fractal dimension of any surface is based on the determination of the number of objects (molecules) of a given size that would completely cover the surface (Figure 5.1). Furthermore, one then also determines the relation between the size of the object used and the effect of the latter on the number. It is obvious that the excluded volume, V_{EX}, would be larger the larger the size of the molecules adsorbed. The various methods that have been used are:

- Molecules of varying sizes (Avnir *et al.*, 1984)
- Numerical simulations (van Damme and Fripiat, 1985; van Damme *et al.*, 1986a,b; Fripiat *et al.*, 1986)
- Latex spheres and polymer molecules (Brochard, 1985).
- Capillary length as the yardstick (Lenormand *et al.*, 1987)

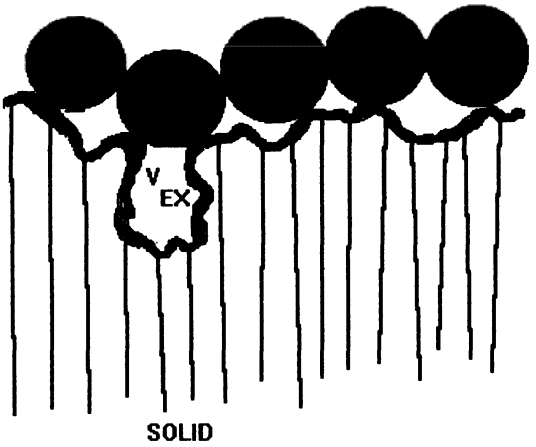

Figure 5.1. Surface coverage of porous solids and the excluded volume (V_{EX}).

5.1. Oil Recovery Processes

Many millions of years ago, forests or materials such as shells were buried in the earth. Depending on the conditions of pressure and temperature, one now finds either coal, oil, or gas. Oil [a mixture of alkanes (mainly) plus some phenyl derivatives and larger molecules such as asphaltenes] and gas (mostly methane, CH_4) are found under the earth's surface (at depths of ~100 m to ~5000 m) in pockets where it has been trapped, unable to move on its own accord (generally under the pressure of gas). The reservoir rock consists of pores of variable size (ca. 10 μm) and shape (noncircular). The efficiency of oil recovery is determined by different physical and geological aspects. The main factor that is generally investigated is the flow of gas or water as it pushes oil through the narrow pores. Knowledge of the exact pore size and shape thus becomes of much importance. It is generally accepted that the average shape of pores in the oil reservoirs is indeed noncircular (i.e., mostly rectangular) (Birdi *et al.*, 1987). In many oil recovery processes, chemicals such as acids are routinely injected into oil reservoirs in order to activate the production (Daccord, 1989). After reaction, the acid produces unstable patterns consisting of highly ramified empty channels. Fractal analysis of this has been reported by various investigators.

The flow is intrinsically unstable for the same reason that viscous fingering is; i.e., as some rock is dissolved, the permeability increases, giving rise to enhanced fluid flow. This increase further increases the dissolution rate. This is the kind of perturbation we have mentioned elsewhere, which changes a smooth flow into a more chaotic one. In the case of reservoirs, very conductive channels ("wormholes") are formed that bypass completely most of the rock matrix.

The multiphase flow in porous media and fluid models of geological hotspots have been reviewed (Lumley *et al.*, 1988; Feder, 1988). The analyses have been aided by digital image processing in flow visualization and secondary instability of boundary layers. The various subjects that have been covered are: fractals in fluid mechanics; multiphase flow in porous media; fluid models of geological hotspots; remote sensing of the sea surface;

initial stage of water impact; surf-zone dynamics; sand transport on the continental shelf; foam flows; instability mechanisms in shear flow transition.

A completely different aspect of oil recovery—the effects of waves on the offshore structures—has become an important area of investigation (Thompson and Stewart, 1988). It has been found that mooring towers exhibited unexpected subharmonic resonance in steady waves. The buoys are actually inverted pendulums. The mooring gives rise to two opposite forces: buoyancy plus mooring and plain buoyancy.

5.2. Fractal Surfaces of Solid Porous Media

The surface property of a solid is characterized by the nature of the surface boundary. A detailed investigation of the surface is necessary because the geometrical arrangement of molecules at the surface is different from that of molecules inside the solid. The surface boundary is expected to be related to its fractal dimension, D, as well as to the pore space. These characteristics can be separated into different fractal spaces (Figure 5.2) (Pfeifer, 1985; Pfeifer and Obert, 1989):

- Mass fractal
- Surface fractal
- Pore fractal
- Subfractal

The power-law relationship's dependence on radius, R, can be given as;

$$M_{\text{mass}}(R) \propto R^{D_{\text{mass}}} \tag{5.1}$$

$$M_{\text{surface}}(R) \propto R^{D} \tag{5.2}$$

$$M_{\text{pore}}(R) \propto R^{D_{\text{pore}}} \tag{5.3}$$

The different fractals (mass, surface, pore) are related as follows.

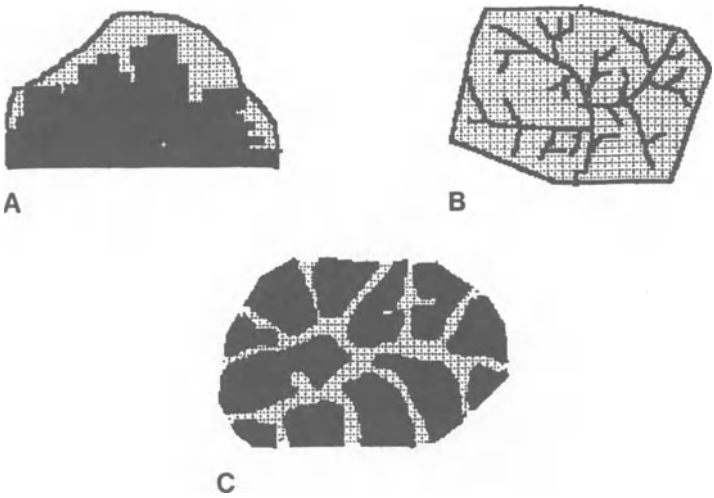

Figure 5.2. Schematic description of the different fractals in porous solid surfaces: (A) Surface fractal; (B) mass fractal; (C) pore fractal.

The values of D, D_{mass}, and D_{pore} can be estimated from such experiments as monolayer capacity, multilayer adsorption, porosimetry, and small-angle scattering.

The Cantor set has also been used to describe the porous structure (see Chapter 1). A three-dimensional porous medium is obtained as given in Figure 5.3. This porous structure is spatially periodic at a large scale and fractal (with $D = 0.63$) at a small scale. The porous medium represents such structures as formed by random packing of solid particles that are identical, such as spheres or needles. Other shapes and forms can be easily drawn by using the Cantor set with a different fractal dimension.

The simple procedure used here to construct such three-dimensional fractal solid surfaces thus shows that the Cantor set can be easily used to draw different forms of fractal surfaces. At this stage, more investigations using this procedure are needed to describe the pore size and distribution of solid surfaces. The Cantor set seems to be very useful for describing such systems. We thus are able to draw by a simple set of rules a shape with a well-defined

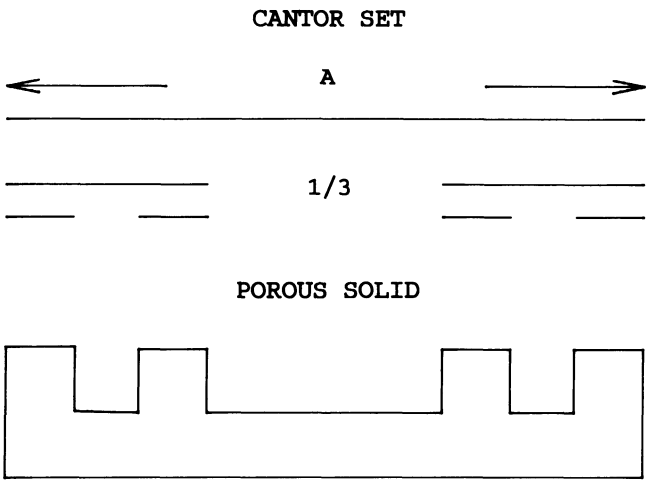

Figure 5.3. The Cantor brush of porous medium (D = 0.63); various geometrical parameters are indicated.

fractal dimension. This example has considerable use in a vast number of systems, as mentioned herein.

As described earlier, geological phenomena are expected to be fractal. It is therefore of interest to determine whether the pores found in rocks exhibit such property. This was analyzed (Bale and Schmidt, 1984) for the case of pore surfaces of lignite coal, and the X-ray scattering data were found to fit the relation:

$$\text{Scattering vector } (S_q) \approx q^{D-6} \tag{5.4}$$

where the scattering relation is the same as described for colloidal aggregates. The magnitude of D was found to be 2.56:

$$\log(\text{scattering intensity}) = 4 \log(\text{scattering angle}) \tag{5.5}$$

Other investigators (Wong, 1985; Wong *et al.*, 1986) have described these scattering data as indicative of rough pore surfaces. The fractal value of sandstone and shale were of magnitude 2.55–2.96, dependent on the rock (Wong *et al.*, 1986).

Surface fractal analyses of coal. An important example of much interest is the surface of coal. Coal is by far the most

abundant source of energy available to man. Its surface is both porous and of very small particle size. The necessity for coal gasification and pollution control has made information about its surface structure of great importance. The combustion reactions of coal (Mohanty *et al.*, 1982; Kerstein and Bug, 1986) can be described as follows:

- Reactions at the outer surface (so-called burning)
- Reactions occurring inside the particles (so-called fragmentation)

The extent of diffusion and reaction will determine the mechanisms involved, especially the reaction products. The combustion has been suggested to lead to the opening of the pores. This leads to more and more fragmentation of the solids. These considerations also apply to analogous systems, such as gasification of straw.

Furthermore, one of the most important groups of porous solids is the so-called amorphous carbon-based materials such as charcoal, activated carbon, and coal. In fact, as far as coal and coal-based materials are concerned, it is usually maintained that their single most important physical characteristic is their surface morphology. In other words, the pore structure mainly determines both the mechanical strength and the access and egress of reactants and products in coal processing.

These models have been applied to the opposite processes, i.e., plugging of porous media. This occurs in the removal of SO_2 or H_2S from smokes by reaction with calcinated limestone (Simons and Garman, 1986), and in deposition of coke on a catalytic pellet.

The use of both small-angle X-ray (SAXS) and neutron scattering (SANS) to characterize porous solids has a long tradition. The use of SAXS to measure porous structure has several advantages over other methods where adsorption or intrusion is used:

- It is nonintrusive.
- No drying or pretreatment such as degassing is needed.
- One can study under dynamic conditions.
- Both open and closed pores can be measured.

However, the disadvantages must be considered:

- Both open and closed porosity are measured, while only open pores may be of interest.
- Only certain length scales may be probed.

However, a combination of gas adsorption [Brunaer–Emmett–Teller (BET) method] liquid intrusion, and SAXS could be the most useful, but obviously a tedious procedure. The X-ray intensity is dependent on the surface morphology. A typical log (intensity) versus scattering angle plot shows a good fit when the assumption is made that $D = 2.44$ (Reich *et al.*, 1990). The different carbon samples that were analyzed by this procedure (Table 5.1) showed varying magnitudes of $D = 2–3$. It has been pointed out that this analysis is of global character and does not describe any of the geometrical shapes. This is due to the fact that in coals there are present some molecular-sized systems. Fractal dimension will be present over a given range of length scales. These data indeed indicated that D may be different for different length scales. Correlation between these fractal dimensions and the combustion rates and efficiency remains to be investigated.

In order to apply SAXS under dynamic conditions, the oxidation of a high-rank coal in a stream of oxygen at 100°C was followed as a function of time (Table 5.2). The data showed that as oxidation proceeded, the magnitude of D decreased slightly (because of the smoothening of the surface) and the surface measure increased (since the pores become more and more open). A similar

Table 5.1. Fractal Data on Porous Carbon-Based Materials[a]

Material	D	r_{max}	r_{min}
Activated charcoal	2.05	4000	305
North Dakota black coal	2.08	2900	370
AJAX activated charcoal	2.21	2800	390
Lignite coal	2.54	3900	230
Brown coal	2.86	4100	520
Glassy carbon film	3.04	3900	420

[a]Source: Reich *et al.* (1990.)

Table 5.2. Change in D versus Time for Oxidized Coal[a]

Days of oxidation	D	r_{max}	r_{min}
0	2.25	2500	390
5	2.05	1300	150
10	2.02	3900	250
20	1.93	4400	250

[a]Source: Reich *et al.* (1990).

trend has been reported for the activation process of charcoal (Avnir *et al.*, 1983).

In the case of porous media (coal), reaction can take place within particles that have accessible porosity. The behavior depends on the relative importance of the reaction outside versus inside the coal particles. Knowledge of the porosity of particles is thus of much importance.

Fractal analyses of porous sandstone surfaces have been carried out using SEM (Katz and Thompson, 1985). The value of $D = 2.78$ was reported (over three to four orders of magnitude; lengths ranged from 10 nm to 100 μm]. From these data, the relation between porosity, φ, and D was given as:

$$\varphi = (l_1/l_2)^{3-D} \tag{5.6}$$

where l_1 (=20 Å) is the lower cutoff of the pore space and l_2 is the upper cutoff (Table 5.3).

Table 5.3. Magnitude of the Fractal Dimension of Porous Rocks[a]

			Porosity (%)	
Sample	D	l_2 (μm)	Calculated[b]	Measured
Sand #965	2.57	2.5	4.7	5.45
Sand #466	2.68	6	7.6	7.3
Coconino	2.78	98	10	11.8
Navajo	2.81	50	15	16.4
St. Peters	2.87	50	27	26

[a]Source: Katz and Thompson (1985).

The exact pore shape and size distribution is not known completely for any solid. Therefore, the relationship given in Eq. (5.6) has been criticized (Roberts, 1986; Katz and Thompson, 1986), and needs further investigations (Birdi and Vu, 1991b).

Flow of liquid around fractal structures. The process by which a fluid flows around a porous medium with fractal structure is an important phenomenon. The flow of fluids with suspended particles is another area of theoretical and practical interest (drinking water treatment).

5.3. Molecular Fractal Surfaces

5.3.1. Porosity and Adsorption

Finely divided, powdered materials have been characterized by adsorption studies. Powdered materials generally exhibit a variable degree of roughness and a diversity of pore shapes. The application of fractal models to such surfaces is of much interest and necessity.

In the case where the surface area is estimated by measuring the amount of gas adsorbed [the well-known BET method (Adamson, 1982), described below], the molecules adsorbed on a rough solid surface may be depicted as shown in Figures 5.1 and 5.4. It is obvious that according to this the excluded volume, V_{EX}, will be related to the radius of the molecules. Multilayer adsorption data on a fractally rough solid surface have been reported (Pfeifer *et al.*, 1989). Hence, adsorption studies carried out by summing molecules of varying radius provide much information about the surface fractal structure.

5.3.2. Molecular Fractal Surfaces

An exact description of solid surfaces at the molecular level has been very difficult. The task is even more complicated when materials used in the catalysis are probed. These materials exhibit such a variety of porous surfaces that the analyses are far from satisfactory (Birdi and Vu, 1991b; Christensen and Topsøe, 1989).

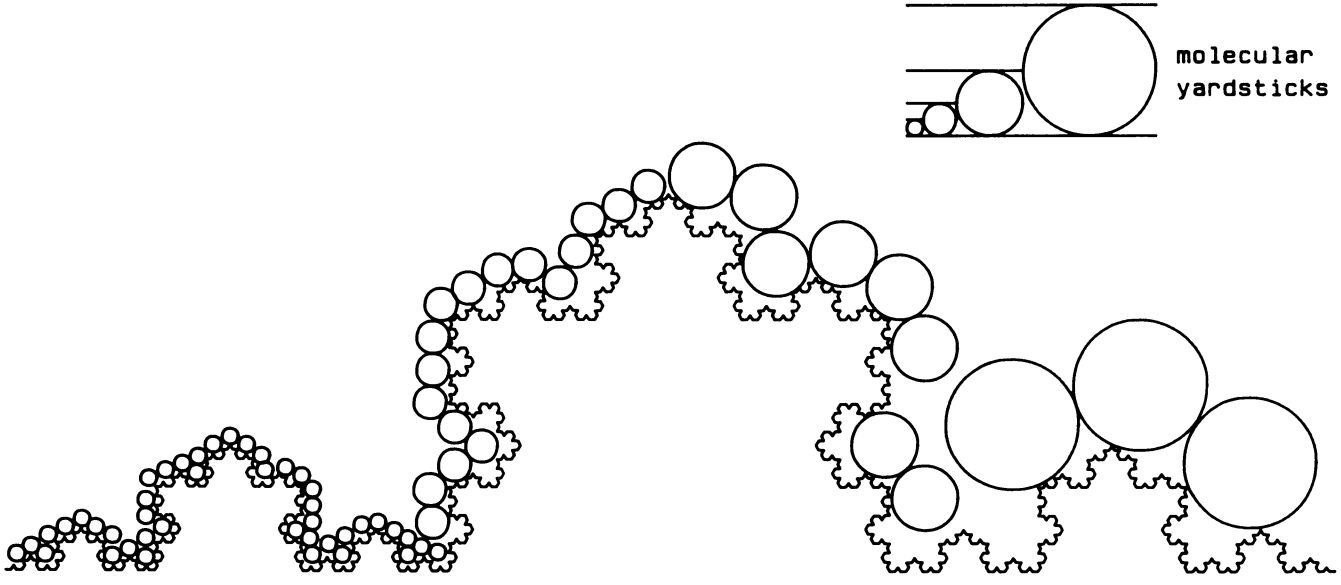

Figure 5.4. A schematic diagram of a monolayer of molecules (of radius r) covering a rough solid surface. (Christensen and Topsøe, 1989).

Recent studies have shown that porous materials often have fractal internal surfaces (Ridgefield, 1987). A brief review is given as to what fractal surfaces are, how they are observed experimentally, why they form, and how they affect the AC electrical transport properties through the media. Theoretical results are compared to real systems such as sedimentary rocks and rough/porous electrodes.

Since the information needed is necessarily in the dimension range of simple molecules such as methane or methanol, one may proceed by determining the adsorption of such molecules (Avnir, 1989).

The experimental data one obtains are based on (Adamson, 1982; Chattoraj and Birdi, 1984):

- n_{ads} = number of molecules adsorbed
- n_m = number of molecules adsorbed at monolayer coverage
- P = pressure of gas

These data are analyzed by using the Langmuir adsorption equation:

$$n_{ads} = (n_m bP)/(1 + bP) \tag{5.7}$$

where b is a constant. The surface area (m^2/g) of a solid material, Σ, can be written as:

$$\Sigma = m_m N_A \sigma_0 \tag{5.8}$$

where N_A is the Avogadro number (6.023×10^{23} molecules/mole) and σ_0 is the area occupied by the adsorbent.

If we suppose that the specific surface of the sample depends on the *size*, δ, (form and shape) of the molecules adsorbed (Avnir *et al.*, 1983, 1984; Avnir and Pfeifer, 1983; Pfeifer and Avnir, 1984; Pfeifer, 1985; Christensen and Topsøe, 1989), then:

$$\sigma_0 = \delta^2 \tag{5.9}$$

The amount adsorbed for each molecule with δ_i is:

$$n_i \leftrightarrow \delta^{-D} \tag{5.10}$$

$$= \sigma^{-D/2} \tag{5.11}$$

As an example, the data regarding the adsorption of small alcohol molecules [assumed to be spherical (this needs further confirmation)] on silica are given in Figure 5.5. This plot shows the variation of millimoles of alcohols adsorbed at monolayer coverage versus the molecular cross section. The data fit the equation (Avnir *et al.*, 1984; Farin and Avnir, 1987):

$$\log n_m = \text{constant} - 1.5 \log(\text{area/molecule of alcohol}) \tag{5.12}$$

the slope gives $D = 3$. It is remarkable that the surface of silica, which is known to be very rough on the molecular scale, still fits the fractal equation. The size range of molecules employed varied from 18 to 35 Å^2. Further investigations need be carried out on the effect of temperature.

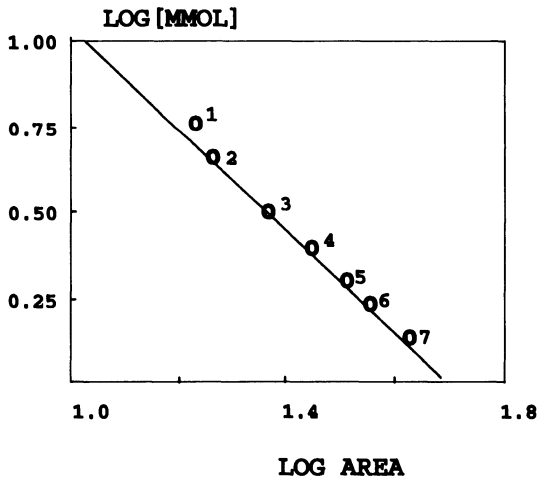

Figure 5.5. Adsorbed millimoles (millimoles adsorbed at monolayer coverage) versus cross section of molecules (adsorbents). 1, N_2; 2, CH_3OH; 3, CH_3CH_2OH; 4, $CH_3CHOHCH_3$; 5, $CH_3CH_3CH_3COH$; 6, $CH_3CH_3CH_3CH_2COH$; 7, $CH_3CH_2CH_3CH_2CH_3CH_2COH$. (Redrawn with modifications from Farin and Avnir, 1987.)

Table 5.4. Surface Area of Silicic Acid Solid Measured by Adsorption of Different Size Molecules[a]

Probe molecule	Cross section ($Å^2$)	Surface area (ζ) (m^2/g)
Methanol	19.9	540
Ethanol	25.5	474
1-Propanol	30.2	438
2-Propanol	30.8	450
1-Butanol	34.4	409
Nitrogen (BET)	16.2	590

[a]Source: Avnir *et al.*, (1983).

Another example is the fractal dimension of silicic acid powder. The amount of different molecules adsorbed from benzene solutions was measured (Table 5.4 and Figure 5.6).

The surface area estimated by this procedure thus is found to increase with a decrease in size of the adsorbed molecule (with the exception of 2-propanol). This is acceptable, since the surface roughness gives rise to this phenomenon. In order to estimate the

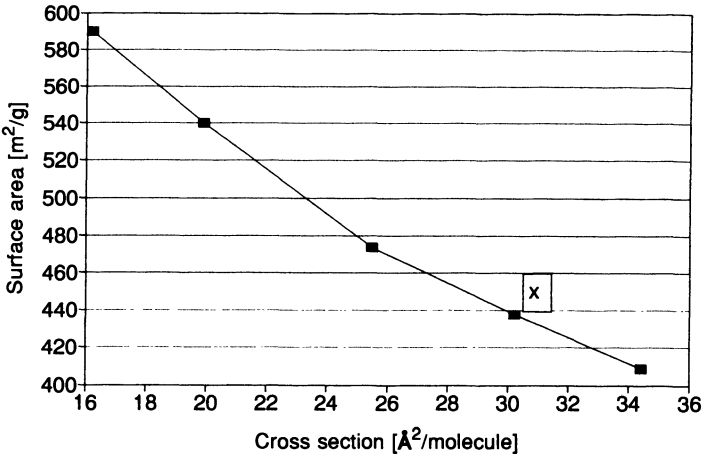

Figure 5.6. Fractal surface analysis of silicic acid powder from adsorption studies. (Redrawn with modifications from Avnir *et al.*, 1983.)

fractal dimension, the data in Table 5.4 were plotted as log A (surface area) versus log ζ (Figure 5.6) (Avnir *et al.* 1983). The slope of these data was found to be $-0.472[=2(2 - D)/2]$ (correlation coefficient 0.994), which gives $D = 2.94$. This value is very close to 3, where maximum coverage would take place, and indicates extreme wiggliness of this surface. Comparing the value of $D = 2.73$ for the Sierpinski gasket, we can conclude that these are similar fractal surfaces. It is also safe to conclude that in general, a high value of D indicates a very rough surface, which in turn means that the value of D would be strongly dependent on the size of the probe, as expected.

5.4. Estimation of Pore and Surface Analyses of Solids: Fractal Surface

In solids, pores that are much smaller than 1 nm in diameter are classified as micropores. These are responsible for the enhanced amount of adsorption observed on porous solid surfaces, e.g., activated charcoal. Further, in some cases they also lead to changes in the physicochemical properties of the adsorbed molecules. Theoretical and experimental studies of these microporous solids of high surface area are required in order to characterize their adsorption and surface properties. For example, nitrogen oxide is reported to be adsorbed as dimer on activated carbon fiber (ACF) (at 30°C; 0.8-nm-diameter micropores) (Kaneko *et al.*, 1987). In another case, the dielectric relaxation of water adsorbed in micropores (1.0-nm diameter) on porous jarosite was 500 times larger than that of ice (at 25°C).

As already mentioned, the micropore structures are not easily measured (Gregg and Sing, 1982). This is mainly ascribed to the fact that the Kelvin equation (which relates the curvature to liquid vapor pressure) is not valid in this region of pore diameter.

In recent studies (Ozeki, 1989), a new method was described that allows one to estimate the micropore structure. In this method, the pore structure of ACF was estimated from the adsorption of dye molecules with varying sizes and shapes. In these experiments, ACF was used after drying at 110°C for 2 h. The

Table 5.5. Different Molecules Used for Adsorption on ACF[a]

Adsorbate	Structure[b]	Molecular area (nm^2)	Amount adsorbed (mmole/g)	Specific area (m^2/g)
OII	$SO_3PNNFOH$	1.05	1.33	841
AR88	$SO_3FNNPOH$	1.2	1.06	766
MB	$Me_2NPNSPNMe_2$	1.0	1.38	831
CV	$[Me_2NP]_3C$	1.4	0.398	335
PCB		1.95	0.234	275
AR27	$SO_3FNNFSO_3SO_3OH$	1.40	0.223	188
NG	FeO_2NFSO_3	3.2	0.074	143
N_2		0.162	14.5	1410
C_6H_6		0.4	4.79	1155

[a]Source: Ozeki (1989).
[b] P, phenyl; F, naphthyl; Me, methyl.

power was equilibrated in dye solutions of various concentrations at 30°C. The amount of adsorbed dye was determined from the difference between the initial and the final concentrations (concentrations of dye were measured by spectroscopic method). The dyes used (Table 5.5) were adsorbed from solutions with concentrations lower than 5 g/liter (=ca. 5 mmole/liter). In this concentration range, one can assume that all dye is adsorbed. The adsorption isotherms are given in Figure 5.7.

The amount adsorbed at saturation from the Langmuir plot is given in Table 5.5. The magnitude of specific area as estimated from these dye adsorption data, assuming flat cross-sectional area (S_{dye}), is also given in Table 5.5. The data are compared with the N_2 (S_{N_2}) and benzene adsorption data ($S_{benzene}$).

In the case of charged dyes, and dyes of large size, we find weaker adsorption (e.g., AR27, PCB, NG, and CV).

In the case of OII, preadsorption experiments were investigated. The amount of N_2 adsorbed (as measured by weight) decreased with the preadsorbed OII. The specific area, S_{NO}, at an OII coverage Θ was calculated from a BET plot of the N_2 adsorption isotherm. S_{NO} corresponds to the N_2 surface area of ACF covered with OII molecules at 0 coverage.

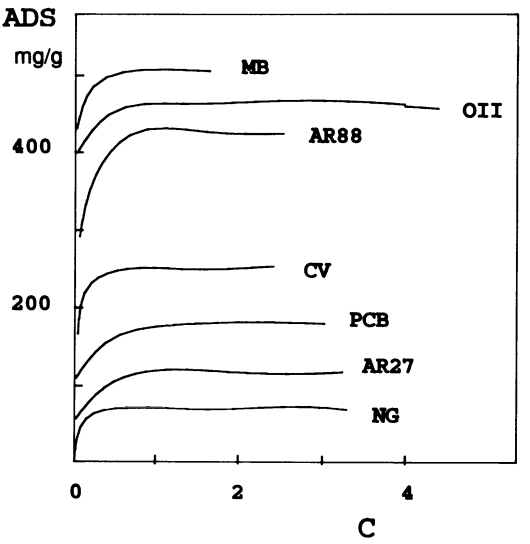

Figure 5.7. Adsorption isotherms of various dyes on ACF (at 30°C). MB, methylene blue; OII, Orange II; AR88, Acid Red 88; CV, crystal violet; PCB, Phthalocyanine Blue; AR27, Acid Red 27; NG, Naphthol Green. (Redrawn with modifications from Ozeki, 1989.)

The magnitude of S_{NO} decreased only slightly below $\Theta = 0.36$ (165 mg OII/g) and then decreased steeply to zero at coverage of $\Theta = 1$ (460 mg/g). The sum of S_{NO} and S_{DO}, on the other hand, first increased with dye adsorption and then decreased to S_{DO} at $\Theta = 1$, passing through a maximum at $\Theta = 0.36$.

The slopes of the S_{NO} versus Θ curve gave apparent occupation areas of a dye on ACF surface that are 0.94 nm^2 below $\Theta = 0.23$ (105 mg/g), and 0.4 nm^2 in the range $\Theta = 0.23$–0.36, and 2.04 nm^2 at larger Θ values (i.e., >0.36).

These data suggest that:

1. OII molecules adsorb on ACF instead of N_2 molecules when the coverage Θ is low.
2. N_2 adsorption occurs on adsorbed dye molecules with increasing Θ. This is expected, as the solubility of gas molecules in dye would be larger than on ACF.
3. When the degree of coverage $\Theta = 0.36$–0.75, each dye molecule adsorbed excludes twice its molecular area.
4. The changes in S_{NO} and $S_{NO} + S_{DO}$ with preadsorbed dye are related to the pore size distribution.

Furthermore, from these data it was found that the pore width decreased gradually from 0.9 nm for bare ACF to 0.85 nm at $\Theta = 0.93$. The pore size distribution was also analyzed. The width of the peak porosity was found to change from 1.08 mm for bare ACF to 0.95 nm for preabsorbed ACF.

As is well known, such adsorption phenomena are complex, due to solvation of the adsorbent and/or adsorbate, competitive adsorption with free ions or molecules, interactions between adsorbates, etc.

These data were analyzed by using the relation described earlier between the monolayer coverage, n_m, and the size of the adsorbed molecule, σ:

$$n_m \propto \sigma^{-D/2} \tag{5.13}$$

where we have the surface roughness or the surface fractal dimension, D. The log n_m versus log σ plot of the data in Table 5.6 gave a value of $D = 2.4$. The fractal dimension ($D = 2.6$–2.8) of three kinds of microporous carbon fibers has been measured from adsorption experiments (Kaneko *et al.*, 1991).

A recent study has reviewed the fractal geometry of fused pigment surfaces (Kaye, 1991) and fractal analyses of catalysts have been reported (Liu and Scott, 1991). The fractal dimensions of geometrically irregularly shaped solid surfaces have also been investigated by the adsorption method (Sokolowska *et al.*, 1989). An analytical and numerical study of the role of local surface

Table 5.6. Fractal Analysis of Rates of Dissolution of Solids in Liquids[a]

Material	Particle size range (μm)	D_R/D
Dolomite $CaCO_3$–$MgCO_3$	163–2606	2.15/2.9
Coral–$CaCO_3$	51–513	1.98/2.73
Quartz	45–1000	2.14/2.0
Silica	0.4–12.6	1.95/2.03

[a]Source: Farin and Avnir (1987).

defects and macroscopic inhomogeneities that might influence the diffusion-controlled reactive processes on a solid surface (Garza-Lopez *et al.*, 1990) showed that for both Euclidean and fractal surfaces (i.e., the triangular lattice and the Sierpinski gasket, respectively), the higher the local valency of the site at which the reaction occurred, the faster the rate. The surfaces that were considered were mainly of two types. First, the difference in reaction efficiency was ascribed to a regular versus a defect center. A very special example considered was the cell membrane. In the membrane, spatial inhomogeneities could be present due to the transmembrane proteins which break the translational symmetry and interfere significantly with the lateral motion of the diffusing molecule. Second, in the case of zeolites, mordenite has a channel structure that allows for two possible sieving mechanisms (suitable in size for small molecules or rare gases).

5.5. Reactive Fractal Solid Surfaces

In a recent study (Farin and Avnir, 1987), fractal analysis at the molecular scale of reactive solid surfaces was undertaken. It is obvious that the parameters expected to dictate the chemical reactivity of such fractal solid surfaces will be both numerous and quite difficult to separate. However, under these conditions, it is reasonable to expect that fractal analyses will be useful, as was also demonstrated. Different stages may be of primary interest in such systems. In some cases, one may be interested in the overall reaction rates. In other cases, the change in particle size distribution during the reaction may become essential. Lastly, the particle shape may change, which will induce some drastic effects.

It was argued that *a priori*, D_R would be expected to be smaller than the surface fractal dimension, $D_{surface}$. This would arise from the selective participation of surface sites in reaction, while on the other hand, heterogeneous reactions might show the opposite, i.e., $D_R > D_{surface}$.

As given above, the fractal surface area, $A_{surface}$, is proportional to its radius, R:

$$A_{surface} \propto R^{D-3} \tag{5.14}$$

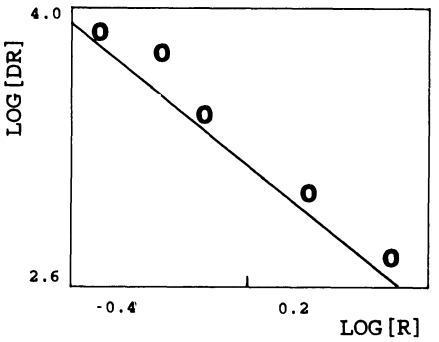

Figure 5.8. The rate of dissolution versus the particle size of tridymite (in 0.1 M HF). (Redrawn with modifications from Farin and Avnir, 1987.)

In the case where the absorbing species reacts with the solid surface, the process would be related to the effective reactive surface sites. In this analysis only the diffusion to the surface was considered, while the diffusion on the surface was neglected. If we now replace the quantity A_{surface} with the corresponding effective area, $A_{\text{effective}}$, we can rewrite the above equation:

$$A_{\text{effective}} \propto R^{D_R-3} \tag{5.15}$$

where D_R is the effective surface reactive fractal dimension of $A_{\text{effective}}$. Since the initial reaction of such a system is proportional to $A_{\text{effective}}$, the magnitude of D_R can be estimated from log (rate) versus log R.

The plot of such a system is given in Figure 5.8 (Table 5.6). The data show that D_R is not the same as D in most cases.

In the case of drug delivery, analogous fractal analyses on the dissolution rates have provided useful information (Loeppert *et al.*, 1984; Avnir, 1987). The magnitude of the dissolution rate of various drugs was found to give values of D_R of ca. 2. This indicated that the dissolution takes place at the outer surface of the drug powder or tablets. The fractal analyses will be useful to understanding the mechanisms of controlled drug release.

5.6. Fractal Dimension at Fluid–Solid Interface (Wettability and Contact Angle)

The process whereby a fluid comes in contact with a solid surface is very common in everyday life. At any interface formed

between two phases (e.g., liquid–solid, liquid–gas, oil–water), the adjacent interfacial multimolecular layers are subjected to an unsymmetric force field and consequently the interfacial tension is the net result of these forces. When a liquid contacts a solid surface, the molecules at the interface are of considerable importance regarding reactions taking place on the solid surface. As already described, the surface of a porous solid can be analyzed by fractal methods. Since the interface where a liquid or gas meets the solid surface will be dependent on the surface roughness, we also expect an interfacial fractal dimension. The fluid–solid interaction requires knowledge of the surface area of the porous solid.

The liquid–solid–gas (or liquid) interface has been described by many investigators (Chattoraj and Birdi, 1984). The proximity of different molecules in the two phases gives rise to interfacial forces with which the phases interact. This interaction creates a specific contact angle, Θ, at the liquid$_{l1}$–solid–liquid$_{l2}$ (or gas) interface:

$$\gamma_{s,l1} = \gamma_{s,l2} + \gamma_{l12} \cos \Theta \tag{5.16}$$

where surface tensions (γ) of the different interfaces are given for solid–liquid$_1$ ($s, l1$), solid–liquid$_2$ ($s, l2$), and liquid$_1$–liquid$_2$ ($l12$). The contact angle, Θ, is the angle obtained when all of the various interfacial forces are at equilibrium. A more extensive analysis of this equation can be found elsewhere (Chattoraj and Birdi, 1984). This is in fact an equation of state for the system gas–solid–liquid or liquid$_1$–solid–liquid$_2$.

In the case of rough solid surfaces, with fractal characteristics, the interfacial force balance as used in the derivation of Eq. (5.16) requires some modification. As seen in Figure 5.9, the contact angle is dependent on the surface roughness. A thermodynamic derivation has been published in which the area of the liquid–solid interface is a function of the fluid that contacts the fractal surface (Hazlett, 1990). The derivation is based on the reference state being a drop of liquid phase$_1$ (with radius R_0) that on the fractal surface spreads to give a contact angle Θ (with radius R) (Figure 5.10). The change in surface free energy, ΔG_s, is given as;

$$\Delta G_s = C\gamma_{s,l1}\sigma_1^{1-D/2} - C\gamma_{s,l2}\sigma_2^{1-D/2} + \Delta A_{12}\gamma_{l12} \tag{5.17}$$

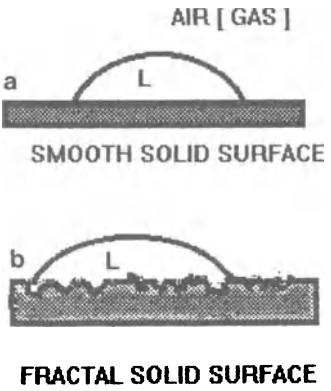

Figure 5.9. Contact angle at gas–liquid (L)–solid interface: smooth (a) or fractal (b) solid surfaces.

where σ_1 and σ_2 are the occupational area of molecular species 1 and 2, D is the fractal dimension, and ΔA_{12} is the change in fluid–fluid interfacial area. Based on these assumptions, the magnitude of cos θ was obtained as;

$$\cos \Theta_{\text{fractal}} = [(1 - \Gamma f^{1-D/2})/(1 - \Gamma)(\sigma_1/\sigma_2)^{1-D/2}] \cos \Theta_{\text{Euclid}} \quad (5.18)$$

where $f = \sigma_2/\sigma_1$, $\Gamma = \gamma_{s,l2}/\gamma_{s,l1}$, and Θ_{Euclid} = Euclidean contact angle.

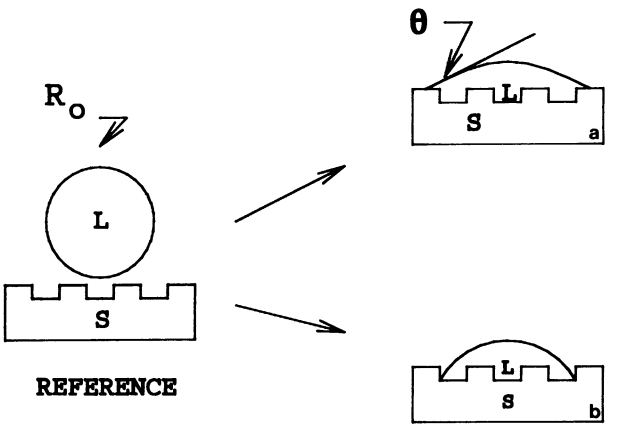

Figure 5.10. Change in surface free energy at the interface between a drop of liquid and a rough surface: (a) $\Theta < 90°$ (wetting); (b) $\Theta > 90°$ (nonwetting).

The application of both fractal and Euclidean concepts obviously requires some crossover point where an object ceases to be fractal. A correlation to the size of water molecules (10.8 $Å^2$) and alkane molecules was used in the analyses of wetting and oil recovery. Further, the degree of wetting or larger molecules (e.g., asphaltenes, 380–1100 $Å^2$) was analyzed.

With the reported differences in fractal and topological dimensions of reservoir rocks, these analyses suggest that such porous media will be either perfectly wetting ($\Theta = 0$) or perfectly nonwetting ($\Theta = 180°$) for most fluid pairs. For example, a fractal dimension of 2.14 is sufficient to shift the contact angle for water on a surface of polytetrafluoroethylene from 108° to 180°, assuming that fractal behavior is exhibited from atomic dimensions to the micrometer range. These results further showed that a new set of wettability indices for reservoir materials is needed, consisting of the fraction of each wetting phase and some measure of the spatial distribution of those types. This is analogous to the wetting phase saturation and scaling behavior for fractal pore models as a function of Laplace pressure (Alder *et al.*, 1985).

As far as oil reservoirs are concerned, it is worth considering the molecular yardsticks (natural) that are present in these systems:

Water	10.8 $Å^2$
CH_4	19.4 $Å^2$
N_2	16.2 $Å^2$
Asphaltenes	380–1100 $Å^2$

The smaller fluids will cover the surface of the reservoir solid better than the larger molecules, such as the higher hydrocarbons or asphaltenes. Analogous phenomena have been observed in other porous solid systems, such as cement or water reservoirs.

In oil recovery, aggregation and deposition poses a very difficult problem in production. Especially asphaltene is known to cause such problems due to its precipitation under certain reservoir conditions. The precipitation is related to the composition of the oil, pressure, and temperature. Fractal aggregation and deposition of heavy organics in petroleum crudes has also been recently

investigated (Park and Mansoori, 1988). The model was based on the concepts of continuous thermodynamics, theory of liquid–solid phase transition, fractal theory of growth, and steric colloidal collapse and deposition. The latter are analogous to the colloidal aggregation processes already discussed above. The phase behavior of asphaltene was discussed based on the kinetics of cluster formation. It is thus reasonable to believe that the cluster size distribution will determine such aggregation processes.

5.7. Gel (Fractal) Chromatography

In certain kinds of chromatographic separation methods, one uses cross-linked gels as the medium upon which the molecular separation takes place (Dubin, 1988). This section describes the potential of such chromatographic methods using gels. This involves the fractal description of the gel phases and the interfacial phenomena.

The liquid space can be accessible to a varying degree to the solvent molecules. This would limit the movement of the solvent molecules throughout the gel matrix. The interface between these regions would be expected to be fractal. The basic model is considered to be the cumulative pore volume, V_p, of the gel matrix, which is dependent on the number N of volume elements of size $f\epsilon^3$, where f is the form factor and ϵ is the measuring yardstick. Size exclusion chromatography and gel permeation are based on (Kuga, 1981; Sernetz *et al.*, 1989):

$$V_{p,\epsilon} = N/\epsilon^3 \tag{5.19}$$

The area of the matrix–liquid phase, A_ϵ, is given as:

$$A_\epsilon = d(V_\epsilon)/d(\epsilon) \tag{5.20}$$

i.e., change in volume with ϵ.

In a different approach, one can use the ϵ^2 elements, which gives:

$$A_\epsilon = Nf\epsilon^2 \tag{5.21}$$

Table 5.7. Fractal Dimension D_f of Gel Pores, Derived from Volume Distributions by Gel Permeation Chromatography[a]

Gel	D_f
Eupergit	2.2
Ultrogel	1.57
Sephadex G100	1.77
Polyacrylamide	1.48

[a]Source: Sernetz *et al.* (1989).

In principle, the separation of molecules on a gel matrix can be described by two different kinds of mechanisms: (1) differential interaction of the solutes with the surface of the stationary gel matrix (arising from adsorption and affinity), and (2) size exclusion chromatography, i.e., based on the different volumes accessible in the liquid and stationary gel phase for solutes of different molecular size. These studies clearly showed that the pore size distribution of gels is fractal.

In the case of size exclusion chromatography (Birdi, 1988), one assumes that there is no interaction (or negligible adsorption energy) between the solute and the gel phase. The magnitudes of the fractal dimension of four gels are given in Table 5.7.

5.8. Application of Fractal Chromatography to Biology

It has been proposed that these fractal investigations can be useful in explaining other biological phenomena. The reason is that the correlation between the self-similarity and the upper and lower limits and a log–logistic distribution, suggests a possible fractal phenomena. Examples that have been given are:

- General adsorption phenomena
- Cooperative enzyme kinetics
- Oxygen-binding isotherm of hemoglobin (Hill exponent)

- Heterogeneity of antibody affinities
- Antibody–antigen interaction
- Enzyme cascades in blood clotting
- Dose–response curve for the general drug–receptor interaction in pharmacology.

6

Fractals and Geochemistry

The fascinating world of patterns and shapes found in geochemistry is indeed worth analysis by the fractal model, since not too many of them can be analyzed by classical Euclidean geometry. Furthermore, since Brownian motion is known to play an important role in geoscience (especially in evolutionary processes), it is reasonable to expect that fractal geometry is useful analytical tool. The time scales involved are of such large dimensions (>1 million years) that newer analytical procedures are needed. The fractal nature of geochemistry is only beginning to be analyzed in more detail. For instance, the following phenomena have recently been examined:

- Landforms made by weathering
- Caves and coral reefs
- Size of islands
- Ore bodies and mineral distribution
- Pollution patterns (weather patterns)
- Earthquakes

The future application of fractal geometry to other geoscience phenomena will likely play a very important role in some of these systems. The reason for using fractal analysis in these systems is that it attempts to give a mathematical picture of seemingly complicated and chaotic structures and physicochemical phenomena. Since in all of these geochemical systems there is a varying degree of surface roughness, the fractal approach is quite logical.

The magnitude of D is expected to have remained constant over large time intervals (i.e., geological time scales). This may be analogous to the counting of rings in a tree. If there has been varying yearly weather, then both the distance between rings and the shapes are affected. This demonstrates geometrical analysis is useful for past ecological processes.

The dependence of pattern and form as mentioned above needs to be considered here in the case of thermatic maps of soil and geology. If the pattern of soil or geology of an area is mapped at a small scale, say 1:1,000,000, the surveyor will divide the landscape into mapping units that express the major sources of variation at that scale. However, if one part of the same area is mapped at a larger scale, say 1:1000, new details will appear that were taken to be uniform previously. This process can be carried further until one has reached a magnification such that different mineral accumulations are identified in thin sections of rocks or soil.

If the real data can be described by the Brownian fractal model, then there must be some validity in this procedure. The knowledge of the fractal dimension of a given geochemical phenomenon could be useful either for a scientific description or when estimating spatial patterns or amounts of resources. Clearly, the larger the fractal dimension, the less easy it will be to make smooth interpolations from point data using well-established conventional mathematical methods.

Some typical data as listed in Table 6.1 give convincing support to such analysis on the fractal dimension of a range of geochemical and geographical distribution. In another study (Gajem *et al.*, 1981), data of minerals in soil gave linear plots for a total area of 2000 m^2 (using dimensions of 0.2, 2, 20, and 200 m). The distribution of gold ore in South African mines has been analyzed by these procedures (Journel and Huijbregts, 1978).

Caves have been regarded as a kind of superpore structure formed by the chemical action of carbon dioxide-rich water on limestone rocks. Further, coral reef formation is in some ways the antithesis of caves. Coral rocks, where chemical deposition takes place, are the precursor of the limestone in which caves form. The surface area of coral reefs is very large. The magnitude of the

Table 6.1. Estimated Fractal Dimension, D, for Geochemical and Topographical Data[a]

Location	Property	D
Wales	Sodium/soil	1.8
Australia	Soil	
	Phosphorus	2.0
	pH	1.5
	Potassium	1.6
France	Iron/rocks	1.4–1.9
England	pH	1.7
Borneo	Caves	1.074–1.546

[a]Source: Burrough (1989).

fractal dimension of coral reefs was reported to be 1.13–1.16 (Laverty, 1987).

Further, it seems that the variation of many properties of soil and geology occurs over many different scales. The reason for this lies in the chemical, biological, and geological processes that shape the earth's surface (or for that matter other planets). The movement of clay in a soil profile may occur over a distance of a few hundredths of a millimeter to a few centimeters. The biological effects of plants and small insects such as ants may affect areas from a few centimeters to a few meters. The river erosion and sedimentation processes may occur over distances from a few meters to several tens of kilometers and the mountain-building processes of plate tectonics act at continental scales (over thousands of kilometers). It is obvious that the sum of all of these effects is the total observed.

6.1. Zipf's Law

Certain phenomena that show similarities can be described by the same fractal analytical procedure. For example, the frequency of words that appear in a text can be analyzed by Zipf's law (Takayasu, 1990). This power law gives a relation between the

probability P_X for the occurrence of X at N times:

$$\log X \propto \log (N - 1)^D \tag{6.1}$$

where $P_X \propto 1/X$. This is a fractal distribution with $D = 1$. This law has been applied in the analysis of mineral reserves, as follows.

6.1.1. Estimation of Mineral Reserves and Pollutant Levels

In general, the presence of minerals varies in different parts of the world. As more and more important minerals become scarce, it becomes very essential to have a useful prediction model. Analogous to the oil reservoirs, where one does find some geographical correlation between oil and other materials such as coal reserves, one would expect some correlation between mineral reserves and other materials or minerals in the surrounding earth.

The assessment of potential reserves of lead and zinc in India was made by using Zipf's law. This procedure could be used to extrapolate from the knowledge of existing deposits to the possible complete but currently unknown set of deposits around India.

The data in Figure 6.1 are irregular and appeared to fit no known distribution. However, by assuming a hyperbolic distribu-

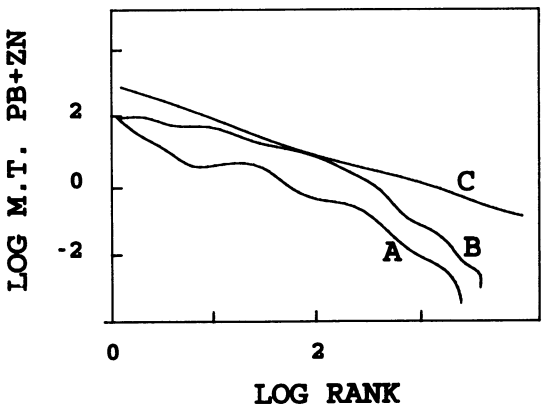

Figure 6.1. Lead and zinc abundance data analyzed by different methods. (A) Original data (+); (B) log-normal distribution; (C) using Zipf's law. (Redrawn with modifications from Paliwal *et al.*, 1986.)

tion, and assuming that there still is 18.7 million tons (twice the current largest deposit), then a reasonably good fit was found. It was concluded that only 25% of the total resources had been discovered. It was therefore suggested that further explorations be made (Paliwal *et al.*, 1986).

It may be argued that fractal analyses cannot be expected to completely map the actual picture of the deposits. On the other hand, one still lacks the relationship between any given geological or soil-forming process and the resulting actual patterns of distribution and their possible fractal dimension.

6.1.2. Soil and Atmospheric Pollution

We are all aware of the need to control and manipulate environmental pollution. Analogous to the mineral resources, one also needs to estimate the degree of pollution in soil, in order to assess and control the amount and distribution of toxic or dangerous materials in the ground. The main idea is to determine whether a given piece of land is suitable or not for a particular kind of usage (e.g., housing, cultivation). It is also clear that the movement of pollutants in the earth will not be easily described by any simple treatment. The same is true in the case of pollution in the sea or rivers or atmosphere. The estimation of various pollutants, such as heavy metals, chlorinated hydrocarbons, and a diversity of other organic and inorganic chemicals, is generally carried out from rather small samples. The ratio of the size of the sample to the size of the polluted area may be some 1:1,000,000. The analyses are much more useful in predicting the extent of pollution if the data fit some well-known fractal model. The data, however, may also turn out to be not as simple as one would expect from the fractal models. The plots in Figure 6.1 show that such analyses give rather useful information.

Furthermore, soil pollution is generally a result of human activity that operates at a given reactivity scale and intensity. True fractal behavior will arise only if the process is self-similar over very many scales, and the scaling is unlikely when the pollution process is dominated by activities at a single, human scale.

Let us consider the distribution of minerals in a piece of rock. Let M be the mass of a certain kind of mineral in the rock. If we divide the rock specimen into two pieces, one piece contains αM mineral and the other piece contains $(1 - \alpha)M$, where α is the fraction. If we again divide the two pieces into two more, then the four pieces of rock of equal volume contain (Takayasu, 1990):

$$\alpha^2 M, \quad \alpha(1 - \alpha)M, \quad \alpha(1 - \alpha)M, \quad (1 - \alpha)^2 M \tag{6.2}$$

The ratio on each division is $\alpha : 1 - \alpha$.

In the case that $\alpha = 1/2$, we find that the mineral is homogeneously distributed, and no matter how many times we divide the original specimen, the mineral is evenly distributed in each subdivided piece. However, it can be shown experimentally that if $\alpha > 1/2$, then the distribution becomes constant and independent of the step of division (Figure 6.2). The limit of this distribution is called de Wijs's fractal (Takayasu, 1990):

$$D = -[\alpha \log_2 \alpha + (1 - \alpha) \log_2(1 - \alpha)] \tag{6.3}$$

If $\alpha = 1/2$, then $D = 1$, whereas if $\alpha > 1/2$, then $D < 1$. For $\alpha = 1$ or 0, $D = 0$. This equation therefore shows that the magnitude of D can indeed become nonuniform.

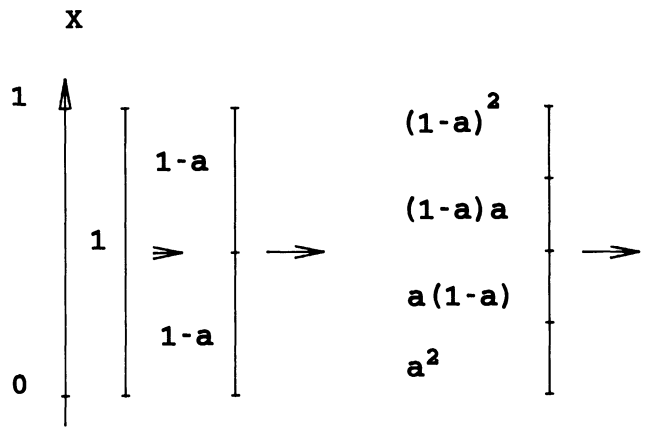

Figure 6.2. de Wijs's fractal (see text for details).

Further, de Wijs's fractal is different from that of Cantor's set in that any integral over a finite interval takes a positive value of $D > 0$. This means that the magnitude of dimension is always 1.

Furthermore, as D decreases, the distribution of the mineral becomes strongly concentrated in a limited region, such that when $D \approx 0$, the mineral is localized at one point. In other words, while most of the mineral will be found in just one rock sample, traces could be present in all of the others. For example, while gold is found singly (almost 100% pure), it is still present in very minor concentrations almost everywhere (e.g., sea water). It seems that the variation of many properties of soil and chemicals occurs over many different scales. This may be ascribed to different scales in the chemical, biological, geomorphological, and geological processes that shape the earth's surface. It is hoped that evolutionary processes may be more useful for such model analyses. This will provide input to pollution control and regulation worldwide.

A new development in these analyses is related to the very small fluctuations (noise) in pollution control. This noise can be analyzed by fractal theory (see Chapter 1), and will be expected to add much useful information in future model analyses. In a recent study, fractal concepts were applied in the analysis of atmospheric inhomogeneities (in the case of smoke plume diffusion) (Ludwig, 1989). Another example is the nuclear winter theory, where sunlight absorbs on smoke as it lifts into the atmosphere, thereby cooling the surface of our planet. This description has been given as an aftermath of a world war where the optical properties of smoke are assumed to produce an inverse greenhouse effect. In early studies, important factors were neglected, e.g., coagulation of individual smoke particles (which are smaller than the wavelength of light) into fractal clusters. The fractal dimension, D, was found to be of magnitude 1.78 (Berry and Percival, 1986). The size of these fractal clusters may be larger than the wavelength of light. This model is also of much interest for theoretical optics studies. It was concluded that fractality would have an adverse effect on the nuclear winter.

Earthquakes have recently been explained based on a self-organized criticality theory (Bak and Chen, 1991). Generally, one explains earthquakes as arising due to the movement of the upper

crust of the earth, e.g., the instability in the San Andreas fault in California. However, these immense movements of materials can be investigated by studying simple models. A model based on the movement of sand corns has been developed. Similarly, avalanches have been explained as a chain reaction. In the initial stages of an avalanche, just a grain of earth moves down hill. If this grain comes to rest somewhere by itself, then nothing more happens. On the other hand, if this grain meets another unstable grain, then there are two grains moving downhill, and if these meet other similarly unstable grains a minor avalanche is growing. The size of an avalanche is thus related to the number of particles that moved altogether. The critical value can be estimated by studying simple models using sand grains.

7

Galaxy Clusters and Fractals

The world is full of clusters, from clusters of quarks to metal and molecular clusters on surfaces and in molecular beams, from ion clusters in the atmosphere to stellar clusters in the galaxy. The big bang theory, which is postulated to describe creation, holds that the matter in the universe has been distributed by natural forces. It is fascinating to study the degree of distribution of stars, galaxies, and planets. The number of atoms and molecules suggested to compose our universe is estimated as follows (Dauvillier, 1963; Shklovskii and Sagan, 1966). According to Einstein's theory of the structure of the universe, the total mass of the universe is some 2×10^{55} grams. This has been transformed into ca. 500 billion galaxies, each with a mass of 20 billion solar systems ($= 2 \times 10^{33}$ g). In the universe, out of each 1000 atoms, there are 875 hydrogen, 124 helium, and 1 oxygen, carbon, or neon; other atoms are negligible in comparison. From these data, the total number of atoms in the universe is 88×10^{77} $[= (2 \times 10^{55})(6 \times 10^{23})/(0.875 + 0.124 \times 4)]$.

At first sight, the stars in the sky seem to be scattered at random. However, stars have a strong tendency to cluster to form galaxies (Mandelbrot, 1982). Each cluster may consist of hundreds of galaxies, forming a so-called supergalaxy. The diameter can be as large as 20 million light-years (1 light-year is the distance traveled by light in 1 year, which equals 9.45×10^{12} km).

From cosmological considerations, one might expect (as a first

approximation) that the distribution of matter follows precisely the same laws for the different systems, regardless of their origin and axes. This means that the distribution of masses would be translationally invariant.

Some 3500 years ago, the Sumerians noticed that stars were arranged such that one could see a lion, a bull, and a scorpion. We also find that the night sky appears to be filled with constellations shaped by straight lines, rectangles, and pentagons. It is therefore quite tempting to imagine that such geometric patterns arise from unknown forces in the cosmos. It was conjectured by Ramsey in 1928 (Graham *et al.*, 1990) that if given enough stars, one could always find a group that very nearly forms a particular pattern. Infact, according to Ramsey's theory, complete disorder in nature is an impossibility.

The correlation function for galaxy distribution (mass versus radius power law) was found to follow the power law, with $D = 1.2$ (Mandelbrot, 1982; Szalag and Schramm, 1985). Compared with $D = 3$, the magnitude of galaxy fractal dimension is much too low. There appears to be no explanation for this result at the present time.

Consider the solar system. Orbiting around the sun at equilibrium with the centrifugal forces are nine planets. The sun is a star, and a very ordinary star compared to others in the universe. It is 93 million miles away from the Earth on the average, and has a diameter of about 863,000 miles. Its volume is 1 million times that of the Earth, yet its mass is only about 250,000 times greater.

The planets orbit the sun in paths that are elliptical and all lie more or less in the same plane. The planets are divided into two groups (see Table 7.1). The planets are at various distances from the sun, and it is interesting to determine the mass (or volume or radius) versus distance relationship and the fractal dimension. The mass (M_R) can be estimated from the volume (from radius) $\times$ escape velocity, as given in Table 7.1. Figure 7.1 is a plot of $\log M_R$ versus $\log R$. The plot can be fitted to the following power-law equation (Birdi, 1992c):

$$M_R \propto R^D$$

$$\log M_R \propto \log R^D = A + D \log R = -29 + 5.2 \log R \quad (7.1)$$

Table 7.1. Planets of the Solar System[a,b]

	Distance from the sun (miles)	Diameter (miles)	Escape velocity (miles/sec)	Density (g/cm^3)
Mercury	36,000,000	3,008	2.12	5.5
Venus	67,250,000	7,575	6	5.2
Earth	93,000,000	7,926	7	5.5
Mars	141,650,000	4,200	3.12	4.0
Jupiter	483,000,000	88,698	60	1.3
Saturn	887,000,000	75,000	—	0.7
Uranus	1,783,000,000	30,000	—	1.3
Neptune	2,796,000,000	27,700	—	1.7
Pluto	4,567,000,000	—	—	—

[a]Source: Birdi (1992c).
[b]Mass (estimated) = volume × escape velocity = $(4/3)\pi R^3$ × escape velocity.

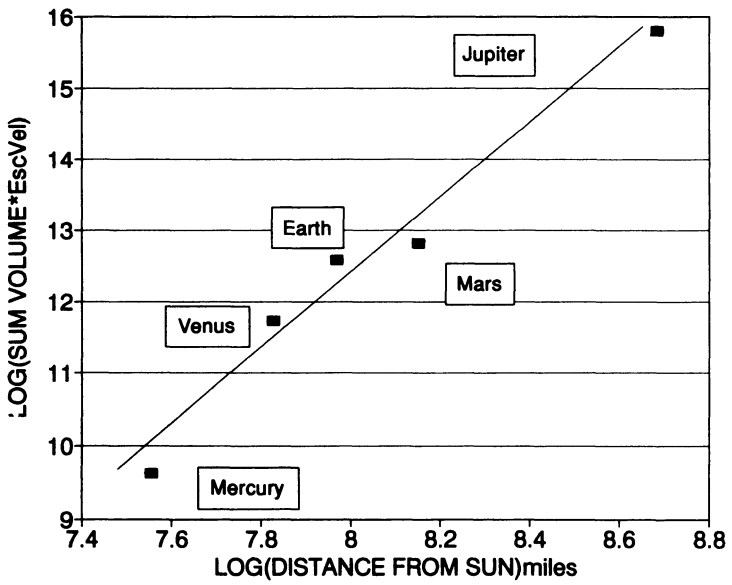

Figure 7.1. Plot of mass of planets versus distance from the sun (Birdi, 1992*c*).

where A is a constant and the magnitude of D is found to be 5.2. The significance of this value of D needs further analysis, since it may be dependent on some evolutionary parameter. If we consider the above-mentioned distribution of mass in the universe as a whole, M_R, the mass inside a sphere of radius R will vary as:

$$M_R \propto R^{D-3} \tag{7.2}$$

where for small R, if we take the origin to be the center of the Earth, $D = 3$. However, as the value of R increases far beyond the Earth's radius, D will go to zero and the system becomes—on the scale of matter—isolated "points," which is what one calls the interstellar scale. At much larger values of R, i.e., in the case of a galaxy or cluster of galaxies, $D \approx 1.23$ (see above). A projection onto a two-dimensional surface such as the "sky," i.e., the surface of the celestial sphere as seen from the Earth, will have the same dimensionality as that of the projected object as long as its dimensionality is less than 2. Hence, all of the stars of the universe will give a projection of $D \approx 1.23$, and thus of zero area on the celestial sphere of the Earth. This provides a geometrical resolution of the so-called blazing sky effect, which states that if $D = 3$ for galaxy distribution, any direction taken from the Earth would sooner or later encounter a star, with the result that the sky would always appear (day and night) uniformly bright. It has been maintained that physical arguments based on relativity theory and the finite lifetime of galaxies (Wesson, 1987) can also explain away the effect even if $D = 3$.

This analysis shows that the mass distribution in the solar system is indeed fractal, and that all of the planets were most likely created under similar force input. In other words, this finding is in accord with the big bang theory. This might additionally suggest that during the creation of planets, a wave of mass erupted from the source. The wave thus seems to have had a fractal nature [perhaps a kind of viscous fingering phenomenon (see Chapter 2)].

We are thus able to predict, with the help of the fractal Eq. (7.1), the magnitude of the mass of a planet at any distance from the sun. We can also imagine that the big bang sent masses of

material in a fractal distribution. Whether this conclusion is valid on more detailed geothermal grounds remains to be analyzed.

7.1. Dynamical Models of Neptune's Dark Spot and Other Phenomena

Based on the information from the recent encounter of the Voyager spacecraft with Neptune, the presence of a large coherent structure in its atmosphere was revealed, the so-called Great Dark Spot (Polvani *et al.*, 1990), which undergoes dramatic variations in its shape. These large oscillations of the Spot were reproduced by using a simple dynamical model of an isolated vortex embedded in a background shear flow. The chaotic zones of a dynamical system are most easily exhibited by computing the Poincaré surface of section. The characteristic property of chaotic motion is that nearby trajectories diverge exponentially from one another. The models imply that there exists a planetary-scale zone of deterministic chaotic convection in the atmosphere of Neptune. It has also been suggested that it would be of much importance to apply this model to the "brown barge"-type vortices on Jupiter, whose aspect ratios have been reported to vary by about 10% over a 15-day period.

Analysis of the dust around Coronae Borealis stars has been reported (Hecht, 1991). The nature of the dust in circumstellar shell was suggested to be of graphite fractal type.

The twinkling of stars arises from fluctuations of the refractive index of the atmosphere. The refractive index is related to the density and humidity of the atmosphere. This turbulence of the atmosphere thus produces the phenomenon of twinkling (Takayasu, 1990). The change in distance during this process of the star (from 2 m to 200 m) is related by a power law to the fractal dimension. The value of D has been found to be 2.5.

7.2. Diameter Distribution of Craters and Asteroids

Examination of the surface of the moon by even a low-power telescope reveals a multitude of craters. These craters have been

analyzed very extensively. Their size can be studied by using the *distribution function.* Let P_R define the probability that any arbitrarily chosen crater has a radius greater than R. The probability of finding such a crater is determined by the probability density Δ_R as follows (Takayasu, 1990):

$$P_R = \int_R^\infty \Delta_R \, dR \tag{7.3}$$

It is known that the only mathematical function that can satisfy such constraints is the so-called power law:

$$P_R \propto R^{-D} \tag{7.4}$$

The $\log P_R$ versus $\log R$ plot will give a straight line with slope equal to D. As an example, in the case of craters, we can determine how the size R affects the results. Let us count the number of craters with radius $\geq R$, which means that craters with radius $<R$ are invisible. If we increase the value of R by a factor of 2, then it can be shown that the number of craters observed will increase by a factor of 2^D.

This example shows how to apply such procedure for the fractal analysis of similar kinds of systems. The term *probability* can cover all kinds of phenomena, e.g., size of particles or stars, magnitude of signal.

The plot of cumulative number of craters versus diameter, d_{crater}, is given as a log–log relation in Figure 7.2. These data can be related to the following equation:

$$N_{\text{diameter}} \propto d_{\text{crater}}^{-D} \tag{7.5}$$

where $D \approx 2$. The term N_{diameter} denotes the number of craters that have diameters larger than d_{crater}. It is very interesting that the value 2 for the fractal dimension has been found to be universal, i.e., it is also the same in the case of craters on Mars and Venus (Mizutani, 1980).

In a recent study the impact craters on Venus were analyzed (Phillips *et al.*, 1991). Their morphology, locations, and size-

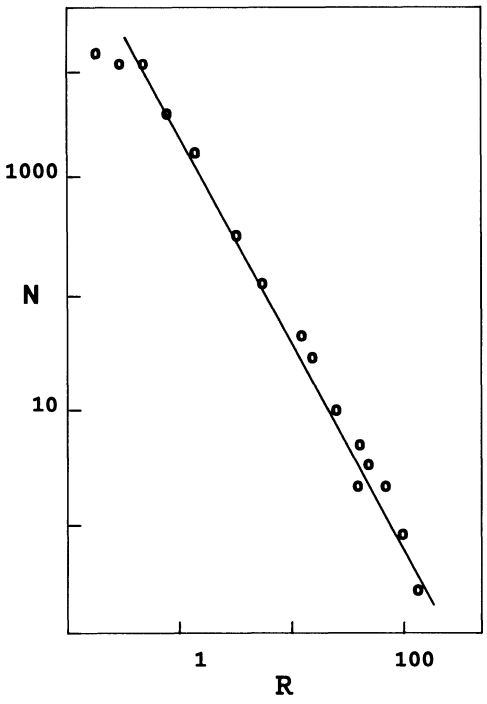

Figure 7.2. Diameter distribution of craters on the moon. (Redrawn with modifications from Mizutani, 1980.)

frequency distributions were studied to provide information about the nature, rate, and timing of Venusian resurfacing processes. It is obvious that if the craters are preserved with time, then the total number increases. From this rate, one can calculate the age of the surface. On the other hand, erosion might remove the craters (or reduce them in size), and this would be useful information. The slope of the log–log plot of Venusian craters was the same as for the moon. Impact craters were found not to be uniformly distributed, and it was concluded that the surface of Venus is active.

In order to determine the theoretical basis of such natural phenomena, one may conduct some model analyses. As mentioned elsewhere, the brittle fracture distribution follows a power law. Furthermore, one can understand this phenomenon if it is compared to the shattering of a piece of rock by a bullet. The distribution of the splinter size has been found to give D of

approximately 2. Thus, we can conclude that if asteroids and meteorites are indeed broken pieces of a larger body, then it would be a natural consequence for their size distribution to follow a power law with $D \approx 2$. The theoretical analyses of fracture need more in-depth investigation at this stage.

8

Fractal Analyses of Macromolecules

Life on our planet is a manifestation of light-element—especially carbon—chemistry. As we know from nature around us, the organization of natural things requires storage of information. This information storage and transmission (through evolution) is of chemical nature and stored in the molecules (*as a molecular computer*). The chemistry of living matter is, in addition, characterized by a sophisticated degree of molecular complexity, i.e., a very precise information content. In this respect there is no difference between the smallest viruses and the most advanced animals: nucleic acids and proteins and the most advanced animals: nucleic acids and proteins are fundamental to both. Furthermore, the capacity for generating, storing, replicating, and utilizing large amounts of information implies an underlying molecular complexity that is known only among compounds found in the biological world (mainly based on carbon). The information that is referred to here (Calvin, 1969) (and is stored as chemical information) is of much larger dimension than is available in any supercomputer. For example, a protein molecule such as hemoglobin (molecular weight of 68,000) may take millions of years to develop, in order to function as a carrier for the transport of oxygen in the blood.

Now let us consider the size of various molecules to be

discussed in the present context. In a system like salt, NaCl (molecular weight 58.5), dissolved in water (H_2O, molecular weight 18), the size ratio is roughly $58:18 \approx 3:1$; in comparison, the size ratio of protein (say hemoglobin) to water in aqueous systems is orders of magnitude greater. In the latter case, the relatively large solute is termed a *macromolecule.* Macromolecules also play a very significant role in various aspects of everyday life: paints, oils, emulsions, plastics, rubbers, and composite materials. The hydrodynamics of macromolecular solutions is an old and important problem in polymer science (Muthukumar, 1985a,b). The hydrodynamic properties and viscosity and the diffusion coefficient are intimately related to the molecular dimensions of the polymers and their measurement provides a useful method of molecular characterization. For instance, determination of the viscoelastic properties of polymer solutions provides considerable information about the nature and rates of the conformational rearrangements. These properties of solutions containing flexible polymer chains, rodlike molecules, spheres, and arbitrary fractals have been discussed (see Chapter 2). Further, the viscosity change, frictional coefficients, relaxation times, hydrodynamic screening, and modifications from the two-dimensional confinement were explained in detail.

The fractal analyses suggested the existence of self-similarity in polymers in solution. The dynamic properties of flexible polymers have been found to be related to scaling laws. It was recognized that the self-similarity of a macromolecule in a dilute solution is related not only to its dilute macroscopic properties, but also controls the equation of state of concentrated solutions.

A review of cluster theory and the effective medium theory of solutions containing flexible polymer chains, rodlike molecules, spheres, arbitrary fractals, etc. has appeared (Muthukumar, 1985a,b). The viscosity change, frictional coefficients, relaxation times, hydrodynamic screening, and modifications from the two-dimensional confinement were discussed.

Apart from linear polymers, the dynamic properties of fractal structures are essentially unexplored (Schaefer *et al.*, 1985). This paucity of data is due to the fact that dynamic light scattering, the technique of choice for such studies, is expected to display unique features only for objects that are fractal over dimensional scales

comparable to the wavelength of light (5000 Å). Recently, however, colloidal aggregates were shown both to be fractal over lengths up to 1 nm and to display interesting dynamics. The dynamics of such aggregates has been reviewed (for polymers and colloidal particles). In all cases, these systems are studied in a dilute suspension by quasi-elastic light scattering.

A characteristic of a synthetic macromolecule is that it is constructed by repetition of a basic unit called a *monomer*. Each monomer has a specific functional property. Macromolecules are thus synthesized by polymerization of the monomer unit. This may produce linear or nonlinear chains. In the case of multifunctional monomers, the nonlinear network gives rise to gel structures. The latter exhibit elasticity, whereas linear macromolecules are viscous liquids.

8.1. Fractal Nature of Polymers

In the case of linear polymers, interpolymer interactions are easily neglected. The random walk model gives the following relationship, in the case of an ideal state (Daoud and Martin, 1989), for a polymer with N monomeric units:

$$N \approx R_0^2 = R_0^{D_0} \tag{8.1}$$

where the characteristic length R_0 can be radius of gyration or end-to-end distance (see Chapter 1). This shows that the fractal dimension D_0 of an ideal chain is 2. In a recent study, the transition temperature of microgels formed by divinylbenzene styrene copolymers was analyzed by fractal theory (Antonietti and Rosenauer, 1991). The fractal analysis was found to be related to the viscoelasticity of the polymer gels.

In real solutions of polymers, two-body interactions are not absent. In the so-called good solvents, the major interactions arise from the volume that each monomer unit excludes from the others, thus preventing any self-intersection of the polymer chain (i.e., self-avoiding walk). This interaction is also the cause of swelling of polymers on the addition of solvent (e.g., a rubber stopper on

exposure to benzene or toluene swells to more than twice its original volume) (Hildebrand and Scott, 1970).

Under these conditions, the more general power-law relationship is found:

$$N \approx R^D \tag{8.2}$$

In a recent study the fractal and statistical mechanics of networks formed by macromolecules were reported (Kardar, 1989).

8.2. Surface Adsorption of Polymers and Biopolymers

Analogous to the adsorption at any interface of surface-active molecules such as soaps and detergents, polymers (such as proteins and biopolymers) are known to adsorb at interfaces (air–water, water–oil, or liquid–solid) (Chattoraj and Birdi, 1984; Birdi, 1989). In the case of air–water interface, this leads to a change in surface tension of a solution, depending on the degree of adsorption, i.e., it is related to the difference in energy when the molecule is in the bulk and at the interface (Birdi, 1989).

The self-similar scaling property has been used to describe the adsorption process (Birshtein, 1983; de Gennes and Pincus, 1983; Binder and Kremer, 1985; de Gennes, 1985). The quantity ρ is used to describe surface contact energy per monomer. Let us consider a system where $\rho < 1$. Since each monomer contributes contact energy individually to the total sum of the polymer molecule, even small contributions can add up to large energetic effects. There are many physicochemical characteristics that are related to the molecular weight, e.g., adsorption and viscosity. It is also important to realize that ρ is dependent on the difference between the surface tension of the solvent and the polymer. This is easily seen from the fact that the surface tension of a liquid under ideal packing conditions (i.e., hexagonal) is just one-half the value of its heat of vaporization (Birdi, 1989).

Consider the adsorption of a single chain of the polymer at the surface:

$$N_s \approx N^{\varphi} \tag{8.3}$$

where N_s denotes the number of monomers at the surface and φ is a crossover exponent (approximately 3/5 for three-dimensional systems). In analogy to the scaling law, a connection between fractal dimension, D, and φ was delineated.

Particles of up to 1000 Å (Lubensky and Pincus, 1984) act like atoms or molecules and come together to form flexible chains, periodic lattices, and entities with fractal geometries. The theoretical models of the growth and properties of these superpolymers, ultraweak solids and aggregates have been discussed briefly.

Adsorption of Polymers on Fractal Solid Surfaces

The adsorption mechanism of polymers on solid surfaces differs from that of small adsorbing molecules (Chattoraj and Birdi, 1984; Birdi, 1989). As already mentioned, the problem of evaluating the cross-sectional area of an adosrbed polymer is sometimes difficult, especially in the case of flexible linear polymers. In the latter case, one has to consider the following:

- Segment–segment interactions with the polymer
- Polymer–solvent interactions
- Polymer–surface interaction
- Solvent–surface interaction

The polymer can therefore assume conformations ranging from complete spreading on the surface, through spheroidal conformations, and up to very elongated prolate conformation in which the polymer is attached through only a few segments, vertical to the surface. These considerations are analogous to the monolayer studies carried out on the surface of water (Birdi, 1989).

One can proceed by assuming that the radius of gyration, R_g, is related to the molecular weight as:

$$R_g \sim M^{\upsilon_p} \tag{8.4}$$

where υ_p is related to the conformation of the polymer. It was shown (Avnir, 1989) that the fractal mass distribution, D_p, is:

$$\upsilon_p = 1/D_p \tag{8.5}$$

The adsorption data of styrene–methyl methacrylate gave verification of this relation (Farin and Avnir, 1987).

8.3. Fractals and Protein Structure

Protein molecules are comprised of some 25 different amino acids, each with specific physical properties (Dickerson and Geis, 1969; Chothia, 1984; Creighton, 1984; Birdi, 1989; King, 1989; Richards, 1991). The polypeptide chain or backbone forms a linear polymer composed of repeating units. There are few cross-linkings, such as disulfide bonds. Proteins vary widely in molecular weight (1000 to 10,000 atoms), composed of 20 to 500 amino acid residues. The protein structures have been elucidated by the technique of X-ray crystallography. In the protein molecule, approximately half of the atoms are hydrogen. The rest are carbon (molecular weight 12), nitrogen (molecular weight 14), oxygen (molecular weight 16), and sulfur (molecular weight 32). The specific property exhibited by a protein is related to both the number of amino acids and their sequence. This is well established from the fact that a difference of a single amino acid in the hemoglobin molecule can give rise to the sickle-cell disease.

The sequence of amino acids, referred to as the primary structure of the protein, actually determines the native conformation, the structure that is stable under physiological conditions. This conformation is the one yielding the minimum in free energy, thus imparting maximum stability (at a given temperature and pH) (Tanford, 1961; Dickerson and Geis, 1969; Chattoraj and Birdi, 1984; Birdi, 1989).

From X-ray crystallography, the folding of portions of the polypeptide chain often shows regularities, referred to as secondary structure. These are characterized as α-helical and β-pleated sheets. The α helix is a compact rodlike structure, whereas the β-pleated sheet is an extended structure. Since a protein has a finite size with a radius of gyration from 16 to 80 Å or so, the secondary structural elements are limited in length. Furthermore, on the average, ca. 25% of the amino acids form helices, 25% sheets, 25% turns, and the remaining 25% the regular configuration (called the random coil) (King, 1989; Birdi, 1989). There can be deviations from this rule. For example, myoglobin shows 85% α-helical structure while the remainder is random coil.

As described elsewhere, the nonpolar amino acids are generally found in the interior of the molecule, while the polar amino acids (Birdi, 1989) are mostly present at the outer part of the molecule. Whenever hydrogen bonds are unavailable for the long-range cross-linking (as found in the α-helical structure), the weaker van der Waals and electrostatic forces are the dominant form of interaction between the polypeptide chain. These peculiar properties ascribed to the weaker interactions are known to determine the anomalous size of the fractal dimension.

The objective of any fractal analysis is to find a relationship of some kind of power law:

$$\text{Physical property} \propto \text{variable}^{\text{fractal dimension}} \tag{8.6}$$

where the variable and the exponent are related to the fractal dimension. This relation is obviously one that can cover a very broad range of protein structures. However, this kind of power law requires some symmetry in these structures.

In biology, the binding of antibody to antigen is a very complex phenomenon. The binding of monoclonal antibodies to surface-immobilized antigen was investigated with regard to fractal theory (Werthen *et al.*, 1990). These studies indicated that such binding processes are indeed complex. The initial binding is a diffusion-rate-limited process. The reaction is slowed down with time. On the other hand, since the reverse reaction is slow, the total reaction behaves as an irreversible adsorption process. The adsorption was followed by using ellipsometry. The rate of adsorption was found to follow a power law (t^{1-D}), where t is time. The magnitude of D was found to be 1.52–1.70.

The aggregation equilibrium of immunoglobulin proteins was investigated by using quasi-elastic light scattering (Feder, 1988). These studies showed that the effective hydrodynamic radius of the protein cluster, R, which grew with time (t) was:

$$R = R_0(1 + \tau t)^{1/D} \tag{8.7}$$

where R_0 is the radius of the monomer and τ is a kinetic temperature-dependent constant (i.e., kinetic energy). The magnitude of D was found to be 2.56.

Nontrivial scaling behavior of various molecular properties has long been known to arise from empirical scaling laws according to power functions, as described above. Thus, in the case of chromatographic separation of proteins, the data yield the following relationship between molecular weight (MW) and molecular radius (R_M):

$$\begin{aligned} \text{MW} &\propto R_M^D \\ &\propto R_M^{2.7} \end{aligned} \tag{8.8}$$

where $D = 2.7$. In the ideal case, one would have expected $D = 3$ (Basedow *et al.*, 1980). The data are shown in Figure 8.1, where a linear plot is found [Eq. (8.8)].

Protein Surface Area and Fractal Dimension

The surface area of a protein molecule is known to determine many of its physical properties, e.g., association, recognition, binding, and diffusion of a ligand. Protein surfaces have been analyzed by using molecular graphic methods. In earlier studies the protein surface area was estimated by rolling a molecule (such as water with a radius of 1.4 Å) over the protein. The surface corrugation can be analyzed by using fractal theory. In various surface analyses, there has been found to be two kinds of fractal

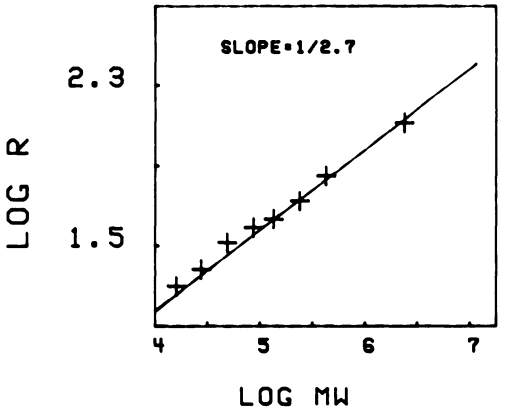

Figure 8.1. Plot of molecular weight (MW) of various proteins versus radius (R_R). (Redrawn with modifications from Felgenhauer, 1974.)

dimensions, D_s. In some cases, only one D_s has been assigned, whereas in other systems various D_s values were used for the different parts of the surface. It is obvious that in order for the scaling law to be valid, the value of D_s must hold for a reasonable length scale.

The surface area of a protein molecule can be estimated by using different procedures. The magnitude of the surface can be estimated by using a probe, which can be a yardstick for a two-dimensional cross section or a small sphere for a three-dimensional representation of the macromolecule. The surface area can be estimated as the area of the probe (molecule) times the number of probes required to cover the surface completely.

In one procedure, D_s was calculated by examining the two-dimensional cross sections of the protein. The length of the contour that closes the cross-section using different step lengths of ϵ was employed. The number of steps N_ϵ required to close the cross section is a function of the step length, ϵ. From the following relation (Lewis and Rees, 1985; Pfeifer *et al.*, 1985; Elber, 1989):

$$N_\epsilon \propto \epsilon^{-D_S+1} \tag{8.9}$$

the value of D_s was estimated (Table 8.1). If a more detailed analysis is preferred, then several values of the fractal dimension can be assigned to different parts of the protein surface (this introduces the concept of multifractal analysis). The magnitudes of D_s are found to vary significantly, with no correlation with the amino acid composition (as regards the polar–apolar amino acid ratio) (Birdi, 1989). Studies analyzing the protein as a function of its fractal data are in progress.

Another question addressed was the relationship between the fractal dimension and the protein flexibility. The effect of thermal fluctuation on this topic has not been investigated. These fractal analyses give an overall average information as regards the surface of the large molecules. This may be useful in the interpretation of the available results, and in some mathematical interpretation of complex properties. The fractal dimesion may also be correlated to the flexibility of the protein molecule. The surface roughness was given a fractal dimensionality. It is important to mention that in

Table 8.1. Magnitudes of Surface Fractal Dimension, D_s, of Various Protein Molecules[a]

Protein	D_s
Immunoglobulin (mouse)	2.145
α-cobratoxin	2.133
Bacterial serine protease	2.088
Lysozyme	2.53
Subtilisin inhibitor BPN complex	2.110
Cytochrome C	2.117
Ribosomal protein	2.132
Retinol binding protein	2.18
Pre-albumin tetramer	2.21
Satellite tobacco necrosis virus	2.15
Trypsin	2.62

[a]Source: Pfeifer *et al.* (1985).

both the physiological and the biochemical sense these analyses are of much value (especially in the molecular design of pharmaceutical molecules).

There are two length scales by which we can analyze a polymer macromolecule. One scale is associated with the monomer unit (in the case of proteins it will be the average size of an amino acid, i.e., ca. $4 \times 4\,\text{Å}^2 = 16\,\text{Å}^2$) (Birdi, 1989). The other scale is much larger and is associated with some length R of the polymer, e.g., its radius of gyration, R_G, or its mean end-to-end length (or approximately $M^{1/3}$, where M is the molecular weight). On the scale of R, the different physical properties of a polymer become independent of the detailed properties of the individual monomer units. Then, in analogy with thermal critical phenomena, there should be some scaling relationship. In the polymer theory of Flory (Flory, 1971; Tanford, 1961), it is known that as the number of monomer units in a polymer, N, increases toward infinitum, the variation of R is:

$$R = a_m N^{\upsilon_F} \tag{8.10}$$

where a_m is a constant on the order of the length of a monomer and υ_F is related to the fractal dimension. Hence, in terms of the fractal

geometry, we can define the fractal dimension D as:

$$D = 1/v_F \tag{8.11}$$

If excluded volume effects can be neglected, then a linear polymer can be modeled by an ordinary N-step random walk with $v_F = 1/2 = 1/D$. Thus, we get:

$$R_{linear} = a_m N^{1/2} \tag{8.12}$$

In the same way, in the case of a branched polymer modeled by independent random walks on each branch and neglecting the excluded volume effects:

$$R_{branched} = a_m N^{1/4} \tag{8.13}$$

Detergents are known to bind to proteins, and a great number of studies have been reported in the literature (Steinhardt and Reynolds, 1969; Birdi and Steinhardt, 1978). The fractal nature of protein–detergent binding was recently reported (Teixeira, 1986). The change in scattering intensity of protein (BSA) on the addition of SDS ($C_{12}H_{25}SO_4Na$) is given in Figure 8.2. The values of D were determined from the slopes of the plots. It is seen that both the

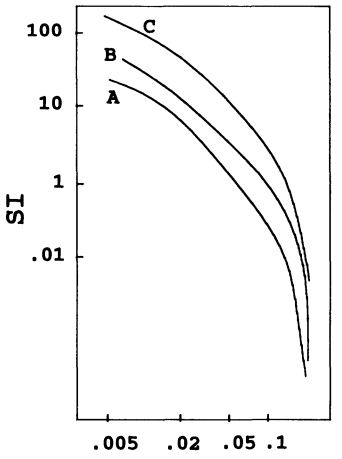

Figure 8.2. Variation of scattering intensity (SI) of 1% BSA (bovine serum albumin) versus radius ($1/R$) and % SDS. The variation in D was (A) x = 1%; 2.3, (B) x = 2%; 1.91, (C) x = 3%; 1.76. (Redrawn with modifications from Teixeira, 1986.)

radius of the complex and the magnitude of D change (from 2.3 to 1.76) with the concentration of SDS, as the protein unfolds on binding.

The class of proteins called *enzymes* exhibit flexible conformation. Due to the Brownian motion of the surrounding solvent molecules, temperature fluctuations and collisions create coupled and rather complex vibrations. Whenever a ligand moves from its location in the solvent phase toward the protein, the conformation of the latter has to change on binding. Thus, this principle requires that the system come to equilibrium with a minimum free energy state. It can be postulated that these changes in the protein molecule have been encoded during the evolution of the macromolecule, i.e., that evolutionary considerations are built into the molecular information. The location and the extent of the conformational change in the enzyme molecule after ligand binding are estimated from the difference in the plot between the enzyme and the acyl-enzyme of the distribution of the flexibility parameter of the peptide chain. A simple model based on an established structural feature, as is commonly known in the case of trypsinlike molecules, to extensive coaxial half cylinders of β sheets, to which previously no mechanistic function could be assigned, is proposed to reveal the attractor in the catalytic phenomenon (Havsteen, 1989). In the case of such enzymes, the reactions may take place after a molecule moves a specific area on the surface of the enzyme. In this approach, Brownian motion thus plays an important role (McCammon *et al.*, 1987). A typical example is the diffusion-controlled reaction between superoxide (O_2^-) and the enzyme superoxide dismutase (SOD). The reaction takes place at the poles of this spherical molecule. A more detailed description of the binding site of O_2^- is as follows. The active-site region contains the amino acids glutamic acid, lysine, and arginine. The distance between the last two amino acids is estimated to be 10 Å. The log (kinetic rate) versus log (ionic strength) plots were linear when the ionic strength was ca. 0.1. The magnitude of D was clearly dependent on the ionic strength (i.e., increasing with increasing ionic strength). Further investigations are needed employing improvements in the electrostatic components of this system. The role of water in the approach of superoxide has not been analyzed. In

another study, it was reported that fractal methodology in enzyme kinetics makes analyses much more meaningful (Lopez–Quintela and Casado, 1989). It was shown that the fractal approach dispenses with calculation of parameters that have no clear physicochemical significance. The magnitude of the fractal dimension was found to vary from $D = 1$ to $D < 1$.

It is clear that the fractal analysis of proteins is a useful approach considering such complicated molecular structures. It is important to remark that segments less than 10 amino acids long may represent secondary structure elements. On the other hand, larger scale segments represent tertiary structure packing. What remains to be discovered is how these power-law relationships are of importance in the biological processes that are dependent on protein structure and function. In a recent study, a fractal dimension of 2.34 was reported for chromosomes and chromosomal DNA replication (Takahashi, 1989). A primary structural unit of DNA is 2 nm in diameter. This can be easily visualized with a scanning tunneling microscope. The DNA molecule is coiled. Coiling is not only a device for making the macromolecule more compact; it also induces structural changes for absoring and releasing torsional stress. An electron micrograph of a chromosome spread as a monolayer at an air–liquid interface shows looplike fibers at least 10–30 μm long that run in parallel. It is thus important to realize that fractal analyses of such complex molecules as proteins will lead to a better understanding of structure at the molecular level.

Adsorption of proteins on solid surfaces. In general, proteins are adsorbed from their aqueous solutions very rapidly when they contact solid surfaces (Chattoraj and Birdi, 1984; Birdi, 1989). Most of these adsorption processes are irreversible. The adsorption mechanism of the protein ferritin on quartz has been investigated (Nygren and Stenberg, 1990). The adsorbed ferritin was analyzed by using electron microscopy. When the concentration of ferritin was 10 μg/ml, molecules were found to be adsorbed initially as monomer. At later stages, clusters varying from 2 to 9 molecules were seen on the quartz surface. After 100 sec, only aggregates were present, 10–100 molecules/aggregate. Similar data have been reported for the surface of carbon. This surface-induced aggrega-

tion of protein molecules from aqueous solution was interpreted as a nucleation and growth phenomenon. It was concluded that the initially monomer-adsorbed species act as nucleation sites. The fractal dimension was found to be 1.05. This agrees with the surface fractal of silica particles on water, i.e., $D = 1.2$. Computer simulations of such surface adsorption processes have been described (Stenberg and Nygren, 1990). The magnitude of the fractal dimension of adsorbed protein aggregates was estimated. These values were larger than the measured values. In the simulation procedure, hexagonal lattices were used as the sites. This may have had some effect on the estimated D.

8.4. Fractal Analyses of Adsorption (of Vapors) on Polymers

As described above in the case of adsorption from liquids to solids, the BET adsorption equilibrium is also valid in the case of gas or liquid vapor adsorption on solids. In this section we consider the fractal analysis of gas vapor adsorption on polymers. When gas molecules are found in the presence of a nonvolatile solid powder surface, they often accumulate on the surface as a result of attractive forces between the solid and the gas molecules. These forces may be chemical or physical (e.g., van der Waals) or intermediate (e.g., hydrogen bonds) (Berry *et al.*, 1980). For simplicity, we restrict ourselves in this section to a special case. It is known that gas adsorption is related to the pressure of the gas or the number of gas molecules in vapor (i.e., vapor pressure). When the gas pressure is extremely low, the equilibrium amount of adsorption is slight and Henry's law is observed, i.e., the amount of adsorption is proportional to the gas pressure. This means that each adsorbed molecule behaves independently of the others (as in a very dilute gas, i.e., low gas pressure). An adsorbed molecule may move freely (mobile adsorption) over the surface if the temperature is high enough. Under these conditions, the adsorbed phase behaves as a two-dimensional ideal gas. On the other hand, at low temperatures an adsorbed molecule is localized or confined to a "site," and it undergoes vibrational motion about that "site."

The "site" is merely a position, on the surface, of minimum potential energy for an adsorbed molecule. It is also known that a localized molecule may occasionally jump from one site to another, which is known as surface diffusion. Intuitively, one can conclude that as pressure increases, the number of molecules adsorbed will increase. However, the adsorption is expected to proceed in such a way that at first a monolayer of adsorption is formed on the polymer; at higher pressures, multilayer adsorption may be observed in some cases.

The adsorption of water vapor and of gas on polymers has been analyzed by fractal theory (Birdi, to be published). It is widely accepted that proteins adsorb water vapor by binding water molecules to specific hydrophilic sites at lower relative humidities followed by condensation or multilayer adsorption as the humidity increases. The nature of these hydrophilic sites has, however, been the subject of much research, and there is no general agreement concerning the helical groupings in proteins to which water is bound. The nature of these binding sites has been studied indirectly by the H_2O sorption capacity of proteins versus that of chemically modified forms of the same proteins and more directly by using such techniques as infrared spectroscopy or calorimetry methods (Berlin *et al.*, 1969; Birdi, 1992d).

The method generally used is based on gravimetric procedure. Equilibrium between water vapor and protein (solid) is typically achieved after 8–12 hrs. A typical adsorption isotherm is shown in Figure 8.3 (Berlin *et al.*, 1969).

The adsorption is seen to increase as humidity (P/P_0) increases, as expected. The monolayer (i.e., a single layer of molecules adsorbed on the surface of the polymer) is complete at the break in the isotherm. The transition from the first to the second layer is usually accompanied by a sharp decrease in the binding energy of the adsorbate, as the first layer is directly held by the substrate (polymer) whereas multilayers involve mostly water molecules. The inflection point thus occurs approximately at the pressure where the substrate is covered with a fully compressed monolayer.

These data can be explained based on multilayer adsorption, and that the principal interaction arises from the dispersion forces.

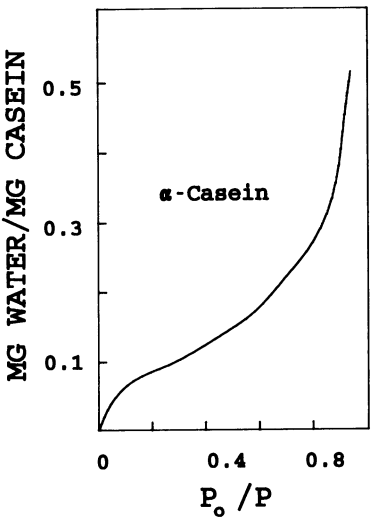

Figure 8.3. Adsorption isotherm of water vapor on α-casein (variation of amount adsorbed versus P_0/P). (Redrawn with modifications from Berlin *et al.*, 1969.)

Under these assumptions, the potential, ϵ_x, will decrease with the increase in the cube of the distance, x (Adamson, 1980):

$$\epsilon_x = \epsilon_0/(a_m + x)^3 \tag{8.14}$$

where a_m is a distance on the order of a molecular radius. The potential is related to the gas pressure, P:

$$RT \ln (P_0/P) = \epsilon_0/(a_m + x)^3 \tag{8.15}$$

A more general relationship is derived from these equations relating amount adsorbed, Γ, and P:

$$(\Gamma/n_m)^D = A/\ln (P_0/P) \tag{8.16}$$

where $A = \epsilon_0/(x_m^n RT)$. The film thickness at the monolayer state is given by x_m. This equation is called the Frenkel–Halsey–Hill, and is useful since it can be transformed into a power law from which the fractal dimension can be estimated (Birdi, 1992d).

The adsorption data of gas (N_2) and water vapor on casein are of much interest as regards the fractal theory. The adsorption

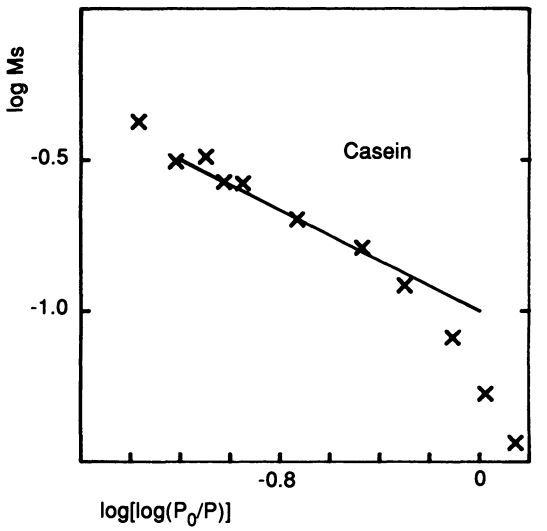

Figure 8.4. A plot of $\log(\Gamma = M_s)$ versus $\log[\log(P_0/P)]$ for water vapor adsorption on casein powder. (Redrawn with modifications from Berlin *et al.*, 1969.)

isotherm given in Figure 8.3 can be analyzed by the above power law (Birdi, 1992d):

$$\log[\log(P_0/P)] = D \log \Gamma + \text{constant} \tag{8.17}$$

The magnitude of D is found to be 2.5 in the case of adsorption of N_2 on casein. On the other hand, the water vapor data (Figure 8.3) showed two linear portions. The first part yielded $D = 2.5$, which is the same as for the N_2 adsorption. It may be safe to conclude that in all such adsorption processes, the value of D will be expected to be 2.5, where strictly only multilayer adsorption is occurring. The higher regions of these isotherms indicate that capillary condensation is occurring in very fine pores such that the sorbent is undergoing swelling. Similar isotherms have been obtained for adsorption of various vapors by polypeptides, and morphological changes were suggested (Brandt and Budrys, 1965). It was concluded that the data in Figure 8.4 reflect swelling in the case of water vapor. Deviations from a linear log–log plot are found useful for the detection of capillary condensation.

9

Biological Systems (Cells, Lungs, Heart)

The biological systems are indeed complex and very difficult to simplify as model studies. However, despite this complexity, one does find much order in some systems. For example, the human body has complicated networks of blood vessels, nerves, and ducts. The shape of the airways of the lung, through evolution and embryogenesis resembles fractals generated by some computer programs. It is worth comparing the fractal analyses of tree branches with lung pathways.

Biological patterns ultimately result from the selective action of genes. The genes are activated in specific spatial and temporal order, which results ultimately in production of a specific structure. Activation leads to cellular organization and creates form and the growth of shapes (such as patterns) (Stanley and Ostrowsky, 1986).

There is no object of study available that offers the fantastic conglomeration of rhythmic motion on scales from macroscopic to microscopic as do the motion of muscles, of fluids, of currents, of fibers, of cells. The lung function and heartbeat are other examples of very complicated systems. The mathematics involved in biological processes has been investigated in early reports (Maynard-Smith, 1971). In spite of all this, we know that these patterns are quite self-similar (Holden, 1987; Goldberger *et al.*, 1987). In fact, it has recently been recognized that the effects of such factors as

stress on the self-similarity in biological systems might be useful for medical treatment of many diseases.

As another example, consider the average temperature of the human body. It is fairly constant at ca. 37°C (98.4°F) in the case of a healthy person, so much so that an individual is considered sick if the temperature is either 36°C or 38°C. A temperature of 41°C is very serious. The lipids of a cell melt at temperature greater than 37°C and the flow of molecules across the membranes becomes nonselective, thus giving rise to fever. The magnitude of heat involved (under dynamic conditions) in producing a 1°C difference in the case of a 100-kg human can be estimated as follows:

Number of calories needed to heat 100 kg by 1°C

$$= 100 \times 1 = \text{ca. } 100 \text{ kcal} = 419 \text{ kJ}$$

The average temperature (i.e., 37°C) is the sum of all of the heat produced by various biological reactions (at different rates) in various types of metabolism (e.g., stomach, heart, lungs, brain, liver). This could be demonstrated by quantifying the heat produced (so-called entropy production) by each metabolism, and the sum at all times being equal to 37°C. In a recent study, the entropy inflow and outflow for the human body due to convection, evaporation of water, and mass flow were calculated using the energy data (Aoki, 1989). The perpetual loss of water from the human body as vapor, from exposed surfaces of apparently dry skin to ambient air, is termed *insensible perspiration.* The amount of water liberated was reported to vary from 5 to 35 g/hr ($=5.5 \times 10^{-4}$ mole/sec). The body's heat control is based on the evaporation rate of water from the surface of the body. Further, the slow dynamics of embryonic development and evolution is suggestive of fractal systems with self-similarity. The evaporation process may be expected to be fractal, since diffusion forces are involved. Then it is reasonable to expect that the temperature locally is fractal (this remains to be shown). Furthermore, apart from evaporation kinetics and dynamics being related to human comfort, they are also important for protecting newborns, burn victims, and skin diseases from dehydration.

The surface area of a system is known to play a very crucial role in many phenomena. This is especially true in the case of lungs. The surface area of the human lung is on the order of a football field. The exchange of CO_2 and O_2 is determined by this large interfacial surface area. The fractal dimension of this surface has been found to be 2.2 (Takayasu, 1990; Mandelbrot, 1982).

An early view assumed that all biochemical reactions inevitably converged rapidly to a thermodynamic steady state (analogous to a stone moving downhill into a valley). Further, if any physiological state was disturbed, it was assumed to move toward some equilibrium state. The current view is much different. At present, complex dynamical behavior is seen as an aspect of almost all kinds of biological regulation and function.

The diameter of blood vessels has been found to exhibit a fractal dimension (Takayasu and Nishikawa, 1986):

$$N_r \propto r^{-D} \tag{9.1}$$

where N_r is the number of vessels with diameter greater than diameter r. The value of D was found to be 2.3.

9.1. Fractal Nature of Heartbeat

The accuracy of blood circulation is so high that our technology has not been able to construct a substitute of equal precision. Arteries and veins are known to be fractal-like (compare with viscous fingering or dendrites) (Goldberger *et al.*, 1990). The contraction of the ventricle is stimulated by a nerve impulse generated upon contraction of the auricle. The patterns of the heart rate of a healthy person at spans of 5, 50, and 500 min (Figure 9.1) reveal a clear self-similarity. In fact, the heartbeat can be compared to the movement of a simple pendulum. If one perturbs the pendulum, it oscillates back to its original rhythm, just as the heartbeat can adjust itself to many minor disturbances. This was further analyzed by the chaos and fractal dimension.

The heart rate fluctuates considerably in young adults (average of about 60 beats/min), while it may vary by 20 beats/min every

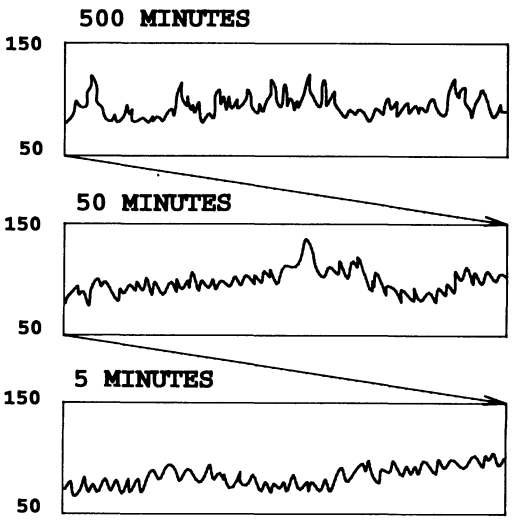

Figure 9.1. Schematic patterns of heartbeat over varying times of observation.

few heartbeats. The variation during a day can be as large as 40 to 180 beats/min.

It has long been known that the fluctuations in heart rate can be explained in terms of homeostasis (i.e., physiological systems normally operate to reduce variability and to maintain a constancy of internal function). This suggests that any biological phenomenon, if perturbed, returns to its normal steady state after some time lapse. This can safely be compared to movement of a pendulum (see Chapter 1); i.e., if one pushes a pendulum that is swinging at a stable rate, the pendulum is found to return to its normal rate after a few minutes. Thus, it is suggested that homeostasis merely arises as a reaction to some transient response in a fluctuating environment. It is also known that the body has difficulty in maintaining a stable heart rate when subjected to illness (fever) or due to old age.

Analysis of the heartbeat carried out for varying time spans—over a day, a few hours, or a few minutes—has provided some insight into the shape of the fluctuations. These beat-to-beat fluctuations have been found to be self-similar. This has been considered to suggest that the heart may fluctuate without any outside perturbation. These kinds of fluctuations are, among other chemical processes, determined by the transport kinetics of ions (calcium, potassium, and sodium).

Analyses of the heart rate (using the Fourier spectrum procedure) have shown that it is indeed chaotic. The mechanism for this chaos in the beat-to-beat variability of the normal heart was suggested to arise from the nervous system. It is universally known that stress causes a rather dramatic change in heartbeat. The question has arisen as to why the heart rate and other systems controlled by the nervous system should exhibit chaotic dynamics. It has been postulated that this plasticity allows systems to cope with the exigencies of an unpredictable and changing (even a sudden change) environment. This was described above in the section on mathematics of chaos (chaotic or periodic). The nonlinear dynamics would thus be useful for such physiological phenomena.

In another report (van der Pol and van der Mark, 1928; Nagumo *et al.*, 1962) an electrical circuit composed of coupled relaxation oscillators was proposed as a qualitative model for the beating heart.

From these considerations, it is clear that physiology should be considered a suitable system for fractal and chaos analyses. The connection between disease and medicine could be a very useful area for fractal dimension analysis. Further, disease and drug toxicity could be better understood if fractal analysis were applied.

The heartbeat can be compared to a pendulum, in a much simplified sense. A pendulum swings with a constant period, and a heart beats with some regular pattern. If we push the pendulum, the period changes for some time, and thereafter returns to its normal pace. Similarly, if we apply a jolt of electricity to the heart, its pattern changes but settles down to its normal rhythm after some time. In fact, chaotic dynamics has been recognized in electrocardiography for a much longer period of time than the recent surge of interest among mathematicians and physicists. It is thus not surprising that fractal geometry has been applied to the heartbeat and disease treatment.

9.2. Mammalian Brain Size Fractal

The brain is a chemical computer with extraordinary state-of-the-art as regards information storage and retrieval. It has been

idealized as a network of neurons that are connected in a random manner by synapses (Krassner, 1983). The stimulus is transmitted by the firing process of a neuron. The latter will fire when the sum of the received stimuli exceeds a certain threshold value. Furthermore, the brain transforms sensory messages into conscious perceptions almost instantly. It has been suggested that there is an analogy to this approach in music. The chaotic arrival of these information signals is sorted out immediately (Freeman, 1991). This may be simply called the taming of chaos in the brain. The chaotic patterns generated by mathematical models (e.g., as produced by the simple equations described in Section 1.5) have been suggested to be useful for the brain function.

The size of the brain in comparison to body weight in different animals is known to be different. It has been suggested that the superior intellect of humans may be due to the large size of the brain. In the same way that the size of the gut varies with the feeding habits of the different animal species, one might expect that brain size could be determined by the information retrieval and storage processes and needs.

Mammalian brain volumes ($\approx$weights) are found to vary from 0.3 to 3000 ml. The human brain weighs ca. 1.3 kg. Some whales have brains as large as 5–8 kg (the brain of elephants weighs 5 kg) (Harvey and Krebs, 1990). It is known that brain weight increases with overall body weight. In one study (Sacher, 1959), the maximum recorded life span was highly correlated with adult brain weight rather than with adult weight among mammalian species. From this analysis it was postulated that life span was controlled by brain weight.

A relationship between brain weight and body weight has been proposed (Gould, 1975). A dependence equal to two-thirds (0.75) power of body weight was proposed. There have been many attempts in the literature to describe the two-thirds dependency. In one case (Armstrong, 1983), it was argued that among extant mammals an increase in brain size keeps pace with an increase in body size when the size is adjusted for the availability of energy. However, it is not clear why mammals should have been selected to supply a constant proportion of their daily basal energy turnover to the brain. In a second analysis (Martin, 1983), it was argued that

the previous postulate was not general. The exponent linking brain and body weight across birds and reptiles was 0.56 and lower than the 0.75. This discrepancy was explained by the argument that if two consecutive metabolic processes were present in birds and reptiles, then $(0.75)^2$ = ca. 0.56.

The metabolic rate (Martin, 1983) in mammals increases with the 0.75 power of adult weight (B), and the weight of the neonatal brain (N) is determined by the maternal metabolic rate. According to this scheme, neonatal brain weight scales to the 0.75 power of maternal body weight. At birth, all neuronal division is complete, such that postnatal brain development consists of the expansion of existing neurons and the addition of glial cells. From this we can add that the adult brain weight (A) is a body-size-independent multiple of neonatal brain weight and therefore scales with the 0.75 power of adult body weight (subscript m denotes mammals):

$$M_m \propto B_m^{0.75} \tag{9.2}$$

and

$$N_m \propto M_m \tag{9.3}$$

From this we get:

$$N_m \propto B_m^{0.75} \tag{9.4}$$

$$A_m \propto N_m \tag{9.5}$$

which gives:

$$A_m \propto B_m^{0.75} \tag{9.6}$$

The two-stage metabolism process limits brain weight in birds and reptiles because of the fact that the mother has to provide for the egg, which must produce the neonatal brain. The egg weight (E) was suggested to be determined by maternal metabolic rate, such that the egg weight scales with the 0.75 power of maternal body weight. The metabolism of the egg (P) is proportional to the egg weight as the power 0.75. The hatching brain weight (H) is directly proportional to the metabolism of the egg. From this one can derive that the hatching brain weight scales with 0.56 ($\approx 0.75 \times$

0.75) of maternal body weight. As it is known (Nottebohm, 1989) that neuronal division determining the size of most components of the adult brain is complete at birth, it has been argued that adult brain weight is a multiple of hatching brain weight and, therefore, scales with the 0.56 power of adult weight, as follows (subscript b denotes birds or reptiles):

$$M_b \propto B_b^{0.75} \tag{9.7}$$

$$E_b \propto M_b \tag{9.8}$$

and one gets:

$$E_b \propto B_b^{0.75} \tag{9.9}$$

$$P_b \propto E_b^{0.75} \tag{9.10}$$

$$H_b \propto P_b \tag{9.11}$$

This gives;

$$H_b \propto (H_b^{0.75})^{0.75} = B_b^{0.56} \tag{9.12}$$

$$A_b \propto H_b \tag{9.13}$$

From these relations one thus finds;

$$A_b \propto B_b^{0.56} \tag{9.14}$$

However, these postulates have not been explained thoroughly (Harvey and Krebs, 1990). Mainly the following questions remain:

- Why should birds, mammals, and reptiles be selected to have as large a brain as their metabolic rates will allow?
- Why should the proportion of metabolic turnover that is allocated to the neonatal brain be the same, irrespective of species difference in adult body weight?
- Why should hatching brain weight scale in proportion to the metabolic rate of the egg, which must provide not only for the chick at the time it hatches but also for the developing embryo?

Recent analysis has, however, indicated that these postulates by Martin are not sufficiently valid and therefore need further examination (Harvey and Krebs, 1990). However, it must be remembered that during the hatching period the formation of the egg shell requires utilization of CO_2 in order to convert it to $CaCO_3$. This arises from the fact that lungs exhale CO_2 while exchanging with O_2. In order to conserve CO_2, the amount exhaled is appreciably decreased during the hatching period.

The volume of gray matter is found to be roughly equal to its thickness multiplied by the area of the brain's surface membrane (termed the *pia*). Assuming that the thickness is the same in all species, the magnitude of the pial area would be proportional not only to the gray matter volume but also to the white matter volume, hence to the total volume, V_{brain}.

The area-volume data were found to give;

$$A \propto V_{\text{brain}}^{D/3} \tag{9.15}$$

where the magnitude of $D/3$ was ca. 0.91–0.93 (Mandelbrot, 1982).

Ever since Huxley (1924) suggested the biological significance of relative size and shape, evolutionary and functional biologists have studied the relation of body size to function. The movement of animals against the gravity of the earth has yielded a wide range of sizes. The size varies by factor of 6 in body mass. The most important criterion is that body structure not break down under motion. Selection therefore may be expected to favor changes in the form, material organization, or mass of biological structures that decrease the probability of their failure during lifetime use. In the case of animals of different sizes, there is used a phrase called "elastic similarity":

$$L^3 \propto D^2 \tag{9.16}$$

where L is the length of the object with diameter D. These relations have further been investigated on the basis of modulus of bone structures and mass (M). From these investigations, the

following have been found (Hokkanen, 1986; Biewener, 1990):

$$D \propto M^d \tag{9.17}$$

$$L \propto M^l \tag{9.18}$$

where allometric (Greek *allouetrov,* meaning "the strange scale") exponents d and l were introduced (Peters, 1983).

The magnitudes of d and l were analyzed (Table 9.1) using the following relation (Hokkanen, 1986):

$$d/l = 1/2 + 1/4l \tag{9.19}$$

It was concluded that evolution may prefer the most simple physical situation. That is, buckling effects of a growing bone under a static load, which is needed to adjust bone proportions, and the dynamic loads are coped "afterwards" with an appropriate choice of running styles. Further, if we accept that only minor changes occur in bone shape, mass-specific forces acting on the skeleton must decrease to maintain a uniform safety factor in larger animals. Rather than alter shape or material strength, selection appears to have forced an allometric change in muscle mechanical advantage and the configuration of the limb elements, as the primary means to lower mass-specific bone and muscle force as animals increase in

Table 9.1. Allometric Exponents for Ungulate Leg Bone Lengths (l) and Diameters (d)[a]

	Experimental			Eq. (9.16)	Predicted [Eq. (9.19)]
Bone	l	d	d/l	d/l	d/l
Femur	0.27	0.35	1.3	1.5	1.43
Tibia	0.22	0.35	1.59	1.5	1.64
Metatarsal	0.2	0.33	1.65	1.5	1.75
Humerus	0.27	0.39	1.44	1.5	1.43
Metacarpal	0.19	0.34	1.79	1.5	1.82

[a]Source: Hokkanen (1986).

size. Consequently, with a greater mechanical advantage, the muscles of larger animals produce greater joint moments for a given mass-specific force. It is found that animals generally exert ground reaction forces that are a constant multiple of body weight (two to three times body weight for each limb) (Biewener, 1990). Based on these assumptions, the analysis gives a fractal dimension of 0.74 for force versus muscle mass data. As regards the speed of movement, in nearly all mammalian species studied, rates of aerobic energy expenditure generally increase with running speed and change of gait. In the case of horses, however, energy use increases as a nonlinear (power greater than 1) function of speed within a gait and actually decreases when the animals change gait.

Diet has also been found to be a determining factor for the fractal dimension of different ratios between brain weight and body weight. It is known that fruit-eating bats have a larger ratio of brain to body weight than do the insectivorous species.

The size of organisms is a good predictor of the biological rates at which they produce energy and consume food. The metabolic rates have been analyzed by fractal theory (Sernetz *et al.*, 1985), since many biological parameters are determined by the size of the organism. An allometric relationship was suggested between species and within the same species. The power law found to describe the metabolic rate (MER) versus body weight (BW) was as follows;

$$\log \mathrm{MER} = \log \alpha + D \log \mathrm{BW} \tag{9.20}$$

The data for different species (rat, dog, man, horse) are plotted in Figure 9.2. These data show that the metabolic rates summed together exhibit a fractal rate. The basic idea assumes that the body is an area that fractally evolves into a volume object. The structures of similar, and more or less comparable, organisms are considered to be made up of similar internal compartments. The kinds and the relative sizes of these biological compartments are also similar. Based on this assumption, one can consider that these systems are self-similar with regard to fractal geometry. Within one organism, self-similar compartmentalization is found over the entire range from macroscopic structures (e.g., the vascular system

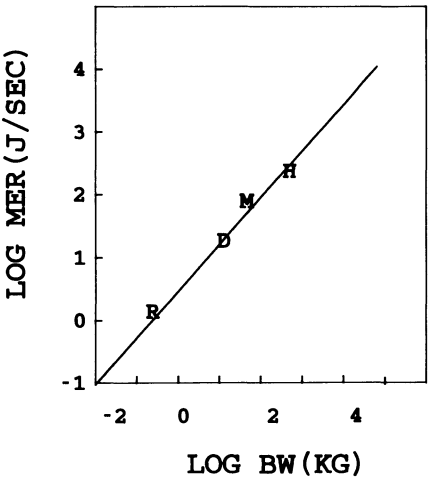

Figure 9.2. Plot of log MER versus log BW of different species: R, rat; D, dog; M, man; H, horse. (Redrawn with modifications from Sernetz *et al.*, 1985.)

and the lungs), to microscopic structures (connective tissue, trabeculae, capillaries) down to the subcellular level (cytoskeleton, organelles). In a recent study (Strathmann, 1990), it has been pointed out that there are probably many pitfalls in testing the hypothesis about the size–abundance relationships. The main difficulty concerns the scatter in the plots. It is clear that more careful analyses need to be performed on this subject. In previous analyses the underlying cause of these scaling relations was seldom well understood. Confidence in the generality of such mathematical relationship depends mainly on the extent of samples used. However, since there are certain subtle differences between these species (e.g., body temperatures are different), further studies are needed concerning these observations.

10

Diverse Fractal Systems

10.1. Ecological and Economic Cycles and Fractals

The driving force in both economic and ecological systems can be considered to be effective under analogous conditions (Smale, 1980; Mandelbrot, 1982). The high oil prices of the 1970s encouraged energy conservation and increased oil exploration, precipitating a predictable drop in prices by the early 1980s. According to conventional economic theory, the equilibrium marks the most reasonable outcome possible under these circumstances. Let us consider a few examples that may be useful in showing fractal trends in economic growth.

Economy. In economic growth, one needs energy input to start a commodity production. This is analogous to ecosystems. Furthermore, economic theory is built on the assumption of diminishing returns (Arthur, 1990).

As an example, competition between two technological products A and B can be considered (Figure 10.1). Which product wins is determined by the path as depicted.

This example shows the tendency of the sales of one product to suddenly switch from one kind of cycle to another. This is analogous to the examples described in the section on chaos (Section 1.5).

The conventional economic texts have described the economy in terms of Newtonian systems, with a unique solution preordained by patterns of mineral resources, geography, population, consumer

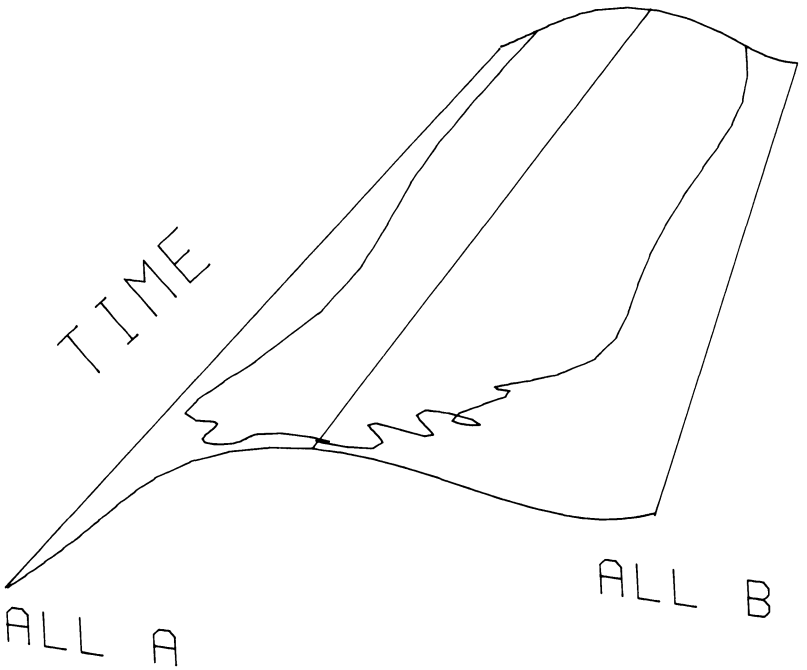

Figure 10.1. Random walk on a convex surface illustrating increasing-return competition between two kinds of technologies [car = A; computer = B]. Chance will determine early pattern formation of adoption and therefore influences how fast each competitor improves. Alternatively stated, as one technology gains more attractors (which is related to movement downhill toward either edge of the surface), further adoption is increasingly likely. (Redrawn with modifications from Arthur, 1990.)

tastes, and technological possibilities. The perturbation events, such as the oil price shock of 1973 or the crash of the stock market of 1987, are quickly weighted by the opposing forces they elicit.

As in many economic cycles, it is generally held that cotton prices exhibit two cycles, one due to orderly and one due to random sources. If observation of these cycles is taken over a long time, then the price cycles could be related to production and trade turnover. The computer has had a very strong impact on prediction of economic price developments. The small-scale ups and downs occurring in a short (24 hr) cycle are just noise, which arise from

very unpredictable sources. However, as already observed for other systems, the effect of changing forces would suggest a coherent effect, even if the cycle was of larger scale.

Well-accepted prediction schemes of corn production in many countries (e.g., India and Egypt) have regarded production to occur in cycles of 7 years, i.e., plentiful crops for 7 years followed by drought for 7 years. Of course, one may correlate this to floods, which may be the result of rains, which in turn may be related to solar flares. To a casual observer, the sum shines constantly with a bright white light that changes to reds and yellow only when scattered or absorbed by dust particles and vapors in the air. A closer look reveals, however, that the sun is far more dynamic than the Earth. Cataclysmic storms periodically erupt on the sun's surface, and these storms sometimes are large enough to easily envelop several Earth-sized planets. One can see this clearly written in the shapes and colors of cliffs on the surface of the Earth, where one sometimes finds repeating patterns, i.e., self-similarity, that have been connected to these activities.

The new theory of chaos may be helpful in setting asset allocation. As is well known, asset allocation seems like a neat and tidy process, conventionally governed by mechanistic rules of economy. The theory of chaos may lead to new insights into the financial market mechanisms and more effective ways of dealing with risk and return in asset allocation. Although the random-walk hypothesis has been proposed to be useful for explaining the ups and down of economy, there are still some who doubt this. On the other hand, it is well accepted that some traders do make above-average profits by following these theories. Current interest toward developing such fractal models is increasingly. However, it is not easy to explain why one finds some trends in the economy's ups and downs. Or it may be that some as-yet-unknown nonlinear developments are driving these trends. It has been suggested that analysis of the stock market by fractal theory is very useful in the interpretation of risk and return measures (Speidell, 1988). It is of further interest to consider whether in some cases the food production cycles may even influence the political balance of a country. In other words, fractal analysis might be regarded as a very useful parameter for such political developments as experienced in recent years in Eastern Europe.

10.2. Distribution of Wealth

It is expected that the distribution of wealth will follow some fractal law, at least within a certain range of yardstick used for the observation. The cumulative income in the United States has been analyzed (Figure 10.2). The income, I, and the cumulative population with a given income, P_I, were related by a power law. The data show that the first part of the population (i.e., from 9 to 90%) follows a straight line with a lower value of D than for the data above that:

$$P_I \propto I^{-D} \approx I^{-1.6} \tag{10.1}$$

This allows us to conclude that the distribution of wealth is fractal, with two different values. This is a typical example of a system that exhibits two (or more) different values of fractal dimension.

This probability relationship may be analyzed as follows. Let P_0 denotes the probability of success of any primary task. If the task requires success from many primary tasks, then (Schlesinger and Montroll, 1983):

$$P_0 = p_1 p_2 p_3 \cdots \tag{10.2}$$

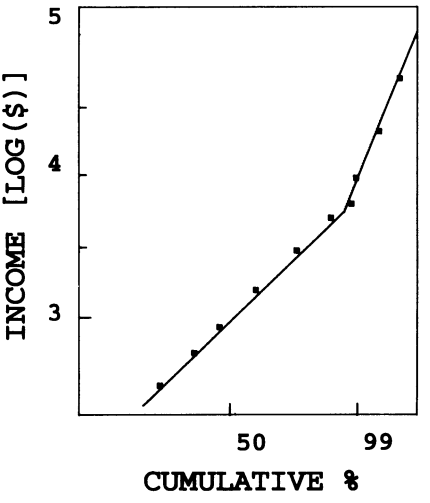

Figure 10.2. Distribution of income (during 1935 in the United States) as log(income/year) versus log(cumulative percentage). (Redrawn with modifications from Takayasu, 1990.)

where p_i indicates the probability of success of the ith subtask. By taking the log of both sides we can write:

$$\log P_0 = \log p_1 + \log p_2 + \log p_3 + \cdots \tag{10.3}$$

Since the terms p_i are independent random variables, the critical limit theorem can be applied, and accordingly the expression $\log P_0$ will have a Gaussian distribution.

Other areas where fractal geometry theory has been applied are filmmaking, town planning, and economics (Lamb, 1987).

10.3. Cellular Automata

As mentioned above, one often finds in nature systems whose overall behavior is extremely complex, yet whose fundamental components are quite simple. It has been argued that the complexity is generated by the cooperative effect of various components. In diverse physical and biological systems, one knows very little regarding the overall complexity.

If we consider the reverse procedure of the above descriptions, it should be possible to produce complicated structures by some simple fractal algorithm or equation. In this context, consider the DNA molecule (molecular weight $>10^6$), which is known to determine the heredity of living systems. Certain fractal procedures, the so-called cellular automata, attempt to analyze these systems (Wolfram, 1984; Hecht, 1990).

The different properties to be considered are:

- A discrete lattice is the basis.
- Time evolution is discrete.
- Number of states at each site is finite.
- Rule of evolution is deterministic.
- Evolution rule is governed by the state of the neighboring sites.

As regards the thermodynamics of such systems, the reversible and irreversible states are of current interest. Most fundamental physical laws appear to be reversible; macroscopic systems often

seem to be irreversible phenomena. These phenomena have been discussed in detail in the literature with respect to cellular automata (Wolfram, 1984).

10.4. Fractal Interfaces in Diffusion and Corrosion

Porous silicon made by anodic reaction of p-doped silicon with hydrofluoric acid displays a ramified microstructure, which is determined by the applied voltage, acid concentration, and amount of doping (Daccord, 1989). These patterns need to be investigated as regards their fractal geometry. Stress corrosion or cracking (due to self-similar patterns) is another area that may be fractal (Avnir, 1989).

Fracture surfaces of metals. The metal surface plays a very important role in everyday life. The surface roughness thus is better analyzed if its fractal dimension can be estimated. The data for the fracture surface of steel gave the following relationship (Shleisinger *et al.*, 1984):

$$A \approx L^{2/D} \tag{10.4}$$

where the value of D was found to be 1.28.

We have seen that self-similarity is observed in various natural phenomena, especially cracks in metals (or cement). The phenomena of material failure and deformation are recognized to be of much importance. The deformation phenomena take place in a variety of systems and over a wide range of time and length scales. They indicate nonlinear behavior under nonequilibrium conditions. The patterns formed in metals are quite similar to the viscous fingering described earlier (Chapter 2). In simulation theory of mechanical properties of metals, the material is represented as consisting of bonds, springs, and beams. These unit structures break down at some rate of failure (Meakin, 1991). It is well known that the rate of failure of many materials increases very rapidly with increasing stress and strain. This shows how the microscopic structure propagates macroscopic failure. In the viscous fingering experiments, cracking patterns are observed when

the concentration of the solids increases. Thus, most of the theory is comparable in these two phenomena. The magnitudes of the fractal dimension have been found to vary from $D = 1.12$ to 1.66.

10.5. Reaction Kinetics and Fractals

In the case where stirring is not possible, such as reactions taking place on solids (porous solids; e.g., oil recovery, groundwater) or in viscous media, the diffusion processes predominate. Furthermore, many physicochemical and biological reactions are diffusion-controlled, for the same reason. Other examples are industrial catalysis and electrode surface reactions, as well as bioenzymatic and membrane reactions.

The concept of fractals, as applied to problems in physical chemistry, has been described in the literature (Argyrakis, 1988). Before describing the fractal analysis (Kopelman, 1989) of such reactions, it is worthwhile to review the classical chemical kinetics (Berry *et al.*, 1980; Argyrakis, 1988). We will consider two examples, i.e., either substance A reacts with A, or A reacts with substance B, as follows:

$$A + A \rightarrow \text{products} \tag{10.5a}$$

or

$$A + B \rightarrow \text{products} \tag{10.5b}$$

These reactions are defined as second-order rates:

$$\text{Rate} = K[A]^2 \qquad \text{for A + A} \tag{10.6}$$

$$\text{Rate} = K[A][B] \qquad \text{for A + B} \tag{10.7}$$

where [A] and [B] are the reactant concentrations of each species, and K is the reaction constant and is independent of [A] or [B] and time. It is obvious that when A = B, then the latter equation is analogous to the former.

The batch and steady-state condition are of interest. Stirring of such reactions seems to provide a quantitative way of controlling their rate, and in a sense provides a new approach to catalysis. In fact, batch reactions are also called *big-bang reactions*. In this case, at time $t = 0$, we have:

$$\text{Rate} = -d[\text{A}]/dt = -d[\text{B}]/dt \tag{10.8}$$

i.e., the rates of disappearance of species A or B per unit time.

From these equations we can obtain:

$$-d\text{A}/dt = K[\text{A}]^2 \tag{10.9}$$

On integration one gets:

$$[\text{A}]^{-1} - [\text{A}_0]^{-1} = Kt \tag{10.10}$$

where $[\text{A}_0]$ is the initial concentration of species A at $t = 0$.

A genuine steady-state reaction (Kopelman, 1989) is independent of time, by definition. The fractal nature now expresses itself in an anomalous reaction order 0. For instance, for the bimolecular A + A reaction:

$$\text{Rate} = K[\text{A}]^X \tag{10.11}$$

where X is not 2 as in Eq. (10.9). If the reaction is diffusion-driven (diffusion-limited):

$$X = 1 + 2/D_s \tag{10.12}$$

where $D_s < 2$. Hence, we expect $X = 2.46$ for the Sierpinski gasket, $X = 2.5$ for the percolating cluster, and $X = 3$ for the one-dimensional (A + A) reaction.

A percolation model of the reactions taking place in the ignition of propellant powders has been reported (Grabski, 1990). It is thus seen that analogous considerations will be valid in heterogeneous reaction kinetics in chemistry, biology, geochemistry, solid-state physics, astrophysics, atmospheric sciences, etc.

Another study (Argyrakis, 1988) has reported some related applications to fractal chaotic motion in polyatomic molecules, and entropy functions as a measure of disorder.

The Belousov–Zhabotinsky Reaction

Oscillations are familiar phenomena in mechanical and electric circuits. The direction of motion of an object or an electric current may repeatedly reverse itself with or without damping of the amplitude of oscillation, and repetitive standing or traveling waves may be generated in a continuous medium. A simple pendulum describes these movements quite satisfactorily (Chapter 1). In stirred-reactor investigations of any chemical reaction, the concentrations are conveniently taken as spatially uniform throughout the phases. Chemical systems are less prone to oscillations, and their evolution usually leads to monotonic change of chemical parameters (Borman, 1991). Electrochemical oscillations have been observed in a variety of electrochemical systems (Kelzer and Noyes, 1980, Koper and Gaspard, 1991). The simplest of this sort of oscillation involves a coupling to the impedance of the external circuit, and the resulting oscillations are easily understood on the basis of elementary circuit theory. A more complicated and picturesque oscillation occurs in the beating mercury heart (Field and Noyes, 1977). In that system, oscillations are triggered by the reduction of a variety of electron acceptors adsorbed on a mercury surface. The switching mechanism, which leads to voltage and shape oscillations of the mercury, involves a periodic short circuit caused by the electrocapillary effect. These oscillations are driven by a corroding metal electrode but do not otherwise depend on the external circuit.

Oscillations have also been observed during homogeneous gas reactions (Noyes and Field, 1974). Living organisms exhibit many processes like heartbeats (see Section 9.1) or nerve impulses that generate repetitive temporal or spatial changes. The mechanisms and energy sources driving these biological processes are ultimately chemical in nature, and the dynamics of many biological and chemical oscillators are likely to contain analogous feature. A review on the theoretical and practical aspects of oscillation in

chemical and biological systems has appeared (Noyes and Field, 1974). In most oscillating reactions, there may be present a metal ion. A typical system that has been investigated consists of methylene blue (a dye), oxygen, and sodium sulfide (Na_2S). This reaction has been analyzed by theoretical models based on noise and bifurcation (Resch *et al.*, 1991). The fluctuations and the amplitude of the reactant species were estimated. The hysteresis was found to be related to these factors.

A general discussion on the aspects of chemical oscillators using a specific model to illustrate some important concepts concerning the theory of chemical oscillators has been published (Field and Noyes, 1977). Although mechanical, electrical, and chemical systems are all susceptible to oscillation, chemical oscillators differ from the others in important ways. In a frictionless (conservative) oscillating mechanical system, the sum of potential and kinetic energies remains constant while they are repeatedly interconverted. Although total energy is sufficient to define the repetitive trajectory in such a conservative system, both a coordinate and a momentum must be stated simultaneously to define the instantaneous state. Inertia repeatedly carries the system through the position of minimum potential energy to which it will eventually decay if any friction is present.

In an electrical oscillator, the voltage and the current behave very much like potential and kinetic energies, respectively, and both must be specified to define the instantaneous state. If there is no external source of power, the oscillations repeatedly carry the voltage through the value to which the system eventually decays; the overshoot arises because induction associated with the current behaves very much like mechanical inertia.

One of the most extensively studied oscillating chemical reactions the so-called Belousov–Zhabotinsky reaction, involves the cerium-catalyzed bromination and oxidation of malonic acid by a sulfuric acid solution of bromate ion (Field and Burger, 1984; Holden, 1987; Zhabotinsky and Rovinsky, 1990). The reaction can be maintained in a steady state away from equilibrium by pumping the chemicals into a stirred flow reactor. The qualitative description is as follows:

$$A + B \underset{k_b}{\overset{k_f}{\rightleftharpoons}} C \tag{10.13}$$

where A reacts with B to produce C, with forward and backward kinetic rates, k_f and k_b, respectively. If in the reactor the flow rate, r, of the chemicals is kept constant (with concentrations A_0 and B_0), then we get a set of nonlinear differential equations:

$$dA/dt = -k_fAB + k_bC - r(A - A_0) \tag{10.14}$$

$$dB/dt = -k_fAB + k_bC - r(B - B_0) \tag{10.15}$$

$$dC/dt = k_fAB - k_bC - rC \tag{10.16}$$

The oscillations observed are very dramatic and can be easily measured, and are dependent on the flow rate, r.

In a recent study of the Belousov–Zhabotinsky reaction, spiral-like shapes were observed (Plesser *et al.*, 1990; Nagy-Ungvarai *et al.*, 1990) (Figure 10.3). The wave profiles and

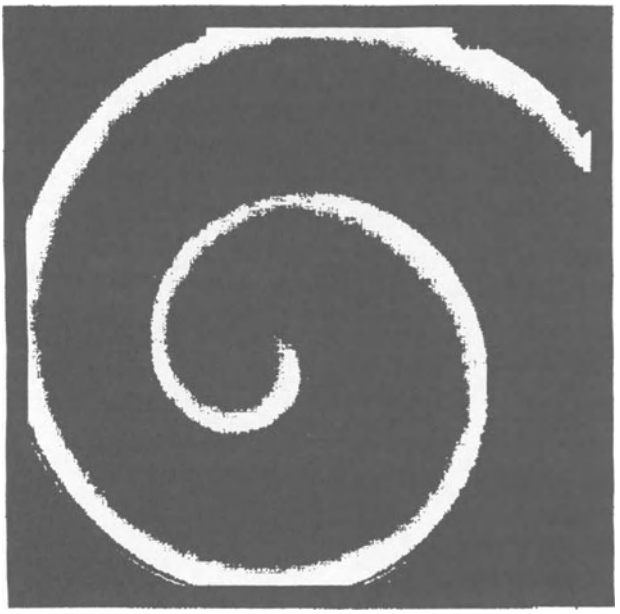

Figure 10.3. Spiral-like shapes in BZ reactions. (Redrawn with modifications from Plesser *et al.*, 1990.)

gradients were analyzed by high-precision two-dimensional measurements. The data suggested clearly that the geometry and the dynamic properties of the spiral waves are predominantly determined by the chemical composition of the reacting species. Since the periodic nature is indeed an indication of fractal and self-similarity, the spiral-like reactions are of much interest at this stage. In another study (Weis and McConnell, 1984, 1985; Keller *et al.*, 1986), spiral-like shapes were observed in mixed monolayers of cholesterol–lecithin spread on the surface of water. Another example where such cycles are observed is in the case of childhood diseases (measles, mumps, chickenpox). Analyses have shown that the data exhibit an interesting yearly cycle with some kind of noise superimposed (Holden, 1987).

In another system, consisting of sodium iodide, malonic acid, sodium chlorate, sulfuric acid, and starch as indicator, one can observe trigger wave patterns (de Kepper *et al.*, 1990). The waves are seen in a dish with a thin (2 mm) layer of reactant solutions. The waves formed annihilate on collision and can be sheared to produce double rotating spirals. This dramatic performance lasts for a short time.

Chemical oscillation has been found in many biological systems. The glycolytic cycle exhibits such oscillations (Pye and Chance, 1966; Hess *et al.*, 1966), and is considered to be central to the process of integration, ordering, and the turnover in living organisms. A new approach was used to determine how encapsulation can aid further ordering of the chemical components. The Belousov–Zhabotinsky reaction in reverse micelles of Aerosol OT [sodium bis(2-ethylhexyl)sulfosuccinate (AOT)] showed that the characteristics of the oscillations are substantially different from those of the same system in water phase (Balasubramanian and Rodley, 1988; Gonda and Rodley, 1990). In a recent study the Belousov-Zhabotinsky reaction was studied in a ternary mixed system: water/isooctane/AOT liquid-crystal phase (Balasubramanian and Rodley, 1991). The purpose of this study was to determine the effects on the length of time that oscillations can be maintained, and the period. It was known that in reverse micelles these parameters were affected. In liquid-crystal structures, the bulk concentrations would be in compartments. In these organized

assemblies, the period decreases toward the end of oscillation. The other effect was period lengthening.

The effect of stirring in such oscillating reactions was reported in a recent study (Menzinger and Jankowski, 1986). It was found that in a stirred batch reactor, large concentration variations did exist and appeared in the ferro–ion–catalyzed Belousov–Zhabotinsky reaction. The reaction was spatially distributed rather than homogeneous. Stirring was found to affect both the amplitude and the spectrum, as well as the period and amplitude of the limit cycle. These data were characterized by use of this macroscopic stirring parameter in terms of noise-induced transitions.

These oscillating reactions create variations in concentrations. If the variation is considered in three-dimensional space, one finds a wide variety of shapes and forms that can be described by using the same procedures (Winfree and Strogatz, 1984). Periodicity was reported to be the main principle cause of these oscillations. A thin layer of excitable medium thus has a finite thickness. The flat spiral is actually a cross section of a three-dimensional wave shaped like a scroll. Three-dimensional images were created by computer programs.

Dynamics of toxic chemicals. The toxicity of different molecules has been investigated in the current literature by using dynamical models (Hallam and Huang, 1989). This arises from the fact that the toxic effects on an organism are determined both by the chemical and by the organism. Further, various toxic phenomena are generally known to be related to biological and interfacial phenomena. Attention has especially focused on the magnitude of the surface area in the assessment of toxic effects. In the dose–response functional analysis, the quantitative structure–activity relationship (QSAR) has been used. The oscillation that sets in arises from the variation in concentration of the chemical as the metabolism affects its concentration (through dilution, uptake, breakdown, etc.). Furthermore, it is of interest to determine whether the toxic property of a chemical arises from its interaction with biological reactions in some catastrophe mechanism. This would then easily explain why some chemicals are 100 million times more toxic than others. The catastrophe model could be initiated by using the procedures described earlier (Section 1.5). In this

model, a single molecule with toxic properties interacts with the bilayer structure of a cell membrane, leading to a cascade of structural breakdown of the lipid bilayer. This mechanism is in accord with the observation that very minute amounts of toxic substances are sufficient to destroy living cells in all kinds of biological systems. Fractal theory is thus the one most appropriate for classification and prediction models of toxic molecules.

10.6. Diverse Chaotic Phenomena

Almost all natural phenomena are governed by chaotic motion. However, as seen above, there are a variety of situations where any phenomenon can exhibit chaos, and it may become increasingly complex as the dimension of the reference space is increased. Some examples follow.

Weather forecasting (Lorenz, 1963). The world climate that we know and consider normal is in fact a geologically recent development. Forty million years ago, most of the planet was both warmer and wetter than it is now. Rainfall tended to be evenly distributed throughout the year, and evergreen and warm forests covered much of the Earth's surface. In many global climate models, a system of equations estimates time-dependent changes in wind as well as temperature and moisture changes in the atmosphere and on the land. We know that part of the motion of the atmosphere is caused by thermal convection, when air warmed near the Earth's surface rises toward the sky. This process may give rise to spontaneous but organized currents of air which may even look like a honeycomb (Figure 10.4).

An example of a similar kind of heat-generated convection is found in cooking. As oil is heated in a pan, one keeps a reasonably constant difference in temperature from top to bottom. The patterns (also called Rayleigh–Benard) produced in the oil look like honeycombs (Velard and Normand, 1980; Bergé *et al.*, 1984; Behringer, 1985). These patterns are found to be related to temperature gradient, distance across the gradient zone, thermal diffusivity and viscosity of the fluid.

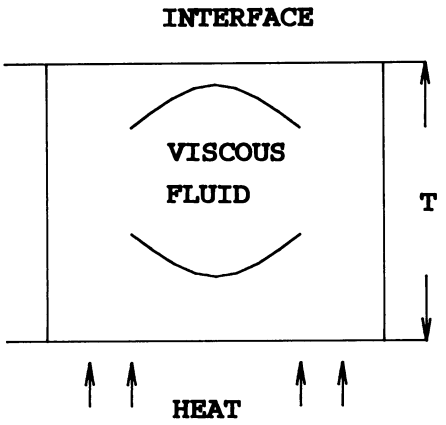

Figure 10.4. An idealized rectangular region of thermal convection as a model used for analysis by Lorentz equations. The temperature difference between the heat at the bottom and the cold at the top is held constant.

Fluid rotation (Couette–Taylor) system. If fluid is subjected to rotational forces when contained between concentric cylinders that rotate with some angular velocity, viscosity-dependent instabilities are observed (Andereck *et al.*, 1983). The patterns are also dependent on the radius of the cylinder and the speed of rotation.

This system can be described by a differential equation:

$$X = -\zeta(X - Y) \tag{10.17}$$

The particle accelerator and dynamics. In celestial mechanics and high-energy physics, there are some important problems that need to be considered as being nonlinear and chaotic systems in the design of particle accelerators (Thompson and Stewart, 1988). Accelerators are used to study subatomic particles, produced upon collision between two beams of heavy particles, protons or electrons. In spite of the very high speeds with which these particles move, the data can be analyzed by some simple nonlinear procedures. Typically, a proton undergoes some 10^{11} revolutions in a storage ring. Accordingly, one must use very sophisticated procedures to obtain stability results.

10.7. Thin-Film Deposition

Man-made solid films are ubiquitous in technological societies. A wide variety of thin-film deposition processes are used to

manufacture magnetic, electronic, optical, and tribological devices. Particles such as atoms or molecules are deposited on a substrate using trajectories that are more nearly ballistic than Brownian because the deposition processes are usually carried out in an atmosphere of very low pressure. In practice, the deposition processes are carried out under conditions of complex physical and chemical processes aimed at obtaining high-quality deposited films or layers with a homogeneous internal structure and a smooth outer surface. Because of the practical importance of these processes, considerable effort has been devoted to achieving a better understanding of the relationships between morphology and deposition conditions.

Two-dimensional structures that are clearly reminiscent of DLA patterns are sometimes observed on the surface of a variety of sputter-deposited thin films, as in the case of $NbGe_2$ thin films sputter-deposited onto quartz substrate. It was found that whereas the fractal dimension of the original clusters with thick outer arms is about 1.88, the underlying skeletal structure obtained by defoliating the thick limbs of the clusters gives $D = 1.7$. This value is very close to that expected for two-dimensional DLA. Similar data were obtained for deposition of gold films on a Nucleopore filter. Local scaling properties of fractal observed in nickel–zirconium alloy films have been reported (Ding *et al.*, 1990). In a recent article (Bales *et al.*, 1990), a macroscopic theoretical approach was used (in combination with scanning tunneling microscopy) to analyze the morphological evolution of thin films grown or eroded by sputtering. The growth surface was found to be very ramified and was, in fact, fractal.

A recent study reported the adsorption isotherms of silver and gold films evaporated onto the surface electrodes of a quartz crystal microbalance (Krim and Panella, 1991). The adsorption isotherms were measured by depositing thin films on the quartz crystal microbalance, in order to increase the sensitivity. This procedure employed as little as 1 cm^2 of surface area. The data were analyzed by the Frenkel–Halsey–Hill equation [Eq. (8.16)]. The data for silver films showed two values of D. In the case of optically polished films $D = 2.0$; for mechanically polished films, 2.4.

In those adsorption processes where the surface reactions are

Table 10.1. Magnitudes of Fractal Dimension, D, for Chemisorption on Dispersed Metal Catalysts[a]

Catalyst	Adsorbate	Metal particle size (Å)	D
$Pt–SiO_2$	H_2	13–40	1.67
$Pt–SiO_2$	CO	66–270	1.6
$Pt–Al_2O_3$	H_2	13–103	1.91
Ag–silica	O_2	55–400	1.82
$Ag–Al_2O_3$	O_2	336–512	2.03
$Rh–Al_2O_3$	O_2	17–150	1.9
$Ni–SiO_2$	H_2	27–87	2.13
Fe–charcoal	CO	$0.11–10^6$	1.6

[a]Source: Farin and Avnir (1989).

dependent on the chemical accessibility at the surface, other procedures are required for the analyses. This has been described for the case where the molecule–surface interaction is the interaction with dispersed metal catalysts (Farin and Avnir, 1989). Even though the metal surfaces are not perfect, it has been observed that D = ca. 2. As seen from the data in Table 10.1, this is indeed correct.

10.8. Thermodynamics of Equilibrium Potential and Fractal Dimension

Gas molecules possess kinetic energy, which is equal to the Boltzmann constant (k) times the temperature (in Kelvin). If we consider the transition between different phases, like gas → liquid → solid, it is obvious that the movement of molecules decreases as we compress the gas to the liquid or solid state. These molecular movements will exhibit fractal properties if self-similarity exists. Accordingly, it is necessary to consider the general thermodynamic properties within this framework.

In the current literature, unfortunately, very few reports have analyzed the fractal dimension of the thermodynamic quantities.

As is well known from thermodynamics, the concept of extensity (Q) is essentially determined by the local existence of a volume density (ρ) such that (Berry *et al.*, 1980):

$$Q = \int_V \rho \, dV \tag{10.18}$$

where the integral is taken over the volume, V. The concept of intensity (μ) is related to Q as follows;

$$\mu = dS/dQ \tag{10.19}$$

where S is the entropy function. In classical thermodynamics, the volume element is easily estimated from Euclidean geometry. However, recently (Fruchter *et al.*, 1986) it has been mentioned that the metric of the medium could have an effect on the value of this thermodynamic quantity. Thus, it has been shown that S is a function of D, i.e., S_D. Further, the fundamental relationship:

$$\mu = h - TS_D \tag{10.20}$$

suggests that provided h, the molar enthalpy, is invariant with change of the metric, a correlation must exist between dimension and chemical potential (μ) (Mehaute and Dugast, 1983). This concept was mentioned above when we considered the fractal nature of the interfacial forces in the gas–solid–liquid systems. The thermodynamics of adsorption phenomena on fractal objects have been reported in a recent study (Yakubov, 1988). An advanced application (Bessis and Moussa, 1985) of fractal structures (using the so-called Julia sets) has been given for explaining: the two-dimensional electrostatic, one-dimensional almost-periodic Schrödinger equation, vibrational spectra, and location of the zeros of the partition function for exactly renormalizable lattice spin systems. In these analyses one may also need to consider the role of fractional calculus. This arises from the fact that the order of differentiation or integration can be elaborated to include fractal dimensions (Holden, 1990; Takayasu, 1990). The dimension of a derivative may be on the order of say 0.24 or integral with a value of 0.35. This has been termed *fractal calculus*.

In another example, the mixing process of two liquids was analyzed by using the fractal theory of molecular packing model (Birdi, 1992a). It was assumed that in the mixing process of alkane and alcohol molecules, the enthalpy was related to the placement of methylene groups ($-CH_2-$) of alkanes around the alkyl part of the alcohol, while avoiding contacts with the hydrogen-bonded hydroxyl groups. The size of the alkane molecule can be considered in terms of surface area of the alkane molecule, SA_{alkane}, as described in the literature (Birdi, 1989). If we imagine that the alcohol associates as a dimer (through hydrogen bonding) (Figure 10.5), then the hydroxyl groups are oriented toward each other. This can be considered as a Cantor set with some appropriate magnitude of D, depending on the alkyl part of the alcohol molecule. The enthalpy data for systems of *n*-alkanes (pentane; hexane; heptane; octane; decane; dodecane) + *n*-alcohols (methanol; ethanol; *n*-propanol; *n*-butanol) were investigated. The enthalpy for mixing $-CH_2-$ units of alkane per mole of an alcohol was found to fit the following model:

1. Alcohol molecules are present mostly as dimers.
2. $-CH_2-$ units of alkanes are arranged around the alkyl part of the alcohol (preferentially).

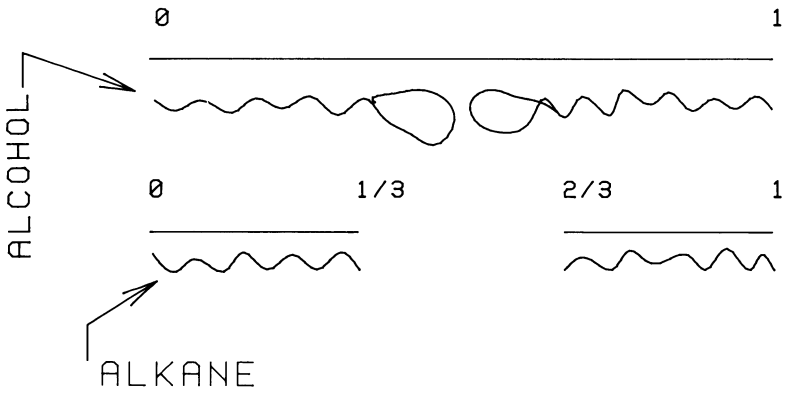

Figure 10.5. A Cantor set model with $D = 0.63$ for the mixing process of alkanes with alcohols [Eq. (10.21)]. (Birdi, 1992d.)

Accordingly, the enthalpy of mixing 1 mole of alcohol, $H_{mix,1}$, will be related to the ratio of moles of alkane to mole of alcohol ($n_{alkane}/n_{alcohol}$), and the fractal geometry as follows:

$$\Delta H_{mix,1} = SA_{alkane}(n_{alkane}/n_{alcohol})^D \tag{10.21}$$

The data for various alkane–alcohol mixtures fit this equation for $D \approx 0.6$, with a correlation coefficient ≥ 0.99. The data are found to fit the Cantor set model of the alcohol dimer with $D \approx 0.63$ (Figures 5.3 and 10.5).

10.9. Liquid Droplet Growth and Evaporation by Diffusion and Fractal Dimension

The phenomena of liquid droplet growth and evaporation play an important role in everyday life (e.g., raindrop to fog; combustion of oil in engines; emulsion formation). Accordingly, these phenomena have been extensively investigated by different methods, and recently by fractal methods. The surface of any liquid, even though it may look very stable, is actually very turbulent at the molecular level. From kinetic theory the number of molecules of water striking 1 cm^2 is found to be 1.2×10^{22} molecules/cm^2-sec. At equilibrium in a closed container, the same number of molecules will be leaving the liquid phase. Despite the enormous traffic, there is no direct method for visualizing this phenomenon. Current studies on evaporation of liquid droplets confirm the presence of noiselike data, which indicates the fractal nature of the process (Birdi, unpublished).

Liquid droplet growth. The growth of a liquid droplet has been described by many investigators (Langer, 1980; Mullins and Sekerka, 1963). The liquid droplet can be imagined to grow in size due to condensation from the supersaturated solution. The molecules execute a random walk, and this diffusion process determines the physical conditions. However, the droplet only grows after a cluster of critical size has been formed, whereafter the growth is very simple. This growth phenomenon has been of interest to many researchers. The main question relates to how many atoms it takes

to form a cluster that changes over to a new phase (say from gas to liquid or liquid to solid). One clue to this number is the point at which the atoms start organizing themselves (with self-similarity) in some regular fashion, such that a cluster stops behaving as a liquid and becomes a solid (Duncan and Rouvray, 1989). An estimate of 1500 atoms has been proposed from experimental studies. A steady state is observed, i.e., rate of mass adsorbed per unit time (dM/dt = flux) becomes constant. In fact, recent investigations carried out on the reverse phenomenon, i.e., rate of evaporation of liquid droplets, have confirmed this very clearly for a variety of fluids (Birdi *et al.*, 1989).

Evaporation of liquid drops. The evaporation of liquid drops in air is of importance in many natural (rain, fog) and industrial processes (spraying fluids in agriculture). In spray ponds, cooling of water is obtained by spraying water into the atmosphere. In pharmaceutical and food industries, certain materials like malt extract, milk, eggs, and different fruits are dried by spray drying. Another example is the ordinary combustion-type engine found in cars, where gasoline droplets evaporate and ignition follows to provide the necessary propulsion force.

Under specific conditions, oscillation of a small drop of liquid is observed under its own surface tension (Srikrishna *et al.*, 1982). Oscillations refer to periodic changes of shape of the drop from spherical to ellipsoidal and back. The oscillation of a small liquid drop under the influence of its own surface tension and in the absence of gravity is given as (Raleigh, 1892):

$$f = (V/2)\Pi \tag{10.22}$$

$$= (1/2)\Pi[(8\zeta)/(\rho R^3)]^{1/D} \tag{10.23}$$

where V = vibrations, and R is the radius of the drop. For a drop of mass m:

$$f = [(8\zeta)/(3\Pi m)]^{1/D} \tag{10.24}$$

The oscillation frequencies of drops of different liquids (drop diameters: 2–8 μm; densities of liquid: 0.66–3 g/cm^3; viscosities:

0.3–20 cP; surface tension: 18–73 dynes/cm) have been investigated by photographic technique. Oscillation frequencies of liquid drops were measured by a stroboscope, with 60 to 60,000 flashes per minute. The flash duration was 50 μsec. These investigations showed that drops of liquids oscillate about a mean drop shape. The frequencies of these oscillations were found to fit Eq. (10.20) (with $D = 2$). The rates of evaporation of liquid drops (of volume 100–5 μl) when placed on smooth solid surfaces have been investigated (Birdi *et al.*, 1989, 1990). The data exhibit fluctuations (noise) with a power-law characteristic (i.e., fractal surface evaporation). These investigations have shown that important information about the solid (especially porous)–liquid interface can be obtained from such dynamic investigations. The rate of evaporation of fluids versus time on glass surface was absolutely linear (i.e., dM/dT = constant). Nonlinear rates were observed on rough or porous solid surfaces (Birdi and Vu, 1991).

11

Physical Applications of Fractals

Cloud boundaries, dendrites, coastlines, lightning, riverbeds, shapes of molecules (macromolecules)—all of these have a form or shape that is much better described by fractal geometrical theory than by Euclidean geometry (i.e., straight lines and smooth curves) (Table 11.1). Fractal theory provides a basis for studying these phenomena by modeling and making predictions.

However, in many cases there would be considerable difficulties trying to apply the mathematical analyses of fractal theory. We showed that the power laws are only valid within the limits of the size of the yardsticks used. The power law would not be valid when the length of the yardstick used is either too large or too small, as well as dependent on the characteristics of the system. In other words, the length of a coastline would increase as the yardstick used (δ) to measure it is decreased from say 200 km to 20 m, while $\log N_\delta$ versus $\log \delta$ is found to be a straight line with slope equal to $D = 1.2$. But if δ used is = 1 nm, the data would be meaningless. On the other hand, in the case of analyses employing electron or scanning-tunneling microscopy, $\delta \approx$ nm would be mandatory.

Under these circumstances, one may question whether true fractals actually are found in nature. One answer is that there is nothing like "frictionless" or an "exact answer." However, it is more appropriate to answer that, within the framework delineated above, fractal analysis is of value when keeping in mind the basis of

Table 11.1. Some General Methods of Estimating D from Measured Data

Method	Relationship	Estimation of D from log–log plots
1. Length of trail dividers method	$L_e = Ke^{1-D}$ e = step size K is constant	log L vs. log e slope = $1 - D$
2. Area/perimeter	$A = KP^{2/D}$ $A \approx$ area $P \approx$ perimeter	log A vs. log P slope = $2/D$
3. Box counting	$N_1 \propto L^{-D}$ N_1 = number of boxes of size 1	log N_1 vs. log L slope = $-D$
4. Variogram	$2g_h = h^{4-2D}$ h = sampling interval	log g_h vs. log h slope = $4 - 2D$
5. Power spectrum	$P_w = w^{-(5-2D)}$ P_w is power w is frequency	log P_w vs. log w slope = $-(5 - 2D)$
6. Korcak/Zipf law	$N_r(A > a) = Fa^{-D/2}$ $N_r A > a$ number of islands larger than size a F is constant	log $N_r(A > a)$ vs. log a slope = $-D/2$
7. Functional box counting	$N_L \propto L^{-D}$ N_L is the number of squares (or cubes) of side L needed to cover set	log N_L vs. log L slope = $-D$

[a]Source: Burrough (1989).

the theory and its limitations (as determined by the theoretical models).

This argument of course is not valid in the case of exact fractals. Under these circumstances, if one compares any natural phenomenon to a model based on exact fractal dimension, one is doing alright. This is analogous to models that accept the Earth as a sphere, when we know that it is puckered at the poles.

Perhaps the most convincing example of a physical phenomenon with a fractal model is that of Brownian motion (Appendix B). The basic assumption—that a particle subject to random molecular

bombardment moves with increments distributed according to a normal distribution—leads to the conclusion that the particle path has a dimension 2. This can be confirmed experimentally using the box-counting method. The motion can also be simulated on a computer, by tracing a path formed by large number of small random increments. The dimension of such computer simulation can also be estimated by the box-counting method.

Thus, fractal analysis is seen to be guided by experimental data, simulation, and theoretical analyses. The procedure is simply that one measures any physical object or phenomenon, and some of its dimension. There can be two levels of results. One is that the analysis shows the presence of a fractal geometry. The second is that the data fit some kind of power law (within the limits related to the yardstick used), without allowing one to attach any clear significance to the fractal geometry. In any case, when considering complicated natural phenomena, it may suffice to take this as a useful conclusion.

Fractals are used to model natural phenomena such as turbulent flow, interactions of plant communities, Brownian motion, and the distribution of stars. Fractals can even describe the activity of the stock market.

Beyond this, one may be able to devise a model that is useful in the analysis. The model could be useful in describing the dependence of different features on the various parameters, and, ideally, may be useful in predictions as well as being descriptive. As expected, in general the fractal phenomena in nature are complicated in terms of mathematical analysis. The main reason is that the time scale in nature is often far too long (millions of years). On the other hand, we have seen that some very complicated phenomena (e.g., dendrites, chaos) can be easily handled by simple mathematical equations. Additionally, in some systems one might need to apply a multifractal theoretical approach (Jensen, 1987; Ahrony *et al.*, 1987).

It is clear that, at least over some range of length scales, many physical structures exhibit fractal geometry. Research has been divided into two main directions. First, attempts have been made to understand the physical mechanics that govern the froth of structures (e.g. aggregates) into their particular shapes. There

remain many open questions to be studied in this direction. In the second direction, the fractal geometry is taken as given, and the physical properties of the structure are then investigated. Different physical properties turn out to be determined by subsets of sites (or bonds, or particles) on the structure, each having its own fractal nature. At the present time, several infinite sets of independent fractal dimensionalities, or critical exponents, have been identified and studied.

Further, it is obvious that in many cases it will not be sufficient to describe the shape or form of an object by just one number, i.e., fractal dimension. This suggests that one will need to use various fractal dimensions, or the so-called multifractal analysis. As these theories are developed, it is hoped that more complicated objects will be subjected to fractal analysis. In this context, the following example extends these ideas even further. The shadow of a circular ring is a circle or ellipse or line, depending on how one orients the ring. In the same way, the shadow of any object with D would give rise to another fractal dimension of its shadow, D_{shadow}, depending on the angle of shadow. This may be considered to be the case when a tumor is analyzed by taking its reflections by a suitable procedure (gamma rays) at different angles. The shape and form can be analyzed by following these transforms.

The current literature is very extensive and covers a variety of topics (see General References). However, there is still much to be investigated by fractal analysis in some areas. One is the relation between the fractal dimension of the surface of a metal and its other surface properties (such as friction or radiation). A second area concerns the natural forces that give rise to the fractal dimension of landscape being 2.2. Another area is the relation between the fractal geometry of tree branches and roots. Fluid flow under turbulent conditions needs to be investigated in more detail.

The reader is now on his or her own to explore the world and grasp the irregular shapes and forms through fractal analysis. Much remains to be learned about the basic principles involved in fractal analysis.

Appendix A

Computer Fractal Programs

A.1. Computer Program for Dragon

The following program listing (in BASIC) can be used to generate the forms given in Figure 1.1. The size of the generator can be changed by using different values of L. A variety of different shapes can be drawn by making the following changes:

- Adding random instruction
- Using circle instead of point
- Using geometrical functions

However, the main idea is to provide computer support for drawing fractal shapes.

Program for Dragon

```
 90 dim sn(14): key off                [14 maximum n]
100 cls: screen 0                      [type of screen]
110 print ''enter even number''
120 input ''or zero to quit:''; nc
130 IF NC=0 THEN KEY ON: END
140 IF NC MOD 2=1 OR NC < 2 OR NC < 14 THEN 100
150 L=128: FOR C=2 TO NC STEP 2: L=L/2: NEXT
160 X=192: Y=133: CLS: SCREEN 2: PSET(X, Y), 1
170 FOR C=0 TO NC: SN(C)=0:NEXT
```

```
180 D=0: FOR C=1 TO NC: IF SN(C-1)=SN(C)
    THEN D=D-1: GOTO 200
190 D=D+1
200 IF D=-1 THEN D=7
210 IF D=8 THEN D=0
220 NEXT
230 IF D=0 THEN X=X+L+L: GOTO 270
240 IF D=2 THEN Y=Y+L: GOTO 270
250 IF D=4 THEN X=X-L-L: GOTO 270
260 Y=Y-L
270 LINE-(X, Y), 1: SN(NC)=SN(NC)+1
280 FOR C=NC TO 1 STEP-1: IF SN(C) < > 2 THEN 300
290 SN(C)=0: SN(C-1)=SN(C-1)+1: NEXT
300 IF SN(0)=0 THEN 180
310 IF INKEY$='''' THEN 310
320 GOTO 100
330 END
```

A.2. Computer Construction of Cantor Set

A simple algorithm can be used to construct the following table (on page 231) that contains the data points for a Cantor set (a spreadsheet program is very easy to use). The generator is a line from 0 to 1 on each side of a square. The Cantor set with $D = 0.63$, where one removes 1/3 of the line, gives the following data.

Data Points for Drawing a Cantor Set with $D = 0.63$

The first set is a line (the initiator), it divides the line into three equal parts (each equal to 1/3), and it is placed at $y = 1/2$ (the generator). This procedure is repeated (ad infinitum if desired). The table is self-similar and easily obtained if using a simple computer program (e.g., a spreadsheet). The magnitude of $D = \log 2/\log 3 = 0.6309$ (Figure 1.30c). The data points for the

→ step.1 . . . 2 . . . . . 3 4							
x_1	y_1	x_2	y_2	x_3	y_3	x_4	y_4
0	0	0	0	0	0	0	0
1	1	1/3	1/2	1/9	1/4	1/81	1/16
		2/3	1/2	2/9	1/4	2/81	1/16
		1	1	1/3	1/2	1/27	1/8
				2/3	1/2	2/27	1/8
				7/9	3/4	1/9	1/4
				8/9	3/4	2/9	1/4
				1	1	1/3	1/2
						2/3	1/2
						7/9	3/4
						8/9	3/4
						25/27	7/8
						26/27	7/8
						79/81	15/16
						80/81	15/16
						1	1

Each series indicates the step that gives rise to the plot in Figure 1.30c. Subscripts denote the stages of iteration.

series for x,y coordinates are after the second step:

$$x \rightarrow 0,\ 1/9,\ 2/9,\ 1/3,\ 2/3,\ 7/9,\ 8/9,\ 1$$
$$y \rightarrow 0,\ 1/4,\ 1/4,\ 1/2,\ 1/2,\ 3/4,\ 3/4,\ 1$$

If one wanted to construct another set with different D, the generators 1/2 or 1/3 can be modified accordingly. For example, if the y axis is changed from 1/2 to 1/10, the series will become, with $D = \log 10/\log 3 = 2.09$:

$$x \rightarrow 0,\ 1/9,\ 2/9,\ 1/3,\ 2/3,\ 7/9,\ 8/9,\ 1$$
$$y \rightarrow 0,\ 1/100,\ 1/100,\ 1/10,\ 1/10,\ 11/100,\ 11/100,\ 1$$

It is also obvious that a large variety of Cantor sets can be constructed by a simple algorithm, such that the curve obtained is similar to some form (data) encountered in practice. This proce-

dure can be used to estimate the magnitude of the fractal dimension of any irregular fractal form (described in Chapter 5).

A.3. Diverse Algorithms for Computing Fractals

The fractal shapes and forms delineated above can be drawn by computer programs with the help of different algorithms. Development in this area has been very active in the past decade. The complete details are beyond the scope of this book, and the reader is given the sources where the details can be found.

In general, the most useful algorithms that have been described are based on computer programs that can be easily developed on an ordinary PC (Barnsley and Sloan, 1988; Barnsley, 1988; Prusinkiewicz and Lindenmayer, 1990; Devaney, 1990). Only those computer programs that are relatively simple to write and run will be given here (Barnsley and Sloan, 1988; Barnsley, 1988; Devaney, 1990).

The main idea is to be able to draw a shape (as a line or curve) with the help of linear equations. If we have two points A and B, then either we can just draw a line between them, or we can carry out an iteration. The iteration makes it a more general type of computer drawing. The Sierpinski triangle can be drawn by using these procedures. This means that the triangle with three points A = 0, 0, B = 0, 300, and C = 300,300 needs to be filled in with dots at random. The dots are only allowed if the calculated values of x,y are within the coordinates of A, B, and C. By using this algorithm, one can draw all kinds of shapes (e.g. leaves, trees, flowers). The number of points to be used can be chosen according to the speed of the computer; a larger number requires a longer time for computation.

In the following program, on an ordinary computer it is useful to begin with $i = 100{,}000$ or more. A random generator;

$$q = 3*RND$$

allows one to choose one of the three triangles of the Sierpinski gasket. If the value of $q < 1$ or <2, then we choose to fill in either

of the three triangles (Devaney, 1990):

```
     if q < 1 goto 10
     if q < 2 goto 20
     M=(300+m)/2    [midpoint]
     N=(300+N)/2    [midpoint]
 10  M=M/2
     N=N/2
     Goto 100
 20  M=M/2
     N=(300+N)/2
100  if i < 1000 then goto 200
     PSET (M, N)
200  next i
end
```

In order to be able to draw other shapes, one can follow the same algorithm. A somewhat different approach has been given by other investigators (Barnsley and Sloan, 1988; Barnsley, 1988).

The figures and shape drawn by this algorithm are also called iterated function schemes (Falconer, 1990). The procedures employed have enabled the capturing of self-similarity and repetition (as in shapes of leaves or trees or skin patterns, etc.), thus reducing the transformations by a factor of 1000 or more. The main approach has been to be able to compress the programs such that even an ordinary computer can be used to draw rather complex figures or shapes. On the other hand, in the compression process, there appears too high a degree of repetition of shape and form. This is sometimes observed in nature, but often is not. Therefore, at this stage, further developments are envisaged in order to provide forms with less repetition.

Appendix B

Basic Aspects of Brownian Motion

Molecules in dense systems are known to move in random, zigzag paths. Examination of a pure substance, for example a drop of liquid, with the most powerful microscope available cannot reveal the presence of any such rapidly moving particles. With regard to how these molecules can be made visible, this is easily done using a macroscopic particle such as a smoke particle in air or a colloidal particle in a liquid. A snapshot of its movement would reveal a chaotic trajectory as shown in Figure B.1 (Perrin, 1923). This motion is called Brownian; it was originally described in 1827 when the botanist Robert Brown noticed that minute particles suspended in a liquid moved in highly erratic paths. This, and a similar phenomenon for smoke particles in air, was explained ultimately as resulting from molecular bombardment of the particles. As is known from kinetic theory, the moleucle moves and collides with other molecules. The diameters of air (i.e., nitrogen) and a dust particle are ca. 3.6 Å and 1 μm, respectively. It is now well known that objects generated by diffusion forces are fractal. In fact, diffusion is characterized as being the consequence of random walks of different particles. In this context, the objects or particles may be electrons, holes, ions, atoms or molecules (or macromolecules), or even bacteria.

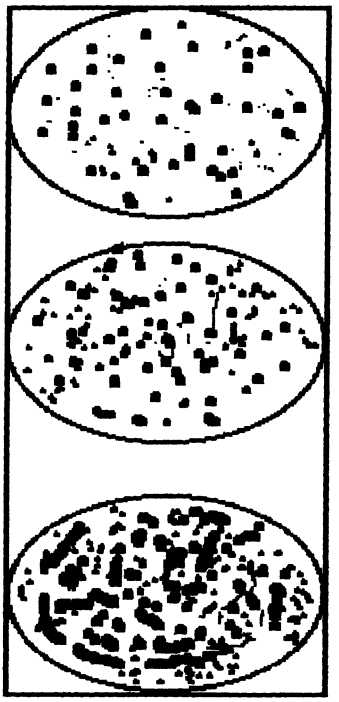

Figure B.1. Micrographs (schematic) of a colloidal solution of mastic at three different levels ca. 12 μm apart.

Let us consider the movement of a particle in only one dimension. The particle is assumed to move in a positive or negative direction with some probability for each direction. This is only demonstrable if we observe the movement over a very long period of time. Although we cannot by any method presently known see the movement of molecules of a liquid, this can be accomplished indirectly, i.e., by stirring into a liquid some insoluble substance (e.g., pollen grains or the like) in a very finely dispersed (colloidal) state. The fast movement of the liquid molecules will be revealed upon collision with the colloidal particles. This was first noticed by Robert Brown in 1827 while observing pollen grains suspended in water. This chaotic movement of pollen was henceforth called *Brownian motion.* In other words, the small visible colloidal particles are knocked about by collisions with the invisible molecules, like footballs in the midst of a crowd of invisible players.

The theoretical analysis of fractional Brownian motion has

been extensively described in the literature. Brownian motion is said to be a statistically self-similar process in the sense that if the intervals are divided by a positive ratio, it exhibits properties with a probability function that is identical with that of the original function (Falconer, 1990). Computational methods for drawing Brownian tracks and three-dimensional surfaces have been described (Voss, 1985; Feder, 1988; Peitgen and Saupe, 1988; Falconer, 1990).

Brownian motion can also be described as follows. Consider a particle that moves a step of length equal to τ at a time. Each step is assumed to be very small (i.e., in terms of molecular dimensions), and is taken randomly. If the probability for each step is entirely independent of the previous history and the location of the particle, then we have the well-known problem of random walk, or Brownian motion or diffusion. If the additional feature is added that the particle tends to avoid places it has already visited, we have the self-avoiding random walk problem (Chapter 1). Diffusion is the overall consequence of random walks of particles. Actually, each observation time yardstick is a self-similar motion. It is thus obvious that qualitatively, Brownian motion will always follow a self-similar fractal path, in general terms.

It was further shown that air molecules move about by Brownian motion, such that the density of air varies with height above the surface of Earth:

$$\log(\delta_1/\delta_2) = [Mg(h_2 - h_1)]/RT \tag{B.1}$$

where δ_1 and δ_2 are the densities of air at heights h_1 and h_2, respectively, M the molecular weight of air ($\approx$28), g the acceleration due to gravity, R (1.98 cal/K-mole or 8.314 J/K-mole) the gas constant, and T the absolute temperature.

In the case of a colloidal suspension, one can derive a similar relation:

$$M = mN_A \tag{B.2}$$

$$m = V\delta_c \tag{B.3}$$

$$= V(\delta_{co} - \delta_{lo}) \tag{B.4}$$

where m is the mass of a colloidal particle, N_A is Avogadro's number, V_c is the volume of the colloidal particle, and the density of the colloidal particle suspended in solution = $\delta_c = \delta_{co} - \delta_{lo}$.

Analogous to Eq. (B.1), we then get:

$$\log(\delta_1/\delta_2) = \log(n_1/n_2) = N_A V(\delta_{co} - \delta_{lo})g(h_2 - h_1)/RT \qquad \text{(B.5)}$$

where n_1 and n_2 are the average numbers of colloidal particles in a given volume at heights h_1 and h_2, respectively.

The magnitudes of n_1 and n_2 were estimated from photographs of colloidal solution of mastic at different levels (see Figure B.1). The measured and calculated values at different levels were very close. For example, measured/calculated were: 116/119; 146/142; 170/169; 200/201.

The path of a colloidal particle was given in Figure B.2. This shows that the horizontal projection of the path of a colloidal particle that initially was at position A at the beginning of the experiment has moved to position B, some t minutes later, while having traversed the indicated zigzag course. The distance from A to B in a direct line is called the horizontal displacement X of the particle during a time interval t. This is determined by the energy of agitation of the particle and the resistance offered to its motion by the viscosity of the suspending liquid. On the assumption that

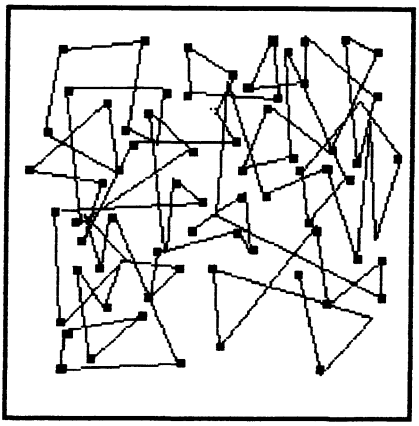

Figure B.2. Brownian motion of a colloidal particle (schematic).

the Brownian motion was the result of the collision of the molecules of the liquid with the colloidal particles, for a large number of observations the average value of the square of the horizontal displacement (X^2) of a spherical particle in time t is:

$$X^2 = RT/N_A 3\pi r\eta \tag{B.6}$$

where r is the radius of the particle and η is the viscosity of the medium. Note that the mass of the particle does not appear explicitly in this equation; the mean square displacement is proportional to its radius, and hence to the reciprocal of the cube root of its volume. This means that smaller the particle, the more extensive the Brownian motion.

In deducing this relation, it was assumed that the motion of the particle under a constant force, f, took place in accordance with Stokes's law:

$$u = f/6\pi r\eta \tag{B.7}$$

where u is the velocity of the particle. Measurements carried out on colloidal systems (gamboge and mastic) gave results in agreement with these equations (Table B.1).

The linear relationship between X^2 and time has been clearly established from experimental data.

Table B.1. Brownian Motion Data[a]

Solution composition	Particle radius (μm)	Mass $\times 10^{15}$ (g)	Number of displace-ments	N_A $\times 10^{-23}$ (calcd)[b]
Gamboge/water	0.5	600	100	8
	0.367	246	1500	6.9
	0.212	48	900	6.9
Mastic/water	0.52	650	1000	7.3

[a] Perrin (1923).

[b] N_A (Avogadro's number) = 6×10^{23} molecules/mole.

Diffusion and random walk. In a dense medium such as a liquid, a particle will be closely surrounded by a set of nearest neighbors and will undergo a series of repeated collisions with them without significantly changing the location of its center of mass. It is easily seen that the mechanism of diffusion is actually one in which particles move in a series of small steps, and thus gradually move away from the reference position (Figure B.2). If it moves a distance d_p after each time interval τ, then:

$$\text{Distance moved after time } t = (t/\tau)d_p \tag{B.8}$$

This is not the distance from the reference point, but the total sum of right (R) and left (L) movements. A simple system is the one-dimensional random walk, where we assume that the molecule only moves a distance d towards the right or left on a straight line.

Let us proceed to find the probability that the molecule is at a distance x from the origin ($x = 0$, $t = 0$) after some given time t. The number of steps, n:

$$n = t/\tau \tag{B.9}$$

Since the step can be either n_L or n_R, then we have;

$$\text{Total number of steps} = n = n_L + n_R \tag{B.10}$$

$$\text{Distance traveled} = x = n_R d - n_L d \tag{B.1))}$$

$$\text{Total number of possibilities} = 2^n \tag{B.12}$$

If we consider a system with only 4 steps, for the sake of simplicity, then there are 2^4 possible step sequences:

LLLL	LLLR	LLRR	LRRR	RRRR
	LLRL	LRLR	RLRR	
	LRLL	LRRL	RRLR	
	RLLL	RLLR	RRRL	
		RLRL		
		RRLL		

and clearly there are 6 ways of taking 2 steps to the right and 2 to the left, which gives $4!/2!2! = 6$. The probability (P) that the particle is at the origin after 4 steps is therefore 6/16. The probability that it is at $x = 4d$ is 1/16. This is because, in order to be there, all 4 steps must be to the right, and there is only way of achieving this. These patterns can be compared with the above-mentioned fractal shapes, such as dragon. Each step may represent the line as drawn in the dragon. It is clear that fractal shapes can be analyzed by this procedure (Falconer, 1990).

A more general expression can now be written:

$$\text{Probability at } x = P_x = n!/[n!\,(n - n_R)!\,2^n] \tag{B.13}$$

We can derive:

$$n_R = (1/2)(n + x/d), \qquad n - n_R = (1/2)(n - x/d) \tag{B.14}$$

thus:

$$P_x = n!/\{[(1/2)(n + s)]!\,[(1/2)(n - s)]!\,2^n\} \tag{B.15}$$

where $s = x/d_p$. This relationship takes the form of the well-known Gaussian distribution under limited conditions (e.g., n is large; s/n is small; x is not far from the origin):

$$P_{x,t} = (2\tau/\pi t)^{1/2}\exp(-x^2\tau/2td^2) \tag{B.16}$$

From this, we find that diffusion can be interpreted as the result of a very large number of small steps in a random direction. This also indicates the region of invalidity of the diffusion equation.

If we compare the two exponents:

$$2d^2/\tau = 4D \tag{B.17}$$

we get the expression:

$$D = (1/2)d^2/\tau \tag{B.18}$$

As an example, consider a molecule with a diffusion constant of $D = 10^{-5}\,\mathrm{cm}^2/\mathrm{sec}$, with effective radius = 206 pm. If we assume that it jumps through its own diameter, then we can estimate τ:

$$\begin{aligned}\tau &= 2(206 \times 10^{-12}\,\mathrm{m})^2/2(10^{-9}\,\mathrm{m}^2/\mathrm{sec}) \\ &= 8 \times 10^{-11}\,\mathrm{sec}\end{aligned} \tag{B.19}$$

This leads to the connection between these microscopic movements and the rather large diffusion movements of macroscopic scales. Further, since average path length is related to the magnitude of D through the equation:

$$D = (1/2)\lambda c \tag{B.20}$$

we get a relation between random walk and the kinetic gas theory.

In the case of a random walk whose mean free path is finite, we get the following. Even though the fractal dimension for a trajectory of ideal Brownian motion is 2 (Takayasu, 1990), in the case of a finite mean free path we expect that the fractal dimension depends on the observation scale. If we use a scale that is much shorter than the mean free path, we will find that the trajectory is nearly a straight line. However, if the yardstick of observation is larger, the random walk may be reduced to the usual Brownian motion. As an example, Figure B.3 depicts the random walk of a particle on a Sierpinski gasket (or some other fractal surface), which would result in $D = 2$. The Sierpinski gasket has attracted much interest since many physical problems using it as a substrate can be solved exactly. This is due to the self-similarity property and to the fact that the Sierpinski gasket is finitely ramified. A fractal is ramified if any bounded subset of the fractal can be isolated by cutting a finite number of bonds, sites, or interactions. The kinetics of diffusion-controlled processes on fractals have been analyzed (Mosolov, 1991). Further, it has been shown that diffusion of Brownian particles on random fractal structures, self-avoiding random walks, and percolation clusters serve as useful model systems for polymers in solutions (Roman *et al.*, 1989). The more detailed relation between the mean free path and the magnitude of D needs to be investigated in greater detail.

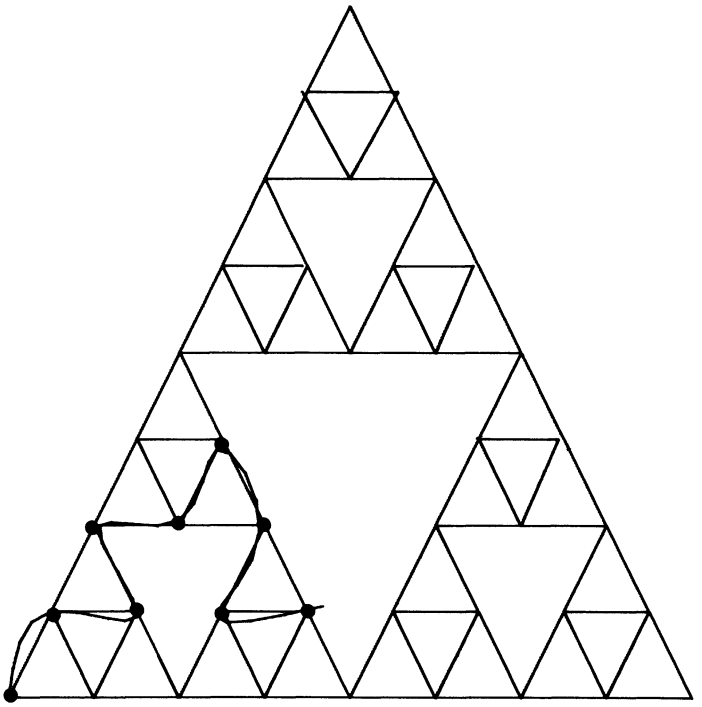

Figure B.3. Diffusion of an object on a Sierpinski gasket.

The role of local defects and inhomogeneities in influencing the diffusion-controlled processes occurring on the solid surface has been reported (Garza-Lopez *et al.*, 1990). The surface reaction was based on a coreactant migrating across a surface where a reaction center is fixed at some particular location. The surface inhomogeneities were considered to be of two kinds. First, there may be differences between reaction sites on regular versus defect sites. As for the second factor, we may consider the cell surface, which has transmembrane protein molecules which may interfere with any movement of a coreactant. In order to consider these inhomogeneities, the Sierpinski gasket was used. The broken structure of this fractal lattice effectively restricts the diffusing coreac-

tant to a subset of the overall sites. This model was used to describe a variety of diffusion-controlled processes taking place on the surface of a supported catalyst or molecular organized assemblies formed by lipids (e.g., cell surface, fatty acid or other lipid monolayer at the air–water or oil–water interface).

References

General References

Anhrony, A., 1986, *6th General Conference of the Condensed Matter,* Stockholm, *Phys. Scr.* **13**:43.

Alder, D., Fritsche, H., and Ovshinsky, S. R. (eds.), 1985, *Physics of Disordered Materials,* Plenum Press, New York.

Avnir, D. (ed.), 1989, *The Fractal Approach to Heterogeneous Chemistry,* Wiley, New York.

Barnsley, M., 1988, *Fractals Everywhere,* Academic Press, New York.

D'Amico, A., and Mazzetti, P. (eds.), 1986, *Noise in Physical Systems,* Elsevier, Amsterdam.

de Gennes, P. G., 1985, in: *Physics of Disordered Materials* (D. Alder, H. Fritsche, and S. R. Ovshinsky, eds.), Plenum Press, New York.

Devaney, R. L., 1989, *An Introduction to Chaotic Dynamical Systems,* Addison–Wesley, Menlo Park, California.

Devaney, R. L., 1990, *Chaos, Fractals and Dynamics,* Addison–Wesley, Reading, Mass.

Falconers, K. J., 1990, *The Geometry of Fractal Sets,* Cambridge University Press, Cambridge.

Family, F., and Landau, D. P. (eds.), 1984, *Kinetics of Aggregation and Gelation,* Elsevier, Amsterdam.

Feder, J., 1988, *Fractals: Physics of Solids and Liquids,* Plenum Press, New York.

Field, R. J., and Burger, M., 1984, *Oscillations and Travelling Waves in Chemical Systems,* Wiley, New York.

Fisher, P., and Smith, W. R. (eds.), 1982, *Chaos, Fractals and Dynamics,* Dekker, New York.

Gleick, J., 1988, *Chaos,* Heinemann, London.

Goodwin, J. W., (ed.), 1982, *Colloidal Dispersion,* Royal Society, London.

Holden, A. V., 1987, *Chaos,* Manchester University Press, Manchester.

Hughes, B. D., and Ninham, B. W. (eds.), 1983, *The Mathematics and Physics of Disordered Media,* Springer–Verlag, Berlin.

Jullien, R., and Botet, R., 1987, *Aggregation and Fractal Aggregates,* World Scientific, Singapore.

Kersten, H., 1982, *Percolation Theory for Mathematicians,* Birkhauser, Boston.

Lumley, J. L., van Dyke, M., and Reed, H. L. (eds.), 1988, *Annual Review of Fluid Mechanics* **20**:551.

Mandelbrot, B. B., 1975, *Les Objects Fractals: Forme, Hasard et Dimension,* Flammarion, Paris: 1977, *The Fractal Geometry of Nature: Form, Chance and Dimension,* Freeman, San Francisco; 1982, *The Fractal Geometry of Nature,* Freeman, San Francisco.

Martin, R. D., 1983, *Human Brain Evolution in an Ecological Context,* American Museum of Natural History, New York.

Mayer–Kress, G., 1987, in: *Directions in Chaos* (B.-L. Hao, (ed.)), Vol. 1, World Scientific, Singapore.

Maynard–Smith, J., 1971, *Mathematical Ideas in Biology,* Cambridge University Press, Cambridge.

Peitgen, H. O., 1988, *The Science of Fractals,* Springer, Berlin.

Peitgen, H. O., and Richter, P. H., 1986, *The Beauty of Fractals,* Springer, Berlin.

Peitgen, H. O., and Saupe, D. (eds.), 1988, *Fractal Images,* Springer, Berlin.

Pietronero, L., and Tosatti, E., (eds.), 1986, *Fractals in Physics, Proceedings of the Sixth International Symposium on Fractals in Physics,* ICTP, Trieste, Italy, North-Holland, Amsterdam.

Prusinkiewicz, P., and Lindenmayer, A., 1990, *The Algorithmic Beauty of Plants,* Springer–Verlag, Berlin.

Pynn, R., and Riste, T. (eds.), 1987, *The Dependent Effects in Disordered Systems,* Plenum Press, New York.

Smale, S., 1980, *The Mathematics of Time; Essays on Dynamical Systems, Economic Processes and Related Topics,* Springer–Verlag, Berlin.

Stauffer, D., 1985, *Introduction to Percolation Theory,* Taylor & Francis, London.

Stevens, P. S., 1974, *Patterns in Nature,* Little, Brown & Co., Boston.

Takayasu, H., 1990, *Fractals in the Physical Sciences,* Manchester University Press, Manchester.

Thompson, J. M. T., and Stewart, H. B., 1988, *Non-linear Dynamics and Chaos,* Wiley, New York.

Vicsek, T., 1989, *Fractal Growth Phenomena,* World Scientific, Singapore.

Conference Proceedings

Ahrony, A., Entin–Wohlman, O., and Orbach, R., 1987, *Proceedings of a NATO Advanced Study Institute, Norway* (R. Pynn and T. Riste, eds.), Plenum Press, New York.

Argyrakis, P., 1988, in: *Proceedings of the NATO Advanced Research Workshop*

on New Theoretical Concepts in Physical Chemistry (A. Amann, L. Cederbaum, and W. Gans, eds.), Kluwer, Dordrecht.

Banaver, J. R., Koplik, J., and Winkler, K. W. (eds.), 1987, *Physics and Chemistry of Porous Media, II,* AIP Conf., Vol. 154, American Institute of Physics, New York.

Barnsley, M. F., and Demko, S. G. (eds.), 1986, *Chaotic Dynamics and Fractals,* Academic Press, New York.

Birdi, K. S., 1982, in: *The Hydrophobic Interaction, Fraday Symp. Chem. Soc.* **17**.

Birdi, K. S., Vu, D. T., Andersen, S. I., Winter, A., Topsøe, H., and Christensen, S. V., 1991, in: *Characterization of Porous Solids II* (F. Rodriguez–Reinoso, ed.), Elsevier, Amsterdam.

Boccara, N., and Daoud, M. (eds.), 1985, *Physics of Finely Divided Matter,* Springer, Berlin.

Cantor, G., 1883, *Mathematische Annalen* **21**:545.

Farin, D., and Avnir, D., 1988, in: *Proceedings of IUPAC Symposium on Characterization of Porous Solids* (K. K. Unger, D. Behrens, and H. Kral, eds.), Elsevier, Amsterdam.

Goodchild, M. F., 1982, in: *Proc. Modeling and Simulation Conference,* Pittsburgh, Vol. 3, p. 1133.

Jensen, M. H., 1987, in: *Proceedings of a NATO Advanced Study Institute, Norway* (R. Pynn and T. Riste, eds.), Plenum Press, New York.

Kaye, B. H., 1989, in: *The Fractal Approach to Heterogeneous Chemistry* (D. Avnir, ed.), Wiley, New York.

King, G. P., Jones, R. and Broomhead, D. S., 1987, in: *CHAOS 87: International Conference on the Physics of Chaos and Systems far from Equilibrium, Nucl. Phys. B Suppl.* **2**:379.

Kolb, M., Jullien, R., and Botet, R., 1985, in: *Scaling Phenomena in Disordered systems* (R. Pynn and A. Skjeltrop, eds.), Plenum Press, New York.

Krim, J., and Panella, V., 1991, in: *Characterization of Porous Solids II* (F. Rodriguez–Reinoso, ed.), Elsevier, Amsterdam.

Long, Q. Y., Suqin, L., and Lung, J., 1991, *J. Phys. D* **24**:602.

Martin, J. E., 1987 in: *TIme-Dependent Effects in Disordered Systems* (R. Pynn and T. Riste, eds.), Plenum Press, New York.

Pynn, R., and Skjeltrop, A. (eds.), 1985, *Scaling Phenomena in Disordered Systems,* Plenum Press, New York.

Sacher, G. A., 1959, in *CIBA Foundation Symposium on the Life Span of Animals* (G. E. W. Wolstenholm and M. O'Connor, eds.), Little, Brown, Boston.

Schlesinger, M. F., and Montroll, E. W., 1983, in: *The Mathematics and Physics of Disordered Media, Proceedings 1983* (B. D. Hughes and N. W. Ninham, eds.), Springer, Berlin.

Shleisinger, M. F., Mandelbrot, B. B., and Rubin, R. J. (eds.), 1984. *J. Stat. Phys.* **36**.

Stanley, H. E., and Ostrowsky, N. (eds.), 1986, *On Growth and Form,* NATO Adv. Study Inst. Vol. E100, Nijhoff, The Hague.

Takayasu, H., and Nishikawa, I., 1986, in: *Proceedings of the 1st International Symposium for Science on Form* (S. Ishizaka, ed.), KTK Science, Tokyo.

Unger, K. K., Behrens, D., and Kral, H. (eds.), 1987, *Characteristics of Porous Solids* (Proceedings of IUPAC Symposium), Elsevier, Amsterdam.
Weitz, D. A., Sander, L. M., and Mandelbrot, B. B. (eds.), 1988, *Fractal Aspects of Materials: Disordered Systems II,* Materials Research Society, Boston.

Articles

Adachi, Y., and Ooi, S., 1990, *J. Colloid Interface Sci.* **135**:374.
Adamson, A. W., 1982, *Physical Chemistry of Surfaces,* 4th ed., Wiley, New York.
Albahadily, F. N., Ringland, J., and Schell, M., 1989, *J. Chem. Phys.* **30**:813.
Alsac, E., Laroche, C., Trauth, D., Massart, P., and van Damme, H., 1990, *Chem. Phys. Lett.* **165**:277.
Andereck, C. D., Dickman, R., and Swinney, H. L., 1983, *Phys. Fluids* **26**:1395.
Antonietti, M., and Rosenauer, C., 1991, *Macromolecules* **24**:3434.
Aoki, I., 1989, *J. Theor. Biol.* **141**:11.
Aoki, K., 1991, *J. Phys. Chem.* **95**:9037.
Armstrong, A. J., Mocklet, R. C., and O'Sullivan, W. J., 1986, *J. Phys. A.* **19**:L123.
Armstrong, E., 1983, *Science* **220**:1302.
Arthur, W. B., 1990, *Sci. Am.* Feb.:**262**(2), 80.
Aubert, C., and Cannell, D. S., 1986, *Phys. Rev. Lett.* **56**:738.
Auerbach, D. J., Paul, W., Bakker, A. F., Lutz, C., Rudge, W. E., and Abraham, F. F., 1987, *J. Phys. Chem.* **91**:4881.
Aviles, C. A., Scholz, C. H., and Boatwright, J., 1987, *J. Geophys. Res.* **92**:331.
Avnir, D., 1987, *J. Am. Chem. Soc.* **109**:2931.
Avnir, D., and Pfeifer, P., 1983, *Nouv. J. Chim.* **7**:71.
Avnir, D., Farin, D., and Pfeifer, P., 1983, *J. Chem. Phys.* **79**:3566.
Avnir, D., Farin, D., and Pfeifer, P., 1984, *Nature* **308**:261.
Bak, P., and Chen, K., 1991, *Sci. Am.* Jan.:**264**(1), 26.
Balasubramanian, D., and Rodley, G. A., 1988, *J. Phys. Chem.* **92**:5995.
Balasubramanian, D., and Rodley, G. A., 1991, *J. Phys. Chem.* **95**:5147.
Bale, H. D., and Schmidt, P. W., 1984, *Phys. Rev. Lett.* **53**:596.
Bales, G. S., Bruinsma, R., Eklund, E. A., Karunasiri, R. P. U., Rudnick, J., and Zangwill, A., 1990, *Science* **249**:264.
Barnsley, M. F., and Sloan, A. D., 1988, *Byte* **13**:215.
Basedow, A. M., Ebert, K. H., Ederer, H. J., and Fosshag, E., 1980, *J. Chromatogr.* **192**:259.
Behringer, R. P., 1985, *Rev. Mod. Phys.* **57**:657.
Beloshapkin, V. V., Chernikov, A. A., Natenzon, M. Y., Petrovichev, A., Sagdeev, R. Z., and Zaslavsky, G. M., 1989, *Nature* **337**:133.
Ben-Naim, A., 1980, *The Hydrophobic Interactions,* Plenum Press, New York.
Benzi, R., Paladin, G., Parisi, G., and Vulpiani, A., 1984, *J. Phys. A* **17**:3521.

Bergé, P., Pomeau, Y., and Vidal, C., 1984, *L'Ordre dans le Chaos,* Hermann, Paris.
Berlin, E., Anderson, B. A., and Pallansch, U. J., 1969, *J. Phys. Chem.* **75**:303.
Berry, M. V., and Percival, I. C., 1986, *Opt. Acta* **33**:577.
Berry, R. S., Rice, S. A., and Ross, J., 1980, *Physical Chemistry,* Wiley, New York.
Bessis, D., and Moussa, P., 1985, *Fizika* **17**:345.
Biewener, A. A., 1990, *Science* **250**:1097.
Binder, K., and Kremer, K., 1985, in: *Scaling Phenomena in Dispersed Systems* (R. Pynn and A. Skjeltrop, eds.), Plenum Press, New York.
Bird, R. B., Armstrong, R. C., and Hassager, O., 1987, *Dynamics of Polymeric Liquids,* Vol. 1, Wiley, New York.
Birdi, K. S., 1988, in: *Aqueous Size-Exclusion Chromatography* (P. L. Dubin, ed.), Elsevier, Amsterdam.
Birdi, K. S.,1989, *Lipid and Biopolymer Monolayers at Liquid Interfaces,* Plenum Press, New York.
Birdi, K. S., 1992a, submitted.
Birdi, K. S., 1992b, submitted.
Birdi, K. S., 1992c, submitted.
Birdi, K. S., and Steinhardt, J., 1978, *Biochim. Biophys. Acta* **534**:219.
Birdi, K. S., and Vu, D. T., 1992, *J. Adhes. Sci. Tech.,* in press.
Birdi, K. S., Vu, D. T., and Winter, A., 1987, in: *Proc. 4th European Symposium on Enhanced Oil Recovery,* Hamburg.
Birdi, K. S., Vu, D. T., and Winter, A., 1989, *J. Phys. Chem.* **93**:3702.
Birdi, K. S., Sanchez, R., and Krog, N., 1990, *Colloid Polym. Sci.* **82**:104.
Birshtein, T. M., 1983, *Macromolecules* **16**:45.
Blanchard, P., 1984, *Bull. Am. Math. Soc.* **11**:85.
Borman, S., 1991, *Chem. Eng. News* **Jan.**:18.
Bouville, C., 1985, *Comput. Graphics USA* **19**:45.
Brandt, W. W., and Budrys, R. S., 1965, *J. Phys. Chem.* **69**:600.
Bremer, L. G. B., van Vliet, T., and Walstra, P., 1989, *J. Chem. Soc. Faraday Trans. 1* **85**:3359.
Broadbent, S. R., and Hammersley, J. M., 1957, *Proc. Cambridge Philos. Soc.* **53**:629.
Brochard, F., 1985, *J. Phys. (Paris)* **46**:2117.
Broecker, W. S., and Denton, G. H., 1990, *Sci. Am.* Jan.:**262**(1), 43.
Bunde, A., 1986, *Adv. Solid State Phys.* **26**:113.
Burrough, P. A., 1989, in: *The Fractal Approach to Heterogeneous Chemistry* (D. Avnir, ed.), Wiley, New York.
Calvin, M., 1969, *Chemical Evolution,* Oxford Press, London.
Chattoraj, D. K., and Birdi, K. S., 1984, *Gibbs Adsorption and the Surface Excess,* Plenum Press, New York.
Chen, J. D., and Wilkinson, D., 1985, *Phys. Rev. Lett.* **55**:1892.
Chothia, C., 1984, *Annu. Rev. Biochem.* **53**:537.
Christensen, S. V., and Topsøe, H., 1989, in: *The Fractal Approach to Heterogeneous Chemistry* (D. Avnir, ed.), Wiley, New York.

Creighton, T. E., 1984, *Proteins: Structures and Molecular Properties,* Freeman, San Francisco.

Culling, W. E. H., and Datko, M., 1987, *Earth Surf. Processes Landforms* **12**:369.

Daccord, G., 1989, in: *The Fractal Approach to Heterogeneous Chemistry* (D. Avnir, ed.), Wiley, New York.

Daccord, G., Nittmann, J., and Stanley, H. E., 1986, *Phys. Rev. Lett.* **56**:336.

Daoud, M., and Martin, J. E., 1989,in in: *The Fractal Approach to Heterogeneous Chemistry* (D. Avnir, ed.), Wiley, New York.

Daoud, M., Bouchaud, E., and Jannink, G., 1986, *Macromolecules* **19**:1955.

Dauvillier, P., 1963, *Les Hypotheses Cosmologoniques,* Masson, Paris.

de Gennes, P. G., and Pincus, P., 1983, *J. Phys. Lett (Paris)* **44**:241.

de Kepper, P. D., Boissonade, J., and Epstein, I. R., 1990, *J. Phys. Chem.* **94**:6525.

Desai, R. C., Benard, P., and Corsten, G., 1989, *J. Phys. Chem.* **93**:6944.

Devaney, R. L., 1986, *Introduction to Chaotic Dynamic Systems,* Benjamin Cummings, Menlo Park, California.

Dewey, T. G., 1991, *Chem. Phys.* **150**:445.

Dickerson, R. E., and Geis, I., 1969, *The Structure and Action of Proteins,* Harper and Row, New York.

Ding, J. R., Wang, F., and Liu, B. X., 1990, *Mod. Phys. Lett. B* **4**:1111.

Domb, C., and Sykes, F., 1961, *Phys. Rev.* **122**:77.

Dubin, P. L., 1988, *Aqueous Size-Exclusion Chromatography,* Elsevier, Amsterdam.

Duncan, M. A., and Rouvray, D. H., 1989, *Sci. Am.* Dec.:**261**(6), 60.

Dziedzini, F., and Botet, R., 1991, *J. Phys. II* **1**:343.

Elber, R., 1989, in: *The Fractal Approach to Heterogeneous Chemistry* (D. Avnir, ed.), Wiley, New York.

Evesque, P., Yang, C. L., and El-Sayed, M. A., 1986, *J. Phys. Chem.* **90**:2519.

Family, F., Platt, D. E., and Vicsek, T., 1987, *Phys. Rev. A* **20**:1177.

Farin, D., and Avnir, D., 1987, *J. Phys. Chem.* **91**:5517.

Farmer, J. D., Ott, E., and Yorke, J. A., 1982, *Physica* **7D**:153.

Felgenhauer, K., 1974, *Hoppe-Seylers Z. Physiol. Chem.* **335**:1281.

Field, R. J., and Noyes, R. M., 1977, *Acc. Chem. Res.* **10**:214.

Flory, P. J., 1971, *Principles of Polymer Chemistry,* Cornell University Press, Ithaca, N.Y.

Fogg, I., 1986, *Micro cornucopia* (USA), **33**:36.

Forrest, S. R., and Witten, T. A., 1979, *J. Phys. A.* **12**:L109.

Freeman, W. J., 1991, *Sci. Am.* Feb.:**264**(2), 34.

Fripiat, J. J., Gatineau, L., and van Damme, H., 1986, *Langmuir* **2**:562.

Fruchter, I., Crepy, G., and Mehaute, A. Le, 1986, *J. Power Sources* **18**:51.

Gajem, Y. M., Warrick, W. A., and Myers, D. E., 1981, *Soil Sci. Soc. Am. J.* **45**:709.

Garza-Lopez, R. A., Rudra, J. K., Davidson, R., and Kozak, J. J., 1990, *J. Phys. Chem.* **94***J. Phys. Chem.* 8315.

Goldberger, A. L., Rigney, D. R., and West, B. J., 1990, *Sci. Am.* Feb.:**262**(2), 42.
Gonda, I., and Rodley, G. A., 1990, *J. Phys. Chem.* **94**:1516.
Gould, S. J., 1975, in: *Approaches to Primate Paleobiology* (F. Szalay, ed.), Karger, Basel.
Grabski, R., 1990, *Int. Annu. Conf. ICT* **21**:70.
Graham, R. L., Rothschild, B. L., and Spencer, J. H., 1990, *Ramsey Theory,* Wiley, New York.
Gregg, S. J., and Sing, K. S. W., 1982, *Adsorption, Surface Area and Porosity,* Academic Press, New York.
Habermann, B., 1960, *Soc. Pet. Eng. AIEME J.* **219**:264.
Hack, J. T., 1957, *U.S. Geol. Surv. Prof. Pap.* **294-B**:45.
Hack, J. T., 1990, *Michigan USGS Prof. Pap.* **504-B**:40.
Hall, R. J., and Bonczyk, P. A., 1990, *Chem. Phys. Processes Combust.* **1**:130.
Hallam, T. G., and Huang, Y., 1989, *J. Theor. Biol.* **141**:65.
Harvey, P. H., and Krebs, J. R., 1990, *Science* **249**:140.
Havsteen, B. H., 1989, *J. Theor. Biol.* **140**:101.
Hazlett, J. D., 1990, *J. Colloid Interface Sci.* **137**:527.
Hecht, C. E., 1990, *Statistical Thermodynamics and Kinetic Theory,* Freeman, New York.
Hecht, J. H., 1991, *Astrophys. J.* **367**:635.
Herrmann, H. J., 1986, *Phys. Rep.* **136**:154.
Herrmann, H. J., Hong, D. C., and Stanley, H. E., 1982, *J. Phys. A* **17**:L261.
Hess, B., Brand, K., and Pye, K., 1966, *Biochem. Biophys. Res. Commun.* **23**:102.
Hildebrand, J. H., and Scott, R. L., 1970, *Regular and Related Solutions,* Van Nostrand–Reinhold, Princeton, N.J.
Hokkanen, J. E. I., 1986, *J. Theor. Biol.* **499**:499.
Holden, C. E., 1990, *Statistical Thermodynamics and Kinetic Theory,* Freeman, San Francisco.
Horne, D. S., 1987, *Fraday Discuss. Chem. Soc.* **83**:259.
Hurd, A. J., and Schaefer, D. W., 1985, *Phys. Rev. Lett.* **54**:1043.
Huxley, J. S., 1924, *Nature* **114**:895.
Jeffrie, C. D., 1985, *Phys. Scr.* **9**:11.
Journel, A. J., and Huijbregts, C. J., 1978, *Mining Geostatics,* Academic Press, New York.
Julia, J. G., 1918, *J. Math. Ser.* **7**:47.
Jullien, R., 1987, *Comments Condens. Matter Phys.* **13**:177.
Jullien, R., Botet, R., and Mors, P. M., 1987, *Faraday Discuss. Chem. Soc.* **83**:125.
Kaneko, K., Fukuzaki, N., and Ozeki, S., 1987, *J. Chem. Phys.* **87**:776.
Kaneko, K., Sato, M., Suzuki, T., Fujiwara, Y., Nishikawa, K., and Jaroniec, M., 1991, *J. Chem. Soc. Faraday Trans.* **87**:179.
Kardar, M., 1989, *Ettore Majorana Int. Sci. Ser. Phys. Sci.* **45**:327.
Katz, A. J., and Thompson, A. H., 1985, *Phys. Rev. Lett.* **54**:1325.

Katz, A. J., and Thompson, A. H., 1986 *Phys. Rev. Lett.* **56**:2112.
Keller, D. J., McConnell, H. M., and Moy, V. T., 1986, *J. Phys. Chem.* **90**:2311.
Kelzer, J., and Noyes, R. M., 1980, *J. Phys. Chem.* **84**:3568.
Kerstein, A. R., and Bug, A. L. R., 1986, *Phys. Rev. B* **34**:1754.
King, J., 1989, *Chem. Eng. News* **April 10**:32.
Kolb, M., Bottet, R., and Jullien, R., 1983, *Phys. Rev. Lett.* **51**:119.
Kopelman, R., 1989, in: *The Fractal Approach to Heterogeneous Chemistry* (D. Avnir, ed.), Wiley, New York.
Koper, M. T. M., and Gaspard, P., 1991, *J. Phys. Chem.* **95**:4945.
Krassner, M. B., 1983, *Chem. Eng. News* **Aug.**:22.
Lamb, J., 1987, *Manage. Today* **Dec.**:129.
Langer, J. S., 1980, *Rev. Phys.* **52**:1.
Langer, J. S., and Muller–Krumbhaar, H., 1978a, *Acta Metall.* **26**:1681; 1978b, **26**:1689.
Laverty, M., 1987, *Earth Surf. Processes Landforms* **2**:475.
Lenormand, R., Soucemarianadin, A., Touboul, E., and Daccord, G., 1987, *Phys. Rev. A* **36**:1855.
Lewis, M., and Rees, D. C., 1985, *Science* **230**:1163.
Liang, S., 1986, *Phys. Rev. A* **33**:2663.
Lianos, P., 1990, *NATO ASI Ser.* **324**:309.
Liu, J., and Scott, S. K., 1991, *J. Chem. Phys.* **94**:4416.
Liu, Z., He, D., and Liu, Q., 1990, *Xibei Daxue Xuebao, Ziran Kexueban* **20**:29.
Loeppert, R. H., Hossner, L. R., and Amin, P. K., 1984, *Soil Sci. Soc. Am. J.* **48**:677.
Lopez–Quintela, M. A., and Casado, J., 1989, *J. Theor. Biol.* **139**:129.
Lorenz, E. N., 1963, *J. Atmos. Sci.* **20**:130.
Lovejoy, S., Schertzer, D., and Tsonis, A. A., 1987, *Science* **235**:1036.
Lubensky, T. C., and Pincus, P. A., 1984, *Phys. Today* **37**:44.
Ludwig, F. L., 1989, *NATO Challenges Modern Sci.* **13**:451.
McCammon, J. A., Bacquet, R. J., Allison, S. A., and Northrup, S. H., 1987, *Faraday Discuss. Chem. Soc.* **83**:213.
Mandelbrot, B. B., 1980, *Ann. N. Y. Acad. Sci* **357**:249.
Mark, D. M., and Aronson, P. B., 1984, *Math. Geol.* **16**:671.
Marquet, P. A., Navarrete, S. A., and Castilla, J. C., 1990, *Science* **250**:1125.
Matsushita, M., 1985, *J. Phys. Soc. Jpn.* **54**:857.
Matsushita, M., Sano, M., Hayakawa, Y., Hanjo, H., and Sawuda, C. Y., 1984, *Phys. Rev. Lett.* **53**:286.
Meakin, P., 1984, *J. Colloid Interface Sci.* **102**:491.
Meakin, P., 1986, *Chem. Phys. Lett.* **123**:428.
Meakin, P., 1991, *Science* **252**:226.
Mehaute, A., Le, and Dugast, A., 1983, *J. Power Sources* **9**:359.
Menzinger, M., and Jankowski, P., 1986, *J. Phys. Chem.* **90**:1217.
Miller, A., and Möhwald, H., 1987, *J. Chem. Phys.* **86**:4258.
Miller, E. E., 1980, in: *Applications of Soil Physics* (D. Hillel, Ed.), Academic Press, New York.

Mizutani, H., 1980, *The Science of Craters,* Tokyo University Press, Tokyo.
Mohanty, K. K., Ottino, J. M., and Davis, H. T., 1982, *Chem. Eng. Sci.* **37**:73.
Moloy, K. J., Feder, J., and Jossing, T., 1985, *Phys. Rev. Lett.* **55**:2688.
Morse, D. R., 1985, *Nature* **314**:731.
Mosolov, A. B., 1991, *Zh. Eksp. Teor. Fiz.* **99**:295.
Mottola, H. A., 1990, *Trends Anal. Chem.* **9**:297.
Mullins, W. W., and Sekerka, R. F., 1963, *J. Appl. Phys.* **34**:323.
Murray, C. D., 1926, *J. Gen. Physiol.* **9**:835; 1927, **10**:725.
Muthukumar, M., 1985a, *J. Chem. Phys.* **83**:3161.
Muthukumar, M., 1985b, *AIP Conf. Proc.* **137**:145.
Nagumo, J., Arimoto, S., and Yoshizawa, S., 1962, *Proc. IRE* **50**:2061.
Nagy–Ungvarai, Z., Tyson, J. J., Muller, S. C., Watson, L. T., and Hess, B., 1990, *J. Phys. Chem.* **94**:8677.
Nittmann, J., and Stanley, H. E., 1986, *Nature* **321**:663.
Nittmann, J., and Stanley, H. E., 1987, *J. Phys. A* **20**:1185.
Nittmann, J., Daccord, G., and Stanley, H. E., 1985, *Nature* **314**:141.
Nottebohm, F., 1989, *Sci. Am.* Feb.:**260**(2), 74.
Noyes, R. M., and Field, R. J., 1974, *Annu. Rev. Phys. Chem.* **25**:95.
Nygren, H., and Stenberg, M., 1990, *Prog. Colloid Polym. Sci.* **82**:15.
Nyikos, L., and Pajkossy, T., 1985, *Electrochim. Acta* **30**:1533.
Onaral, B., Tsao, Y. Y., Moussavi, M., and Sun, H. H., 1987, *Proceedings of the Ninth Annual Conference of the IEEE,* Engineering in Medicine and Biology Society, IEEE, New York.
Ottino, J. M., Leong, C. W., Rising, H., and Swanson, P. D., 1988, *Nature* **333**:419.
Ozeki, S., 1989, *Langmuir* **5**:186.
Paliwal, H. V., Bhatnagar, S. H., and Haldar, S. K., 1986, *J. Math. Geol.* **18**:539.
Park, S. J., and Mansoori, G. A., 1988, *Energy Sources* **10**:109.
Peng, B., Petrov, V., and Showalter, K., 1991, *J. Phys. Chem.* **95**:4957.
Perrin, J., 1923, in: *Atoms* (D. L. Hammick, ed.), Van Nostrand, New York.
Peters, R. H., 1983, *The Ecological Implications of Body Size,* Cambridge University Press, Cambridge.
Pfeifer, P., 1985, *Chimia* **39**:120.
Pfeifer, P., and Avnir, D., 1984, *J. Chem. Phys.* **80**:4573.
Pfeifer, P., and Obert, M., 1989, *The Fractal Approach to Heterogeneous Chemistry* (D. Avnir, ed.), Wiley, New York.
Pfeifer, P., Welz, U., and Wippermann, H., 1985, *Chem. Phys. Lett.* **113**:535.
Pfeifer, P., Wu, Y., Cole, M. W., and Krim, J., 1989, *Phys. Rev. Lett.* **62**:1997.
Phillips, R. J., Arvidson, R. E., Boyce, J. M., Campbell, D. B., Guest, J. E., Schaber, G. G., and Soderblom, L. A., 1991, *Science* **252**:288.
Plesser, T., Muller, S. C., and Hess, B., 1990, *J. Phys. Chem.* **94**:7501.
Poincaré, H., 1890, *Acta Math.* **13**:1.
Politowicz, P. A., and Kozak, J. J., 1988, *Langmuir* **4**:305.
Polvani, L. M., Wisdom, J., DeJong, E., and Ingersoll, A. P., 1990, *Science* **249**:1393.

Pospisil, L., 1988, *J. Phys. Chem.* **92**:2501.
Power, W. L., Tullis, T. E., Brown, S. R., Boitnott, G. N., and Scholz, C. H., 1987, *Geophys. Res. Lett.* **14**:29.
Pye, K., and Chance, B., 1966, *Proc. Natl. Acad. Sci. USA* **55**:868.
Quellet, C., Eicke, H. F., and Sager, W., *J. Phys. Chem.* **95**:5642.
Raherendeen, K., 1981, *J. Theor. Biol.* **91**:607.
Raleigh, L., 1892, *Philos. Mag.* **34**:177.
Reich, M. H., Russo, S. P., Snook, J. K., and Wagenfeld, H. K., 1990, *J. Colloid Interface Sci.* **135**:353.
Resch, P., Munster, A. F., and Schneider, F. W., 1991, *J. Phys. Chem.* **95**:6270.
Richards, F. M., 1991, *Sci. Am.* **Jan.**:**264**(1), 34.
Richardson, L. F., 1961, *Gen. Systems Yearb.* **6**:139.
Ridgefield, C. T., 1987, *AIP Conf. Proc.* **154**:304.
Roberts, J. N., 1986, *Phys. Rev. Lett.* **56**:2111.
Roman, H. E., Bunde, A., and Havlin, S., 1989, *Ber. Bunsenges. Phys. Chem.* **93**:1205.
Saffman, P. G., 1986, *J. Fluid Mech.* **173**:73.
Saffman, P. G., and Taylor, G., 1958, *Proc. R. Soc. London Ser. A* **245**:312.
Samson, R. J., Mulholland, G. W., and Gentry, J. W., 1987, *Langmuir* **3**:272.
Saupe, D., 1987, *Physica (Utrecht)* **28D**:358.
Schaefer, D. W., Martin, J. E., Wiltzius, P., and Cannell, D. S., 1984, *Phys. Rev. Lett.* **52**:2371.
Schaefer, D. W., Martin, J. E., and Hurd, A. J., 1985, in: *On Growth and Form,* NATO Adv. Study Inst. Vol. E100, Nijhoff, The Hague.
Schell, M., and Abahadily, F. N., 1989, *J. Chem. Phys.* **90**:822.
Sernetz, M., Gelleri, B., and Hofmann, J., 1985, *J. Theor. Biol.* **117**:209.
Sernetz, M., Bittner, H. R., Willems, H., and Baumhoer, C., 1989, in: *The Fractal Approach to Heterogeneous Chemistry* (D. Avnir, ed.), Wiley, New York.
Shanks, H., and Wrench, K., 1962, *Math. Computation* **XVI**:77.
Shklovskii, I. S., and Sagan, C., 1966, *Intelligent Life in the Universe,* Holden–Day, San Francisco.
Simons, G. A., and Garman, A. R., 1986, *AICHE, J.,* **32**:1491.
Sokolov, I. M., 1986, *Usp. Fiz. Nauk* **150**:221.
Sokolowska, Z., Patrykiejew, A., and Sokolowski, S., 1989, *Langmuir* **5**:938.
Sood, A. K., 1987, *Hyperfine Interact. (Switzerland)* **37**:365.
Speidell, L. S., 1988, *Pension and Investment Age* **16**:26.
Srikrishna, M., Sivaji, K., and Narasimhamurty, G. S. R., 1982, *Chem. Eng. J. (Loughborough)* **24**:27.
Stanley, H. E., 1984, *J. Stat. Phys.* **36**:843.
Steinhardt, J., and Reynolds, J. (eds,), 1969, *Equilibria in Proteins,* Academic Press, New York.
Stenberg, M., and Nygren, H., 1990, *Prog. Colloid Polym. Sci.* **82**:10.
Strathmann, R. R., 1990, *Science* **250**:1091.
Stutzer, M. J., 1980, *J. Econ. Dyn. Control* **2**:353.
Szalag, A. S., and Schramm, D. N., 1985, *Nature* **314**:718.

Szep, J., Cserti, J., and Kertesz, J., 1985, *J. Phys. A* **18**:413.
Tabeling, P., Zocchi, G., and Libchaber, A., 1987, *J. Fluid Mech.* **177**:67.
Takahashi, M., 1989, *J. Theor. Biol.* **141**:117.
Takayasu, H., Nishikawa, I., and Taskai, H., 1988, *Phys. Rev. A* **37**:6.
Tanford, C., 1961, *Physical Chemistry of Macromolecules,* Wiley, New York.
Tanford, C., 1980, *The Hydrophobic Effect,* 2nd ed., Wiley, New York.
Teixeira, J., 1986, in: *On Growth and Form* (H. E. Stanley and N. Ostrowsky, eds.), Nijhoff, The Hague.
Tence, M., Chevalier, J. P., and Jullien, R., 1986, *J. Phys. (Paris)* **47**:1989.
van Damme, H., 1987, *J. Phys. Chem.* **48**:87.
van Damme, H., and Fripiat, J. J., 1985, *J. Chem. Phys.* **82**:2785.
van Damme, H., Obrecht, F., Levitz, P., Gatineau, L., and Laroche, C., 1986a, *Nature* **320**:731.
van Damme, H., Levitz, P., Beraya, F., Alcover, J. F., Gatineau, L., and Fripiat, J. J., 1986b, *J. Chem. Phys.* **85**:616.
van der Pol, B., and van der Mark, J., 1928, *Philos. Mag.* **7**(6):763.
Velard, M. G., and Normand, C., 1980, *Sci. Am.* **243**(1):92.
Verwey, E. J. W., and Overbeek, J. T. G., 1948, *Theory of the Stability of Lyophobic Colloids,* Elsevier, Amsterdam.
Vicsek, T., 1984, *Phys. Rev. Lett.* **53**:2281.
Vicsek, T., 1985, *Phys. Rev. A* **32**:3084.
Vicsek, T., 1987, *Phys. Scr.* **19**:334.
Vicsek, T., and Kertesz, J., 1990, *Phys. Rev. Lett.* **65**:1388.
Voss, R. F., 1985, in: *Fundamental Algorithms in Computer Graphics* (R. A. Earnshaw, ed.), Springer–Verlag, Berlin.
Weis, R. M., and McConnell, H. M., 1984, *Nature* **310**:47; 1985, *J. Phys. Chem.* **89**:4453.
Weitz, D. A., and Oliveria, M., 1984, *Phys. Rev. Lett.* **52**:1433.
Weitz, D. A., Huang, J. S., Lin, M. Y., and Sun, J., 1985, *Phys. Rev. Lett.* **54**:1416.
Werthen, M., Stenberg, M., and Nygren, H., 1990, *Prog. Colloid Polym. Sci.* **82**:349.
Wesson, P., 1987, *Astrophys. J.* **317**:601.
Williams, G. O., Singh, V. A., and Corbett, J. W., 1987, *Phys. Status Solidi B* **144**:1.
Winfree, A. T., and Strogatz, S. H., 1984, *Nature* **311**:611.
Witten, T. A., and Cates, M. E., 1986, *Science* **232**:1607.
Wolfram, S., 1984, *Nature* **311**:419.
Wong, P.-Z., 1985, *Phys. Rev. B* **32**:7417.
Wong, P., Howard, J., and Lin, J., 1986, *Phys. Rev. B* **32**:7417.
Xu, Y., and Schell, M., 1990, *J. Phys. Chem.* **94**:7137.
Yakubov, T. S., 1988, *Dokl. Akad. Nauk SSSR Phys. Chem.* **303**:425.
Zhabotinsky, A. M., and Rovinsky, A. B., 1990, *J. Phys. Chem.* **94**:8001.
Zhou, Z., and Chu, B., 1991, *J. Colloid Interface Sci.* **143**:356.

Index